This project has received funding from the European Union's Horizon 2020 research and innovation programme under grant agreement No. 700748

LIQUEFACT

Assessment and mitigation of Liquefaction potential across Europe: a holistic approach to protect structures/infrastructure for improved resilience to earthquake-induced Liquefaction disasters.

H2020-DRA-2015

GA no. 700748

DELIVERABLE D2.7

Methodology for assessment of earthquake-induced risk of soil liquefaction at the four European testing sites (*microzonation*)

This project has received funding from the European Union's Horizon 2020 research and innovation programme under grant agreement No. 700748

Author(s):	UNIPV- Eucentre: Carlo G. Lai, Claudia Meisina, Francesca Bozzoni, Daniele Conca, Antonino Famà, Ali G. Özcebe, Elisa Zuccolo, Roberta Bonì, Valerio Poggi, Renato M. Cosentini UPORTO: António Viana da Fonseca, Cristiana Ferreira, Cláudia Coelho, João Coelho, Julieth Quintero, Sara Rios, Maxim Millen, Diana Cordeiro Istan-Uni: Sadik Oztoprak, Ilknur Bozbey, Cihan Oser, Sinan Sargin, Namık Aysal, Ferhat Ozcep, M. Kubilay Kelesoglu ULJ: Matej Maček, Aleš Oblak, Dušan Petrovič, Mirko Kosič, Jasna Smolar, Sebastjan Kuder, Janko Logar
Responsible Partner:	Università degli Studi di Pavia/Eucentre
Version:	1.0
Date:	31/07/2019
Distribution Level (CO, PU)	CO

This project has received funding from the European Union's Horizon 2020 research and innovation programme under grant agreement No. 700748

DOCUMENT REVISION HISTORY

	Version	Editor	Comments	Status
31/07/2019	1	UNIPV- Eucentre: Carlo G. Lai, Claudia Meisina, Francesca Bozzoni, Daniele Conca, Antonino Famà, Ali G. Özcebe, Elisa Zuccolo, Roberta Bonì, Valerio Poggi, Renato M. Cosentini UPORTO: António Viana da Fonseca, Cristiana Ferreira, Cláudia Coelho, João Coelho, Julieth Quintero, Sara Rios, Maxim Millen, Diana Cordeiro Istan-Uni: Sadik Oztoprak, Ilknur Bozbey, Cihan Oser, Sinan Sargin, Namık Aysal, Ferhat Ozcep, M. Kubilay Kelesoglu ULJ: Matej Maček, Aleš Oblak, Dušan Petrovič, Mirko Kosič, Jasna Smolar, Sebastjan Kuder, Janko Logar	First Draft	Draft

LIST OF PARTNERS

	Name	Country
UNIPV/Eucentre	Università degli Studi di Pavia/Eucentre	Italy
UPORTO	Universidade do Porto	Portugal
Istan-Uni	Univerza v Ljubljani	Turkey
ULJ	Istanbul Universitesi	Slovenia

GLOSSARY

Acronym	Description
GIS	Geographical Information System
CH	Cross-Hole
CPT	Cone Penetration Test
C_{QL}	Quality Score
C_{QT}	Quantity Score
CRR	Cyclic Resistance Ratio
DMM	Minimum Average Distance
FA	Factor of amplification
FS	Safety Factor
HVSR	Horizontal to Vertical Spectral Ratio
LDI	Lateral Displacement Index
LPI	Liquefaction Potential Index
LSN	Liquefaction Severity Number
MASW	Multichannel Analysis of Surface Waves test
R	Minimum Range
RP1	Return Period = 475 years
RP2	Return Period = 975 years
RP3	Return Period = 2475 years
SASW	Spectral Analysis of Surface Waves test
SDMT	Seismic Dilatometer Test
SPT	Standard Penetration Test
SR	Seismic Refraction test

This project has received funding from the European Union's Horizon 2020 research and innovation programme under grant agreement No. 700748

T1	Seismic Action Type 1 (Eurocode 8); Distant large magnitude earthquake
T2	Seismic Action Type 2 (Eurocode 8); Near medium magnitude earthquake
V_S	Shear Wave Velocity

CONTENTS

LIST OF FIGURES AND TABLE

FIGURES

TABLES

1. INTRODUCTION

One of the main goal of the Work Package 2 (WP2) of LIQUEFACT project is to set-up a methodology for localized assessment of liquefaction potential (*microzonation*). Microzonation of a territory for liquefaction risk is the subdivision of the territory in areas characterized by the same probability of liquefaction manifestation, under free-field conditions, in case of an earthquake of specified severity. Microzonation for liquefaction risk is hereinafter considered as the subdivision of a territory at a municipal or submunicipal scale. The liquefaction risk at a site depends on the severity of expected ground shaking and thus on the seismic hazard and the susceptibility to liquefaction of that site. This in turn depends on geological, geomorphological, hydrogeological and geotechnical factors. Thus, liquefaction risk implies the existence of areas characterized by a moderate to high seismic hazard in the sense of intensity of ground shaking.

The four areas under investigation are located in Marmara region (Turkey), Ljubljana area (Slovenia), Lisbon area (Portugal) and Emilia region (Italy). The four testing sites were selected on the basis of the following criteria: availability of geological and geotechnical data, presence of liquefiable soil deposits, documented cases of liquefaction manifestations occurred in past earthquakes, representativeness of different geological setting, density of population in selected areas. The microzonation, objective of Task 2.6, must be based on the results obtained from ground characterization carried out at each of the four selected areas in Task 2.1 (Deliverable 2.1, 2017).

The roles of the partners involved in this activity is as follows:

- UNIPV-Eucentre has responsibility over the Emilia area;
- UPORTO has responsibility over the Lisbon area;
- ULJ has responsibility over the Ljubljana area;
- Istan-Uni has responsibility over the Marmara area.

It is worth noting that UNIPV and Eucentre drafted the "*Guidelines on the methodology for localized assessment of Earthquake Induced Soil Liquefaction potential at the four European testing sites (Microzonation)*" (v1.0 July 15, 2017) with the aim of establishing a shared framework among the partners involved in this task in order to deliver at the four selected areas compatible and to a certain degree homogeneous microzonation maps for liquefaction risk. They are recommendations aimed to guarantee an acceptable degree of compatibility among the maps that will be produced at the four testing sites. LIQUEFACT is a research project and as such each partner should have the freedom to carry out their activities according to its own strategies and ideas. Finally, this document represents the base for the preparation of the present Deliverable 2.7.

2. MICROZONATION OF THE ITALIAN TESTING AREA: THE TERRITORY OF CAVEZZO MUNICIPALITY

2.1 Geological and Seismotectonic setting

Cavezzo municipality is located within the northern sector of the Modena province (Italy), on the right side of the Secchia River. The study area sits within the western margin of the Po plain, a large foreland sedimentary basin originated by the progressive convergence of the Africa/Adria and Eurasia plates initiated during the late Cretaceous and still ongoing. Such compressional regime led to the development of large thrust and folds structures with roughly WNW-ESE trending, but of opposing vergence to the North and to the South of the longitudinal valley axis. Some of the southern buried structures have demonstrated to be still under active shortening, causing non-negligible historical seismicity, whose noticeable expression was the recent 2012 Emilia sequence.

The sedimentary infill of the Po plain consists of a thick sequence of sediments of Tertiary-Quatertiary age, from fine Pliocene muds to more course silt, sand and gravel alternations due to transition to continental deposition from the Pleistocene. Depositional sequence is heavily perturbed by the ongoing deformation process and the alternation of episodes of erosion and glaciation, which have generated several noticeable angular unconformities and gaps (Mascandola et al. 2019).

At local scale, Cavezzo is on the southern limb of the buried Mirandola antiform (Boccaletti et al., 2004; Martelli et al., 2017). The lithostratigrafic succession of the area is composed by alluvial deposits ranging in thickness from around 130 m in the northern area to 280 m in the southern one (RER-ENI, 1998). The bedrock is constituted by interbedded marlstones and sands of the Pliocene and Lower Pleistocene “Argille Azzurre” Formation and Middle Pleistocene “Imola Sands” Formation (RER-ENI, 1998). The alluvial deposits in the Cavezzo area are characterized by interbedded fine silty-clayey soils with layers rich of peat and interbedded sands and silty sands. These surficial sediments were deposited by the Secchia River, whereas the deeper sand layers were deposited by the Po River (Castaldini, 1989).

From the morphological point of view, the study area is located in the alluvial plain of the Secchia River, ranging in elevation from 34 m a.s.l. in the southern and western sector to around 20 m a.s.l. in the northern part. It is worth noting that the highest topographic level is reached in correspondence of the modern artificial levees of the Secchia River, which raise about 7-8 m above the surrounding area (Figure 2-1). The study area includes different geomorphological features interpreted as floodplain, fluvial ridges and crevasse splays. The subsoil of Cavezzo is mainly characterized by silty-clayey sequences including channel-filling and crevasse splay sand layers (Pellegrini and Zavatti, 1980).

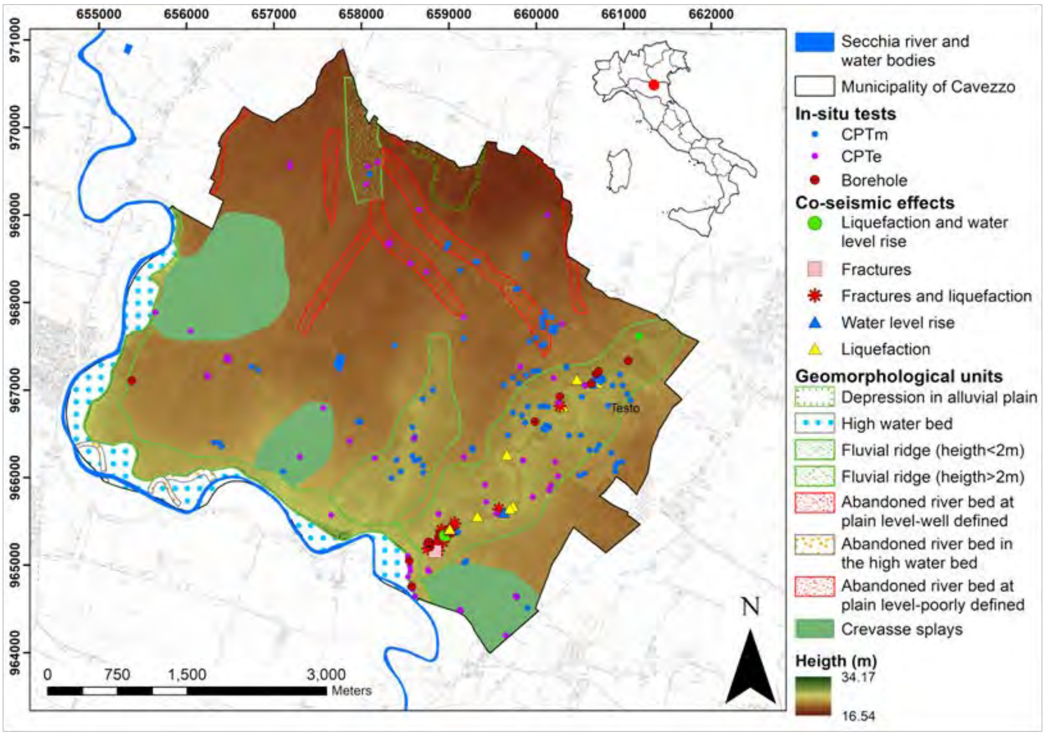

Figure 2-1: Main geological and geomorphological features of the area of Cavezzo (from Meisina et al., 2019).

2.2 Methodology

Starting from the creation of a comprehensive and unified GIS database of available geotechnical and geophysical measurements, a lithological model was first constructed from the analysis of boreholes and CPT data. From that, homogeneous areas identifying the major lithological units (LU) were outlined. Stratigraphic vertical cross sections were developed oriented longitudinally and transversally with respect to the main geomorphological features. A 3D geological model was then constructed for the territory under study down to a depth of 30 m and for an area of approximately 27 km^2.

Next, a large-scale, a pseudo-3D, seismo-stratigraphic model was developed based on old and newly acquired data from seismic geophysical surveys which included passive measurements of ambient noise using 2D arrays and high resolution reflection prospecting. Concerning data analysis, advanced processing techniques were used, such as the combined inversion of multi-component surface wave datasets (Poggi et al. 2010), based on a joint interpretation of travel-times, dispersion and polarization data. This has led to the definition of different realizations of 1D seismo-stratigraphic profiles at each of the 2,984 nodes of a grid with a 0.001 degrees spatial resolution (about 100 meters) covering the Cavezzo territory. Overall, 11 complementary 1D seismo-stratigraphic models were defined at each node. The resulting 3D model has then been used for the calculation of the seismic amplification factors through numerical stochastic ground response analyses taking into account the epistemic uncertainty associated to the input models. More specifically, at each of the 2,984 nodes and for each of the 11 seismo-stratigraphic models, 1D site response analyses were carried out using the linear-equivalent soil constitutive model. The input motions referred to outcropping bedrock conditions were defined for 475, 975, and 2,475 years return periods in terms of suites of 7 seismo- and spectrum-compatible real accelerograms. For each return period, 229,768 analyses were carried out considering 2,984 nodes, 11 seismo-stratigraphic models and 7 accelerograms. Results were finally combined using the logic-tree approach to rationally account for the epistemic uncertainty associated with the 3D seismo-stratigraphic model and the variability of reference input motion while predicting ground motion amplification.

2.3 Ground characterization dataset

To carry out ground response analyses, an accurate knowledge of the geotechnical characteristics of the shallow subsoil at the site is required. At this purpose, the territory of Cavezzo was thoroughly characterized from geomorphological, geological, hydrogeological, seismological, geotechnical and geophysical viewpoints.

As a start, existing data retrieved from trench pits, boreholes, piezometric, in situ and laboratory geotechnical and geophysical investigation campaigns were gathered. Figure 2-2a shows the existing data available for ground characterization of the territory of Cavezzo before the LIQUEFACT project started. Based on the quality and quantity of the retrieved existing data, then, complementary ground investigation campaigns were purposely devised (Figure 2-2b).

In-situ geotechnical investigations included: cone penetration tests with acquisition of the excess pore water pressure (CPTu) and the shear wave velocity Vs (SCPTu), standard penetration tests (SPT) and drilling of boreholes. Laboratory tests were also performed on undisturbed soil samples retrieved with the standard Osterberg sampler and the innovative gel-push technique for coarse-grained materials (Cubrinovski et al., 2016). A number of non-invasive geophysical tests were also performed. These included 3D electric tomography, active and passive multi-channel analysis of surface waves (MASW). In this regard, fundamental was the contribution of the National Institute of Geophysics and Volcanology (INGV Milano) and the National Institute of Oceanography and Applied Geophysics (OGS, Trieste), who respectively led a large-scale ambient vibration survey (including single-station H/V spectral ratio and 2D array measurements) and a high-resolution P/S reflection seismic survey. Such combined geophysical prospecting allowed illuminating large volumes of soils and at great depths (> 200 m from the ground surface) to identify the location of the seismic bedrock, while providing a mean to correlate the results obtained at different locations from the conventional geotechnical tests.

All data gathered on the subsoil of Cavezzo were organized into a purposely-developed GIS database, which now includes the data of more than 1,000 geotechnical and geophysical tests, as shown in Figure 2-2b. Data of both 1m and 5m resolution DEM were also included.

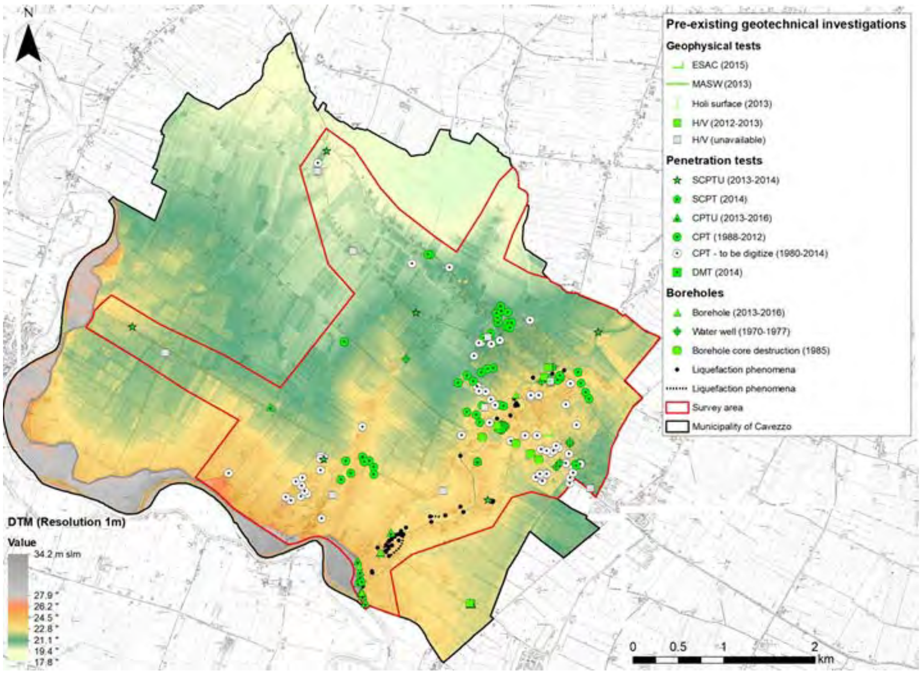

(a)

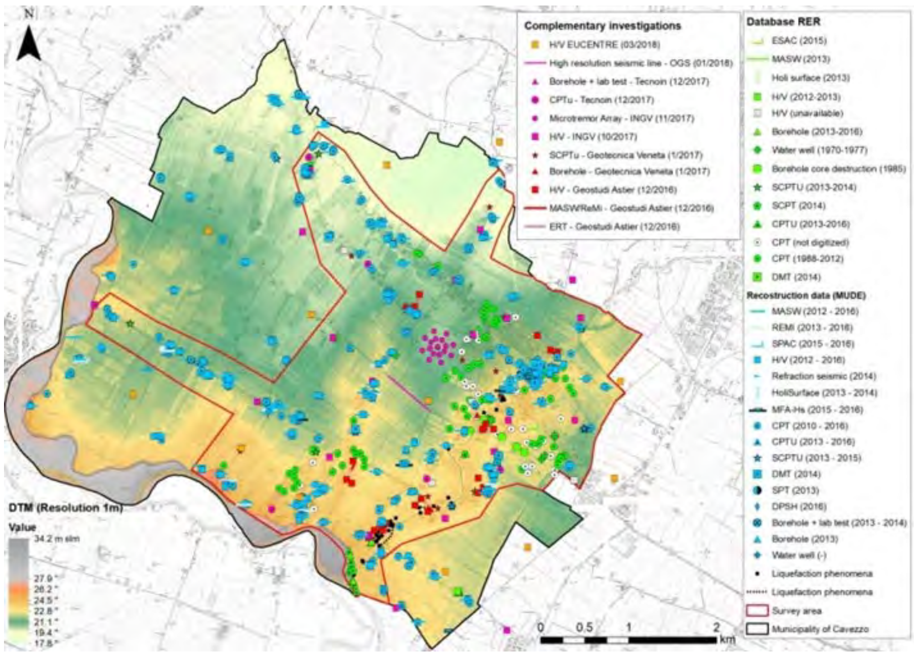

(b)

Figure 2-2: Comparison between the map showing the existing geotechnical data available for the territory of Cavezzo before the LIQUEFACT project started in 2016 (a) and the map showing data acquired during the LIQUEFACT project for improving ground characterization of the territory (b). The manifestations of soil liquefaction occurred in 2012 sequence (black dots) and 1m resolution DEM are superimposed. Modified from Lai et al. (2019).

Moreover, the water table position has been surveyed in both dry and wet seasons. In particular, two field campaigns were planned to measure the depth of the water level in April and September 2018, taking into account that the period of minimum and maximum depth corresponds to higher and lower risk for the liquefaction, respectively.

More precisely, the measurements were performed in civil wells of Cavezzo in order to obtain the distribution of the depth of the water level over the entire study area. Then, the measurements of the depth of the water level, respectively 36 and 23 measuring, respectively for the first and the second field campaigns, have been interpolated using the Kriging approach (Oliver, 1990). Figure 2-3 and Figure 2-4 show the location of the points at which the water table has been measured and the map of the interpolated values with reference to the wet season and dry season, respectively. The maps of the depth of the water level in Cavezzo show lower values in proximity of the Secchia river (See the location in Figure 2-1) and increasing value in the northern part of the study area (Figures 2-3 and 2-4). The map acquired during the period (April 2018) of minimum depth of the water level from the g.l. shows values lower than 1 m near the Secchia river and highest values of about 4-5 m in the norther sector of the study area. These evidences highlight the higher risk for liquefaction in the southern part of Cavezzo where the depth of the water level is lower respect the northern one.

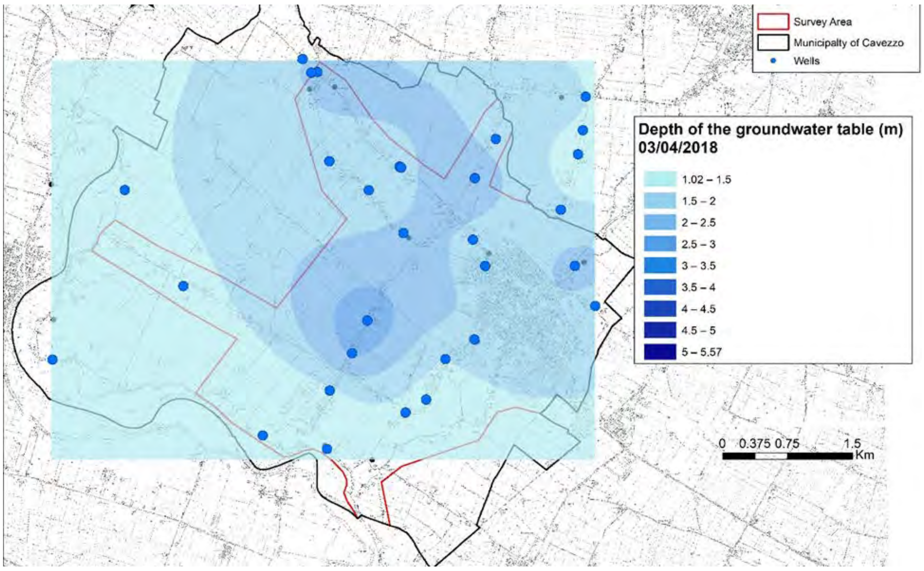

Figure 2-3: Map of water table depth in mostly wet season.

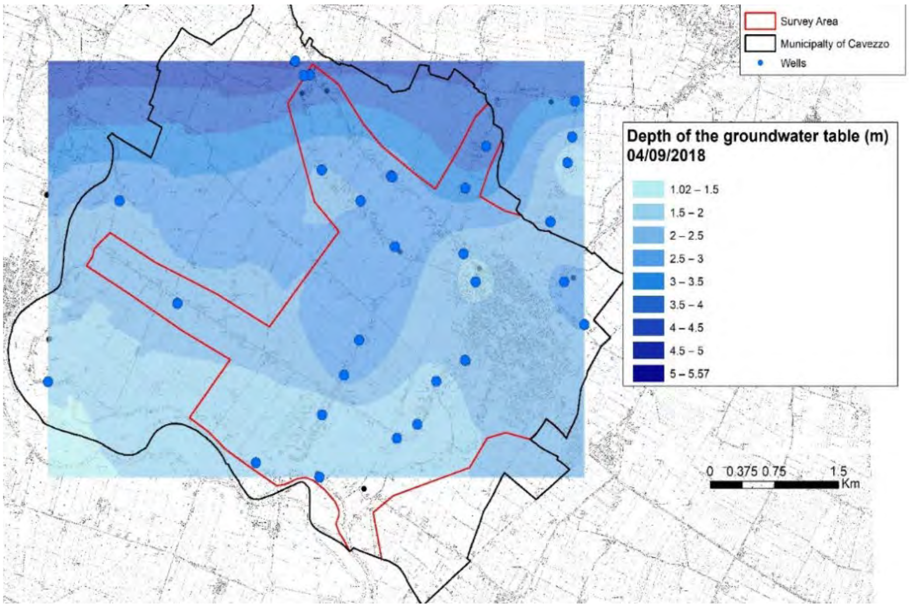

Figure 2-4: Map of water table depth in mostly dry season.

2.4 Modeling of the subsoil

2.4.1 Geological model

Based on a joint analysis of stratigraphic, lithological and geomorphological data, the territory of Cavezzo was tentatively subdivided into a number of geologically homogenous zones. The lithological units for liquefaction hazard assessment named "MOPS" represents homogeneous areas from the geomorphological and lithological point of views characterized by a rep-resentative stratigraphic profile representing the stratigraphic sequence (thickness and strat-igraphic succession) and boundaries of the different strata.

First, the main lithological classes of the study area were recognized by interpreting the stratigraphic profiles obtained from the borehole simplification using sample classification tests in order to analyse the first 30 m from the ground level. Then, the stratigraphic profile from cone penetration tests interpretation was performed. For the stratigraphic interpretation of cone penetration test data, it was used a correction of Soil Behaviour Index (Ic, Robertson 2009) calibrated using the available cone penetration tests and boreholes data in order to identify the mixture layers falling within the transition zone of the reference chart (Robertson, 2009). After that, a 3D geological model was built by using the stratigraphic profiles obtained from the boreholes and cone penetration tests interpretation, by means of the "horizons to solids" algorithm via the Groundwater Modelling System (GMS) Aquaveo software.

Finally, the MOPS identification was achieved thanks to the analysis of the stratigraphic profiles performed using the 3D geological model (Figure 2-5) and the geomorphological map (Figure 2-1). First, for each geomorphological unit, the type of lithologies in the surface and in the first 30 m from the ground level was determined. Subsequently, the boundaries of the MOPS were manually drawn using the boundaries of the landforms and the subsoil architecture as guide.

Seven dominant lithologies (the lithological classes) were identified in the study area, that are: man-made deposits (R), silty sand (Sl), sandy silt (Ls), clay (A), clay with peat (At) and sand (S) (Figure 2-5).

The results of the analysis have given insight about 9 main lithological units for liquefaction hazard assessment (MOPS) (Figure 2-6). Liquefiable layers were identified in all the MOPS, except for the MOPS 9 corresponding to the sector of alluvial plain (Table 2-1). These layers were located at depths between 2 and 15 m from ground level and are composed of sandy silts or silty sands. Liquefiable deposits were alternated sometimes with clayey layers, generally at depths between 7-10 m from ground level. In MOPS 5 and 7, these materials were silty sands and sandy silts present at depths between 2 and 12 m from ground level, which sometimes presented clay levels, of 1 m in thickness, at their top. In MOPS 6, silty sands and sandy silts responsible of liquefaction were not covered by clayey deposits (Table 2-1). Moreover, the 3D geometry of the silty sands and sandy silts layers in MOPS 5, 6 and 7 highlighted that these materials are confined by clayey and silty deposits both vertically and laterally, forming bodies which were extended not more than few hundreds of meters in lateral direction. This geometrical and depositional feature represented a difference respect to the sandy silts and silty sands layers identified in the other MOPS, where no liquefaction phenomena were identified. These layers were not interrupted by clayey-silty deposits, including continuous bodies within the units.

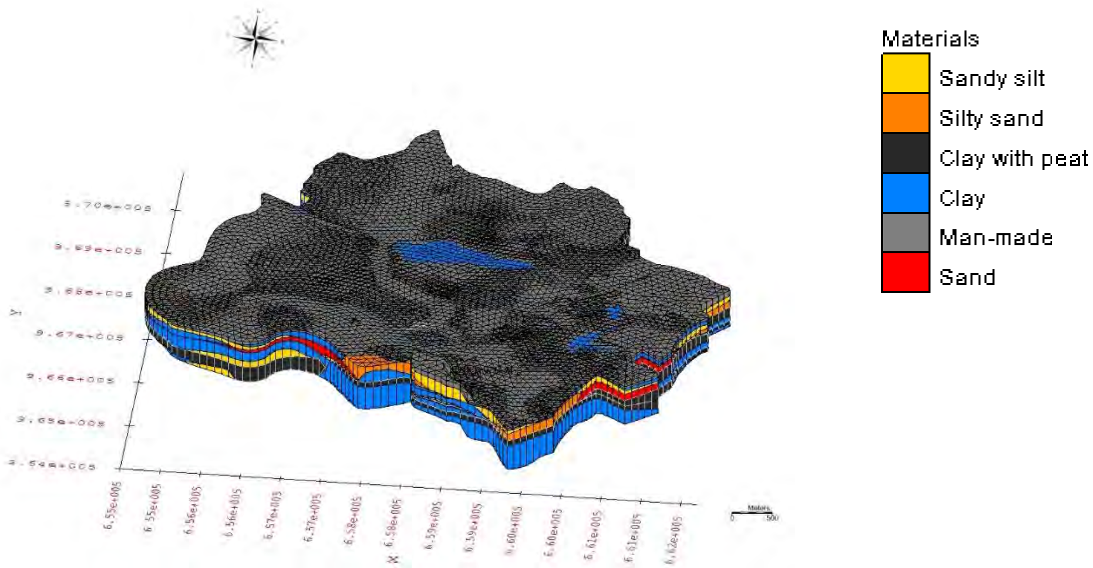

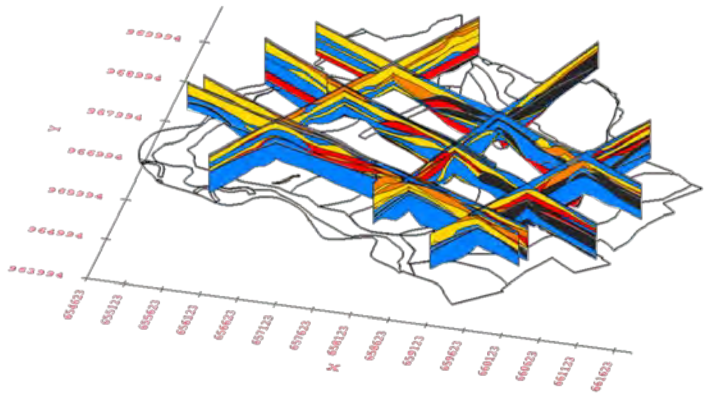

Figure 2-5: 3D lithological model of Cavezzo and cross-sections of the model.

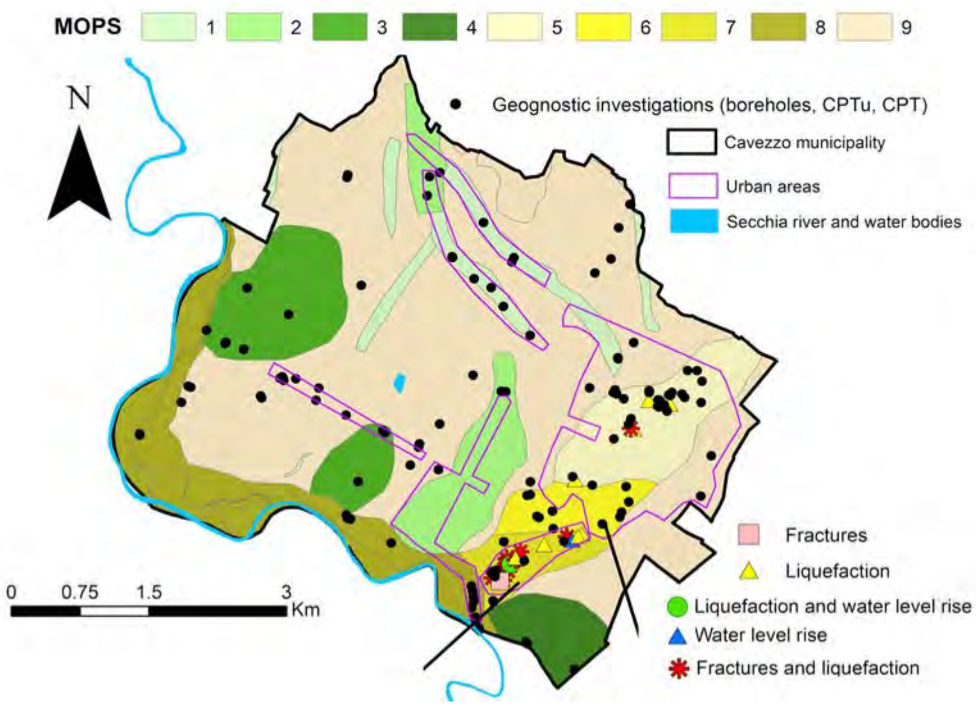

Figure 2-6: Map of 9 homogenous geological zones defined for Cavezzo municipality. Modified from Meisina et al. (2019).

Table 2-1: Lithological and geomorphological characteristics of the MOPS in Cavezzo.

Lithological units	Main lithostratigraphic features for microzonation studies	Depositional environment
1	Liquefable sandy silt layers between 2 and 9 m from ground level	Abandoned river bed
2	Liquefable sandy silt layers between 2 and 12 m from ground level	Abandoned river bed and ancient fluvial ridge
3 **4**	Liquefable sandy silt layers between 2 and 9 m from ground level	Crevasse splay
5	Liquefable sandy silt and silty sand layers between 2-9 m and 9-12 m from ground level, respectively	Abandoned river bed and ancient fluvial ridge
6	Liquefable sandy silt and silty sand layers between 2 and 8-9 m from ground level	Abandoned river bed and ancient fluvial ridge
7	Liquefable sandy silt and silty sand layers between 2-9 m and 9-15 m from ground level, respectively	Abandoned river bed and ancient fluvial ridge
8	Liquefable sandy silt layers between 9 and 14 m from ground level	Levees and actual river bed
9	Non-liquefable silt/clayey soils	Alluvial plain

2.4.2 Seismo-stratigraphic model

The previously described lithological model was preliminary to the definition of the seismo-stratigraphic idealization of the subsoil, which was obtained by integrating existing geophysical data (mostly from MASW investigations) with purposely-planned seismic acquisitions. Assuming a smooth lateral variability of the geophysical parameters over the investigated area, a pseudo-3D model was defined starting from a set of 1D velocity profiles obtained from the combined inversion of multi-component surface wave datasets (Figure 2-7). Two independent families of shear wave velocity profiles were calculated: the first (hereinafter called the INGV model) from ambient vibrations whereas the second from the processing of high-resolution reflection of P/S seismic data (hereinafter called the OGS model), for a total of 11 independent profiles. The two seismic techniques have shown to produce consistent results down to about 100 m depth from the ground surface, while some deviations were observed at larger depths (Figure 2-8). Such discrepancy has been considered as epistemic uncertainty of the reference seismo-stratigraphic models and accounted for in the data processing by means of a logic-tree approach.

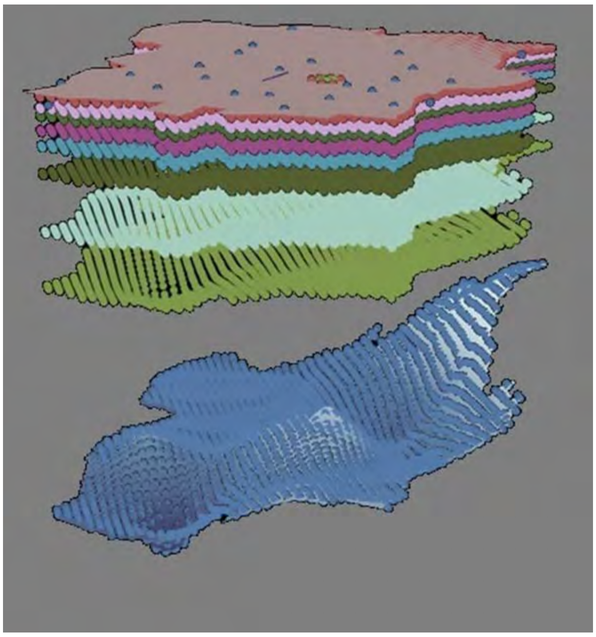

Figure 2-7: Pseudo-3D model developed starting from seismic data acquired from old and new geophysical surveys using the combined inversion of multi-component surface wave datasets based on a joint interpretation of travel-times, dispersion and polarization data. This led to the definition of 11 different realizations of 1D seismo-stratigraphic profiles at each of the 2,984 nodes of a grid with a 0.001 degrees spatial resolution (about 100 meters) covering the Cavezzo territory.

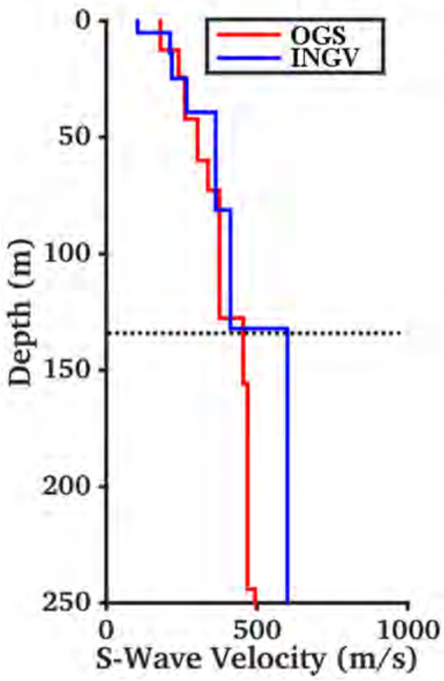

Figure 2-8: Comparison between two sample models from surface wave inversion of ambient vibration data (acquired by INGV) and from high-resolution P/S seismic reflection survey (OGS). The models show an overall good match down to a depth of about 140m, where an interface assumed to represent the seismic bedrock is located. Velocity is progressively mismatching the deeper layers.

2.4.3 Mapping subsoil variability over the area of study

In a subsequent step, at each point of the pseudo-3D model, the shear wave velocity profiles have been adjusted to match the observed variability of both the shallow subsoil and the deepest resonating layer interface (which was assumed to be the local seismic bedrock). For that, a map of the surface Rayleigh and Love wave velocity variability was first obtained by interpolating the V_{S30} estimates from 83 MASW analyses (Figure 2-9). It should be noted that being the results from MASW data heterogeneous (e.g. they were obtained from different surveys and using different processing schemes), it was decided to homogenously reassess the V_{S30} of each measurement by means of a simplified procedure as proposed by Brown et al. (2000) and further developed by Martin and Diehl (2004) and Albarello and Gargani (2010) (see also Comina et al. 2011 for clarifications). In short, the V_{S30} at each site was obtained empirically from the Rayleigh wave dispersion curve by extracting the phase velocity corresponding to a wavelength (λ) of 40 m, which provided estimates of V_{S30} comparable with those obtained from independent processing. Spatial interpolation of the V_{S30} values was performed using Geostatistics (through the ordinary Kriging algorithm). This provided a mean shear wave velocity and the corresponding expected uncertainty at each point of the interpolated grid. Finally, at each location, the reference velocity profiles have been adjusted to be compatible with the identified local value of V_{S30}. The adjustment was performed by applying a depth dependent correction factor, whose effects progressively decreases with the increase of depth (following a negative exponential function). This ensure that the observed shallow variability of V_S does not sensibly impact the seismo-stratigraphic model at large depths.

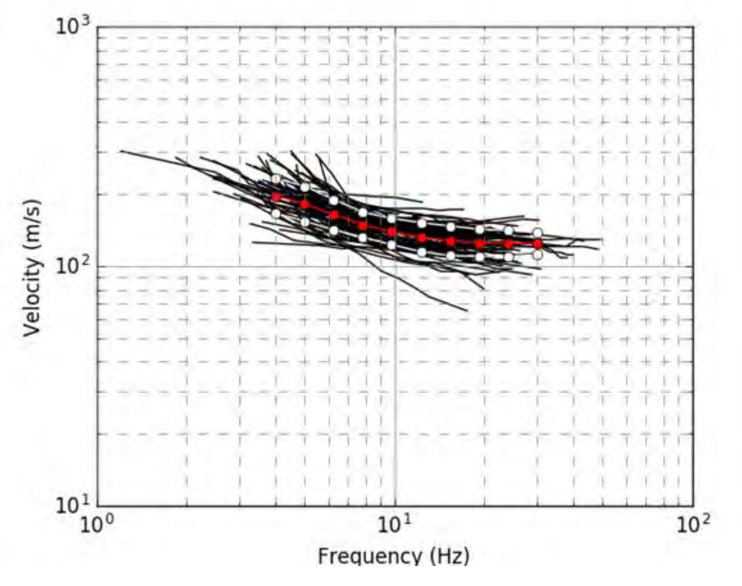

(a)

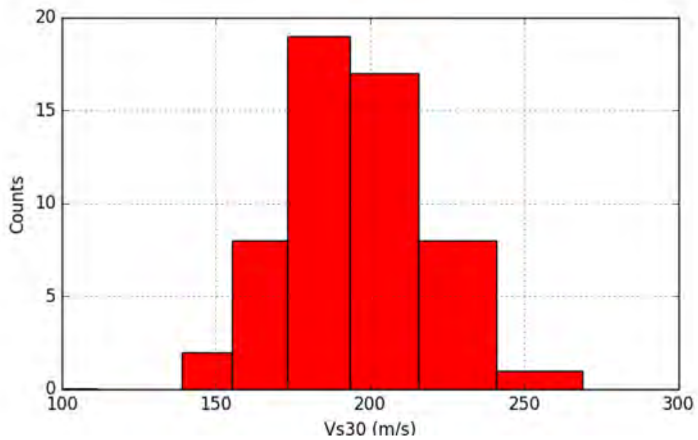

(b)

Figure 2-9: (a) Rayleigh wave dispersion curves form MASW analysis available for the territory (in black). Mean (red dots) and standard deviation (white dots) of the distribution is also presented to show the overall variability. (b) Distribution of the V_{S30} values obtained from the λ_{40m} empirical approximation.

2.4.4 Seismic bedrock constraints

The seismic bedrock was defined from the inversion of the fundamental frequency at the site (f_0) from horizontal-to-vertical-ratio spectral analysis (e.g. Nogoshi & Igarashi 1971; Nakamura 1989; Haghshenas et al. 2008) of 26 single station ambient vibration measurements performed over the area of study. For the inversion, it was used the procedure proposed by Poggi et al. (2012) based on Rayleigh wave ellipticity peak matching. Consistently with the procedure used to map shallow velocity variability, spatial interpolation between inverted bedrock depths was finally performed using ordinary Kriging, with an estimate of the associated uncertainty.

2.4.5 Final geotechnical-seismic model

The final geotechnical-seismic model of the area of study was defined starting from the pseudo-3D seismo-stratigraphic model, consisting of 10 V_S INGV profiles each with an associated weight of 0.05 (overall weight equal to 0.5), and an OGS V_S profile from seismic reflection survey to which a weight of 0.5 was associated. Each independent 3D model consisted of 2,984 1D V_S-profiles at each node of a reference grid that covers the territory of Cavezzo. Therefore, a total of 32,824 V_S profiles (2,984x11) were defined and used for ground response analysis. Furthermore, for each profile a unique seismo-geotechnical model was created by merging the soil properties of the geological/lithological and geophysical models (Table 2-2). At this purpose the 9 geologically homogeneous zones discussed in § 3.2 were used jointly with their associated uncertainties. In each homogeneous zone, the nodes of the reference grid falling within its boundaries have been identified

This project has received funding from the European Union's Horizon 2020 research and innovation programme under grant agreement No. 700748

for each layer of 11 seismo-stratigraphic models and a statistical analysis of the corresponding thicknesses was performed (Figure 2-10). Since the assessment of ground amplification was performed using 1D linear-equivalent analysis, a purposely-devised calibration of the shear modulus and damping ratio decaying curves was accomplished following the methodology proposed by Darendeli (2001) coupled with the experimental data from laboratory tests performed in the area of study in December 2017 (Figure 2-11)).

MOPS 1

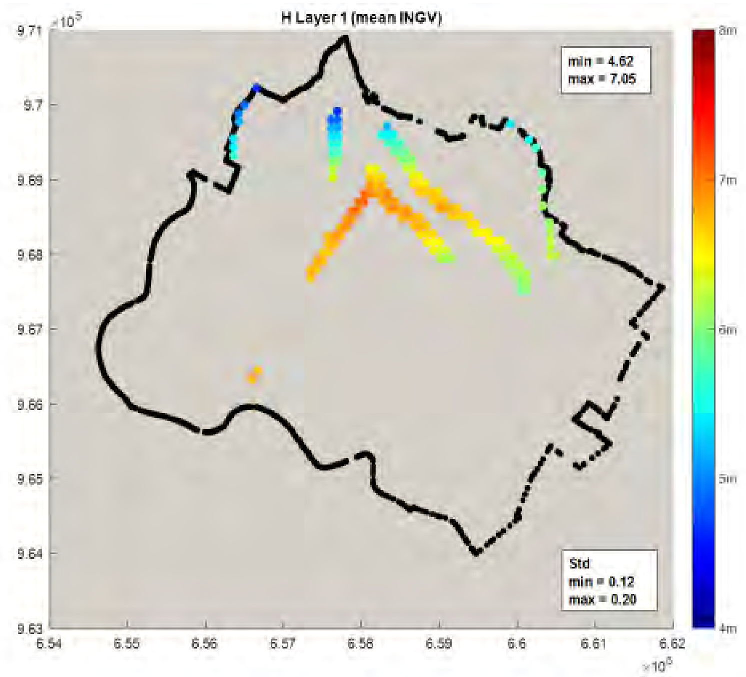

Figure 2-10: Statistical analysis of the corresponding thicknesses performed in each homogeneous zone for each layer of 11 seismo-stratigraphic models

Table 2-2: Merging of soil properties of the geological/lithological and geophysical models performed for one of 2984 nodes with reference to one of Vs INGV profiles.

Pseudo 3D geophysical model					Geological/lithological model				
n°	H(m)	V_p(m/s)	V_s(m/s)	ρ (kg/m³)	H	H(%)	material	pi	ϕ(°)
1	6.5	370	140	2100	2	0.31	fill	-	35
					4.5	0.69	Sandy silt	10	-
2	11.3	550	225	2100	3.8	0.34	Sandy silt	10	-
					7.5	0.66	clay	55	-
3	23.5	570	230	2100	1.5	0.06	sand	-	33
					22	0.94	clay	30	-

This project has received funding from the European Union's Horizon 2020 research and innovation programme under grant agreement No. 700748

4	23.5	875	350	2100	23.5	1	clay	30	-
5	35.7	880	360	2100	35.7	1	clay	30	-
6	123.3	1130	460	2100	123.3	1	clay	30	-
7	bedrock	2010	800	2100	-				

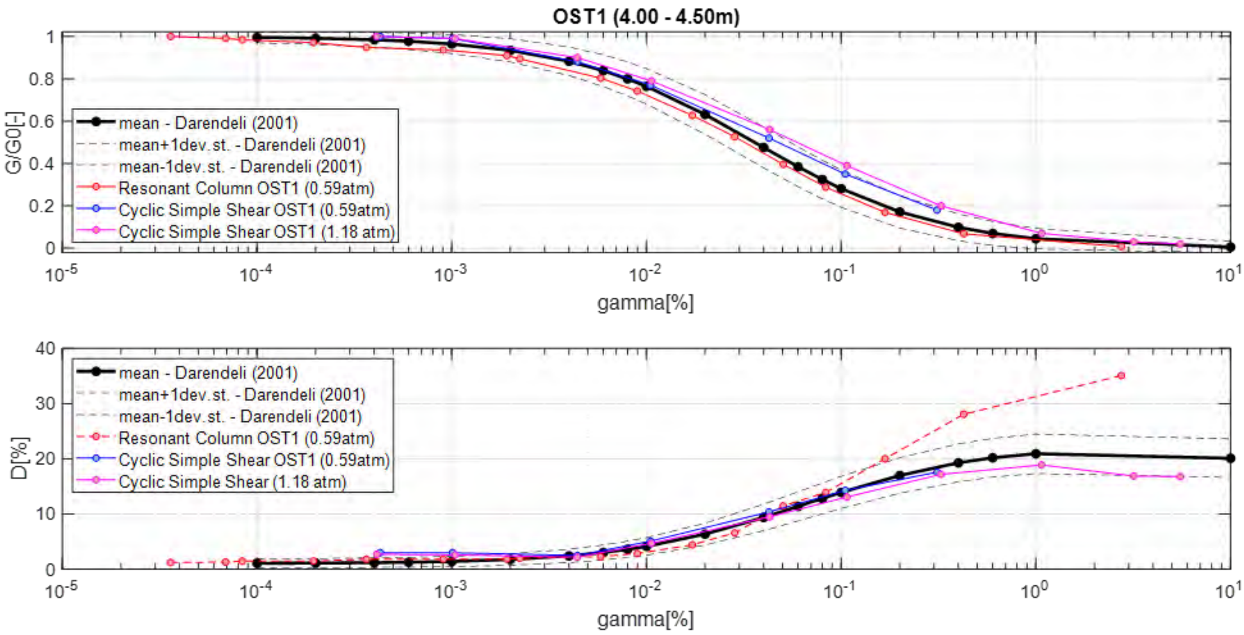

Figure 2-11: Calibration of shear modulus and damping ratio decaying curves as proposed by Darendeli (2001) using data from laboratory tests performed in December 2017 in Southern area of Cavezzo municipality.

2.5 Seismic response for microzonation

2.5.1 Definition of the reference seismic input and its variability

Emilia-Romagna region issued in 2015 (DGR n.2193) regional guidelines to support territorial and urban planning, which are consistent with the national "Guidelines for Seismic Microzonation" (SM Working Group, 2015). These regional guidelines provide 3 real accelerograms recorded on outcropping bedrock to be used as input motion for ground response analyses. However, these signals are not independent of each other; in addition, they are referred only to the 475 years return period. Thus, they are unsuitable to the scope of the study. Consequently, the seismic hazard at the site was redefined in terms of seismo- and spectrum-compatible natural accelerograms for three return periods (475, 975 and 2475 years). Spectrum-compatibility was enforced with reference to 5% damped, elastic acceleration response spectra (horizontal component of motion) referred to stiff ground conditions specified by the current Italian building code (NTC, 2018).

This project has received funding from the European Union's Horizon 2020 research and innovation programme under grant agreement No. 700748

Table 2-3 summarizes, for each considered return period, the parameters required to define the elastic response spectra for soil class A with reference to Cavezzo: a_g is the horizontal peak ground acceleration on a rigid reference site, F_0 is the amplification factor of the horizontal acceleration spectrum and T_{C^*} is the upper limit of the oscillator period of the constant spectral acceleration branch.

For each return period, a suite of 7 independent natural accelerograms recorded on free-field rock ground conditions, spectrum-compatible with the elastic response spectrum defined by the NTC (2018) for the territory of Cavezzo was selected. The selection was made using an updated version of ASCONA computer program (Corigliano et al., 2012), which provides a set of strong motion recordings satisfying specific seismological criteria (e.g., magnitude and distance ranges, spectral shape), with the additional requirement of being compatible with a target spectrum (in this case, the elastic acceleration response spectrum prescribed by the current Italian building code), in a specified oscillator period range (in this case, from 0.15 s to 2 s). Regarding record scaling, the PEER (2010a, 2010b) approach was adopted. Among different accelerogram sets that satisfy the requirements, the set returned by ASCONA is the one characterized by the minimum average deviation of the average response spectrum (of the 7 accelerograms) with respect to the target spectrum.

Table 2-3: Parameters adopted for the definition of the seismic hazard in Cavezzo, according with NTC (2018).

Return period (years)	**a_g (g)**	**F_0 (-)**	**T_c^* (s)**
475	0.151	2.588	0.270
975	0.202	2.535	0.276
2475	0.290	2.436	0.291

The following figures (Figure 2-12 to Figure 2-17) show the set of 7 accelerograms selected for the three considered return periods and their reponse spectra.

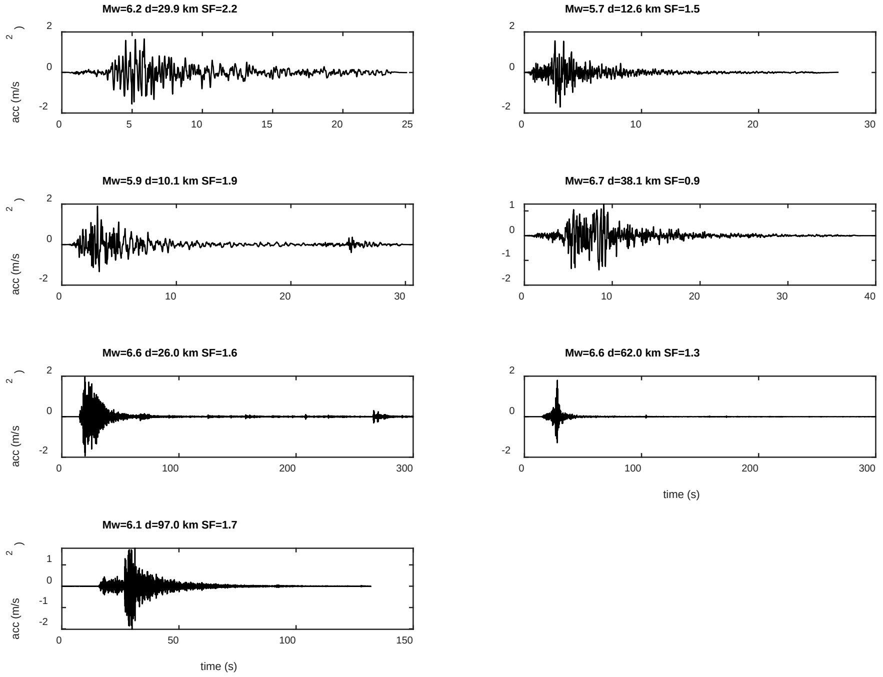

Figure 2-12: Group of 7 accelerograms (horizontal components) selected for the return period of 475 years. Above each accelerogram, the associated magnitude (Mw), distance (d) and adopted scaling factor (SF) are also reported.

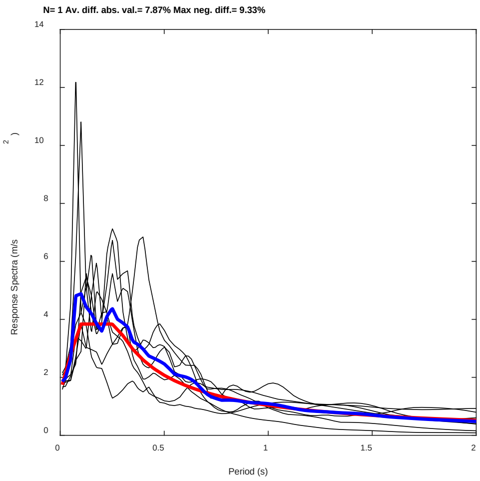

Figure 2-13: Response spectra of the 7 accelerograms selected for the return period of 475 years (black lines) along with their average spectrum (blue line) and the reference spectrum (red line). The average misfit between the spectral ordinates of the average spectrum and the reference spectrum in the range of periods [0.15–2.0 s] is 7.87%, while the maximum negative misfit in the same range of periods is 9.33%.

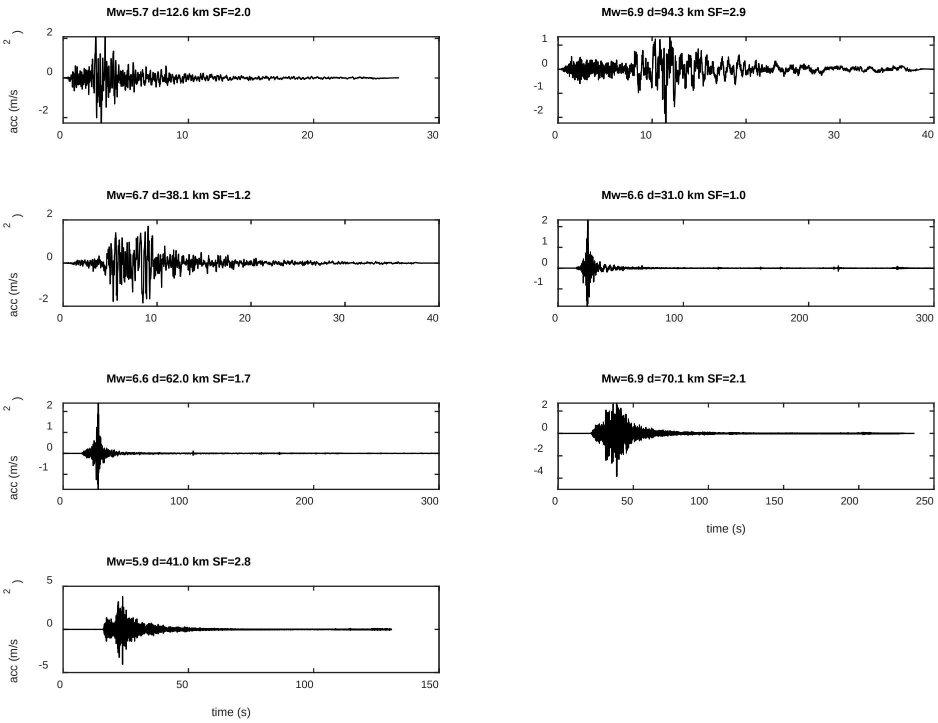

Figure 2-14: Group of 7 accelerograms (horizontal components) selected for the return period of 975 years. Above each accelerogram, the associated magnitude (Mw), distance (d) and adopted scaling factor (SF) are also reported.

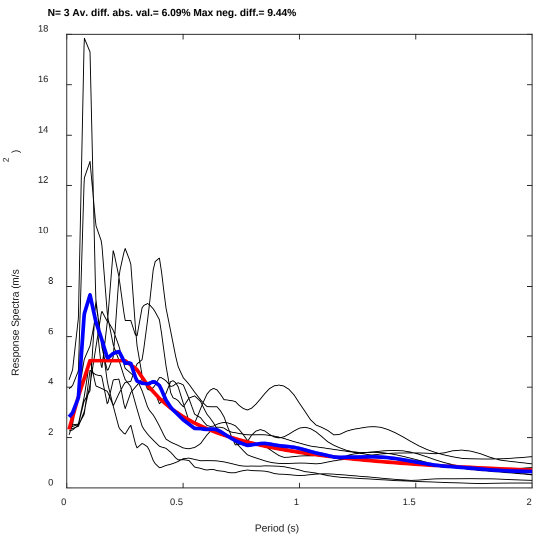

Figure 2-15: Response spectra of the 7 accelerograms selected for the return period of 975 years (black lines) along with their average spectrum (blue line) and the reference spectrum (red line). The average misfit between the spectral ordinates of the average spectrum and the reference spectrum in the range of periods [0.15–2.0 s] is 6.09%, while the maximum negative misfit in the same range of periods is 9.44%.

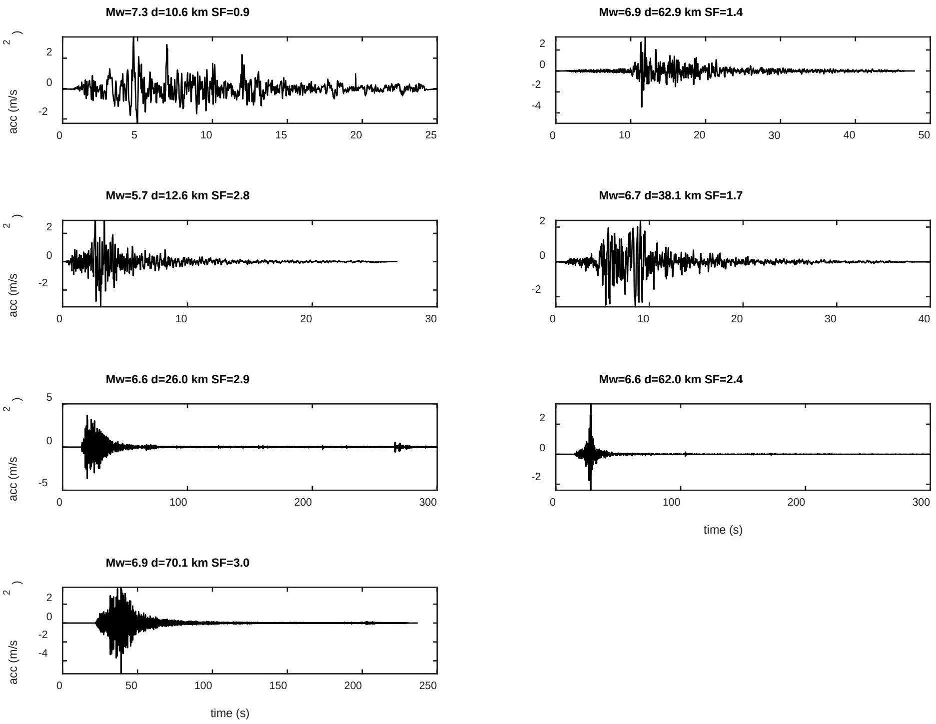

Figure 2-16: Group of 7 accelerograms (horizontal components) selected for the return period of 2475 years. Above each accelerogram, the associated magnitude (Mw), distance (d) and adopted scaling factor (SF) are also reported.

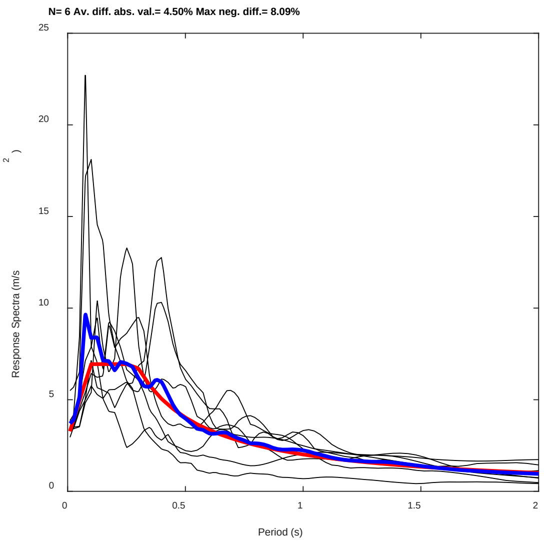

Figure 2-17: Response spectra of the 7 accelerograms selected for the return period of 2475 years (black lines) along with their average spectrum (blue line) and the reference spectrum (red line). The average misfit between the spectral ordinates of the average spectrum and the reference spectrum in the range of periods [0.15–2.0 s] is 4.50%, while the maximum negative misfit in the same range of periods is 8.09%.

2.5.2 Ground response analyses

One-dimensional ground response analyses were carried out in Cavezzo territory using SHAKE91 (Schnabel et al., 1972; Idriss and Sun, 1992) coupled with the linear-equivalent soil constitutive model. The analyses were conducted for 3 return periods, 7 accelerograms, 2,984 nodes of the reference grid for which the geotechnical-seismic pseudo 3D (P3D) model was defined and 11 V_S profiles, for a total of 229,768 analyses. For each analysis, amplification factors (F_i) in terms of peak ground acceleration, Housner intensity ratio (computed considering 4 different oscillator period ranges) and acceleration response spectrum integral ratio in the spectral interval between 0.1s and 0.5s were computed. At each node of the grid and for each return period, the F_i values computed from the 7 accelerograms and 11 V_S profiles were averaged as follows:

$$F^i = \sum_{j=1}^{7} w\_acc_j \sum_{k=1}^{11} w\_\mathrm{mod}_k \, F^i_{jk} \quad (1)$$

where w_acc_j is the weight of the accelerogram, assumed to be the same for all accelerograms (w_acc_j=1/7), w_mod_k is the weight of the P3D model (w_mod_k=0.05 for each of the 10 models based on INGV data and w_mod_k=0.5 for the OGS model), while F^i_{jk} is the amplification factor F_i associated with the j-th accelerogram and the k-th P3D model.

It should be remarked that the suitability of 1D modelling in Cavezzo, mostly characterized by a stack of homogeneous flat and parallel layers with a negligible slope of the bedrock roof (around 5% in its steepest part), was confirmed by a 2D ground response analysis performed with QUAD4M (Hudson et al., 1994). In fact, the 2D analyses, which were performed with reference to a 110 m – long section crossing Cavezzo along the NS direction (i.e. the one with the largest variability in the sloping of the bedrock roof), allowed to obtain amplification factors similar to those obtained by 1D analyses.

2.5.3 Results

Figure 2-18 shows the map of the amplification factors computed for the municipality of Cavezzo for the 475 years-return period. The amplification factors (F_i) are showed in terms of peak ground acceleration FPGA expressed as PGA/PGA0 ratio (top-left) and Housner intensity ratio expressed as SI/SI0 and computed for 3 different oscillator period ranges: FH0.1-0.5s (top right), FH0.5s-1.0s (bottom left), FH0.5-1.5 (bottom right). The terms PGA0 and SI0 are respectively the peak ground acceleration and Housner intensity related to the reference input motion. The largest amplification factors are expected in the northern part of the municipality, in the proximity of the culmination of the Mirandola anticline (Figure 2-8), which is clearly visible in the four maps. Moreover, it is interesting to note that these maps clearly reflects even the homogeneous zones defined based on lithological and genetic depositional environment. The boundaries of these areas can be seen in trend with the values of the amplification factors. For instance, this fact is clearly visible in the high period range, namely FH0.5s-1.0s (bottom left) and FH0.5-1.5 (bottom right); lower values were obtained in homogeneous zones named 3 and 4 showed in Figure 2-6.

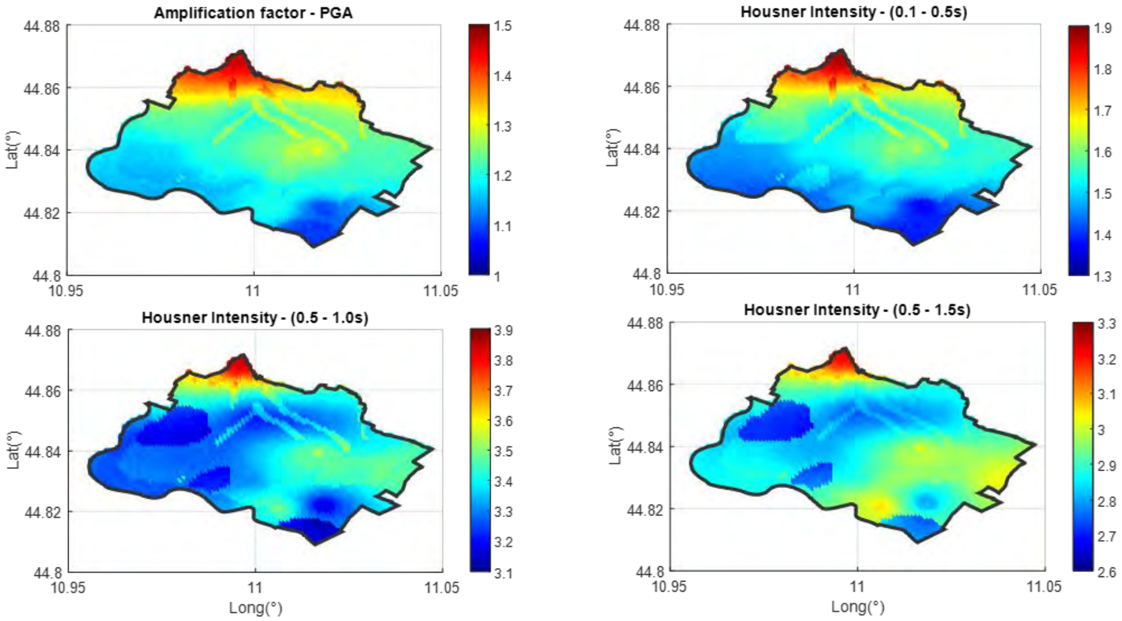

Figure 2-18: Map of amplification factors computed for Cavezzo considering the 475-years return period. Top left: PGA; Top right: Housner intensity ratio (0.1s≤T≤0.5s); Bottom left: Housner intensity ratio (0.5s≤T≤1.0s); Bottom right: Housner intensity ratio (0.5s≤T≤1.5s).

2.6 Microzoning Cavezzo territory for the liquefaction risk

The work described in the previous Sections was in a way preliminary to that needed to perform the microzonation of Cavezzo for earthquake-induced liquefaction risk. Several methods are available from the literature to assess the susceptibility of soils to liquefaction and their selection depends on the purpose of the study (e.g. research projects, land planning, important site-specific projects, etc.). For instance, laboratory testing as the primary means to assess liquefaction susceptibility is rarely used in ordinary practice since it requires high quality undisturbed samples of granular materials to capture the influence of fabric on cyclic soil response. Undisturbed sampling of coarse-grained soils requires the adoption of expensive in situ ground freezing techniques or emerging methods such as the gel-push technology.

The in-situ tests typically used to assess the resistance of soil deposits to earthquake-induced liquefaction include the standard penetration (SPT) and the cone penetration testing (CPT). Shear wave velocity measurement is also used as a method to estimate the soil resistance to liquefaction despite the limitations of this approach thoroughly discussed in the NASEM Report (2016). Assessment of liquefaction risk requires a comparison of the anticipated level of loading imposed on a soil deposit by the ground shaking with the inherent resistance of soil to liquefaction. Since both loading and resistance vary with depth, the liquefaction risk must be evaluated at different depths within the soil profile of interest. A stress-based approach for evaluating whether liquefaction may be triggered at a site was originally proposed in 1971 by Whitman and Seed & Idriss. While the details of the methodology, often referred to as the "*simplified procedure*" (or the "*Seed-Idriss simplified method*"), have been the subject of continuous updates since 1971, its basic framework is unchanged and it remains the most commonly used approach to evaluate liquefaction triggering in everyday practice (NASEM, 2016). Furthermore, current guidelines for microzonation of liquefaction risk including the Italian recommendations (ICMS-LIQ, 2018) suggest the use of the Seed-Idriss simplified method to identify liquefaction-prone sites. In this method, the factor of safety (F_S) against liquefaction triggering is defined at each depth as the ratio between the cyclic stress ratio CSR, which is a measure of the intensity of cyclic shear stress induced in the soil by the earthquake, and the cyclic resistance ratio CRR, which is a measure of soil resistance (i.e., the cyclic stress ratio expected to cause liquefaction).

The cyclic stress approach defines the earthquake loading in terms of cyclic shear stress amplitude, which can be obtained from site-specific ground response analyses or by a correlation with the PGA. The peak ground acceleration is usually tied to a prescribed hazard level, as represented by the mean annual rate of exceedance or the return period. The duration effects of ground motion are accounted for by specifying the earthquake magnitude, which is used to adjust the cyclic shear stress amplitude via a *magnitude scaling factor*. Since the severity of ground shaking is typically defined by means of probabilistic seismic hazard analyses (PSHA), a specific level of ground motion intensity comprises contributions from different earthquake magnitudes and epicentral distances (earthquake scenarios). Therefore, an accurate assessment of liquefaction risk would require consideration of a set of magnitudes compatible with the results of a PSHA. Details on the definition of moment magnitude at Cavezzo are illustrated in Lai et al. (2018).

In the simplified procedure, soil resistance to liquefaction at a certain depth is estimated using empirical or semi-empirical correlations linking CRR to penetration resistance from CPT or SPT or via direct measurement of in-situ shear wave velocity V_S although the NZGS (2016) report states that "*shear wave velocity liquefaction triggering procedures are still not considered to be as robust as CPT-based procedures*". If CPT data are available then liquefaction resistance is estimated using the using the *normalized Soil Behavior Type Index* I_C (Robertson et al., 2009). A value of I_C=2.6 is considered as a threshold for separating between liquefiable (sand-like) and non-liquefiable (clay-like) soils (NZGS, 2016).

The Seed-Idriss simplified procedure requires the calculation of the Factor of Safety F_S=CRR/CSR at various depths. The point-wise assessment of F_S at different depths is then combined into an overall scalar or vector parameter to yield the liquefaction risk in term of Liquefaction Potential Index, LPI as originally proposed by Iwasaki et al. (1978) or considering the modification introduced by Sonmez (2003) or in terms of the Liquefaction Severity Index, LSI, as introduced by Yilmaz (2004) or in terms of the Liquefaction Severity Number, LSN as proposed by Van Ballegooy et al. (2014). Empirical or semi-empirical approaches are also adopted for the estimation of liquefaction-induced settlements and lateral displacements which can also be expressed in terms of indices such as the LSN, the Lateral Displacement Index, LDI (Zhang et al., 2004) and the ground settlements (Zhang et al., 2002).

Parameters such as LPI, LSI or LSN can be used to construct microzonation maps for liquefaction risk (e.g. Cramer et al., 2017). To do so the results of calculations along a vertical soil profile is statistically averaged over neighbouring points. Interpolation can be performed by using any of the several numerical techniques currently available including geostatistical algorithms (Isaaks and Srivastava, 1989). Significant epistemic uncertainties are associated with all variants of the simplified Seed-Idriss approach to liquefaction triggering assessment (NASEM Report, 2016). The epistemic uncertainty can be taken into account using the *logic tree approach*.

2.6.1 Monte Carlo simulations

At Cavezzo, data from 444 CPT including 375 mechanical versions of the test (CPTm), 44 CPTU executed with the piezocone and 25 SCPT (seismic CPT) were used to assess the liquefaction risk. Three independent empirical CPT-based procedures, namely Robertson (2009), Boulanger & Idriss (2016) and Moss et al. (2006) were chosen based on the most recent recommendations from the literature (e.g. Cubrinovski et al., 2017). A logic tree approach (Figure 2-19) was then implemented to take into account the epistemic uncertainty. A larger weight was attributed to the branch associated with the CPT-based method by Boulanger and Idriss (2016) as suggested by the literature (e.g. NZGS, 2016). Finally, data from CPTm were corrected using the formulas proposed by Facciorusso et al. (2017). The logic tree shown in Figure 2-19 is characterized by two main branches. The second branch refer to empirical correlations based on critical state theory a relatively recent innovative approach. In particular, two models were considered: the one by Jefferies and Been (2015) and the correlation by Giretti and Fioravante (2017). A larger weight was attributed to the latter since this model was developed on data from soil deposits that liquefied during the 2012 Emilia sequence.

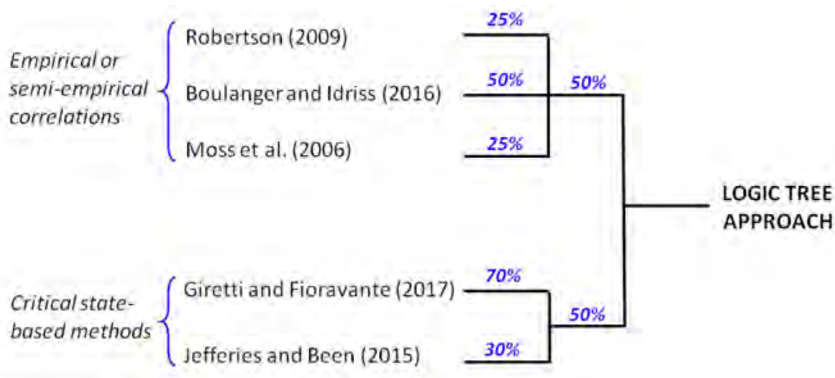

Figure 2-19: Logic tree implemented in this study to assess the liquefaction risk in the territory of Cavezzo (microzonation) taking into account the epistemic uncertainty.

The logic tree presented in the previous section is used as the engine of a novel algorithm purposely developed in this study to carry out Monte Carlo simulations for a probabilistic assessment of liquefaction risk in a territory of relatively large size. The uncertainty of soil parameters and that of the seismic input is considered by treating them as random variables whose individual realizations feed a deterministic model that is repeatedly used to assess the liquefaction risk until the results are stabilized.

The following parameters affecting the liquefaction risk at Cavezzo are considered as random variables in the Monte Carlo simulations:

- Water table depth: a normal distribution was assumed. The mean value was extracted from the map obtained by interpolating the measured data from the monitoring survey carried out during the spring season. This corresponds to the most conservative scenario for the liquefaction risk assessment. The coefficient of variation was assumed equal to 20%;

- The threshold value of the Soil Behavior Type Index I_C separating clay-like (i.e. non-liquefiable soil) from sand-like (i.e. liquefiable soil) response: a discrete distribution of the parameter I_C was assumed. In each realization of input parameters, the threshold value for I_C is uniformly sampled from the values of the vector v = [2.4 2.5 2.6 2.7]. These three values were defined based on the recommendations provided by Boulanger and Idriss (2016) and they have the same probability of being sampled.

- PGA value at free surface: a discrete distribution was assumed for PGA considering that the results obtained from ground response analyses at each return period were determined using as reference input motion 7 real accelerograms.

During each simulation, a random value is sampled for the each of the above variables. The analysis proceeds with those sampled parameters and the index of interest are calculated. At the end of the Monte Carlo analysis, the results for each simulation are aggregated and a mean value is extrapolated.

Monte Carlo simulation was applied as well in order to carry on liquefaction potential analysis starting from V_s data. Soil resistance to liquefaction at a certain depth was thus estimated via direct measurement of in-situ shear wave velocity V_S, using the approach proposed by Kayen et al. (2013; 2014).

2.6.2 Fully nonlinear coupled effective stress analyses at a few sites in Cavezzo

In this section, fully nonlinear coupled effective stress analyses will be presented for two verticals which showed the evidences of liquefaction during M6.1 20 May 2012 Emilia event. In the relevant analyses, PM4 sand model v3.0 (Boulanger and Ziotopolou, 2015) implemented in finite difference solver FLAC 7.0 (Itasca, 2011) is utilized. Target return period is selected as 475 years.

This section is organized to show explicitly the procedure for Site 1 (Uccivello School located at southwestern part of Cavezzo) from model calibration to presentation and discussion the results of nonlinear dynamic time history analyses. For Site 2, on the other hand, only the key results and discussions will be presented for the sake of brevity.

2.6.2.1 Calibration of the constitutive model

PM4sand model is an upgraded version of the boundary surface plasticity model proposed by Dafalias and Manzari (2004). The constitutive model has twenty-one parameters among which three are categorized as primary and the rest are categorized as secondary parameters. As shown in Table 2-4, ten parameters carrying out physical meaning are calibrated based on the available data, whereas remaining eleven are remained as default. Readers are referred to Boulanger and Ziotopolou (2015) for complete definition of the constitutive model parameters.

Table 2-4: Definition of parameters whose values are modified according to the mentioned sources and their values assigned in Site 1

Parameter	Definition	Parameter tye	Estimated from/as:	Value (Site 1)
D_r	Relative density	State-related parameter	CPT-based formulation (Kulhawy and Mayne, 1990)	0.40
G_o	Shear modulus coefficient	Primary	Available seismostratigraphic velocity-thickness models	519.86
h_{po}	Contraction rate parameter	Primary	CRR-N (Cyclic resistance ratio versus effective number of cycles) obtained after CPT-based interpretation (see Figure 2-22)	0.18
p_a	Atmospheric pressure	Primary	-	98.1 kPa
e_{max}	Maximum void ratio	Secondary	Defined according to the relation proposed by Giretti and Fioravante (2017) on San Carlo Sand (SCS)	1.00
e_{min}	Minimum void ratio	Secondary	See e_{max}	0.58
ϕ'_{cv}	Effective internal friction angle at critical state	Secondary	See e_{max}	34.5°
ν_o	Poisson's ratio of the skeleton	Secondary	$=K_o/(1+K_o)$ with $K_o=1-\sin(\phi'_{cv})$ according to Jaky (1948)	0.302
Q	Bolton's Q parameter	Secondary	From critical state line (CSL) defined in Giretti and Fioravante (2017) on SCS. See e_{max}	6.5
R	Bolton's R parameter	Secondary	See *Q*	0.5

Parameter	Definition	Parameter tye	Estimated from/as:	Value (Site 1)
n	Porosity	Continuum parameter	Obtained from emax, emin, and Dr	0.454
Kwater	Bulk modulus of pore water	Continuum parameter	-	2.2e6 kPa

According to Giretti and Fioravante (2017), index parameters (emin and emax) for San Carlo Sand (SCS) are 1.00 and 0.58, respectively. Internal effective friction angle at critical state is assigned as 34.5 degrees and Bolton's Q and R parameters are calibrated based on the critical state line (CSL) presented in Equation (2.2) in terms of in terms of void ratio (e_{cr}) at isotopic confinement pressure (p'_0).

$$e_{cr} = 0.99 - 0.12(p'_0/98.1)^{0.59} \tag{2.2}$$

In Figure 2-20, CSL for SCS is approximated sufficiently well by imposing Q=6.5 and R=0.5, which seem a little off the expected values of Q=10 and R=1 in Bolton (1986). Yet, the reproduced curve seems to model the initial states in a relatively accurate manner in the range of confinement pressures between 0 to 200 kPa.

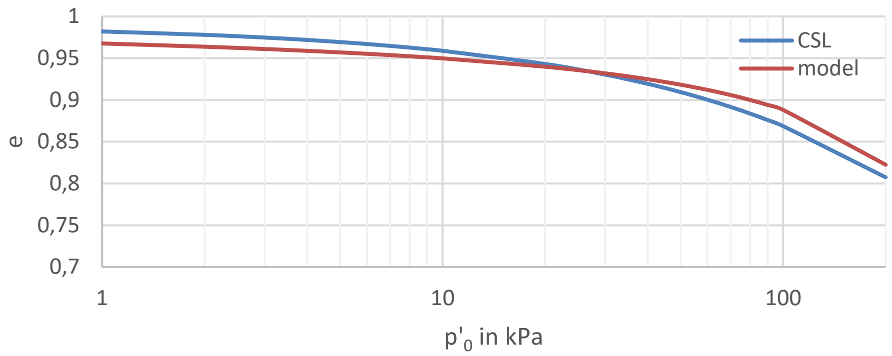

Figure 2-20: Modelled and measured CSL for SCS. CSL represents the measurements presented in Giretti and Fioravante, 2016) computed according to Equation (2.2).

As presented in Equation (2.3), shear modulus coefficient (G_o) is assigned for each sandy layer according to its state of mean effective stress (p'_{ref}) in 2D plane by respecting the measured shear wave velocities at mid-depth.

$$G_o = \frac{\rho V_S^2}{98.1\left(p'_{ref}/98.1\right)^{1/2}} \tag{2.3}$$

Where; ρ is the total unit density (t/m^3), V_S (m/s) is the shear wave velocity according to the seismo-stratigraphic model, p'_{ref} (kPa) is the mean effective stress (in 2D stress state) at mid-depth of the layer.

Having assigned all the relevant parameters presented in Table 2-4 apart from Dr and hpo, the steps below are followed to conclude the calibration procedure.

This project has received funding from the European Union's Horizon 2020 research and innovation programme under grant agreement No. 700748

1. For each vertical, first the idealization of soil profiles is carried out to identify potentially liquefiable sand-like layers from more stable clay-like layers through the soil behaviour type index (I_c) proposed by Robertson (2009). Once the layer identification is completed, initial states (mean effective confining stress - *p'* - and relative density -D_r-) at mid level of the layers is computed. All in all, all the sandy layers showed around 40% relative density according to Kulhawy and Mayne (1990). See Figure 2-21 for characterization of Site 1.

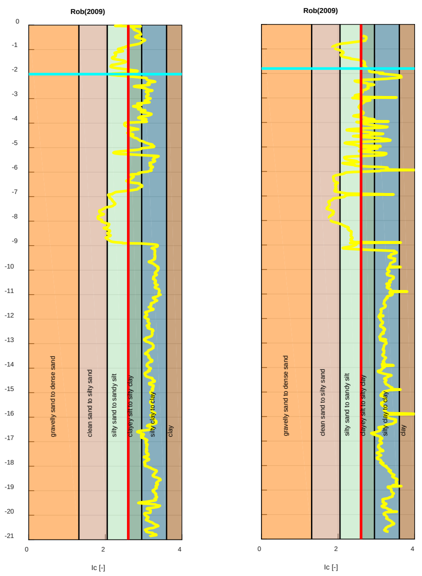

INGV			OGS		
Depth (m)			Depth (m)		
From	To	Vs (m/s)	From	To	Vs (m/s)
0	1.75	145*	0	1.75	145*
1.75	3.25	145*	1.75	3.25	145*
3.25	6.5	145*	3.25	6.5	145*
6.5	9	145*	6.5	9	145*
9	13	208	9	13	157
13	15.5	208	13	17.25	157
15.5	17.25	216	17.25	24.75	207
17.25	34.5	216	24.75	39.5	254
34.5	39.5	308	39.5	54.75	302
39.5	53.25	308	54.75	82.25	319
53.25	73.25	368	82.25	141.25	399
73.25	99.25	368	141.25	197.75	482
99.25	206.75	475	197.75	198.75	750
206.75	207.75	800			

Figure 2-21: SBT-n characterization of CPT profiles according to Robertson (2009) [left: U998, middle: SU909] and idealized depth velocity structures used in the coupled numerical analyses for Site 1. Note that potentially liquefiable layer is highlighted with grey color. Shear wave velocities indicated with (*) are replaced from the recordings of SCPTu of SU909.

2. Following the determination of the initial state, cyclic resistance ratio (*CRR*) versus effective uniform cycle (*N*) relation is obtained from the flowchart presented in Figure 2-22. It is underlined that cycle to obtain the final curve is repeated for five times considering all the methods presented in the logic tree presented in Figure 2-19.

This project has received funding from the European Union's Horizon 2020 research and innovation programme under grant agreement No. 700748

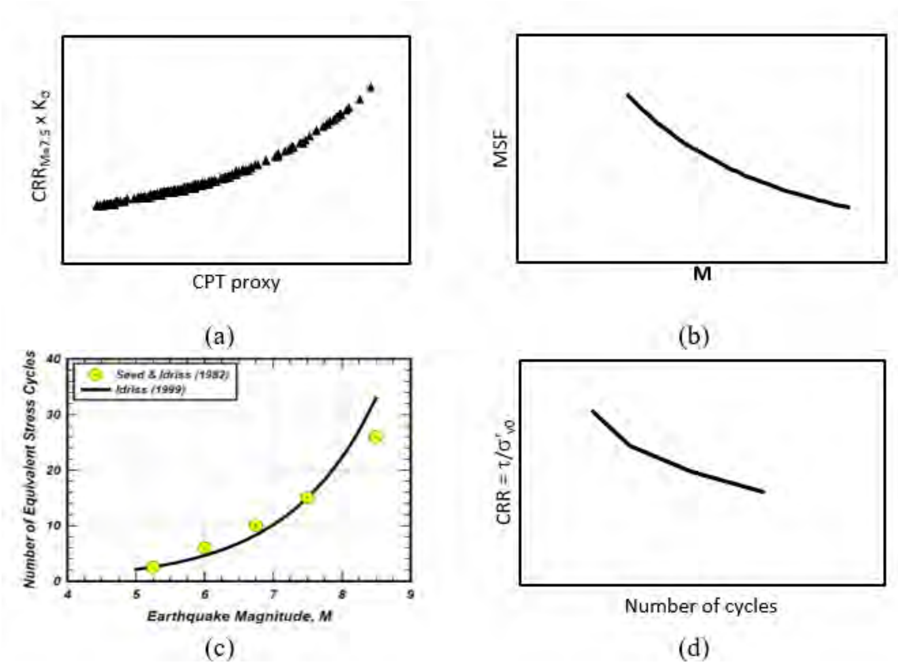

Figure 2-22: Estimation of CRR-number of equivalent cycles according to CPT-based interpretation. (a) obtaining CRRM7.5,σ'vo value corresponding to CPT proxy (a single representative value for entire layer), (b) applying the magnitude – magnitude scaling factor (MSF) relation to multiply the resistance ratio computed at step a and obtain CRRM,σ'vo, (c) converting magnitudes to effective uniform cycles, (d) plotting CRRM,σ'vo computed in step (b) with respect to number of equivalent cycles calculated in step (c).

3. Weighted average of CRR-N relation is obtained by using the weighting coefficients provided in Figure 2-19.
4. Series of plane strain 2D single element tests subjected to various cyclic shear stress are carried out to match the target CRR-N relation through changing h_{po} parameter. For the onset of liquefaction, double amplitude 6% shear strain is used. In Figure 2-23, an example cyclic shear test conducted on the numerical model is presented.
5. Best h_{po} parameter is decided to provide the closest match of CRR for the cycle number from 4 to 6, to represent the closest range to the target magnitude (~6.0) at considered retun period of 475 years. In Figure 2-24, result of calibration for Site 1 is provided.

This project has received funding from the European Union's Horizon 2020 research and innovation programme under grant agreement No. 700748

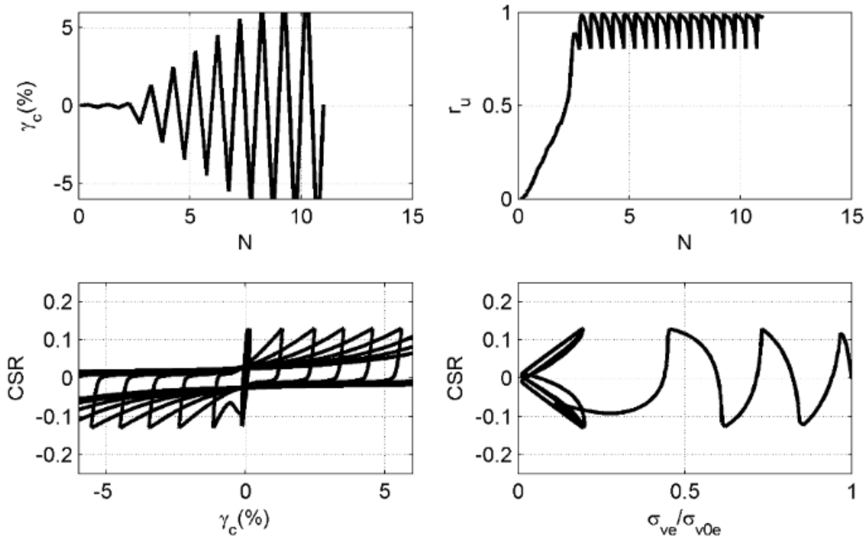

Figure 2-23: Sample single element test output to calibrate the parameter hpo. Top left: shear strain-uniform number of cycles. Top right: excess pore water pressure ratio (=Δu/σ'vo) – uniform number of cycles. Bottom left: Cyclic stress ratio (τ/σ'vo) – cyclic shear strain. Bottom right: stress path in effective stress domain. In this example, number of cycles to 6% DA shear strain is found as 5.17.

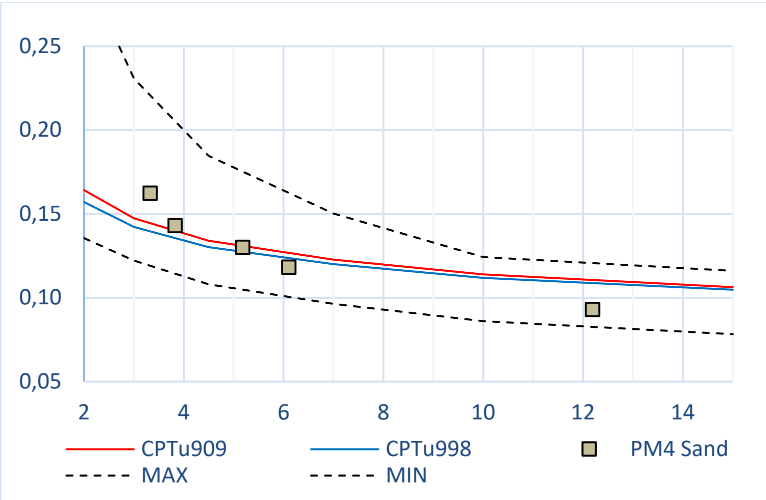

Figure 2-24: Target and calibrated CRR-N relations for Site 1. Continuous lines represent the weighted average lines according to the logic tree approach. Dashed lines show variablity. Markers show CRR-N relation at liquefaction onset corresponding to 6% double amplitude shear strain.

2.6.2.2 Details on numerical models

Finite difference models are created as soil column models by respecting the steps below:

- Step 1: Creating the vertical as a soil column and defining all the materials as elastic. Defining the geostatic pore water pressure, fixing saturation, pore water pressures as well as mechanical fixities (horizontal at sides, vertical at bottom)
- Step 2: Pore water pressure fixities are removed and the model is further cycled to make sure that stress histories do not change.
- Step 3: The constitutive model of the liquefiable zone is updated to elasto-plastic, BCs are removed instead equal degree of freedom (attach command in FLAC) are provided to lateral boundaries. Model is cycled to detect any kind of perturbation.
- Step 4: The time stepping scheme is updated to be real dynamic one, such that features of Rayleigh damping (0.005 at 1Hz), hysteretic curves for non-liquefiable materials and PM4sand model for liquefiable layer are activated. The model is cycled to observe any kind of perturbations. The very base of the model is kept as linear viscoelastic, without any sort of hysteretic dissipative response.
- Step 5: PM4sand parameters are initialized (FirstCall=0). Absorbing (quiet) boundary conditions are added to model base, then the model is excited from the model base by making use of a shear stress time history ($\tau=\rho_{rock}*V_{srock}*vel_{free\text{-}field}$) computed by considering the rock outcrop ground motion under interest.
- Step 6: At the end of the shaking, post shake flag of PM4 sand is activated (post_shake=1), excess pore water pressure in the liquefiable layer is dissipated.

From Figure 2-25 to Figure 2-30, illustrative screenshots are presented corresponding to the end of each step under consideration.

This project has received funding from the European Union's Horizon 2020 research and innovation programme under grant agreement No. 700748

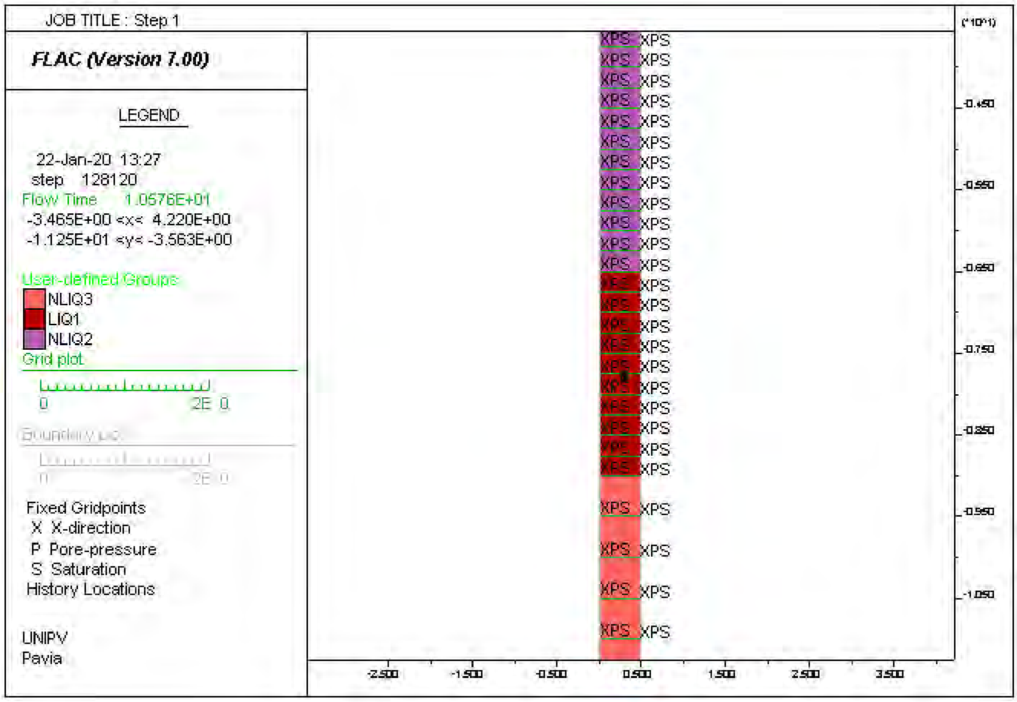

Figure 2-25: Initial set-up of boundary conditions. Geostatic water pressure distribution is introduced. Saturation and pore water pressure values are fixed. Mechanical boundaries are introduced on the outward normal directions of quadrilateral soil elements. Linear elastic properties are introduced for the soil material. Then, the model is cycled.

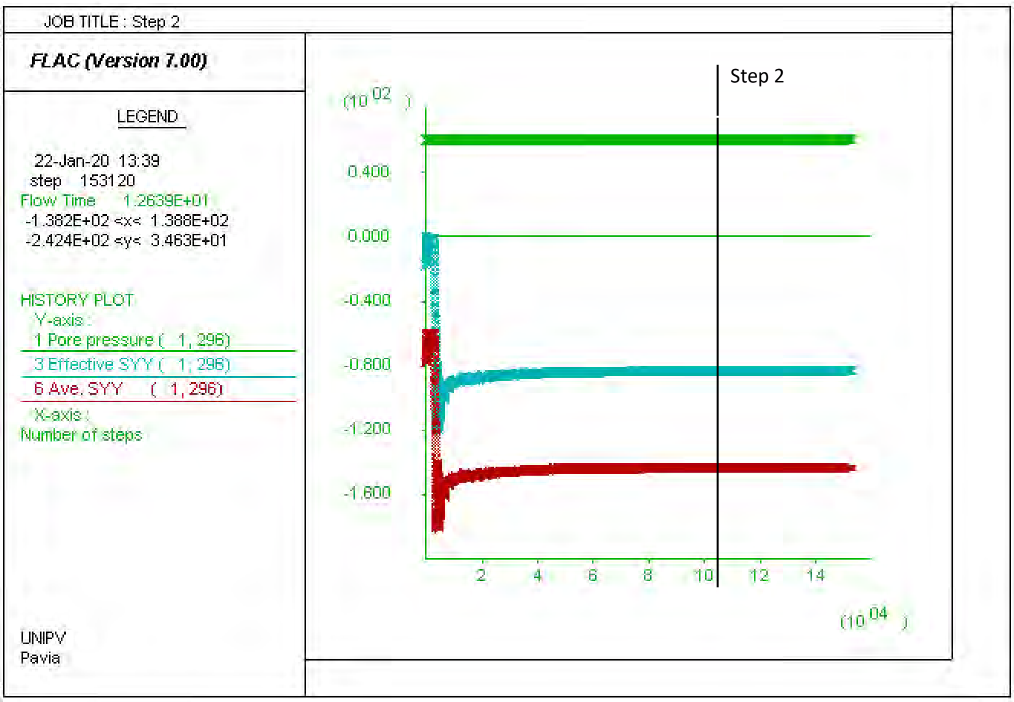

Figure 2-26: Second step. Pore water pressure fixity restraints are released. Model is cycled.

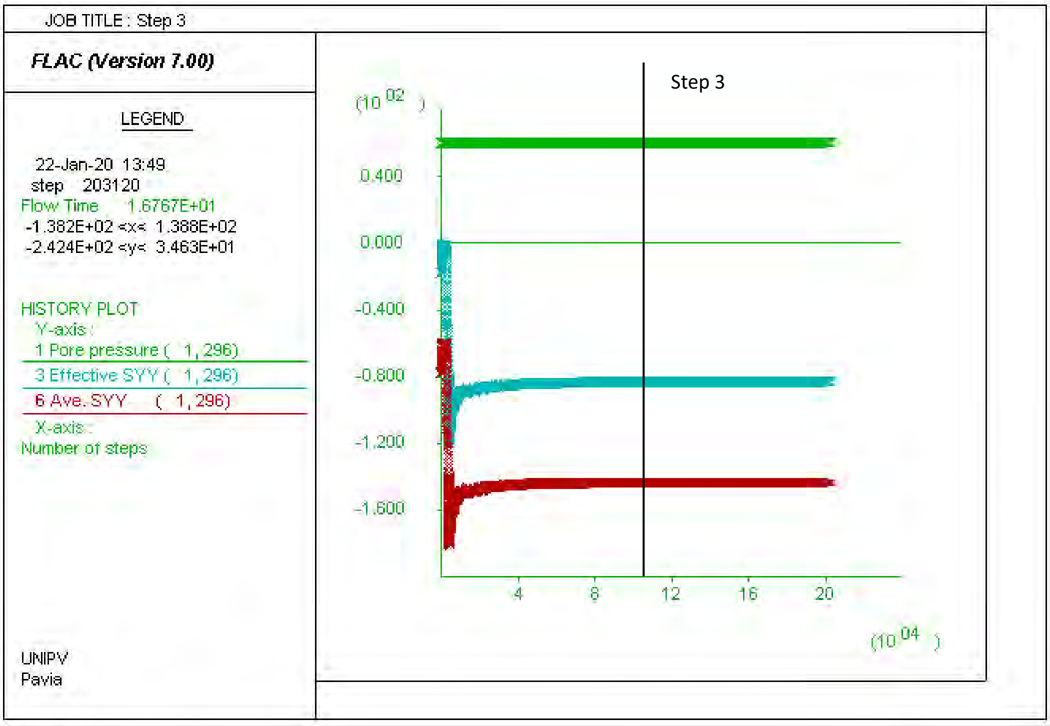

Figure 2-27: Third step. Constitutive model for the liquefiable zone (shown with LIQ1 in Figure 2-25) is updated to Mohr-Coulomb, lateral boundary conditions are removed. Model is cycled.

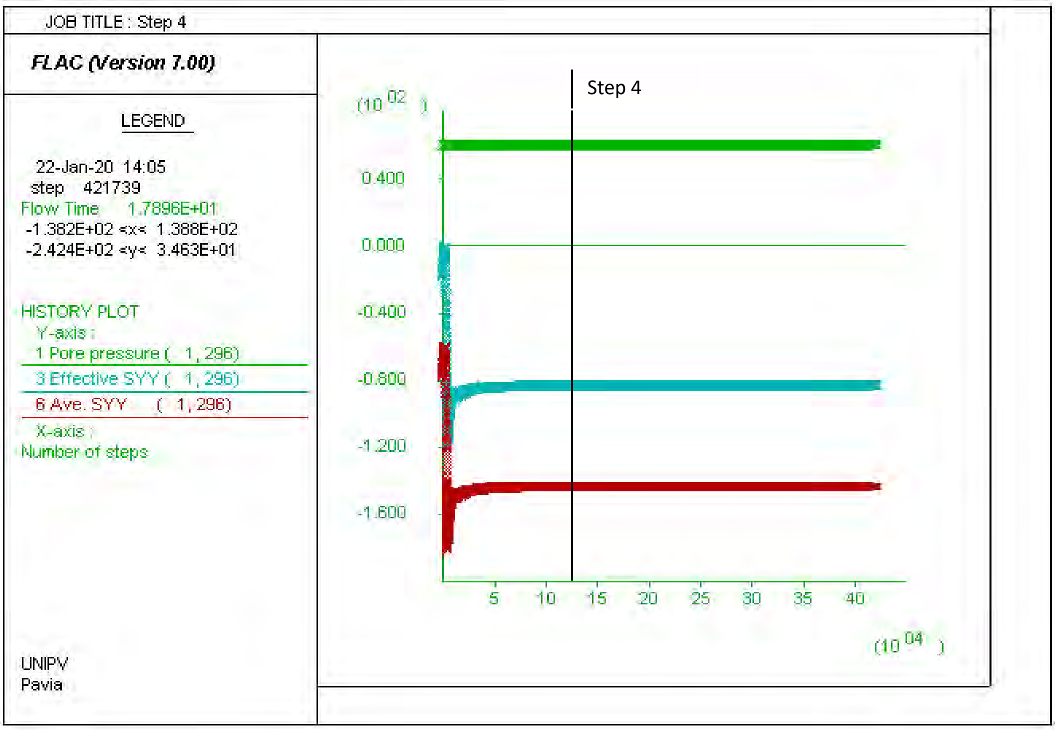

Figure 2-28: Fourth step. Rayleigh damping is introduced. Hysteretic curves are assigned for NONLIQ materials (apart from the bedrock at the base, which is linear visco-elastic) and PM4 sand is assigned for LIQ1. Model is cycled.

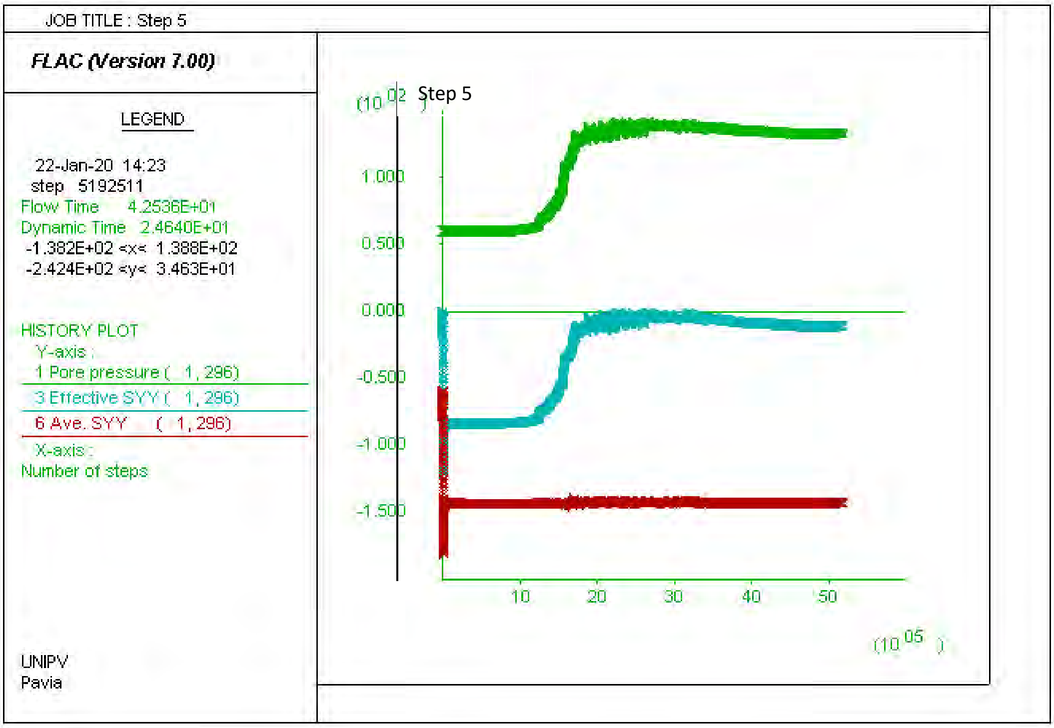

Figure 2-29: Fifth step. PM4 sand parameters are re-initialized. Dashpot is added to model bottom as an absorbing boundary. Rock-outcrop earthquake motion is introduced in terms of shear stress input. Model is cycled until the end of motion.

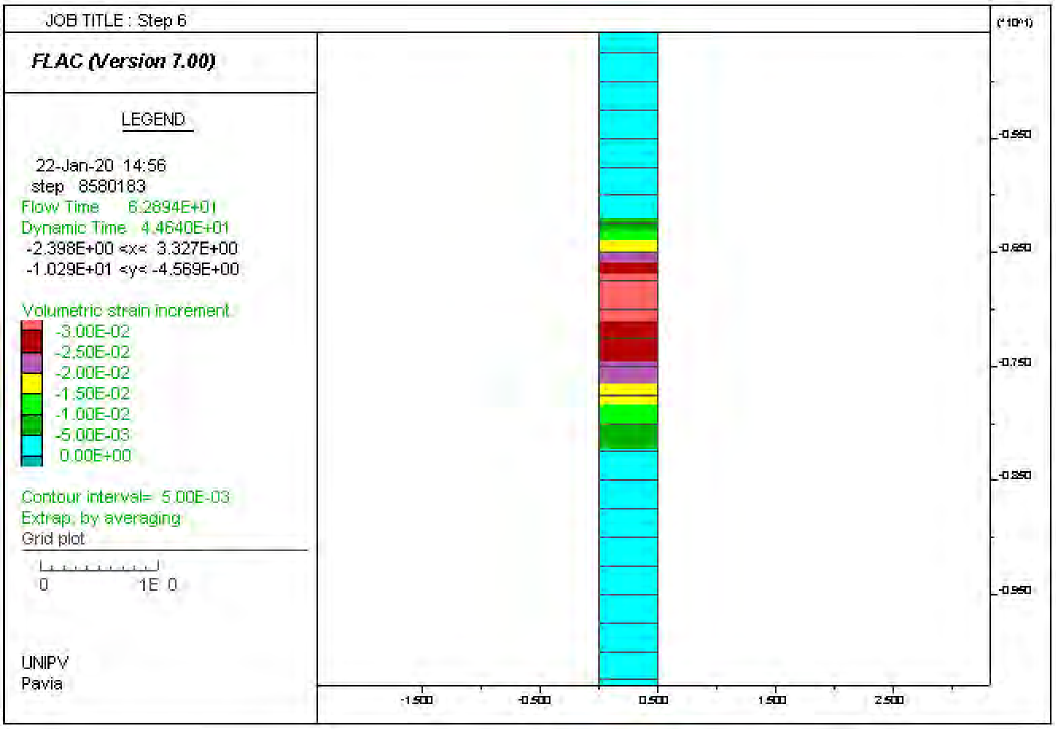

Figure 2-30: Sixth step. Post-shake flag of PM4 sand is activated. Model is cycled to make sure that excess pore water pressure generated during the ground motion is dissipated.

2.6.2.3 Comparison of results

Site 1

In Figure 2-31, factor of safety profiles computed through de-coupled approach is compared with the maximum excess pore water pressure ratio ($r_{u,max}=\Delta u_{max}/\sigma'_{vo}$) considering two distinct soil layering system of Site 1. While calculating the factor of safety profiles, cyclic stress ratio values are directly computed from site response analyses with equivalent linear constitutive model, whereas CRR is computed the corresponding weighted resistance ratio.

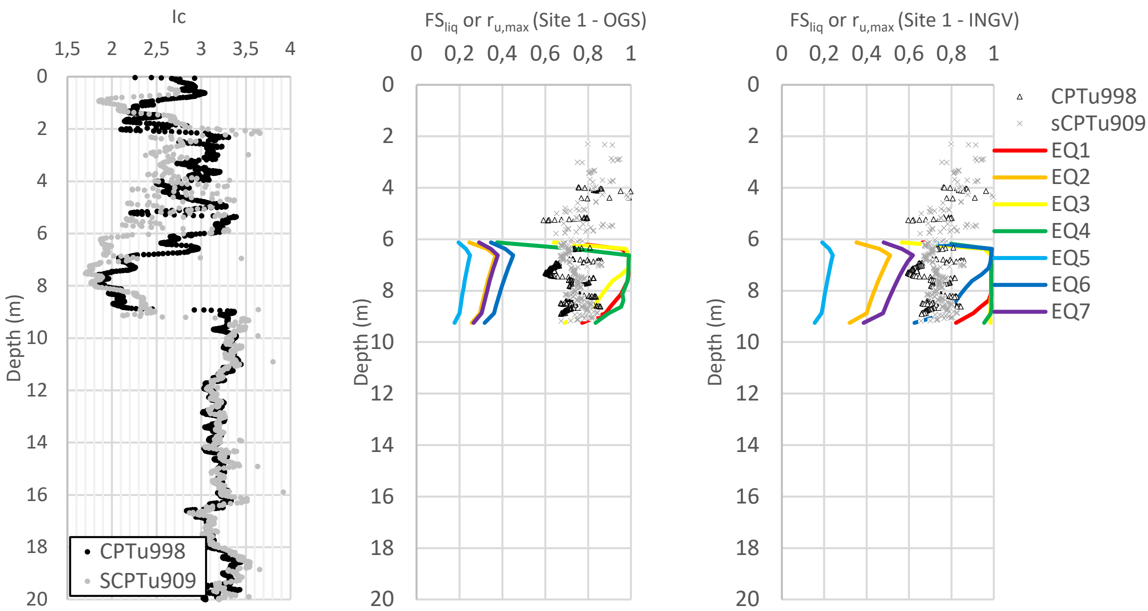

Figure 2-31: Left: Ic profile calculated from two CPT data. Middle: factor of safety against liquefaction triggering (markers) and maximum excess pore water pressure ratio, ru,max (continuous lines) considering OGS profile at Site 1. Right: Same of middle but with INGV profile.

It could be observed from Figure 2-31 that within the thick liquefiable zone (I_c < 2.6) between 6 to 9 meters, de-coupled methodologies end up with factor of safety values around 0.7 – 0.8 and coupled numerical analyses confirm the presence of liquefaction through high excess pore water ratios ($r_{u,max}$ > 0.9) in half of the simulations, which is found consistent with the relatively high level of factor of safety values.

It is interesting to note that numerical analyses considering the INGV profile predict the triggering of liquefaction with higher values of $r_{u,max}$ because of the presence of stronger impedance contrast between the liquefiable layer and stable layer lying beneath it.

Another interesting point is that in case of a strong one/two cycle exists but without many repetitions in terms of deformations (such as the case of EQ2 motion response), due to overestimation of cyclic strength ratio, corresponding generation of excess pore water pressure is underestimated.

In Table 2-5, post-liquefaction settlement values are compared with those predicted by Zhang et al. (2002)-Zea02- based on factor of safety against liquefaction triggering. It is noted that relatively good agreement is found at the upper portion of the stratum (i.e. 6.5 to 7.0-8.0 meters), whereas the comparison gets worse at deeper portions where the maximum excess pore water pressure ratio gets smaller than unity.

Table 2-5: Post-liquefaction volumetric strains in liquefiable layer in Site 1.

	Depth (m)	**EQ1**	**EQ2**	**EQ3**	**EQ4**	**EQ5**	**EQ6**	**EQ7**	**Zea02**
INGV	6.5-7	2.7 %		2.6 %	2.7 %		3.1 %		3.8 %
	7-8	2.5 %		2.0 %	2.1 %		0.7 %		3.5 %
	8-9	0.8 %		1.2 %	1.1 %		0.0 %		4.0 %
OGS	6.5-7	3.3 %		3.4 %	3.1 %				4.0 %
	7-8	2.2 %		0.8 %	2.0 %				3.5 %
	8-9	0.3 %		0.1 %	0.7 %				4.0 %

Site 2

In Table 2-6, conditions of liquefaction triggering are compared with the factor of safety against liquefaction triggering for three different zones under consideration. It could be observed that for the upper 1m layer, almost all simulations predict the liquefaction triggering. On the other hand, for the deeper zone, the sandy matrix is not expected to liquefy, yet the level of excess pore water pressure generation is found to be too low. This artefact is thought to be stemming from the overestimation of CRR at fewer number of cycles, as it had previously been discussed.

Table 2-6: Synthesis of maximum excess pore water pressure ratios and factor of safety against liquefaction triggering at Site2.

		Maximum excess pore water pressure ratio							**FS_{liq}**
	Depth (m)	**EQ1**	**EQ2**	**EQ3**	**EQ4**	**EQ5**	**EQ6**	**EQ7**	**Simplified**
INGV	4-5	0.99	0.30	0.98	0.98	0.23	0.98	0.48	0.7 – 1.0
	20-23.8	0.26	0.24	0.27	0.34	0.17	0.22	0.16	0.9 – 1.2
	23.8-25	0.22	0.20	0.23	0.29	0.15	0.19	0.15	0.9 – 1.2
OGS	4-5	0.99	0.54	0.98	0.98	0.29	0.98	0.98	0.7 - 0.9

	20-23.8	0.22	0.19	0.22	0.31	0.15	0.17	0.12	1.0 – 1.2
	23.8-25	0.19	0.18	0.19	0.27	0.13	0.14	0.11	1.0 – 1.2

In Table 2-7, volumetric strains are computed through numerical means are compared with the ones estimated through factor of safety-based simplified expressions of Zhang et al. (2002). Same order of magnitude in shear strains are noted (1 to 2), however with lower results obtained by numerical means.

Table 2-7: Synthesis of volumetric strains at Site 2.

		Volumetric strain							
	Depth (m)	**EQ1**	**EQ2**	**EQ3**	**EQ4**	**EQ5**	**EQ6**	**EQ7**	**Zea02**
INGV	4-5	2.8 %		2.8 %	2.6 %		1.1 %		3.8 %
OGS	4-5	2.0 %		2.0 %	1.9 %		1.9 %	1.3 %	3.1 %

2.6.3 Liquefaction microzonation results

The maps of liquefaction risk for the Municipality of Cavezzo with reference to the return period of 475 years are shown in Figure 2-32. The left image (Figure 2-32a) illustrates the mean values of LPI (according to the procedure proposed by Sonmez, 2003) obtained from the logic tree of Figure 2-19 whereas the right image (Figure 2-32b) shows the mean LPI obtained from Monte Carlo simulations. Figure 2-33 shows the results in terms of LSN (Figure 2-33a) and LSI (Figure 2-33b), whilst Figure 2-34 show the results in terms of ground settlements (Figure 2-34a) and in terms of LDI (Figure 2-34b). The reults for the return periods have been computed also with reference to 975 and 2475 years with the Monte Carlo simulations, although a validation of these results could not be carried on, because there are no data regarding possible liquefaction manifestations linked to the two return periods. In any case, the results appear consistent with the higher ground motion intensity.

1,000 simulations were needed at each node of the 3,052 nodes grid to obtain stable results. At each node, the LPI parameter was computed using the logic tree of Figure 7 then this parameter was spatially interpolated. A comparison of Figure 8a and Figure 8b suggests that although the results obtained with Monte Carlo simulations are less conservative, yet they seem to better capture the liquefaction manifestations occurred in the 2012 Emilia sequence. For what concerns ground settlements and lateral displacements, the values are low except for the areas affected by the liquefaction manifestations of 2012.

Figure 2-35 shows the results in terms of LPI (Figure 2-35a) and LSI (Figure 2-35b) calculated via the V_s-based approach, applying the same Monte Carlo simulation.

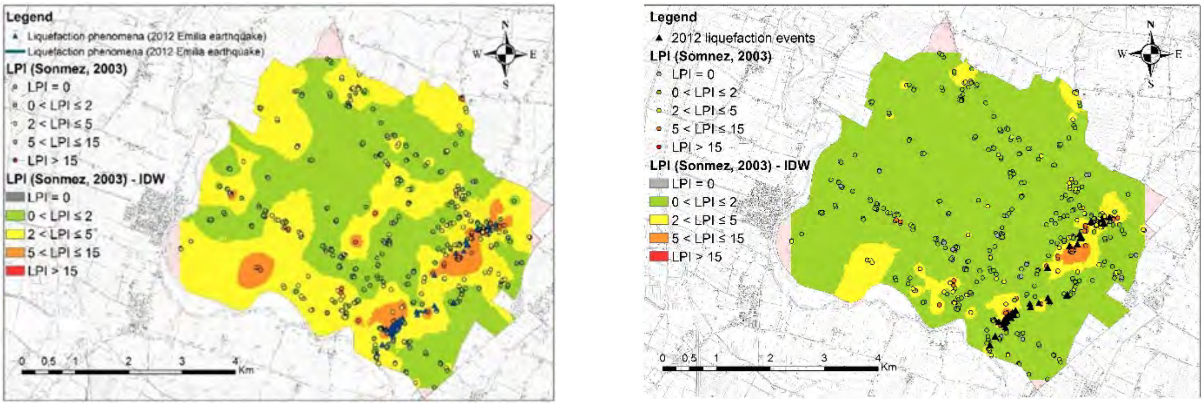

(a) (b)

Figure 2-32: Map of the liquefaction risk at the Municipality of Cavezzo with reference to the return period of 475 years: (a) spatial interpolation of LPI (defined according to Sonmez, 2003) computed adopting only the logic tree in Figure 2-19 and (b) using Monte Carlo simulations. The manifestations of soil liquefaction occurred in 2012 sequence are also superimposed (in blue color).

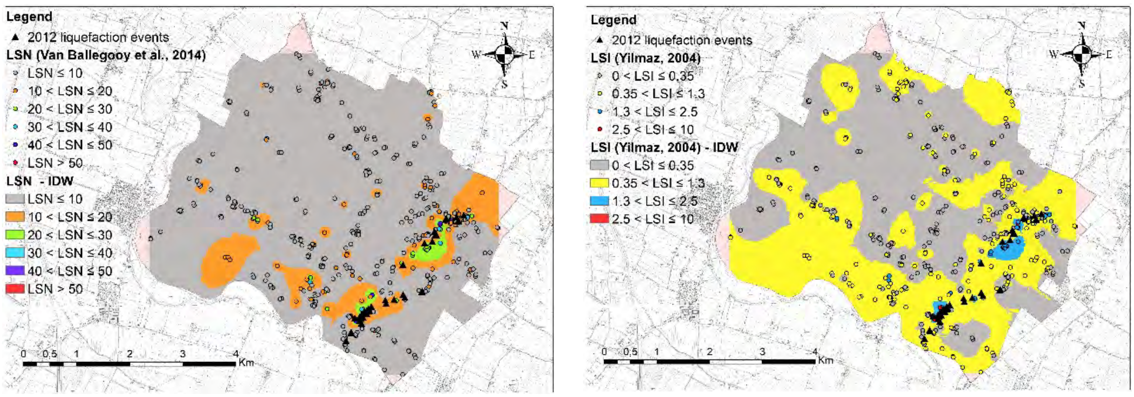

(a) (b)

Figure 2-33: Map of the liquefaction risk at the Municipality of Cavezzo with reference to the return period of 475 years: (a) spatial interpolation of LSN (defined according to Van Ballegooy, 2014) and (b) spatial interpolation of LSI (defined according to Yilmaz, 2004) both calculated using Monte Carlo simulations. The manifestations of soil liquefaction occurred in 2012 sequence are also superimposed (in blue color).

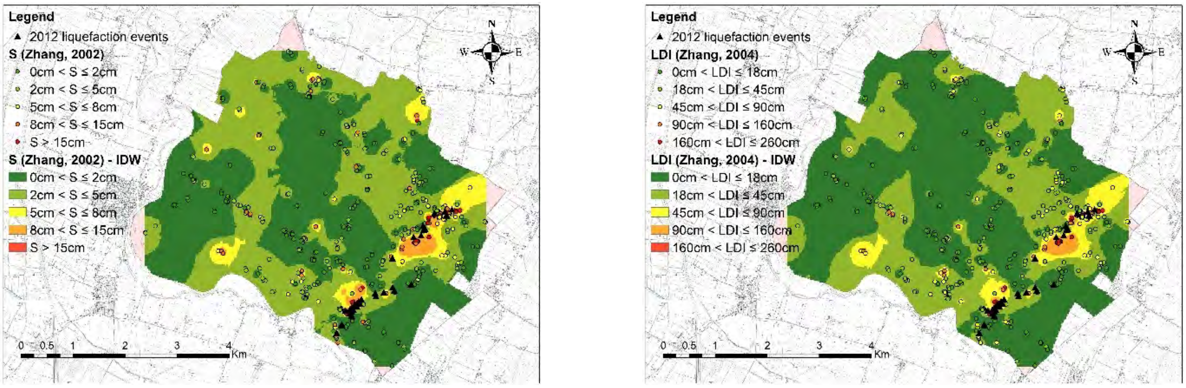

(a) (b)

Figure 2-34: Map of the liquefaction risk at the Municipality of Cavezzo with reference to the return period of 475 years: (a) spatial interpolation of CV (defined according to Zhang, 2002) and (b) spatial interpolation of LDI (defined according to Zhang, 2004), both computed using Monte Carlo simulations. The manifestations of soil liquefaction occurred in 2012 sequence are also superimposed (in blue color).

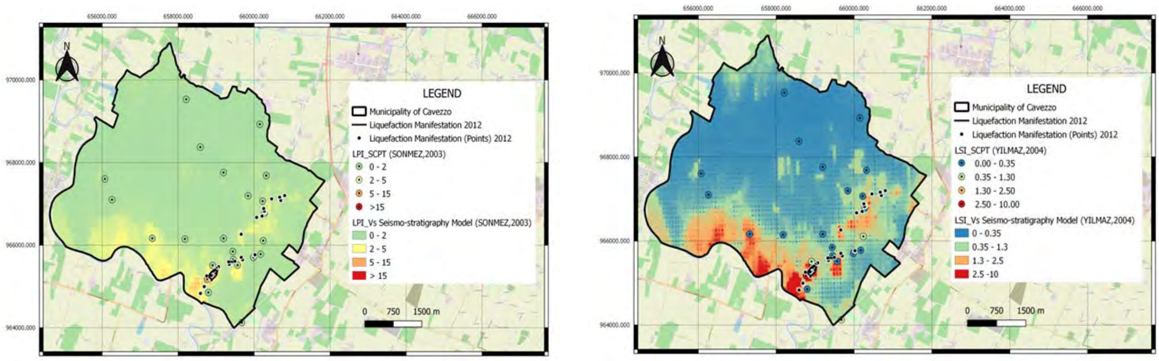

(a) (b)

Figure 2-35: Vs-based map of the liquefaction risk at the Municipality of Cavezzo with reference to the return period of 475 years: (a) spatial interpolation of LPI (defined according to Sonmez, 2003) and (b) spatial interpolation of LSI (defined according to Iwasaki, 1978) using Monte Carlo simulations. The manifestations of soil liquefaction occurred in 2012 sequence are also superimposed (in blue color).

The stability of the Monte Carlo simulations was assessed monitoring the trend of the moving average LPI value of a random CPT borehole (Figure 2-36). It can be seen that the moving average stabilizes at around 500 simulations.

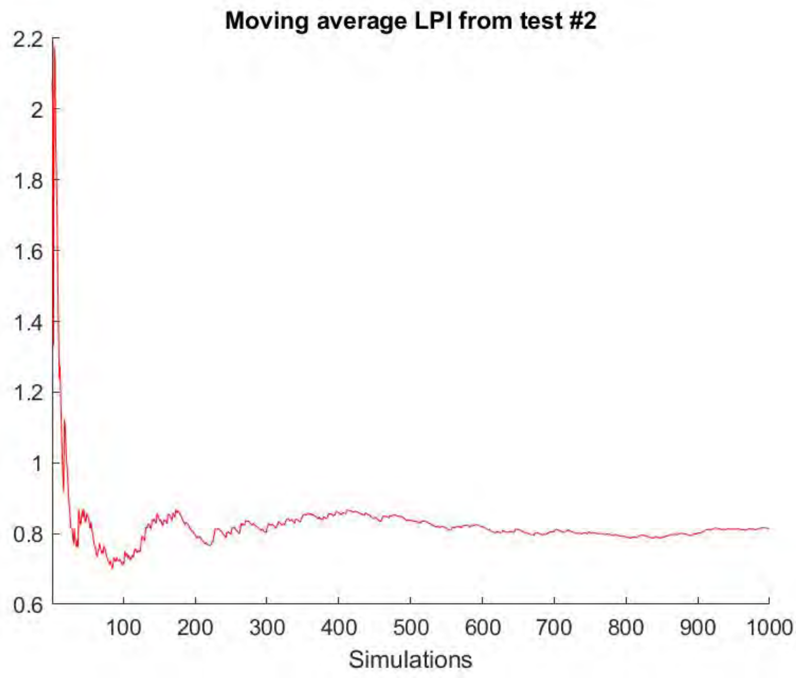

Figure 2-36: moving average LPI value relative to the CPT test data number 2.

2.7 Discussion and conclusions

From the results of ground amplification analyses it is readily apparent the correlation between the spatial variability of surface ground motion within Cavezzo territory and the characteristics of the adopted seismic-geotechnical and seismo-stratigraphic models. This clearly highlights the importance of the interplay and complementarity among different methodological approaches and spatial resolution scales characterizing a seismic microzonation study when tackled from a geological, geophysical, seismological and geotechnical prospective. The challenge to succeed in such a study consists in explicitly recognizing its intrinsic multi-disciplinary nature in pursuing the goal of defining a unified subsoil model that harmonizes coherently the different scales at which it can be visualized.

It must be remarked however that the procedure illustrated in this article, strictly applies to situations where the geological setting is such that a smooth spatial variation of the subsoil properties over the territory, is an acceptable approximation, at the points of the calculation grid. In case of evident 2D/3D response, the use of more advanced numerical models will be unavoidable. Nonetheless, such condition must be evaluated carefully on a case by case scenario, e.g. by a preliminary inspection of the H/V spectral ratio variability across the area, in order to justify the increased investment required for such advanced and computationally very expensive analysis. So far, very few attempts are available in the literature to objectively quantify the possibility of 2D/3D morphological effects, which makes this subject an open field of research.

It is also important to underline that ground response analyses were conducted using a linear equivalent soil constitutive model. This approach of adopting one-constituent, equivalent-linear viscoelastic rheology for the soil is inadequate to correctly reproducing the seismic response of geomaterials exhibiting strong nonlinearities in the hydro-mechanical behavior. An example is constituted by liquefiable soils, which require ground response analyses to be more correctly conducted using effective stress-based soil constitutive models.

Finally, an advancement of the current achievements in the seismic microzonation of Cavezzo territory could be represented by a complete randomization of all soil parameters and other input data for ground response analyses so to produce a fully stochastic set of amplification factors.

In this framework a development of a methodology for localized assessment of liquefaction potential (*microzonation*) was carried out. This paper illustrated a few outcomes from these activities which are still on-going. A sensitivity analysis to assess the impact of different liquefaction models (epistemic uncertainty) and assumptions on the results is underway also using LSI and LSN as indexes of liquefaction risk.

Calibration of fully coupled constitutive model requires attention on modelling the cyclic resistance ratio versus number of equivalent cycles relation as due to the presence of succesive transmissions and reflections in complex soil layer systems number of equivalent cycles may differ at different positions inside the soil profile. Yet, classical relation between magnitude and effective number of cycles proposed initially by Seed and Idriss is suggested to be followed. It is shown that once an advanced constitutive model is well calibrated, resulting predictions of liquefaction triggering and consequences in terms of volumetric strains may also be predicted in relatively good agreement with respect to the emprical methods, of course with a margin of uncertainty that is always present in earthquake geotechnics.

2.8 References

- Boccaletti, M., Bonini, M., Corti, G., Gasperini, P., Martelli, L., Piccardi, L., Severi, P. & Vannucci, G. 2004: Carta sismotettonica della Regione Emilia-Romagna, scala 1:250.000. Note illustrative. Regione Emilia-Romagna–SGSS, CNR-IGG. SELCA, Firenze.
- Bolton, M. D. (1986). Strength and dilatancy of sands. *Geotechnique* 36(1): 65-78.
- Boulanger, R.W., Ziotopolou, K. (2015). PM4SAND (version 3) a sand plasticity model for earthquake engineering applications. Center for Grotechnical Modeling. Department of Civil & Environmental Engineering College of Engineering, University of California at Davis. Report no: UCD/CGM-15/01.
- Boulanger, R.W., Idriss, I.M. 2016. CPT-based liquefaction triggering procedure. J. Geotech. Geoenviron. Eng., 142(2).
- Castaldini, D. 1989. Evoluzione della rete idrografica centropadana in epoca protostorica e storica. Atti Conv. Naz. Studi "Insediamenti e viabilità nell'alto ferrarese dall'Età Romana al Medioevo". Cento 8-9 May 1987 Acc. delle Sc. di Ferrara, 115-134, Ferrara.
- Corigliano, M., Lai, C.G., Rota, M., Strobbia, C.L. (2012). “ASCONA: automated selection of compatible natural accelerograms”. Earthquake Spectra, 28(3): 965-987.

- Cramer, C.H., Bauer, R.A., Chung, J.W., Rogers, J.D., Pierce, L., Voigt, V., Mitchell, B., Gaunt, D., Williams, R.A., Hoffman, D., Hempen, G.L., Steckel, P.J., Boyd, O.S., Watkins, C.M., Tucker, K., McCallister N.S. 2017. St. Louis Area Earthquake Hazards Mapping Project: Seismic and Liquefac-tion Hazard Maps. Seismological Research Letters, 88 (1).
- Cubrinovski, M., Stringer, M., Haycock, I. (2016). Experience with gel-push sampling in New Zealand. http://www.nzgs.org.
- Cubrinovski, M., Rhodes A., Ntritsos, N., Van Ballegooy, S. (2017). "System response of liquefiable deposits". Proceedings, 3rd International Conference on Performance-Based Design in Earthquake Geotechnical Engineering, PBD-III, Vancouver, Canada, July 16 - 19, 2017.
- Dafalias Y.F, Manzari M.T. (2004). Simple plasticity sand model accounting for fabric change effects. Journal of Engineering Mechanics, 130(6): 622-634.
- Facciorusso, J., Madiai, C., Vannucchi, G. 2017. Corrections to mechanical CPT results for use in liquefaction evaluation. Bull. Earthquake Eng., 15, 9, 3505–3528.
- Giretti, D., Fioravante, V. 2017. A correlation to evaluate cyclic resistance from CPT applied to a case history. Bull. Earthquake Eng., 15, 1965-1989.
- Haghshenas, E., Bard, P.-Y., Theodulidis, N. & SESAME WP04 Team, 2008. Empirical evaluation of microtremor H/V spectral ratio, Bull. Earthq. Eng., 6(1), 75–108.
- Hudson, M.B., Beikae, M., Idriss, I.M. (1994). "QUAD4M, a Computer Program to Evaluate the Seismic Response of Soil Structures Using Finite Element Procedures and Incorporating a Compliant Base Center for Geotechnical Modeling", Department of Civil and Environmental Engineering, University of California, Davis.
- ICMS-LIQ 2018. Microzonazione sismica. Linee guida per la gestione del territorio in aree interessate da liquefazioni (LQ). Versione 1.0. Commissione tecnica per la microzonazione sismica. Roma, 2017.
- Idriss, J., Sun, J.I. (1992). SHAKE91 - a computer program for conducting equivalent linear seismic response analyses of horizontally layered soil deposits. University of California, Davis, USA.
- Itasca Consulting Group (2011). Fast Lagrangian Analysis of Continua (FLAC), version 7.0. Computer code and documentation.
- Iwasaki, T., Tatsuoka, F., Tokida, K., Yasuda, S. 1978. A practical method for assessing soil liquefaction potential based on case studies at various sites in Japan. In Proceedings of the 2nd International Conference on Microzonation for Safer Construction. Amer. Society of Civil Eng., New York. 2, 885-896.
- Jefferies, M., Been, K. 2015. Soil liquefaction. A critical state approach, Taylor and Francis, London.
- Kayen, R., Moss, R.E.S., Thompson, E.M., Seed, R.B., Cetin, K.O., Der Kiureghian, A., Tanaka, Y. & Tokimatsu, K. 2013. Shear-Wave Velocity–Based Probabilistic and Deterministic Assessment of Seismic Soil Liquefaction Potential. Journal of Geotechnical and Geoenvironmental Engineering 139(3): 407-419.
- Kayen, R., Moss, R. E. S., Thompson, E. M., Seed, R. B., Cetin, K. O., Der Kiureghian, A., Tanaka, Y. and Tokimatsu, K. (2014). Closure to "Shear-Wave Velocity–Based Probabilistic and Deterministic Assessment of Seismic Soil Liquefaction Potential" by R. Kayen, R. E. S. Moss, E. M. Thompson, R. B. Seed, K. O. Cetin, A. Der Kiureghian, Y. Tanaka, and K. Tokimatsu." J. Geotech. Geoenviron. Eng., 140(4), 07014006.

- Kulhawy, F.H., Mayne P.W. (1990). Manual on estimating soil properties for foundation design. No. EPRI-EL-6800. Electric Power Research Inst., Palo Alto, CA (USA); Cornell Univ., Ithaca, NY (USA). Geotechnical Engineering Group.
- Lai, C.G., Meisina, C., Bozzoni, F., Conca, D., Famà, Özcebe, A.G., Zuccolo, E., Bonì, R., Poggi, V., Cosentini, R.M. (2019). Mapping the liquefaction hazard at different geographical scales. Proceedings 7th International Conference on Earthquake Geotechnical Engineering, 7ICEGE, Rome, Italy, 17-20 June, 2019.
- Martelli, L., Bonini, M., Calabrese, L., Corti, G., Ercolessi, G., Molinari, F. C., Piccardi, L., Pondrelli, S., Sani, F. & Severi, P. 2017. Carta sismotettonica della Regione Emilia-Romagna e aree limitrofe. Note illustrative. Regione Emilia-Romagna, Servizio geologico, sismico e dei suoli. D.R.E.AM. Italia.
- Meisina, C., Bonì, R., Bordoni, M., Lai, C.G., Bozzoni, F. et al. 2019. 3D Geological model reconstruction for liquefaction hazard assessment in the Po Plain. Proceedings 7th International Conference on Earthquake Geotechnical Engineering, 7ICEGE, Rome, Italy, 17-20 June, 2019
- Moss, R.E.S., Seed, R.B., Kayen, R.E. et al 2006. CPT-based probabilistic and deterministic assessment of in situ seismic soil liquefaction potential. J. Geotech. Geoenviron. Eng., 132:1032-1051.
- NASEM Report (2016). State of the Art and Practice in the Assessment of Earthquake-Induced Soil Liquefaction and Its Consequences. National Academies of Sciences, Engineering, and Medicine (NASEM).
- Nakamura, Y., 1989. A method for dynamic characteristics estimation of subsurface using microtremor on the ground surface, Quart. Records Railway Tech. Res. Inst., 30, 25–33.
- Nogoshi, M. & Igarashi, T., 1971. On the amplitude characteristics of microtremor, Part II, J. seism. Soc. Japan, 24, 26–40.
- NTC (2018). Norme tecniche per le costruzioni. Ministero delle Infrastrutture e dei Trasporti, Decreto Ministeriale del 17 gennaio 2018, Supplemento ordinario alla G.U. n. 8 del 20 febbraio 2018 (in Italian)
- PEER (2010a). Technical report for the PEER ground motion database web application-Beta Version-October 1, 2010. Pacific Earthquake Engineering Research Center (PEER).
- PEER (2010b). User's Manual for the PEER ground motion database web application-Beta Version-October 1, 2010. Pacific Earthquake Engineering Research Center (PEER).
- Pellegrini, M. & Zavatti, A. 1980. Il sistema acquifero sotterraneo tra i fiumi Enza, Panaro e Po: alimentazione delle falde e scambi tra falde, correlazioni idrochimiche". Quaderni IRSA, 51(1), Roma.
- Poggi, V. and Fäh, D., 2010. Estimating Rayleigh wave particle motion from three-component array analysis of ambient vibrations. Geophys. J. Int., Volume 180, Issue 1, 251-267.
- Poggi, V., Fäh, D., Burjánek, J. and Giardini, D., 2012. The use of Rayleigh wave ellipticity for site-specific hazard assessment and microzonation. An application to the city of Luzern (Switzerland). Geophys. J. Int., Volume 188, Issue 3, 1154-1172.
- RER–ENI. 1998. Riserve idriche sotterranee della Regione Emilia-Romagna. G. M. Di Dio. Regione Emilia-Romagna, ENI Agip Divisione Esplorazione e Produzione. S.EL.CA., Firenze, pp 120.
- Robertson, P.K. 2009. Performance-based earthquake design using the CPT. In Proceedings of IS Tokyo 2009: International Conference on Performance-Based Design in Earthquake Geotechnical Engineering, Tokyo, Japan, 15-18 June 2009.

- Schnabel, P.B., Lysmer, J., Seed, H.B. (1972). SHAKE: A computer program for earthquake response analysis of horizontally layered sites. Rep. No. EERC 72-12, EERI, Berkeley, Calif.
- SM Working Group (2015). Guidelines for Seismic Microzonation". Conference of Regions and Autonomous Provinces of Italy – Civil Protection Department, Rome, 2015.
- Sonmez, H. 2003. Modification of the liquefaction potential index and liquefaction susceptibility mapping for a liquefaction- prone area (Inegol,Turkey). Environmental Geology, 44, 862-871.
- Van Ballegooy, S., Malan, P., Lacrosse, V., Jacka, M.E., Cubrinovski, M., Bray, J.D., O'Rourke, T.D., Crawford, S.A., Cowan, H. 2014. Assessment of liquefaction-induced land damage for residential Christchurch. Earthquake Spectra, 30(1), 31-55.
- Zhang, G., Robertson, P.K., Brachman, R. W. I. (2002). Estimating liquefaction-induced ground settlements from CPT for level ground. Can. Geotech. J. 39, 1168-1180, DOI: 10.1139/T02.
- Zhang, G., Robertson, P.K, Brachman, R.W.I. 2004. Estimating Liquefaction-Induced Lateral Displacements Using the Standard Penetration Test or Cone Penetration Test. J. Geotech. Geoenviron. Eng., 130 (8), 861-871.

This project has received funding from the European Union's Horizon 2020 research and innovation programme under grant agreement No. 700748

3. MICROZONATION OF THE LISBON AREA IN PORTUGAL

3.1 Definition of geological model

3.1.1 Introduction

This report includes the description of the methodology and results obtained in the geological modeling and liquefaction microzonation of the Vila Franca de Xira / Benavente region in the Lisbon area, included in Work Package 2 of the LIQUEFACT project.

A georeferenced database was created in SQLite with data obtained from lithological surveys and geotechnical and geophysical tests. The data, according to their nature, was modeled in 2D (maps) or in 3D (models). The tool selected for modeling was Rockworks17 from Rockware®. Details of the adopted algorithm and modelling options are provided in Appendix 3A.

The pilot site area is located in the Greater Lisbon region, more precisely in the municipalities of Vila Franca de Xira and Benavente, on the left bank of the river Tagus. The polygon that delimits the study area, presented in Figure 3-1, with a total area of 146.9 km^2, is located between longitudes 501,550.0 m and 518,300.0 m and latitudes 4,307,650.0 m and 4,320,600.0 m. The specific coordinates of each point of the polygon are provided in the Appendix 3A.

This project has received funding from the European Union's Horizon 2020 research and innovation programme under grant agreement No. 700748

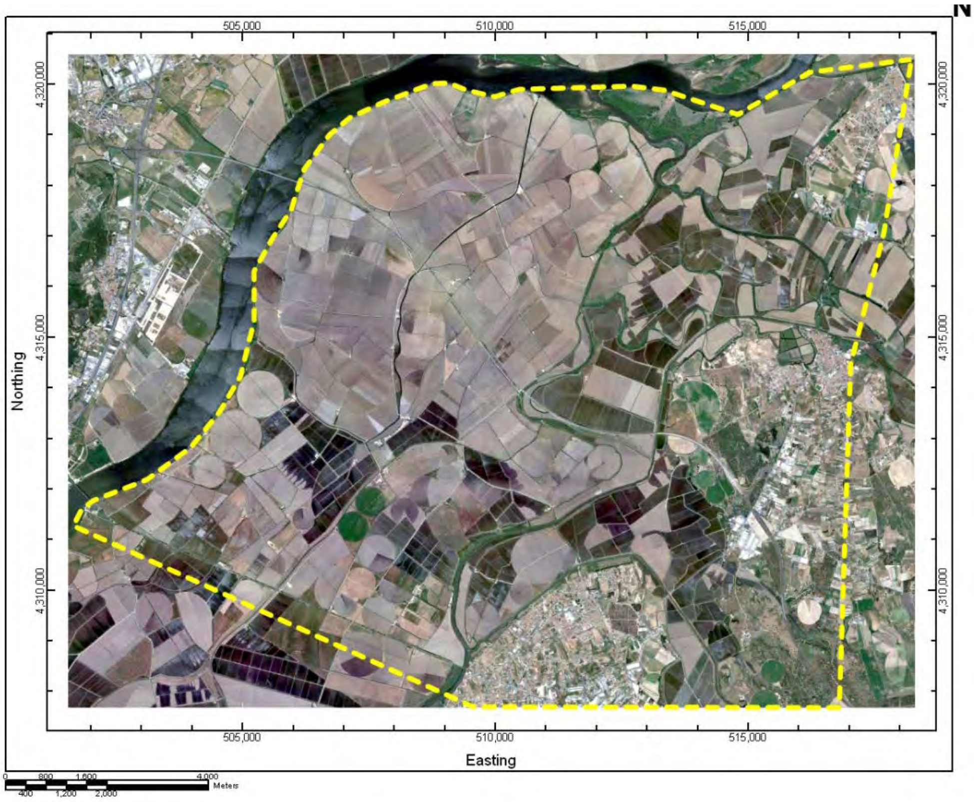

Figure 3-1 Map of the pilot site area

The database used in this work consisted of geological, geotechnical and geophysical information obtained through:

- Data collection from several public institutions and private companies that operate or have operated in the pilot site area (Figure 3-2), details in D2.1;
- Geological charts at scale 1: 50,000 (30D - Alenquer; 31C - Coruche; 34B - Loures and 35A - Santo Estevão) and respective explanatory notes;
- In situ testing campaigns carried out under the LIQUEFACT project (1st campaign - Figure 3-3); additional testing locations defined based on the distribution of data previously mentioned (2nd Campaign - Figure 3-4).
- Topographic data obtained from the original SRTM free data, with a resolution of 25 meters (http://www.fc.up.pt/pessoas/jagoncal/srtm/).

Based on the distribution of the collected data and the tests carried out during the 1st campaign, additional testing locations were found to be necessary to complete the geological and geotechnical models with reasonable reliability. Several additional testing locations were defined in which a total of 11 CPT, 4 SDMT and 28 HVSR measurements were performed (Figure 3-4). Table 3-1 presents a summary of the pre-existing information and the tests carried out in the two in situ testing campaigns of LIQUEFACT.

This project has received funding from the European Union's Horizon 2020 research and innovation programme under grant agreement No. 700748

Table 3-1 Number of tests resulting from the collection of pre-existing information and the in situ testing campaigns

Testing technique	Pre-existing data	1st in situ campaign	2nd in situ campaign	Total
Borehole (lithology)	122	3		125
SPT	91	2		92
CPT/CPTu/SCPT	28	14	11	53
Cross-Hole	13	1		14
Seismic refraction (SR)	5	8		13
DMT/SDMT		5	4	9
HVSR		24	28	52
MASW			3	3
SASW		1		1

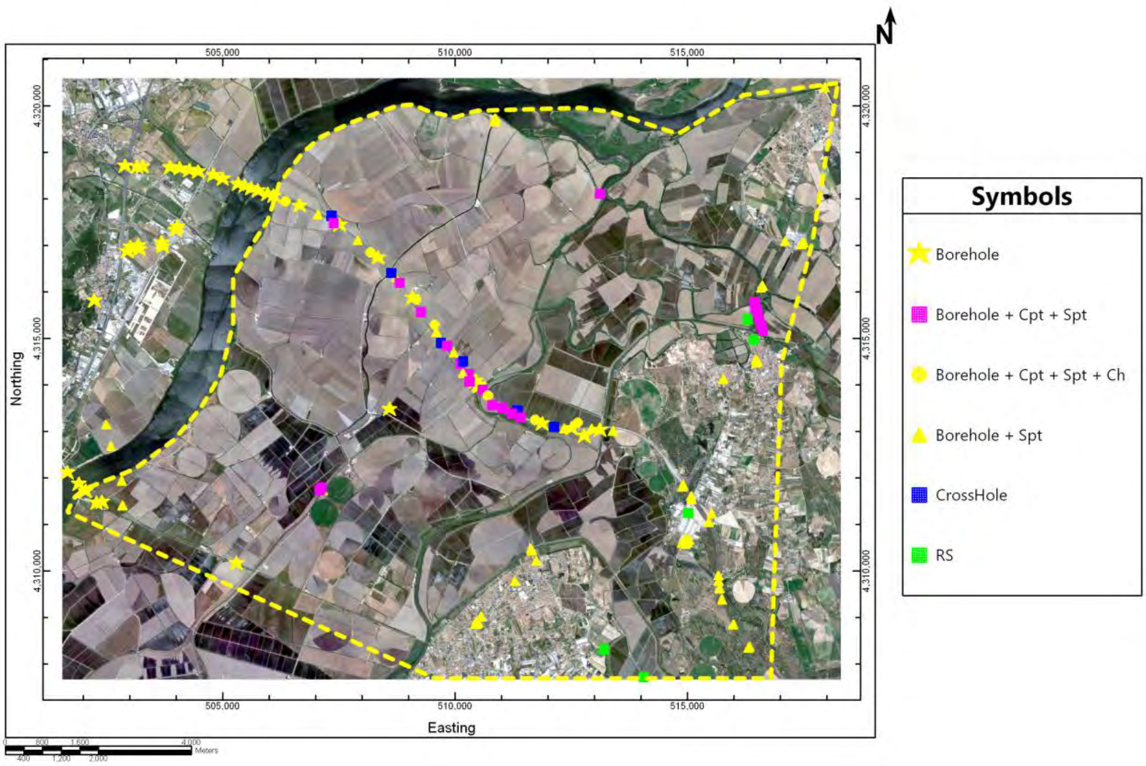

Figure 3-2 Map of the pre-existing in situ tests

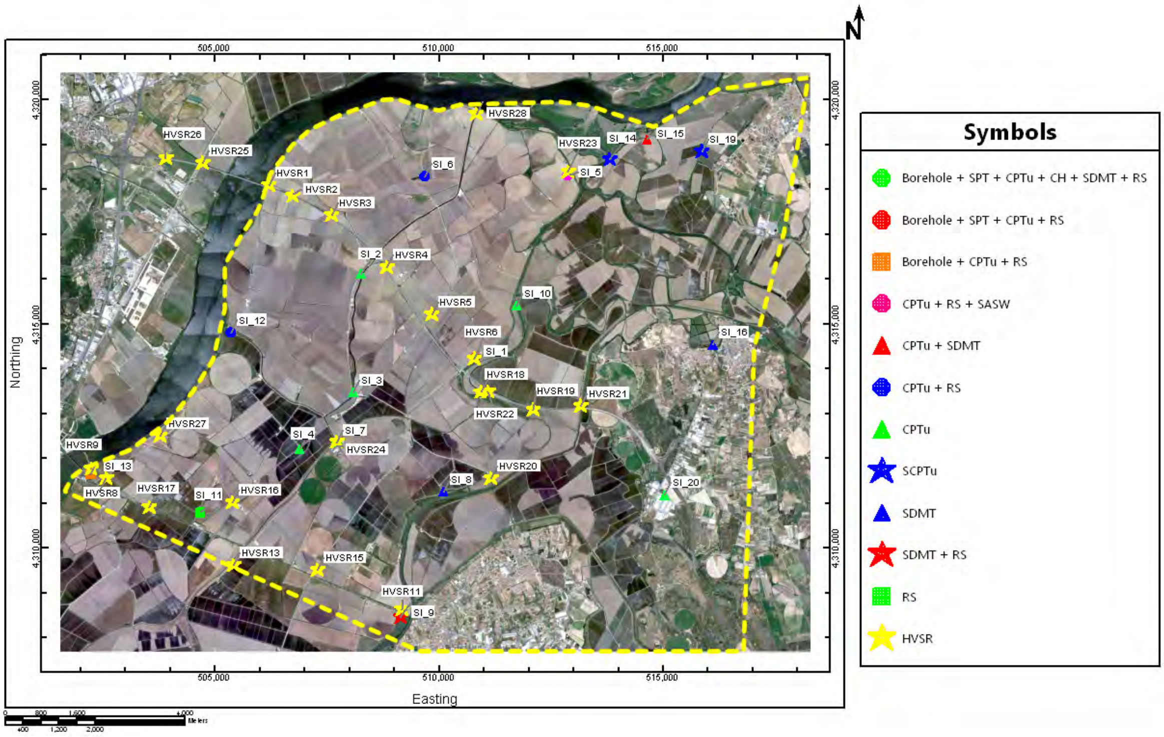

Figure 3-3 Map of the 1st in situ testing campaign (including HVSR measurements)

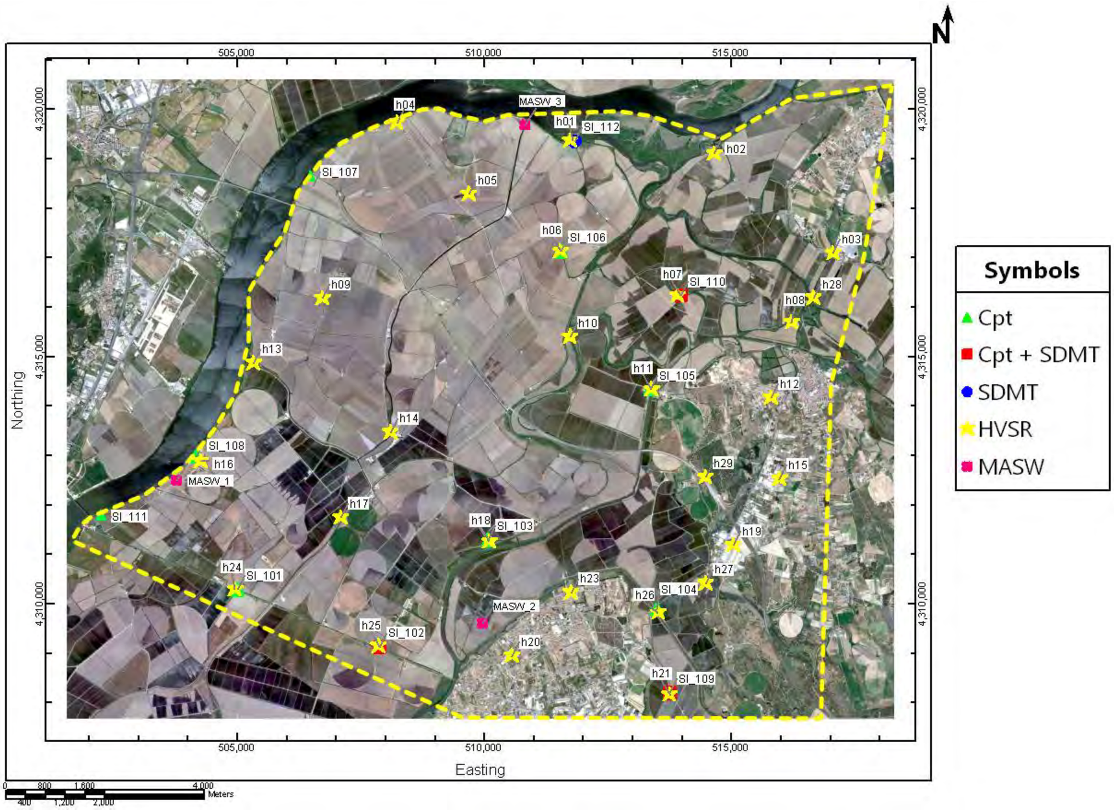

Figure 3-4 Map of the 2nd in situ testing campaign (including HVSR measurements)

3.1.2 Stratigraphic model

The pilot site area consists of a basin that evolved as a tectonic depression, controlled by faults, resulting in an elongated rectangle oriented in the NE-SW direction. The basin rests on top of the *Soco Varisco* and/or Mesozoic formations and it is filled by fluvial and marine sediments, whose age ranges from the Paleogene to the Holocene (Carvalho et al., 2006; Vis et al., 2008, Mannupella et al., 2011). The sediments of the basin present vertical and lateral variations of composition and texture and, locally, stratification irregularities, with lenticular or beveled layers. The large stratigraphic and lithological variability of the area, coupled with a database of numerous pre-existing reports produced by various geotechnical investigation companies (and within the same company by different technicians), for the creation of a single stratigraphic table for this project, proved to be a very complex task.

It was necessary to compile all the lithological descriptions provided in the various reports, to standardize them and often to reinterpret them, taking into account the surrounding areas and the existing knowledge about the area. The stratigraphic units are defined according to the formation process and/or age of a set of lithological units.

The study area is covered by the following geological charts: 30D - Alenquer; 31C - Coruche; 34B - Loures and 35A - Santo Estevão (LNEG). According to the analysis of the charts and their explanatory notes (Zbyszewski & Torre de Assunção, 1965; Zbyszewski & Veiga Ferreira, 1968; Mannupella et al., 2011; Zbyszewski & Veiga Ferreira, 1969) the following stratigraphic units were defined (Figure 3-5):

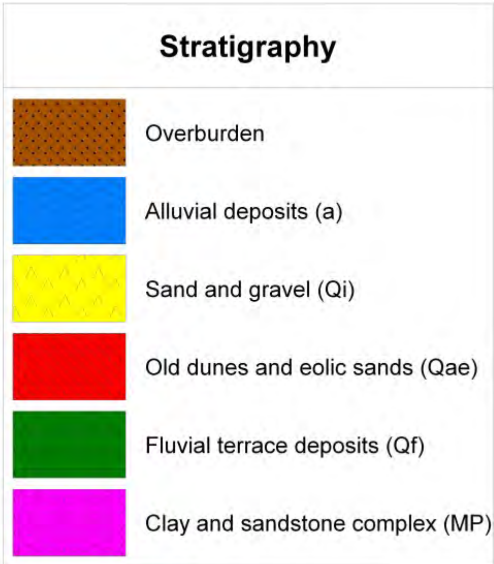

Figure 3-5 Colour scheme of the stratigraphic model

1) Overburden cover - the most recent and superficial layer, composed of organic soil and landfill. It is generally a thin layer, varying between 0.1 m and 0.5 m, reaching in some locations a maximum thickness of 3.5 m for organic soils and 4.5 m for landfill. This can be considered partly anthropogenic, since it includes landfills created to protect water lines and organic soil resulting from the agricultural activity in the area.

2) Alluvial deposits (a) - alluvial deposits are the most abundant stratigraphic unit of the pilot site area, reaching 70 m depth. It is composed of mud, sands of various gradings and of gravel. Particularly in the transition to the Miocene substrate (the clay-sandstone complex - MP), a gravelly layer usually appears, composed of coarse sands with passages of silicious pebbles and cobbles.

3) Sand and gravel (Qi) - only occur in the NE part of the area and correspond to sands and gravel of undifferentiated genesis.

4) Old dunes and eolic sands (Qae) - correspond to ancient dunes and eolic sands, which cover the fluvial terrace deposits (Qf). This stratigraphic unit only occurs in the East zone in Benavente and Samora Correia.

5) Fluvial terrace deposits (Qf) - fluvial terrace deposits can be found to the East (Salvaterra de Magos, Benavente and Samora Correia) and West on the right bank of the Tagus. This stratigraphy can reach a thickness of almost 30 m.

6) Clay-sandstone complex (MP) - the clay-sandstone complex is considered the bedrock substrate. It is the oldest (Miocene-Pliocene) stratigraphy of fluvio-deltaic genesis. This unit emerges at the edges of the basin.

3.1.3 Lithological model

The lithological units correspond to the actual layers intersected by the boreholes. Within each stratigraphic unit, there may be a repetition of several lithological units. Taking into account the purpose of the project, a more detailed differentiation of the sands was adopted. Due to the large variety of existing lithological units, and in order to be able to identify them in the 3D models, the color scheme of each lithology is attributed according to the stratigraphy in which it is inserted (Figure 3-6).

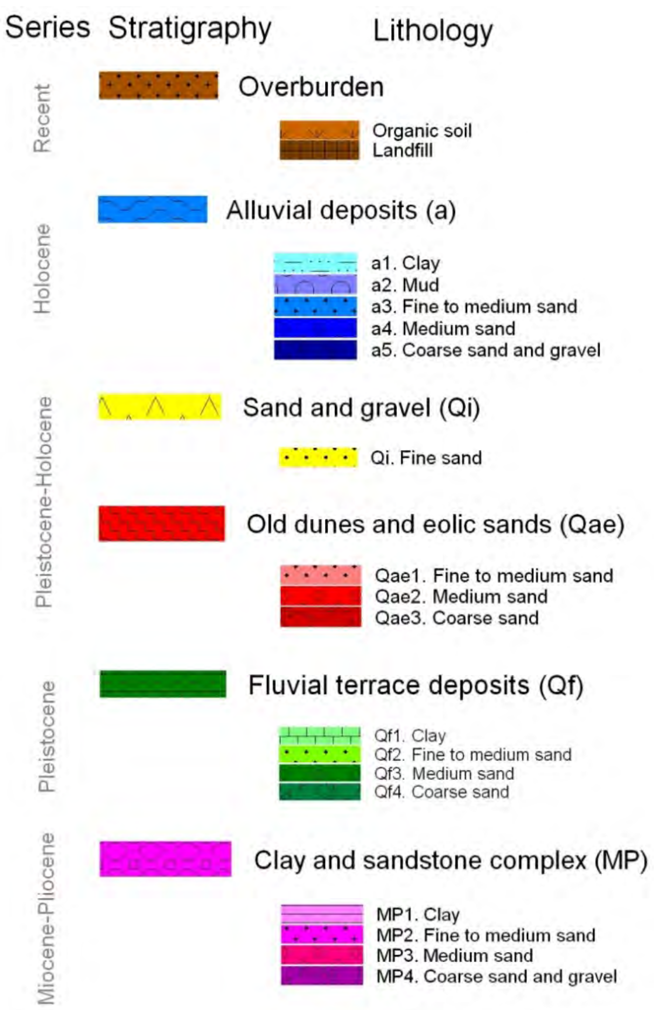

Figure 3-6 Colour scheme of the stratigraphic and respective lithological model (Note that the lithological units follow the same colour hue of the respective stratigraphic unit)

3.1.4 Main results of the geological model

The following sections illustrate the main results of the geological model of the pilot site area in Lisbon. The maps and 3D models were produced based on different algorithms, as summarily listed in Table 3-2. The topographic map and 3D model are presented in Figure 3-7 and Figure 3-8, respectively.

Table 3-2 Algorithms used in the maps and 3D models of the pilot site

Data	Type of output	Algorithm
Topography	Map	Inverse distance
Ground water level	Map	Inverse distance
Stratigraphy	Model + Map	Inverse distance
Lithology	Model + Map	Lateral blending
Geological bedrock	Map	Inherited from the stratigraphic model
V_S (CH + SDMT + SCPT + RS + SASW)	Model	IDW – Anisotropic
V_{S30}	Map	Inverse distance
Seismic bedrock	Map	Inherited from the Vs model
CRR	Model	Lateral Blending
FS	Model	Lateral Blending
LPI	Map	Inverse distance
LSN	Map	Inverse distance
LDI	Map	Inverse distance
Ground Shaking + Amplification factor	Map	Inverse distance

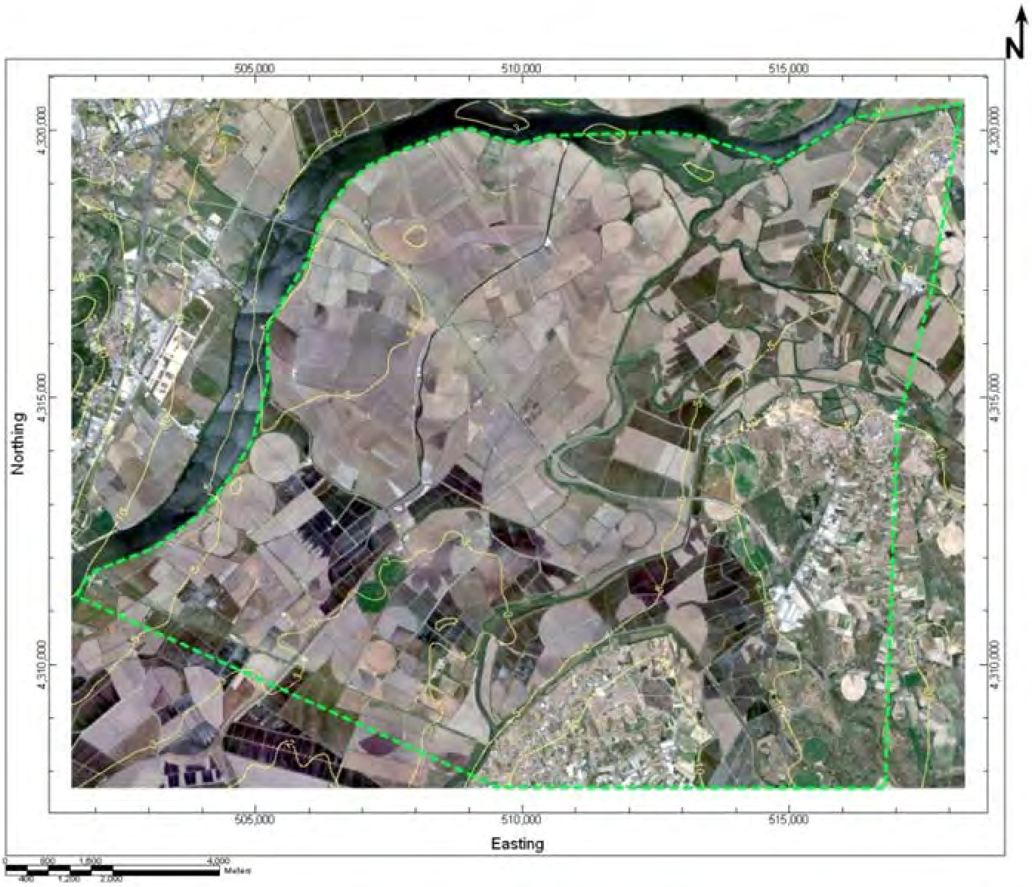

Figure 3-7 Topographic map of the pilot site

This project has received funding from the European Union's Horizon 2020 research and innovation programme under grant agreement No. 700748

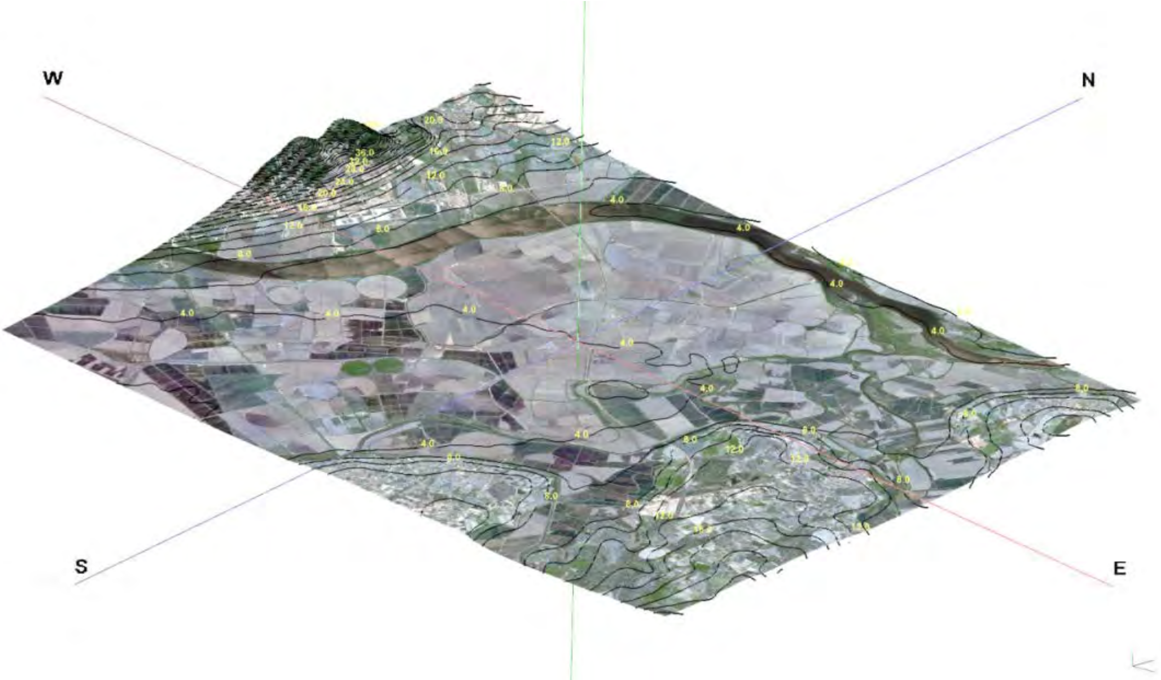

Figure 3-8 View of the topographic map in 3D

The stratigraphy outputs are illustrated in Figure 3-9 to Figure 3-12. The lithology outputs are shown from Figure 3-13 to Figure 3-16.

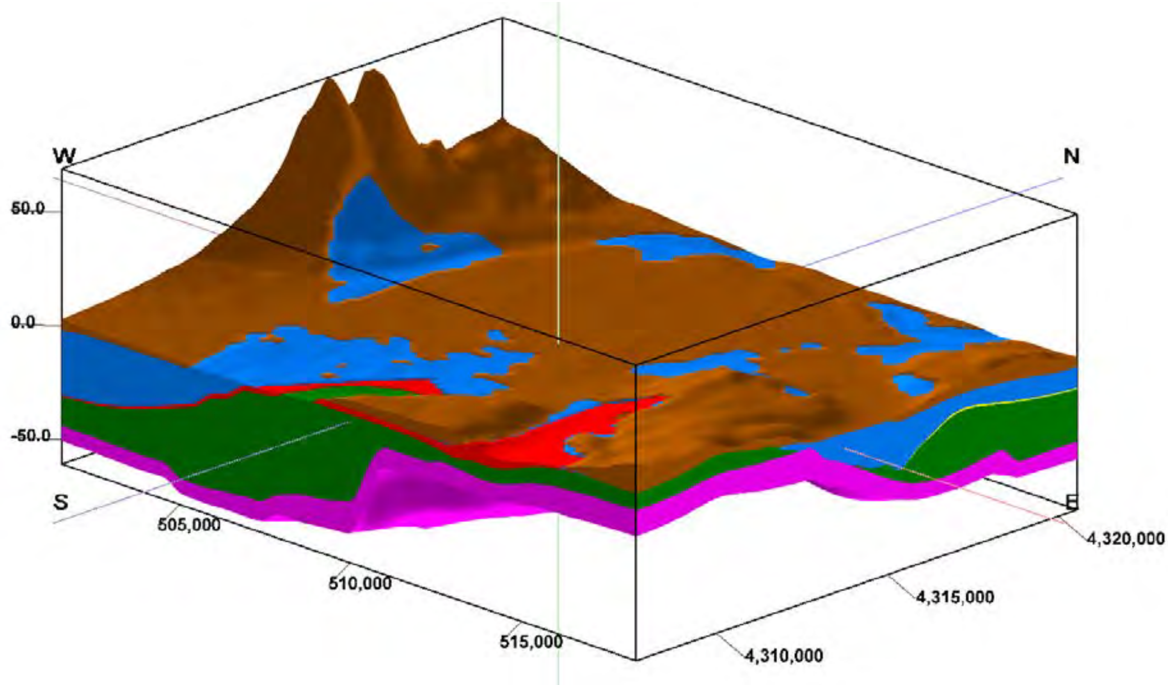

Figure 3-9 View of the stratigraphic model in 3D

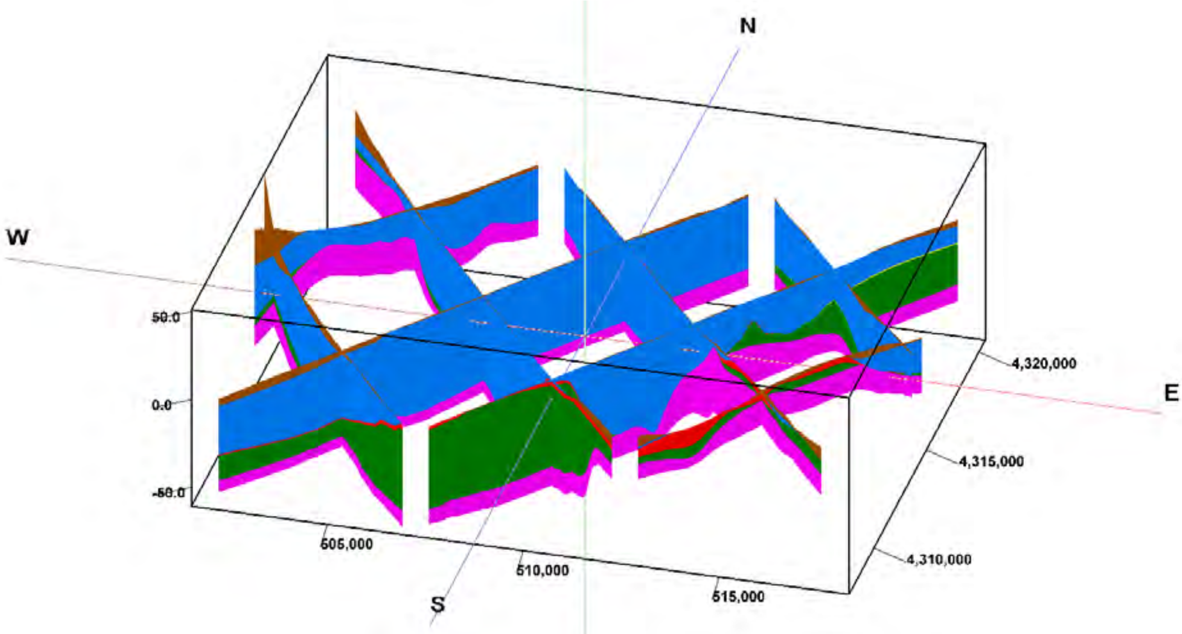

Figure 3-10 Fences (cross-sections) of the stratigraphic model

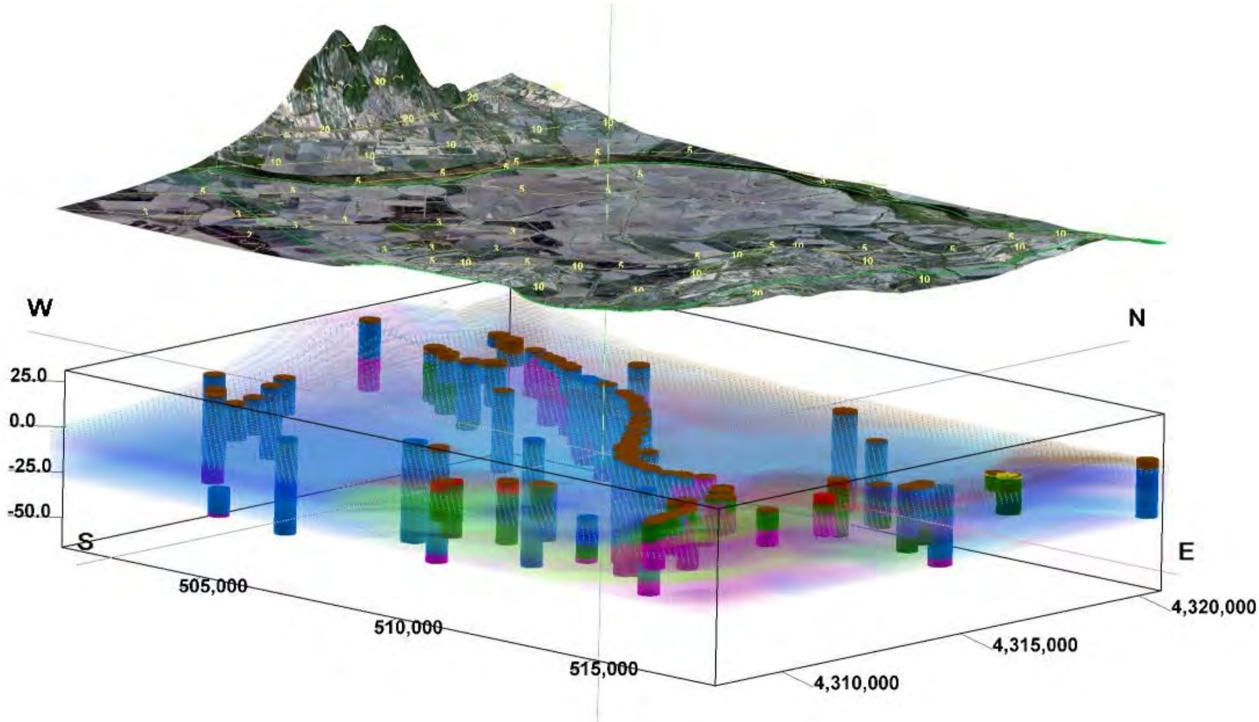

Figure 3-11 Representation of the topographic model and the stratigraphic boreholes

This project has received funding from the European Union's Horizon 2020 research and innovation programme under grant agreement No. 700748

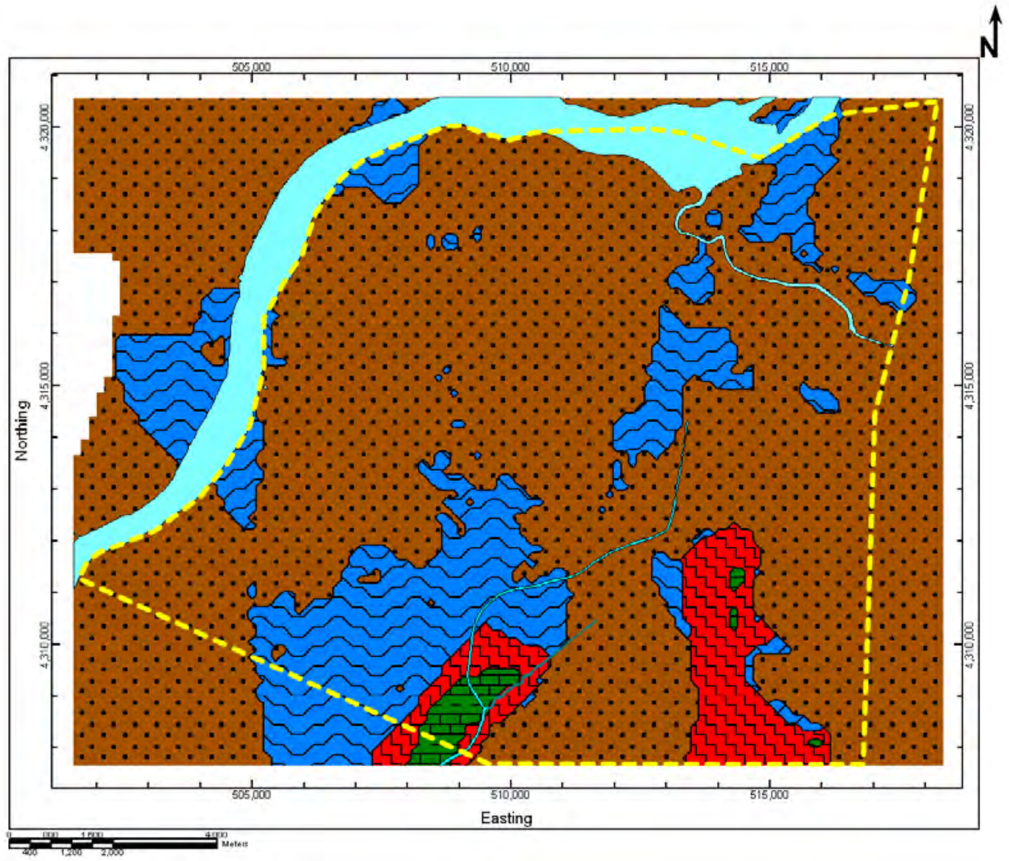

Figure 3-12 Stratigraphic map with the main water lines

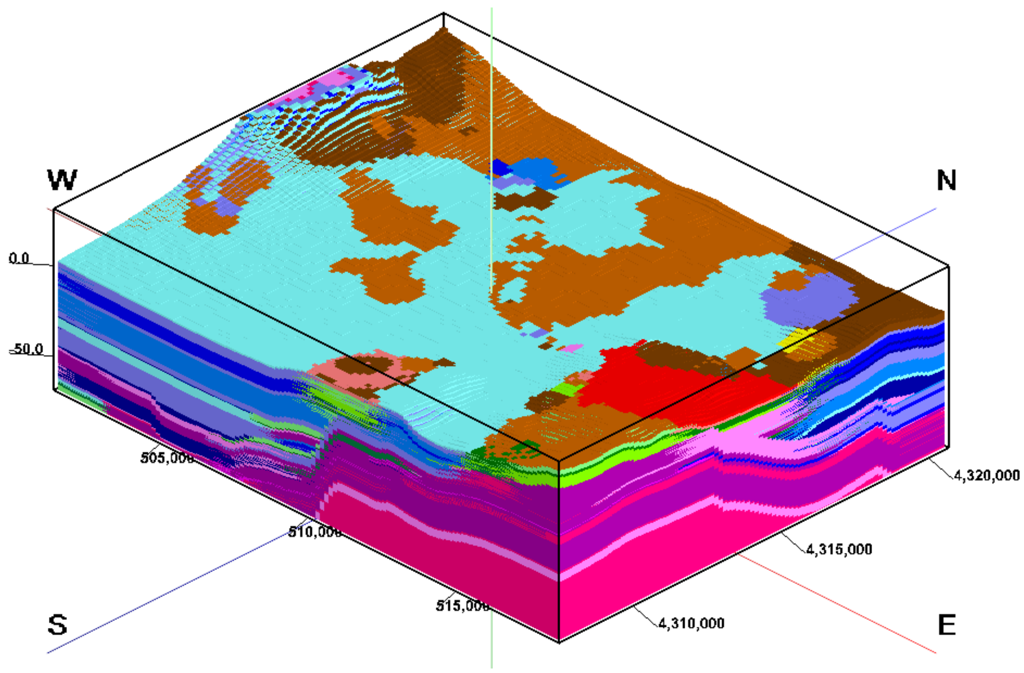

Figure 3-13 View of the lithological model in 3D

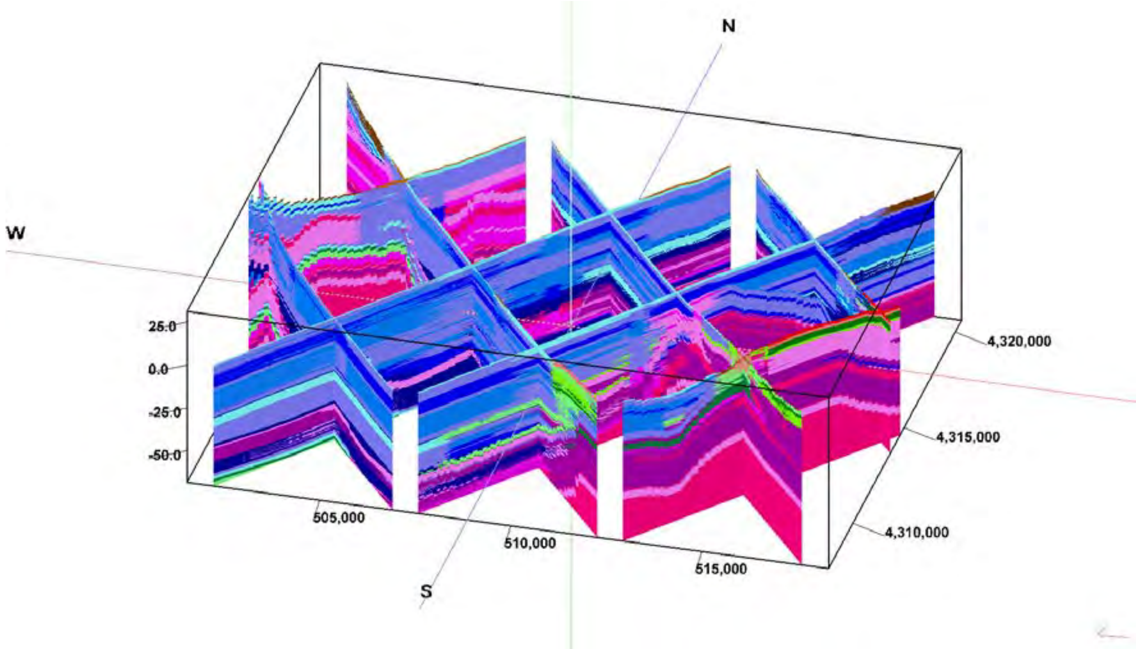

Figure 3-14 Fences (cross-sections) of the lithological model

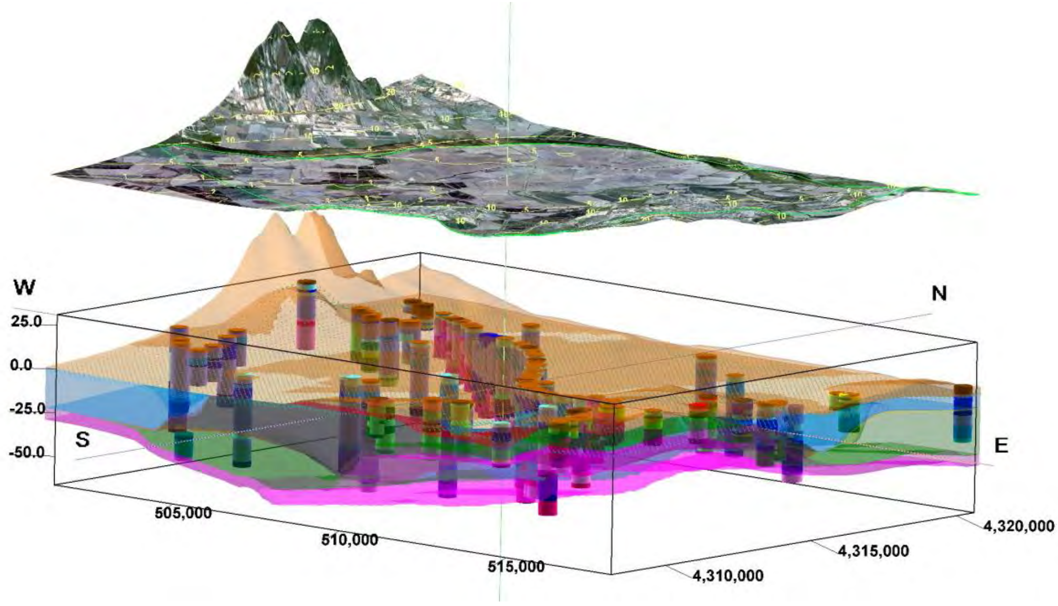

Figure 3-15 Representation of the topographic model and the lithological boreholes

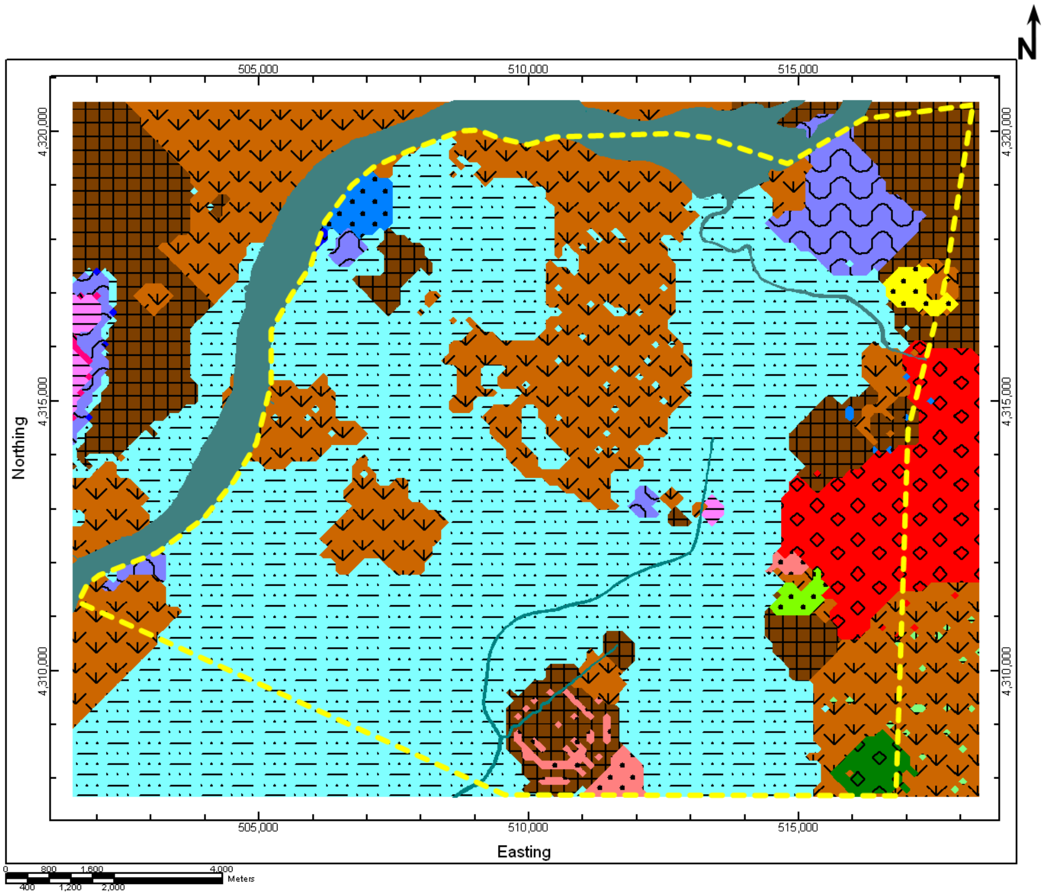

Figure 3-16 Lithological map with the main water lines

For the definition of the ground water table depth, the data in the reports and tests carried out were compiled and analyzed. It should be noted that for each testing location, only one reference is made to a water table level measurement, valid for the date of its execution, which varied between 1969 and 2019. The map with the groundwater level depth in the pilot site is provided in Figure 3-17.

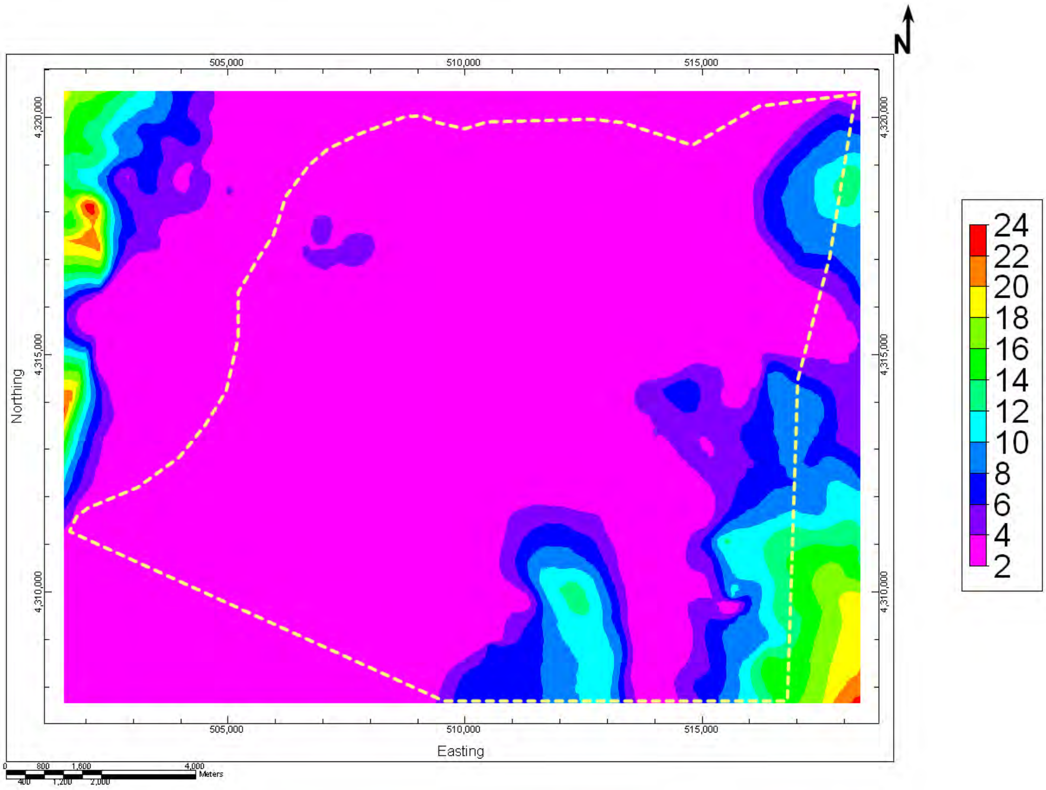

Figure 3-17 Map of the groundwater level depth

With regard to the definition of the geological bedrock, two scenarios were considered, based on the analysis of the existing stratigraphy. The first scenario is more conservative, where the bedrock is defined at the top of the Miocene layer (Figure 3-18 to Figure 3-22).

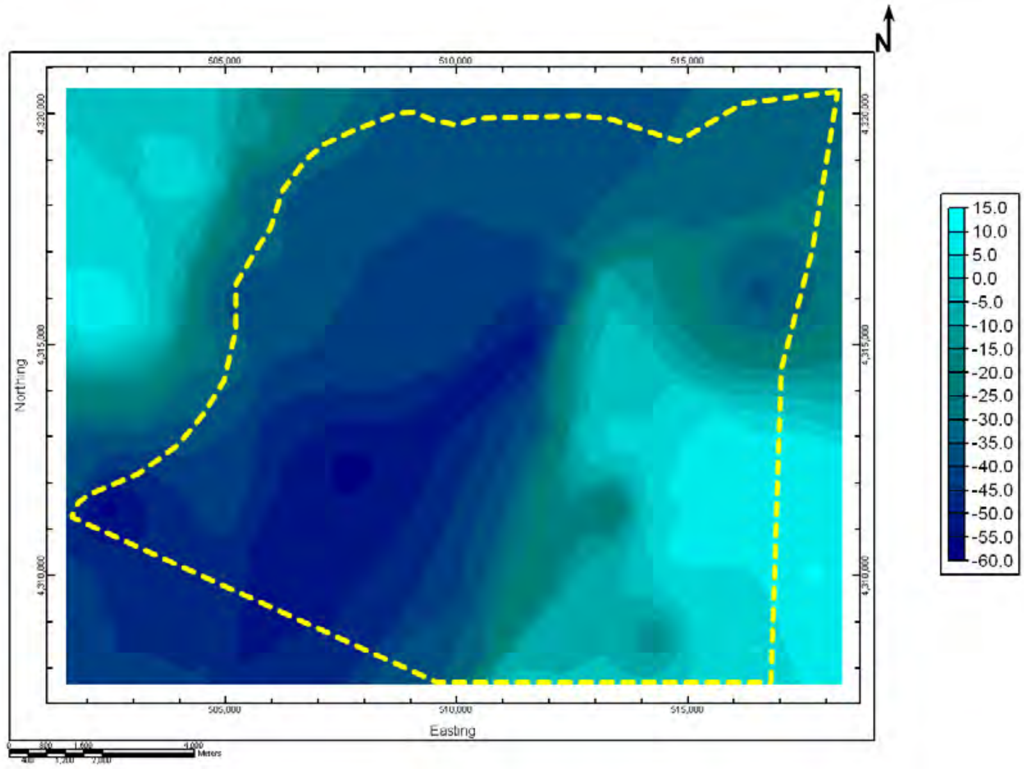

Figure 3-18 Map of the elevation of the geological bedrock (corresponding to the Miocene lithology)

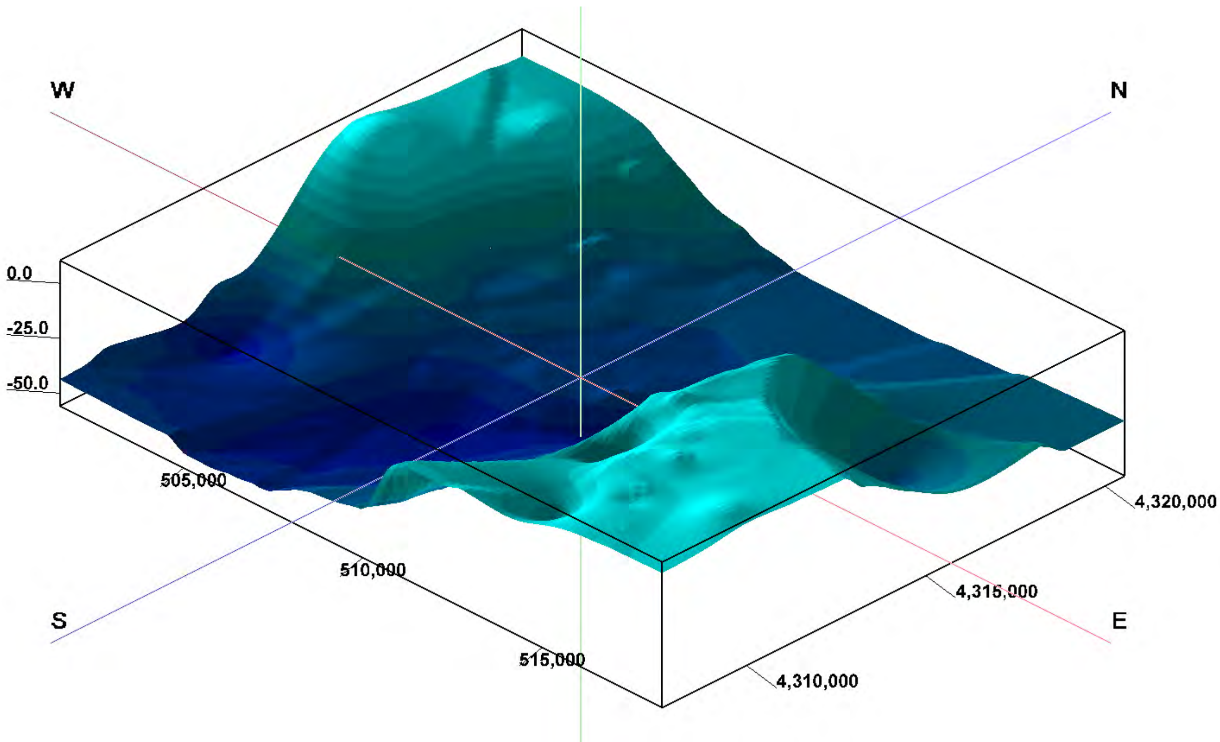

Figure 3-19 View of the geological bedrock in 3D (corresponding to the Miocene lithology)

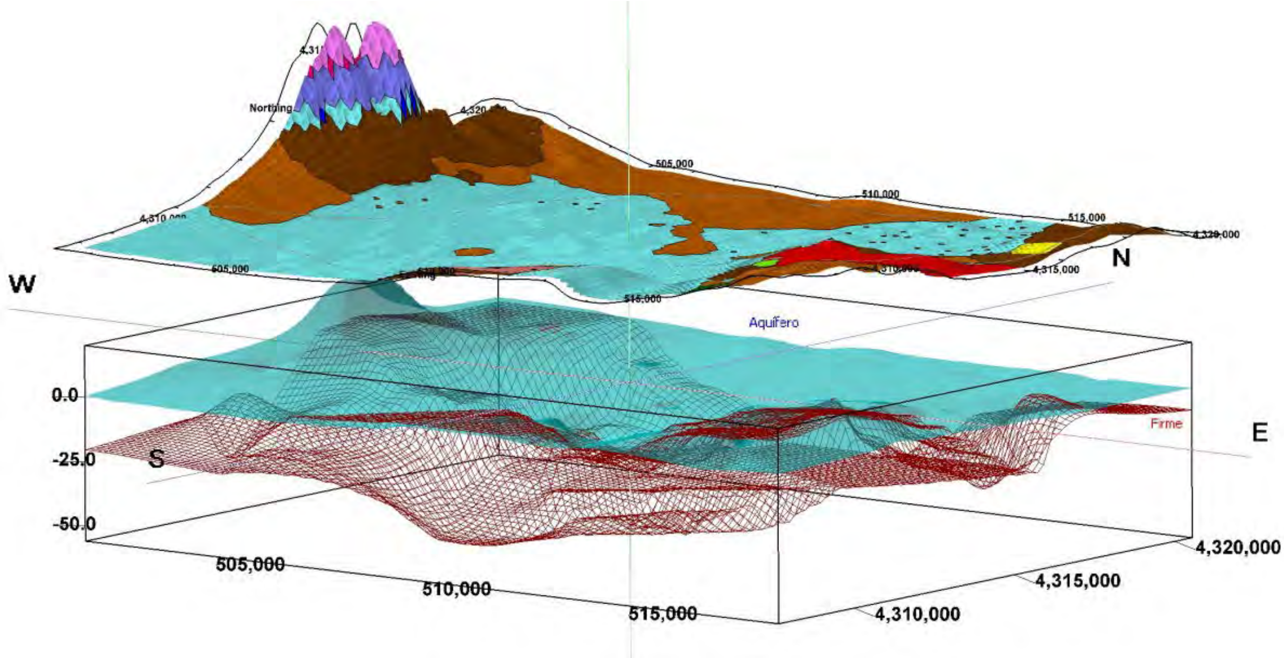

Figure 3-20 View of the lithological model (top), groundwater level (middle blue) and geological bedrock (red mesh) in 3D

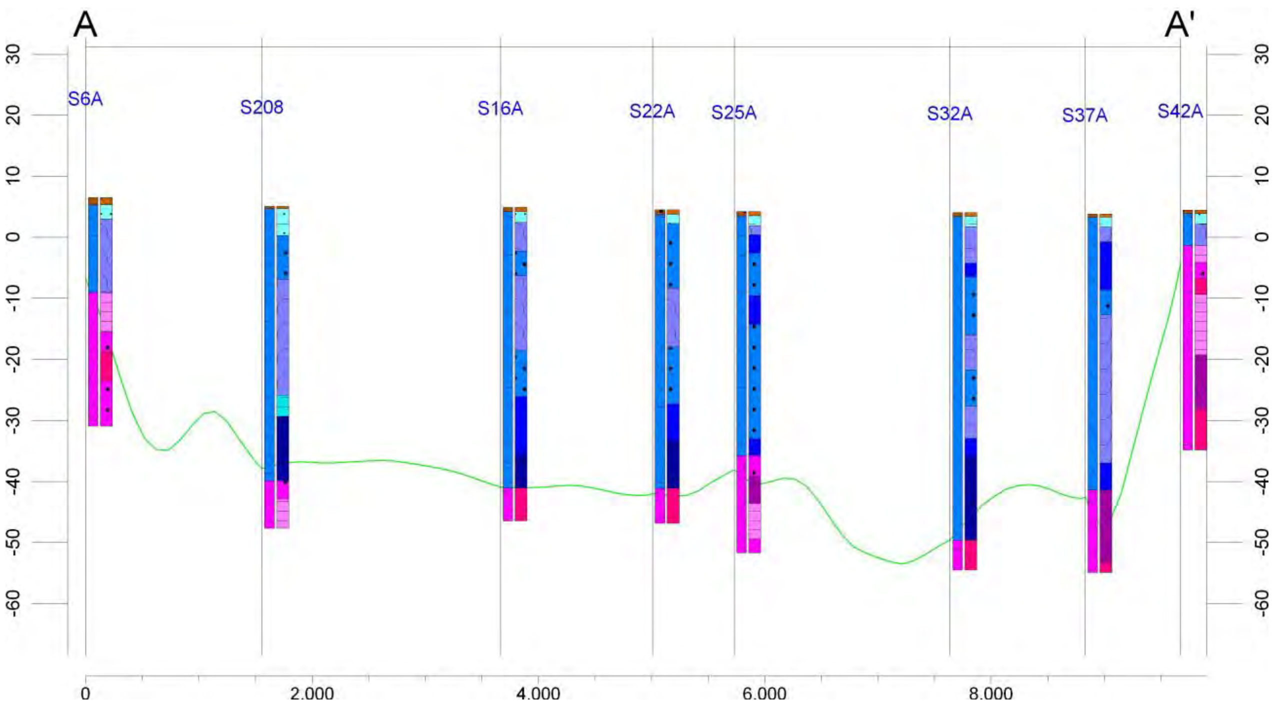

Figure 3-21 Cross-section along the A10 with representation of the stratigraphic (left) and lithological (right) boreholes and the geological bedrock (green line)

This project has received funding from the European Union's Horizon 2020 research and innovation programme under grant agreement No. 700748

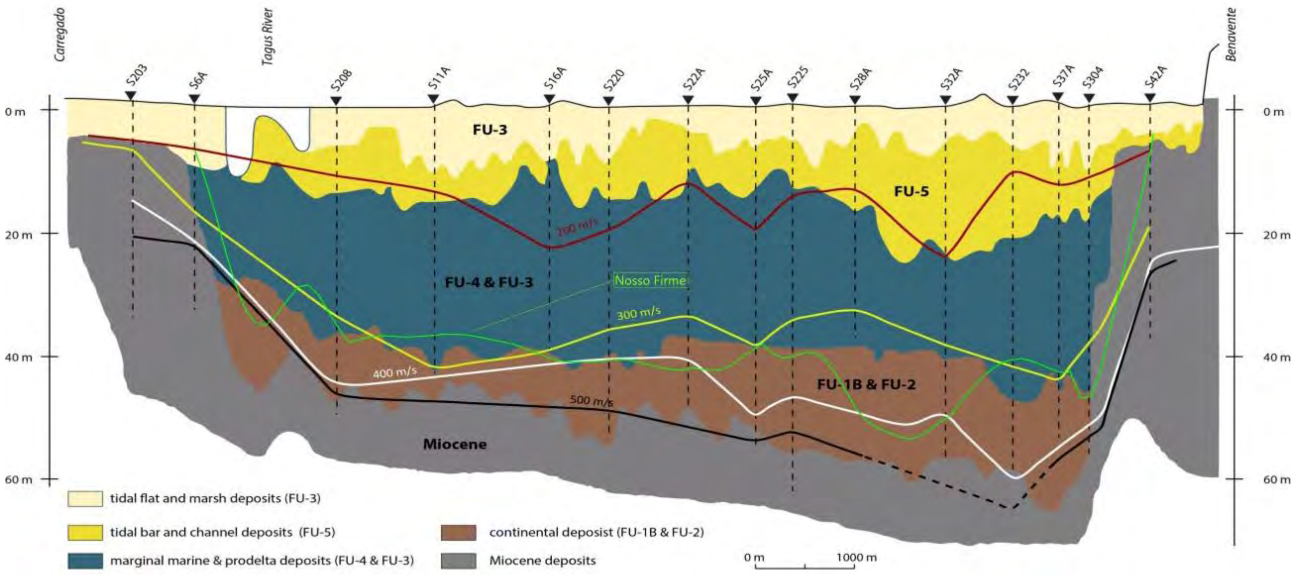

Figure 3-22 Representation of the geological bedrock (green line) in the interpretative cross-section along the A10 produced by Vis et al. (2008)

The second scenario for the geological bedrock considers not only the Miocene but also the old fluvial terrace deposits (Figure 3-23 to Figure 3-24).

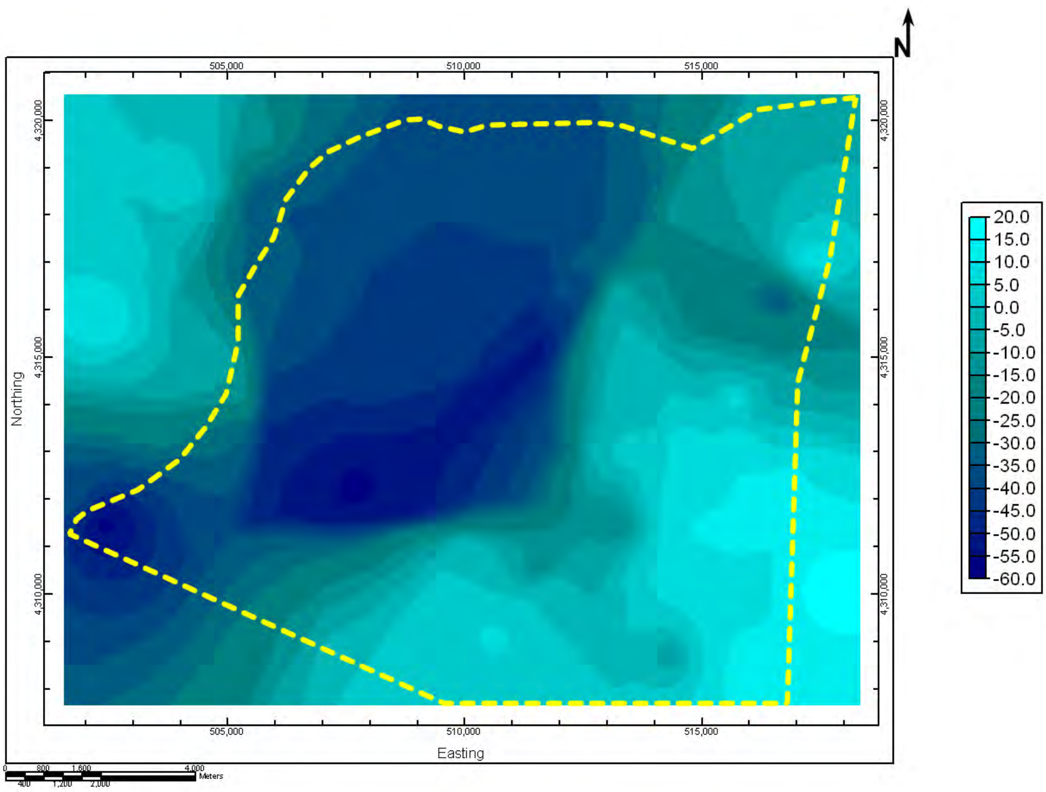

Figure 3-23 Map of the elevation of the geological bedrock (considering the fluvial terrace deposits and Miocene lithologies)

This project has received funding from the European Union's Horizon 2020 research and innovation programme under grant agreement No. 700748

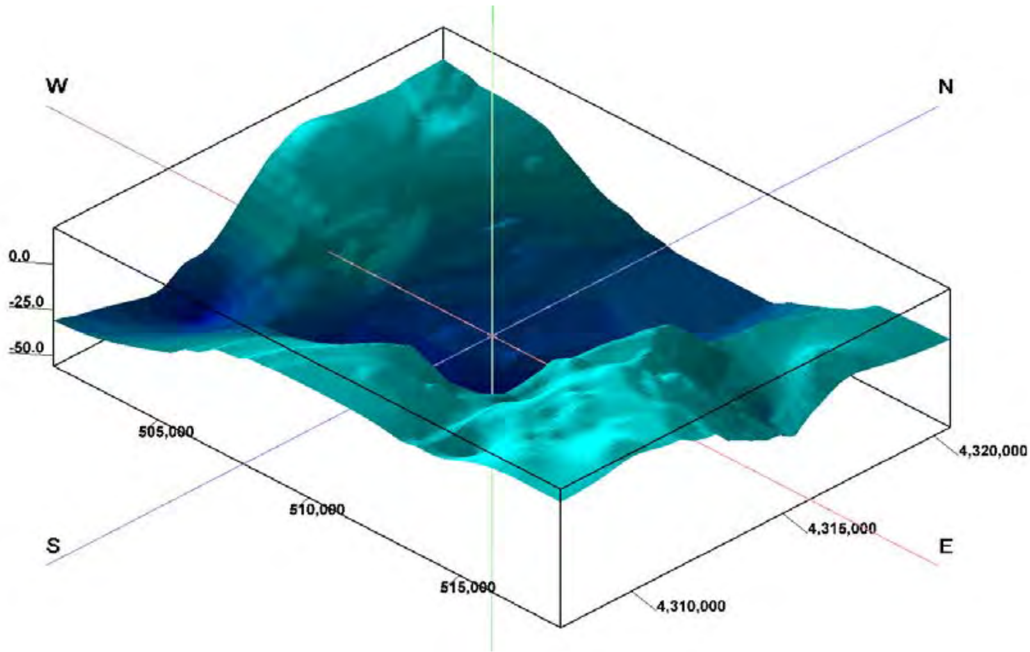

Figure 3-24 View of the geological bedrock in 3D (considering the fluvial terrace deposits and Miocene lithologies)

3.2 Definition of geotechnical model

Based on the data collected in the geological-geotechnical characterization of the pilot site, a geotechnical model was defined. This model will serve as the basis for the assessment of the local ground response and for the construction of the map of ground surface motion, as well as the ground motion profiles, which will then be used to calculate the intensity of seismic demand. Furthermore, this geotechnical model will enable to produce site-specific liquefaction risk maps and more complete 3D models, for the final goal of microzonation of the pilot site. A summary table of the main geotechnical characteristics of each lithology is provided in Table 3-3.

For the purpose of illustrating the variability of the generated geotechnical model in the pilot site, a map of the distribution of the time-averaged shear wave velocity at 30 meters (V_{S30}) is presented in Figure 3-25. This map clearly shows an increase of V_{S30} from West to East, predominantly in the NW-SE direction. Although this parameter alone cannot be considered indicative of liquefiable soils, as soil type is not discernible directly from V_{S30}, it provides useful information regarding the stiffness and seismic response of the soils in this region.

This project has received funding from the European Union's Horizon 2020 research and innovation programme under grant agreement No. 700748

Table 3-3 Geotechnical characteristics of the different lithological units of the pilot site

Lithology	Depth range (m)		Thickness range (m)		V_S range (m/s)	
0. Landfill	0	0	0	1.8	100	100
0. Organic soils	0	13.9	0.2	8.6	75	220
a1. Clays	0	26.8	0.9	20	62	170
a2. Muds	0	40.5	0.6	26	78	258
a3. Fine to medium sands	0	37.5	0.4	21.5	125	393
a4. Medium sands	1.8	44.8	0.6	15.8	114	565
a5. Coarse sands & gravels	30.8	47	2.5	16.5	270	393
Qae1. Fine to medium sands	1.8	1.8	0	2.9	158	158
Qf1. Clays	4.7	27.6	1	9.6	107	222
Qf2. Fine to medium sands	12.1	27.3	0.3	4.8	200	230
Qf3. Medium sands	7.5	27.4	2	4.8	213	633
Qf4. Coarse sands	19.5	19.5	0	1.8	268	268
MP1. Clays	5.8	59	0.8	9.9	178	460
MP2. Fine to medium sands	8.6	53.6	1.4	3.4	258	513
MP3. Medium sands	11.2	57.2	1.5	7.8	269	530
MP4. Coarse sands	23.7	45.2	4.4	12	304	400
Bedrock	19.9	64.8	-	-	-	-

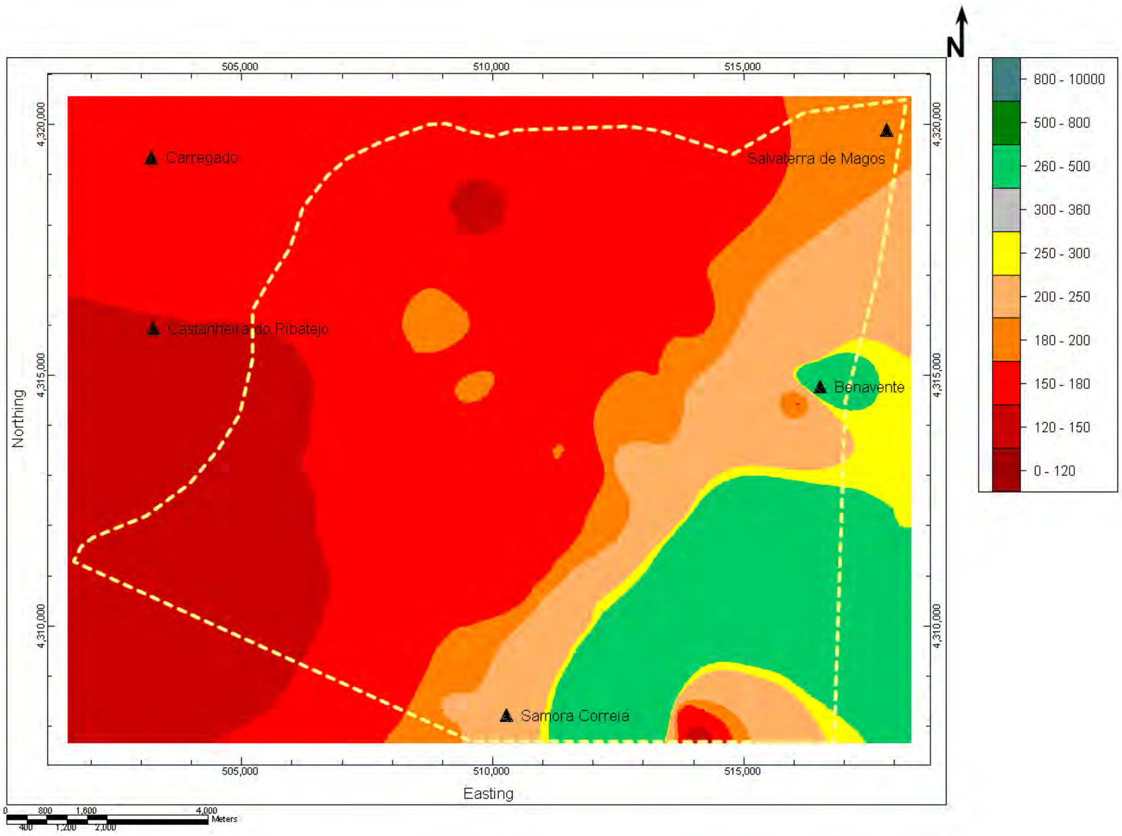

Figure 3-25 V_{S30} map

Within the scope of the geotechnical interpretation of the pilot site, a new soil profile classification has been proposed. Conventional liquefaction assessment focuses only on triggering; however, earthquake-induced liquefaction is also responsible for considerable structural damage. For this reason, a new hazard-independent liquefaction classification has been proposed where the soil profile is defined as an equivalent 3-layered soil profile. The classification consists of only three features, considered the most relevant to the performance of shallow-founded buildings: the depth of the non-liquefying crust, and the thickness and liquefaction resistance of the potentially liquefiable layer. A procedure to obtain the 3-layered soil profile from CPT data was developed and a set of soil profile classes are generated for rapid loss assessment purposes. The use of this ESP classification for bearing capacity analysis in liquefied soils has the advantages of being capable of reproducing the actual response of the soil profile across the full hazard range using just three intuitive parameters, while providing simple implementation for numerical simulations, as the information can be directly related to the performance of shallow-founded buildings. The procedure and classes were demonstrated on a case study site considering 100 CPT from Christchurch where a comparison was made regarding the computed LSN value for the equivalent and CPT profiles (Millen et al., 2019a). This hazard-independent but risk sensitive classification has the distinct advantage of being independent of regularly updated seismic hazard maps. Furthermore, liquefaction triggering assessments that use different assumptions can provide considerably different results. Recent investigations of the performance of soil deposits in Christchurch during the 2011 earthquake by Cubrinovski et al. (2017) identified the role of pore water flow and seismic isolation as key differences between the CPT-based simplified triggering procedure from Boulanger & Idriss (2016) and nonlinear effective stress analyses. In turn, soil layers in terms of the normalised cone tip resistance and the information criterion were readily identified and consistent across both assessment procedures. This methodology and the calibration for specific case-studies is presented more in detail is Deliverable D3.2 of Liquefact worpackage 3 (Viana da Fonseca, 2018b).

For this purpose, a total of 38 points were selected, taking into account the considerable amount of in-situ tests available to characterize the subsurface soil (Figure 3-26).

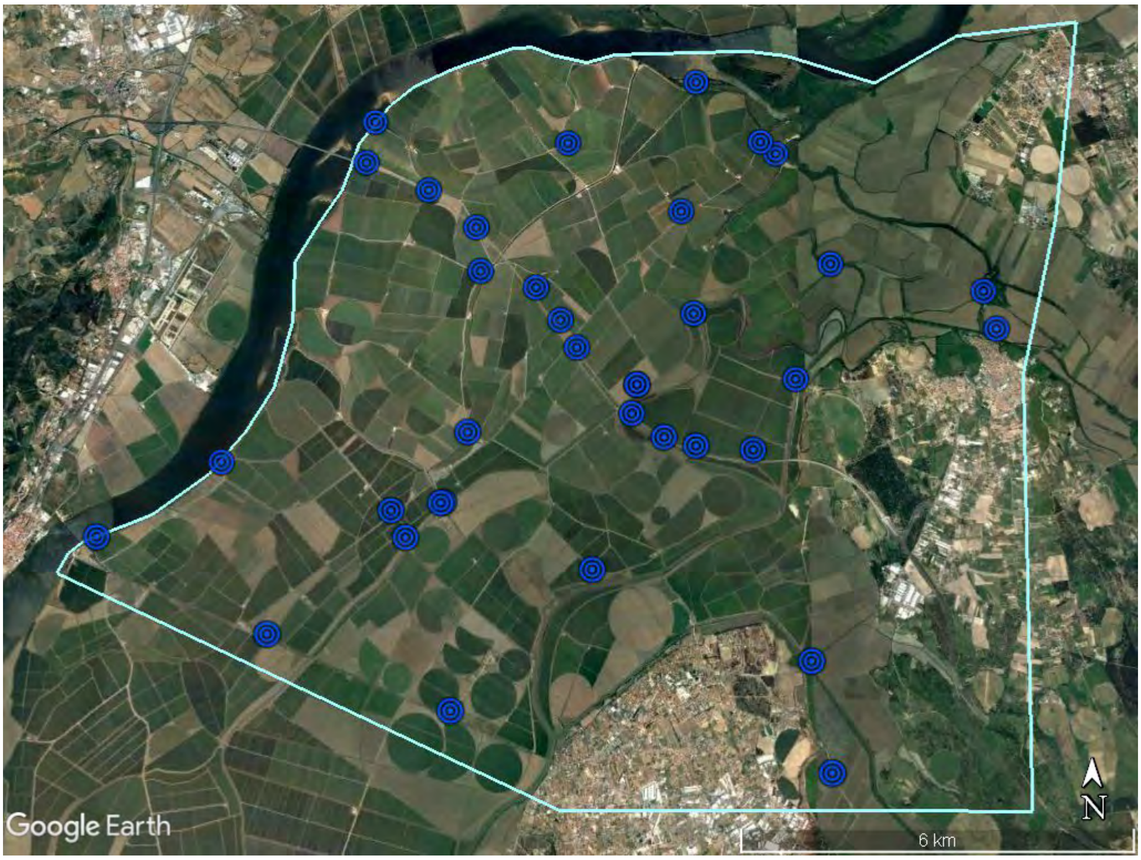

Figure 3-26 Location of the selected points

The soil profiles in the 38 points were classified following the methodology in Millen et al. (2019a). As said, this new methodology for obtaining a simplified equivalent three-layered soil profile is based on the liquefaction assessment of the soil profile from CPT data. The equivalent soil profile (ESP) is defined as a soil profile classification tool for the purpose of the seismic response of shallow-founded buildings in liquefied soils. As mentioned above, this methodology uses three governing parameters: the depth of the crust (D_{liq}), the thickness of the liquefied layer (H_{liq}) and its shear strength (CRR_{n15}). Typical ranges of values for each of these variables have been defined, from which 22 different soil profile classes are derived (Figure 3-27).

This project has received funding from the European Union's Horizon 2020 research and innovation programme under grant agreement No. 700748

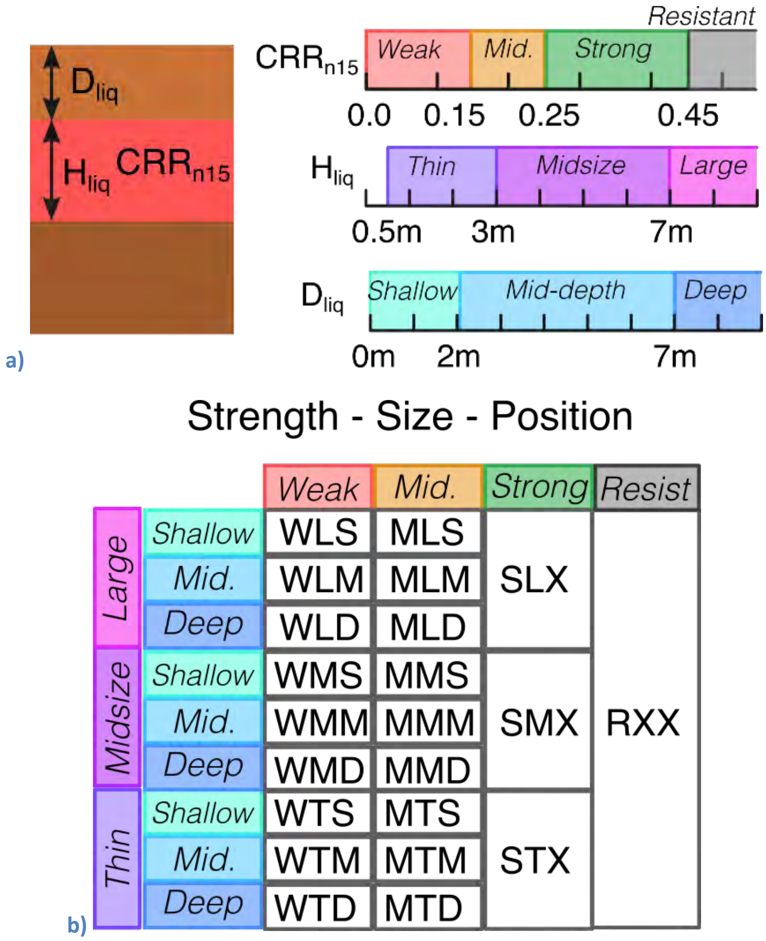

Figure 3-27 Equivalent soil profile classification: a) range definition; b) classes

From the application of this procedure to the 38 points, the distribution of equivalent soil profiles in the pilot site was obtained, as shown in the pie chart in Figure 3-28. The following distribution was obtained: a large majority (more than 65%) are weak soil profiles, almost 24% are mid-strength, about 3% are strong and almost 8% are resistant soil profiles, predominantly located at medium depths (between 2 to 7 m).

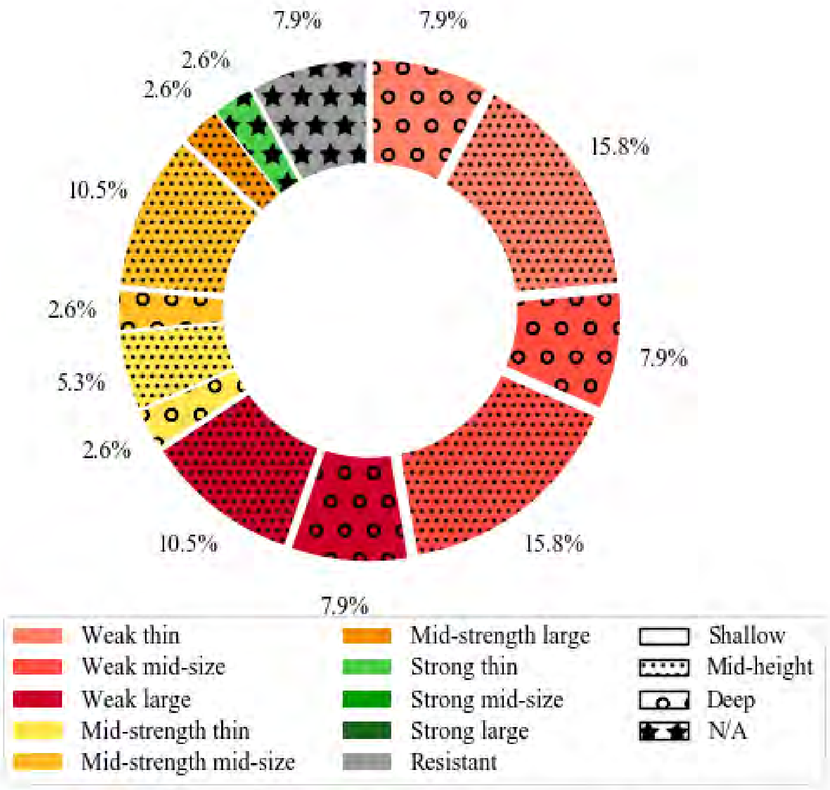

Figure 3-28 Equivalent soil profile distribution

3.3 Description of seismic input

3.3.1 Selected ground motions

Two earthquake types and three return periods identified in Eurocode 8 (475 years, 975 years, and 2475 years) were used to perform the analyses. Type 1 seismic action corresponds to a "far" earthquake, with epicentre in the Atlantic Ocean. Type 2 corresponds to a "near" earthquake, with epicentre in Continental Portugal.

For each return period of type 1 six motions were selected, while for type 2 seven motions were adopted for each return period, giving 39 different motions. Table 3-4 and Table 3-5 summarize the information associated to type 1 and 2 seismic actions for Benavente in the South of Portugal, which were kindly provided by Dr. Alexandra Carvalho, from the Portuguese National Laboratory of Civil Engineering (LNEC).

The ground motion accelerograms were generated in UPavia by Dr. Elisa Zuccolo, under the supervision of Prof. Carlo Lai.

For the seismic action 'Type 2' the accelerograms were generated for each required return period (i.e. PGA) selecting accelerograms spectrum-compatible to the EC8 type-1 response spectrum (corresponding to Ms>5.5). These accelerograms were scaled to match, on average, the EC8 response spectrum in the spectral period range 0.1-1.5s, so they could be used without any further scaling.

For the seismic action 'Type 1' the accelerograms were selected with a criterion different from that used to select the accelerograms "Type 2". Although they do not match the EC8 response spectrum, each accelerogram was selected in order to have a magnitude, distance and tectonic regime (i.e. subduction) compatible with the scenario event. The accelerograms were retrieved from the Japanese http://www.kyoshin.bosai.go.jp/ portal, they were recorded at rock-like stations and they were scaled to math the PGAs provided in Table 3-4 for three return periods of interest.

The seismic action 'Type 1' corresponds to an earthquake scenario whose main seismological parameters (moment magnitude and hypocentral distance) and focal mechanism (subduction) are controlled by a single seismogenic structure which is the Ferradura fault. Under these conditions, a characteristic earthquake governs the seismicity at the site, which is anything but Poissonian. The magnitude does not change much with the return period (Table 3-4). In addition, the distance from the site to the main fault is about 300 km. Under these conditions, it was not considered necessary to enforce spectrum compatibility because the shape of the spectrum is essentially controlled by a M8.0 deterministic earthquake occurring at a relatively large distance. The spectrum-compatibility needs to be enforced when the seismicity at a site is controlled by several faults each characterized by a different seismogenic potential (i.e. different maximum moment magnitudes) and distance from the site. Finally, the selected accelerograms have been scaled to the PGA in Table 3-4 for the three different return periods of interest.

The single degree-of-freedom (SDOF) acceleration response spectra of the motions is shown in Figure 3-29.

Table 3-4 Type 1 Seismic action: Distance to the main fault: 300 km to the Ferradura fault

Year interval	maximum magnitude	corresponding PGA (cm/s2)
400-550	M7.8	100
>900-1500	M8.0	159
>2200	M8.2	301

Table 3-5 Type 2 Seismic action: Distance to the main fault: 10 km to the Vila Franca de Xira fault

Year interval	maximum magnitude	corresponding PGA (cm/s2)
450-600	M6.6	170
>800-1000	M6.8	224
>2000-3500	M7.0	329

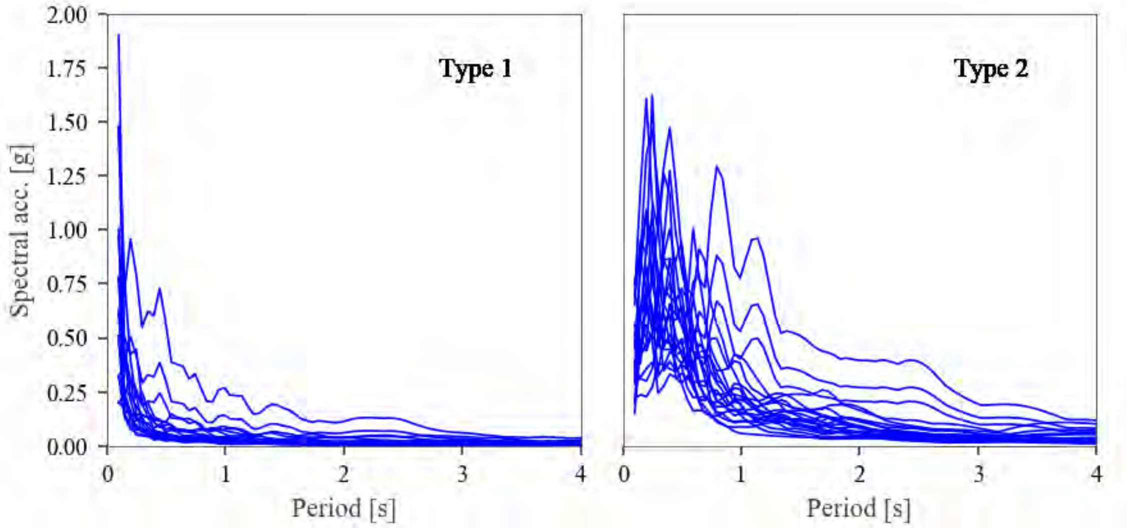

Figure 3-29 Ground motion SDOF response spectra

3.4 Microzonation for ground motion

3.4.1 Methods for estimating surface ground motion

There are different methods to estimate surface ground motion. In the following sections, three ground response models will be detailed.

3.4.1.1 Linear approach

In this approach, the input motion at the bedrock in the form of a time history is represented as a Fourier series, usually using Fast Fourier Transform, FFT (Cooley & Tukey, 1965). Each term in the Fourier series of the bedrock motion is then multiplied by a transfer function to produce the Fourier series of the ground surface motion. This latter can then be expressed in the time domain using the inverse FFT. Thus, the transfer function determines how each frequency of the bedrock motion is amplified or de-amplified by the soil deposit. However, this transfer function depends on the soil parameters, namely of shear modulus and damping ratio, which are considered constant in this analysis.

3.4.1.2 Equivalent Linear approach

Since the soil behaviour is nonlinear, the linear approach needs to be modified to provide reasonable estimates of ground response. The real nonlinear hysteretic stress-strain behaviour of cyclically loaded soils can be approximated by equivalent linear soil properties. The equivalent linear shear modulus, G, is generally taken as a secant shear modulus and the equivalent linear damping ratio, D, as the damping ratio that produces the same energy loss in a single cycle as the real hysteresis loop. Since the linear approach requires G and D to be constant for each soil layer, the aim is to determine the values that are consistent with the level of strain induced in each layer. However, G and D are generally obtained in laboratory tests made with simple harmonic loading where the peak shear strain amplitude characterizes the strain level. Instead, the shear strain time history of a typical earthquake motion is highly irregular with peak amplitude being only approached by few spikes in the record (Kramer, 1996). As a result, it is common to characterize the strain level of the transient record in terms of an effective shear strain often taken as 65% of the peak strain. Idriss and Sun (1992) proposed that this shear strain ratio (α) depends on the earthquake magnitude and can be estimated by Equation (3.1). This means that, for a magnitude of 7.5, the value of α is 0.65.

$$\alpha = \frac{M-1}{10} \tag{3.1}$$

Since the computed strain level depends on the values of the equivalent linear properties, an iterative procedure is required to ensure that the properties used in the analysis are compatible with the computed strain levels in all layers. So, the linear procedure described above is repeated several times with different G and D values (calculated for an assumed strain level) until the difference between the computed and assumed strains are below a certain tolerance.

To do this comparison, the variation of the shear modulus G and damping D with the strain level for a particular soil is required. In this work, the curves proposed by Darendeli (2001) were used. The reduction of modulus values and decreasing damping curves takes into account the confining pressure (σ'_0), the plasticity index (PI), the overconsolidation ratio (OCR), the excitation frequency (f) and the number of cycles of loading (N) as explained in what follows.

The model used for the shear modulus reduction curve is a hyperbola defined by:

$$\frac{G}{G_{max}} = \frac{1}{1+\left(\frac{\gamma}{\gamma_r}\right)^a} \tag{3.2}$$

$$\gamma_r = \left(\frac{\sigma'_0}{p_a}\right)^{0.3483} (0.0352 + 0.0010 \cdot PI \cdot OCR^{0.3246}) \tag{3.3}$$

where a is 0.9190, γ is the shear strain, γ_r is the reference shear strain (not in percent), σ'_0 is the mean effective stress and p_a is the atmospheric pressure in atm.

The damping ratio is calculated from the minimum damping ratio (D_{min}) at small strains and from the damping ratio obtained from the Masing law (D_{Masing}) using the following equations:

$$D = b\left(\frac{G}{G_{max}}\right)^{0.1} \cdot D_{Masing} + D_{min} \tag{3.4}$$

$$b = 0.6329 - 0.0057\ln(\mathrm{N}) \tag{3.5}$$

$$D_{min}(\%) = (\sigma'_0)^{-0.2889}(0.8005 + 0.0129 \cdot PI \cdot OCR^{-0.1069})[1 + 0.2919\ln(f)] \tag{3.6}$$

$$D_{Masing}(\%) = c_1 D_{Masing,a=1} + c_2 D^2_{Masing,a=1} + c_3 D^2_{Masing,a=1} \tag{3.7}$$

$$D_{Masing,a=1}(\%) = \frac{100}{\pi}\left\{4\left[\frac{\gamma - \gamma_r \ln\left(\frac{\gamma+\gamma_r}{\gamma_r}\right)}{\frac{\gamma_r{}^2}{\gamma+\gamma_r}}\right] - 2\right\} \tag{3.8}$$

$$c_1 = -1.1143\,a^2 + 1.8618\,a + 0.2533 \tag{3.9}$$

$$c_2 = 0.0805\,a^2 - 0.0710\,a - 0.0095 \tag{3.10}$$

$$c_3 = -0.0005\,a^2 + 0.0002\,a + 0.0003 \tag{3.11}$$

3.4.1.3 Non-linear approach

Although the equivalent linear approach is computationally convenient and provides reasonable results in many cases, it remains an approximation to the actual non-linear process of seismic ground response. For instance, in strong ground motions leading to very large strain levels, the equivalent linear approach may not be adequate (Pyke, 1979). An alternative approach is to analyse the actual non-linear response of a soil deposit using direct numerical integration in the time domain (Carlton and Tokimatsu, 2016). Any elastic or inelastic stress-strain model or advanced constitutive model can be used for this purpose, as for example QUIVER using the Hardin and Drnevich (1972) backbone curve (Kaynia, 2012) or the Davidenkov (1938) model for unloading-reloading with the results of the General Quadratic/Hyperbolic (GQ/H) model (Groholski et al., 2015), implemented in the 1D site response analysis program DEEPSOIL [Hashash et al. 2015). In this case, a simple elastic stress-strain soil model was used within NERA software (Bardet and Tobita, 2001).

3.4.2 Calibration of α value

The Equivalent Linear approach (ELA) was used to obtain the PGA value at the surface based on the bottom ground motion and the soil profile characteristics. As a first step, a calibration of α value was performed using non-linear analysis (NLA). As mentioned above α can be obtained by Equation (3.1) based on the earthquake magnitude. However, the equivalent linear method underestimates the acceleration in the case of deep soft soils deposits (Kausel & Assimaki, 2002) (Yoshida et al., 2002). This happens because the equivalent linear approach uses constant values of shear modulus and damping ratio for the entire spectrum of frequencies. Therefore, larger damping ratios and smaller shear moduli (associated to the large strains occurring at low frequencies) are used even in high frequencies (where the strains are smaller). This is particular important in deep soft soil deposits where the fundamental frequencies are lower. To overcome this problem Andreotti et al., (2018) suggested that the α value should be reduced to the lower boundary of this coefficient, the value of 0.2, corresponding to the most conservative PGA. In this case, the equivalent linear analysis becomes closer to the linear analysis because the strain-compatible shear modulus and damping ratio are defined for an effective strain corresponding to 80% reduction of the maximum shear strain.

To better understand this problem for this specific case, ELA analyses using α values equal to 0.2 and 0.65 were compared with NLA analyses, in order to check which α for ELA would be more appropriate for this specific site (Lower Tagus Valley area). To perform this calibration, from the 38 points, 2 points (A2 and A19) along A10 highway, in the alluvial deposits, and 1 point (BS1) in the crest of the valley (corresponding to older, consolidated deposits) were selected (Figure 3-30). Points A2, A19 and BS1 were classified as WMD, WMT and RXX respectively (Figure 3-27). Additionally, some type 1 ground motions with three different return periods were used as well as type 2 ground motions with the higher return period (2475 years).

The following parameters were assumed in the calculation of the modulus reduction and damping ratio curves:

- OCR = 1
- Number of cycles (N) = 10

- Excitation frequency = 1 Hz
- Plasticity index = 0 (for sand layers) and 30 (for clay layers)
- Soil unit weight = 20 kN/m3

The other parameters related to the height of the soil profile and the layer thickness as well as the shear wave velocity for each layer are presented below for the three selected points (Table 3-6 to Table 3-8). The shear wave velocity (V_S) of each layer was obtained using results from correlations with CPTu (preferably) or with SPT (in the absence of CPT data), and previously calibrated using adjacent measured V_S values by seismic tests (SCPTU, SDMT, Cross-Hole and SR) in these points (Viana da Fonseca et al., 2019).

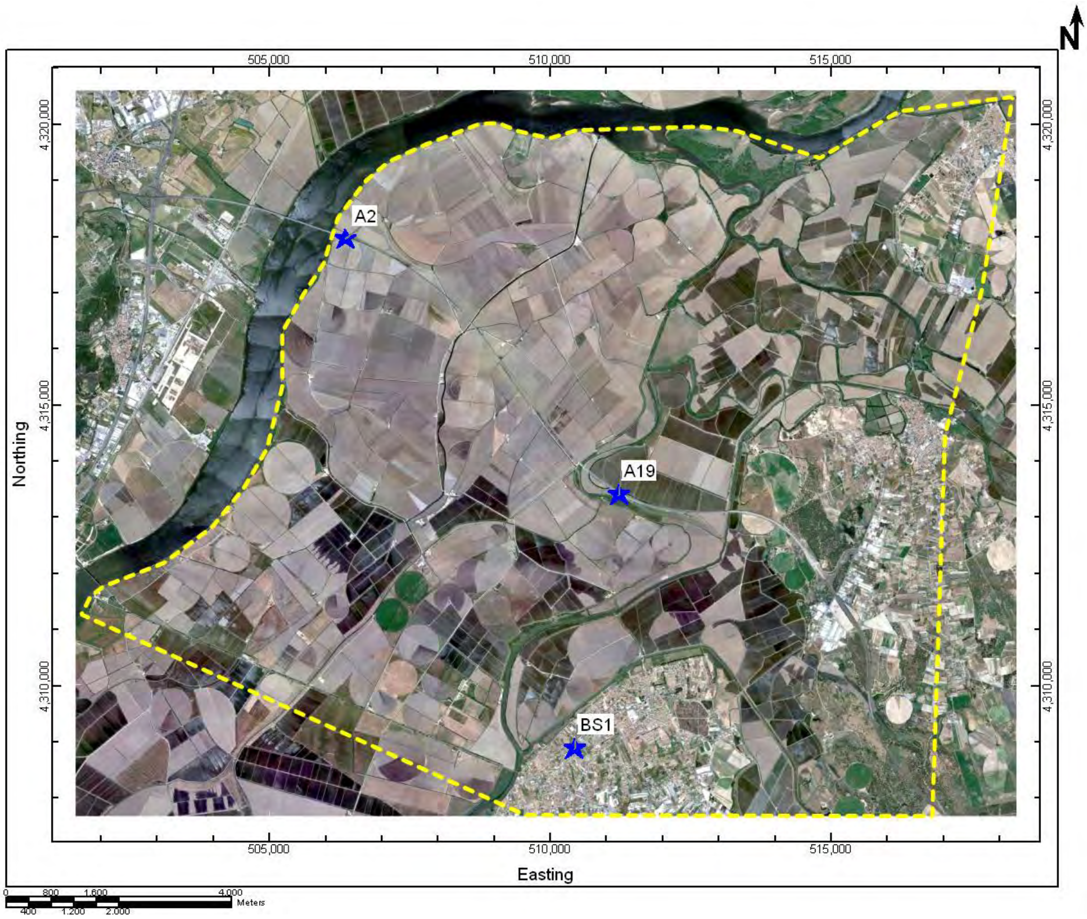

Figure 3-30 Points Location of the selected points for further analyses

Table 3-6 Soil profile for point A2 (WMD)

Layer	Soil	Thickness (m)	Depth at top of layer (m)	Vs (m/s)
1	Organic soils	0.40	0.00	220
2	a1. Clay	4.40	0.40	150
3	a3. Fine-medium Sand	3.00	4.80	168
4	a3. Fine-medium Sand	4.20	7.80	181

5	a2. Mud	3.00	12.00	188
6	a2. Mud	3.00	15.00	163
7	a2. Mud	3.00	18.00	172
8	a2. Mud	3.00	21.00	176
9	a2. Mud	3.00	24.00	170
10	a2. Mud	3.00	27.00	174
11	a2. Mud	4.50	30.00	211
12	a5. Coarse Sand (Gravel)	3.00	34.50	313
13	a5 Coarse Sand (Gravel)	3.00	37.50	318
14	a5. Coarse Sand (Gravel)	4.50	40.50	335
15	MP2. Fine-medium Sand	3.00	45.00	446
16	MP1. Clay	4.79	48.00	460
17	Bedrock		52.79	

Table 3-7 Soil profile for point A19 (WTM)

Layer	Soil	Thickness (m)	Depth at top of layer (m)	Vs (m/s)
1	Organic soils	1	0	165
2	a1. Clay	1.3	1	168
3	a2. Mud	2.2	2.3	171
4	a4. Medium Sand	3	4.5	173
5	a4. Medium Sand	3	7.5	182
6	a4. Medium Sand	3.3	10.5	189
7	a3. Fine-medium Sand	3.5	13.8	190
8	a3. Fine-medium Sand	3.5	17.3	191
9	a3. Fine-medium Sand	3.5	20.8	191
10	a2. Mud	3	24.3	189
11	a2. Mud	3.5	27.3	191
12	a2. Mud	4	30.8	204
13	a3. Fine-medium Sand	3	34.8	211
14	a3. Fine-medium Sand	3	37.8	224
15	a3. Fine-medium Sand	2.8	40.8	292
16	MP4. Coarse Sand	3	43.6	326
17	MP4. Coarse Sand	3	46.6	287
18	MP4. Coarse Sand	2.9	49.6	299
19	MP3. Medium Sand	2.3	52.5	306
20	MP1. Clay	3.5	54.8	301
21	MP1. Clay	3.56	58.3	360
22	Bedrock		61.86	

Table 3-8 Soil profile for point BS1 (RXX)

Layer	Soil	Thickness (m)	Depth at top of layer (m)	Vs (m/s)
1	Landfill	1.80	0.00	100
2	Qae1. Fine-medium Sand	2.90	1.80	158
3	Qf1. Clay	2.80	4.70	180
4	Qf3. Medium Sand	4.80	7.50	212
5	Qf1. Clay	2.90	12.30	222
6	Qf2. Fine-medium Sand	0.30	15.20	230
7	Qf3. Medium Sand	4.00	15.50	250

8	Qf4. Coarse Sand	1.83	19.50	268
9	Bedrock		21.33	

In Figure 3-31, Figure 3-32 and Figure 3-33, the ELA with two α values of 0.2 and 0.65 and NLA are compared for the selected points A2, A19 and BS1, respectively, for the three return periods of type 1 earthquake. For these cases, the surface PGA in the ELA with α equal to 0.65 is closer to the one in NLA than the one of ELA with α equal to 0.2, indicating that the 0.65 is probably the best value. According to Table 3-4 for an earthquake type 1 the magnitude is 7.8, 8.0 and 8.2 respectively for the return period of 475 years, 975 years and 2475 years, and therefore an α value of 0.68, 7.0 and 7.2 would be obtained using Equation (3.1). Since $ELA_{\alpha=0.65}$ PGA profiles plot in the middle of $ELA_{\alpha=0.2}$ and NLA PGA profiles, it is expected that higher values of α (as obtained by Equation (3.1)) would led to PGA profiles closer to NLA.

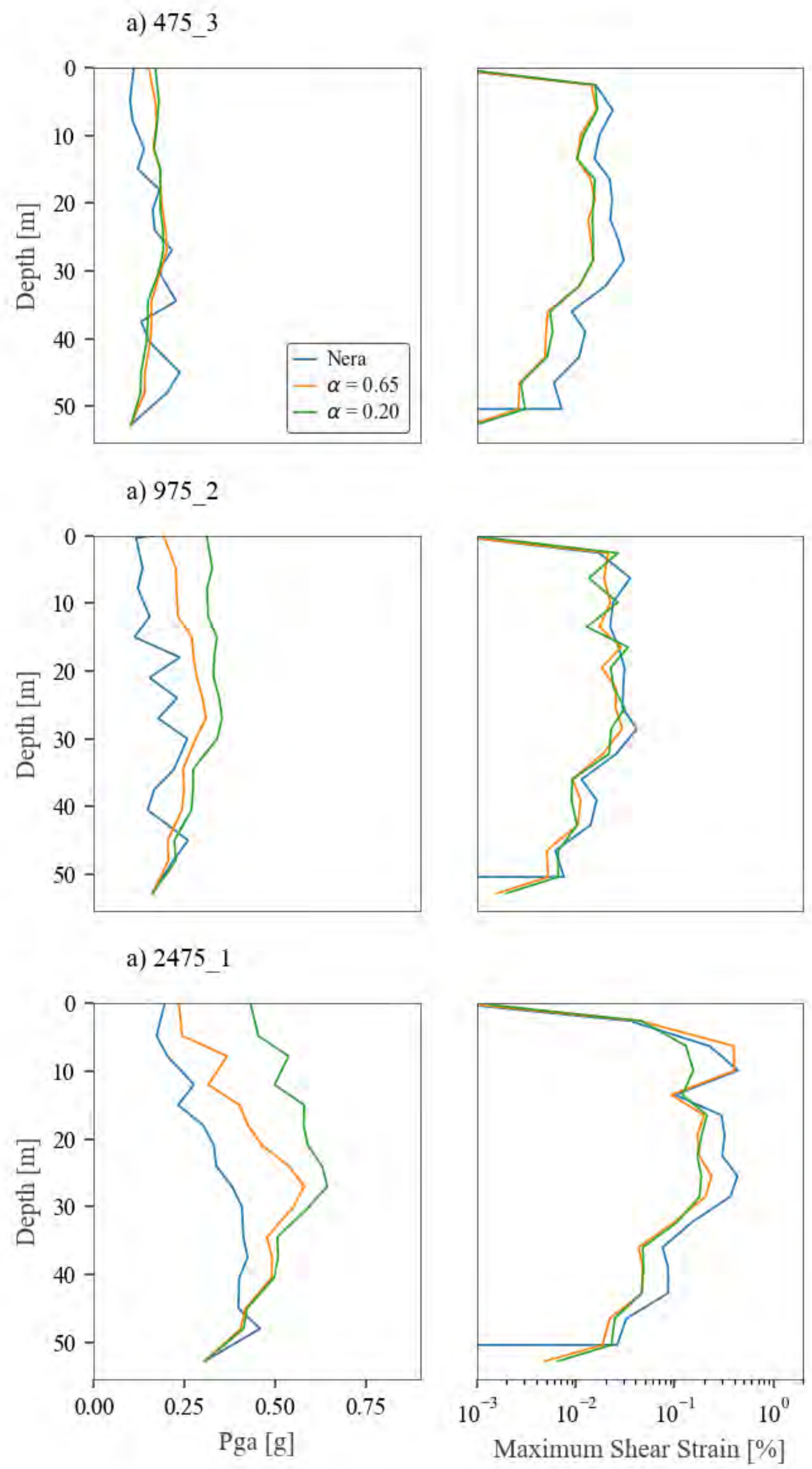

Figure 3-31 Maximum acceleration and shear strain (Point A2) with ELA for two α values and with NLA (with NERA) for the three return periods of type 1 earthquake: a) 475 years, b) 975 years and c) 2475 years.

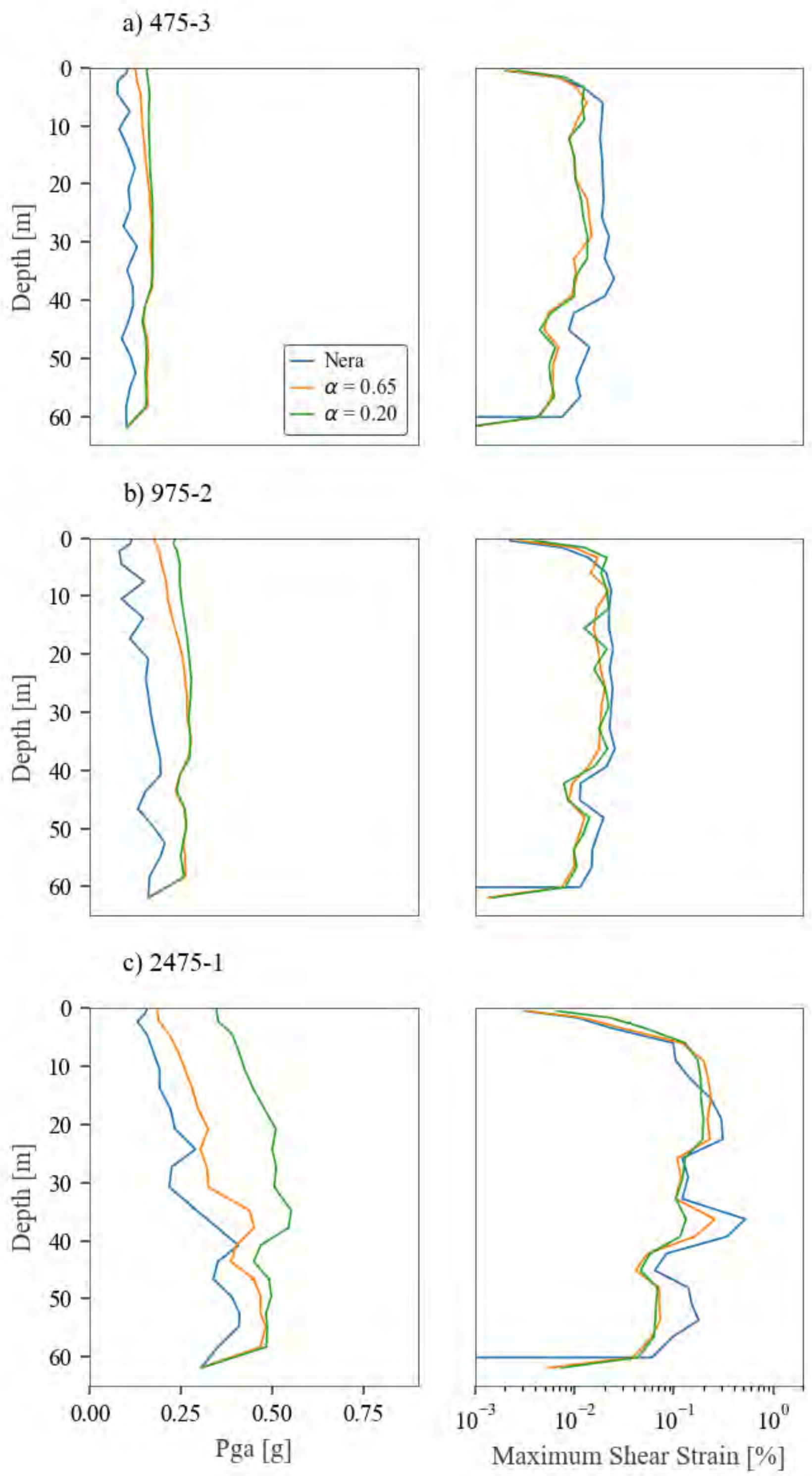

Figure 3-32 Maximum acceleration and shear strain (Point A19) with ELA for two α values and with NLA (with NERA) for the three return periods of type 1 earthquake: a) 475 years, b) 975 years and c) 2475 years.

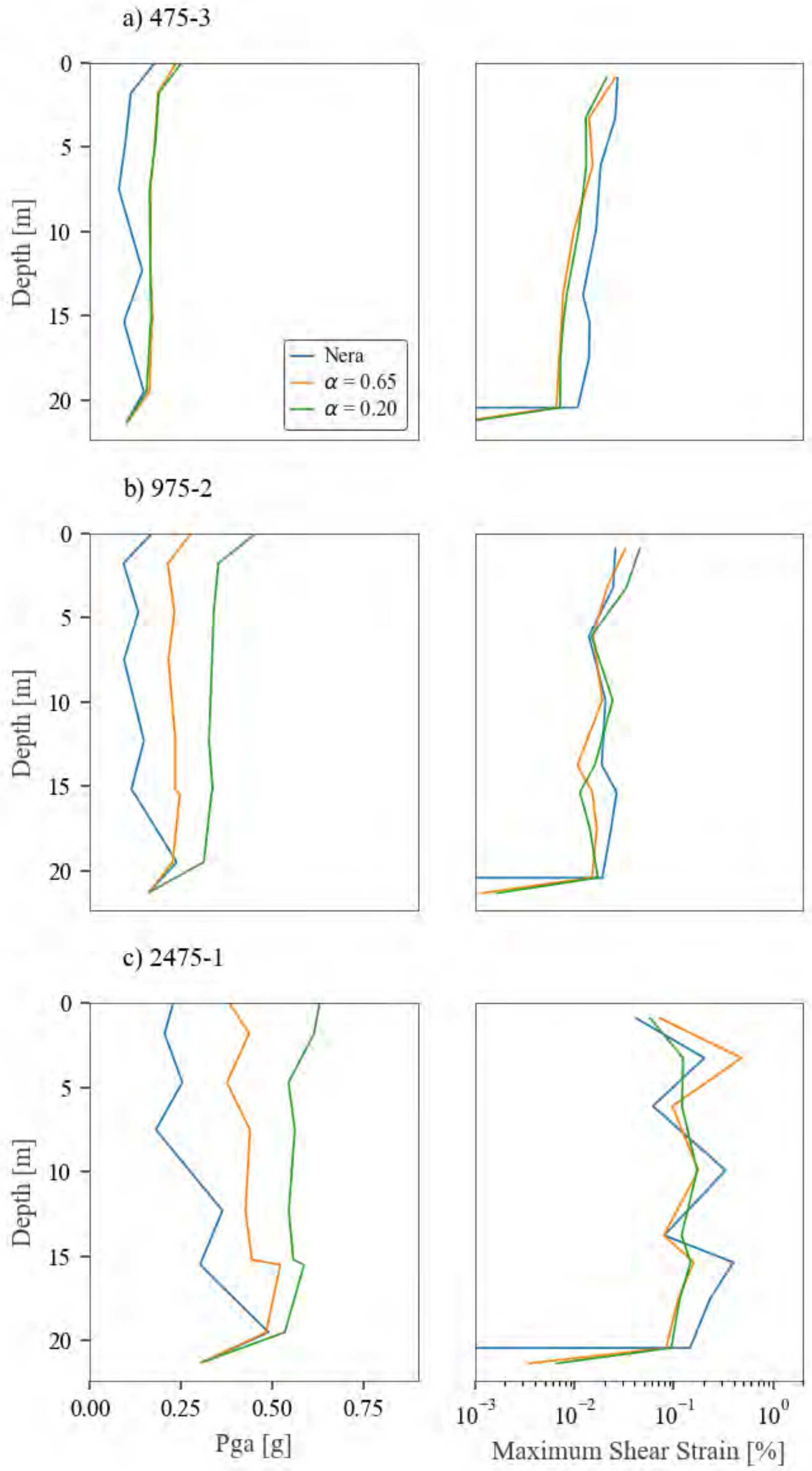

Figure 3-33 Maximum acceleration and shear strain (Point BS1) with ELA for two α values and with NLA (with NERA) for the three return periods of type 1 earthquake: a) 475 years, b) 975 years and c) 2475 years.

This project has received funding from the European Union's Horizon 2020 research and innovation programme under grant agreement No. 700748

For point A2, an uncertainty related to the position of the bedrock led to the analysis of three different options (A, B and C) compared in Figure 3-34 and in Figure 3-35. The deeper soil profile option (A2-A) is shown in Table 3-6 and the results were plotted in Figure 3-31. For the A2-B option, the first 40.5 meters (14 layers) were considered and for A2-C option, just the first 30 meters (11 layers) were considered. Figure 3-34 shows the maximum acceleration profiles for the three return periods (type 1) and Figure 3-35 shows the maximum shear strain for the same ground motions. The plots in the first column show the results using NLA, the second column shows the results using ELA for α equals to 0.65 and the third column shows the results using ELA for α equals to 0.20. In each graph, the three lines represent the different depths considered for the point A2 (Table 3-6). It is clear that a very similar pattern was observed for the three profiles.

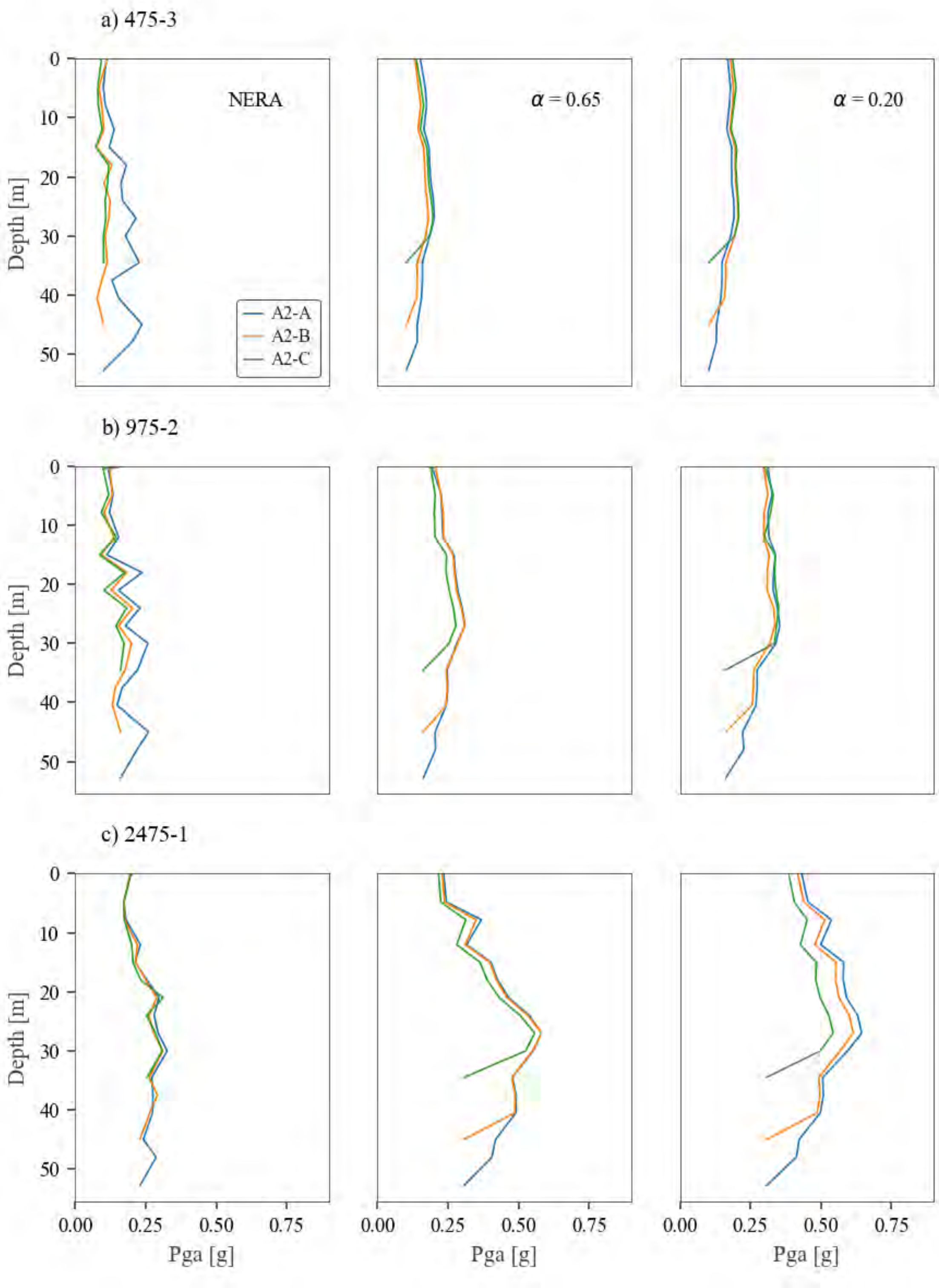

Figure 3-34 Maximum acceleration for different positions of the bedrock (Point A2) with ELA for two α values (columns 2 and 3) and with NLA (with NERA – column 1) for the three return periods of type 1 earthquake: a) 475 years, b) 975 years and c) 2475 years.

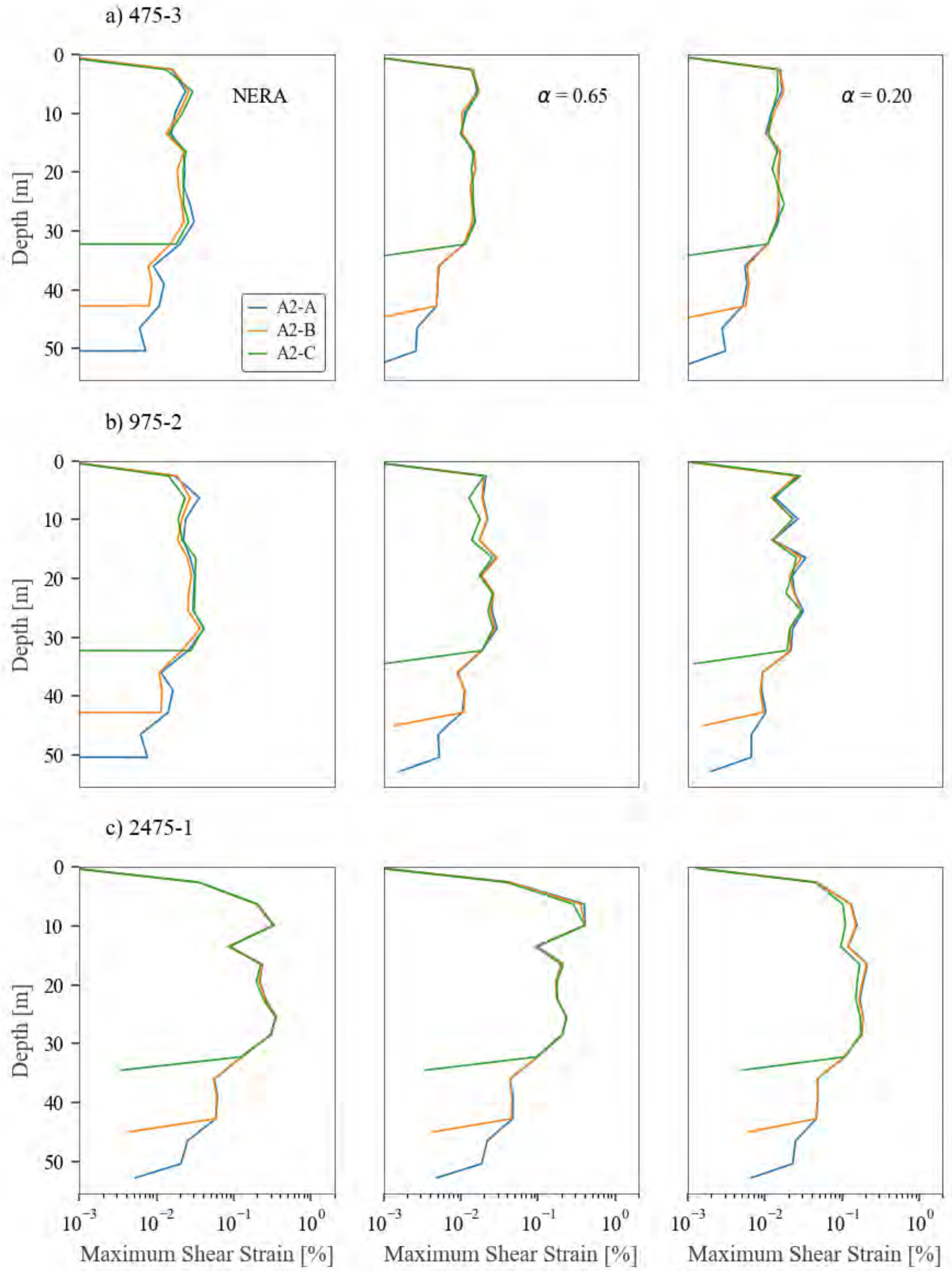

Figure 3-35 Maximum shear strain for different positions of the bedrock (Point A2) with ELA for two α values (columns 2 and 3) and with NLA (with NERA – column 1) for the three return periods of type 1 earthquake: a) 475 years, b) 975 years and c) 2475 years.

It is now interesting to see what happens when a type 2 earthquake is used. As observed in Figure 3-34 and Figure 3-35, the results obtained for the three profiles are very similar. For that reason, in Figure 3-36 the results are presented just for one profile (A2-A indicated in Table 3-6). As seen before the $ELA_{\alpha=0.65}$ plots in the middle of $ELA_{\alpha=0.20}$ and NLA indicating that the value of 0.65 is still the most appropriate for this case. It should be noted that in this case, the alpha values calculated with Equation (3.1) are lower than 0.65 (0.56, 0.58 and 0.60 for 475, 975 and 2475 years) since the magnitudes are also smaller. Consequently, it was expected that for this case the NLA would be situated in the middle of the two ELA analysis. However, this was not verified, since the $ELA_{\alpha=0.65}$ results are still closer to those from NLA. Considering these comparisons, the value of 0.65 was considered most appropriate for the general analyses and finally adopted.

In addition, it should be noted that the maximum shear strains obtained in NLA are always much closer to the $ELA_{\alpha=0.65}$ than to $ELA_{\alpha=0.20}$ for all studied cases. Regarding the values obtained for the induced shear strains, it should be highlighted that the high values obtained with NLA (especially for the higher return period where values of 0.7% were achieved) can be considered excessive for an ELA approach. Still, for the present work, and in view of the amount of analyses to cover the large area for microzonation purposes, it was decided to proceed.

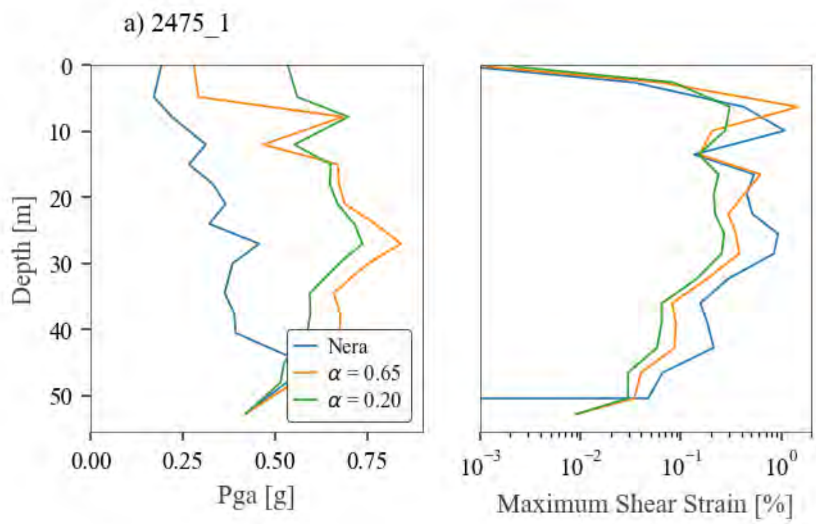

Figure 3-36 Maximum acceleration and shear strain in point A2-A for type 2 earthquake and return period of 2475 years

To support the previous studies evaluated in specific points, and in view of the shape of the Low Taggus Valley in this area, a site-factor sensitivity study was performed. The transfer function in one of the sections of the valley was analysed in non-linear elastic analysis using a Finite Difference model in FLAC®, to understand how would the valley transversal geometry could affect the surface PGA, that is, to analyse if the valley amplifications can lead to higher α values, as obtained in the previous calculations.

The 475 and 2475 years ground motions (type 1) were selected to be applied in the base of the numerical model and the accelerations at the surface were measured to be compared with the ELA results. The considered soil profile model has a total thickness of 75 m and width of 10.000 m (Figure 3-37a). The lateral nodes (vertical boundaries) at each depth were attached so they could move together. Elastic model was used to represent the behaviour of the soils and the same soil parameters used in the ELA were used.

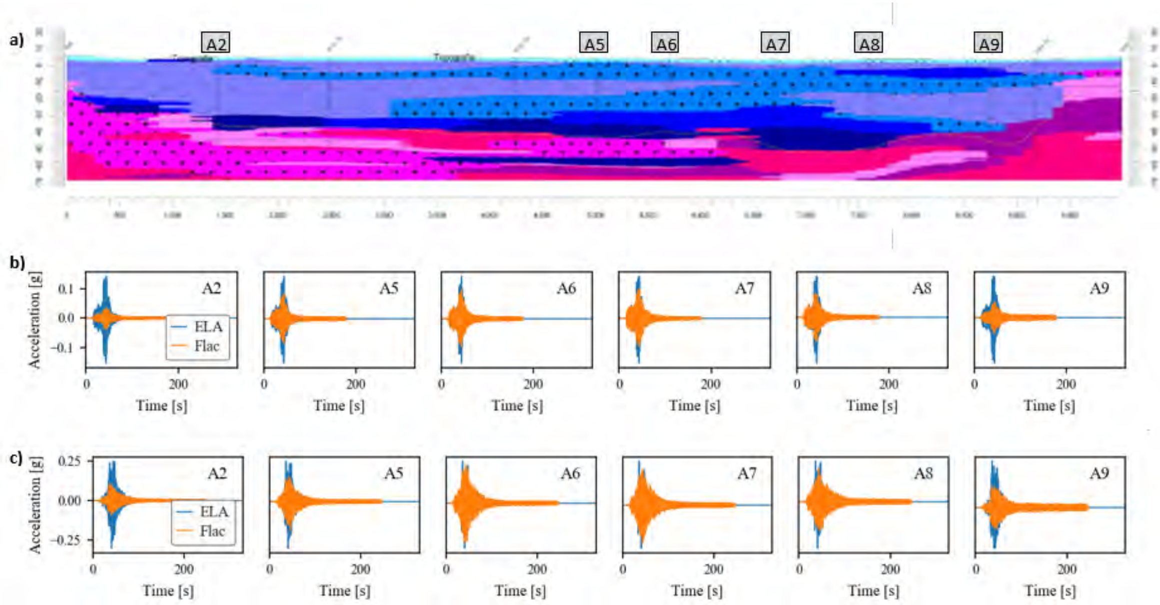

Figure 3-37 a) FLAC® 2D non-linear model ; b) Results for ground motion 475-4; c) Results for ground motion 2475-3

Figure 3-37b and Figure 3-37c show the comparison between numerical model and ELA results in 6 points along A10 highway. For the points in the middle of the valley (A6 and A7) where the stiffer material is deeper the surface accelerations are in close agreement with ELA results. At the points where the stiffer material is shallower (A2 and A9) the surface acceleration results obtained with ELA are more conservative.

In view of these results, the 1D analyses equivalent linear analysis were considered appropriate for microzonation purposes, taking into account the large area involved in the Portuguese Pilot-Site.

3.4.3 Site response results

After comparing ELA, NLA and numerical modelling results, the surface acceleration time series for the 38 points in the Tagus valley area were estimated using ELA using an α equal to 0.65. Figure 3-38 shows the PGA values calculated from surface accelerations for the 38 points. The PGA values for the type 2 earthquakes (T2-RP1, T2-RP2 and T2-RP3) are higher than PGA values for type 1 earthquakes, as expected. In addition, PGA values for RP3 earthquakes (return period of 2475 years) are higher than PGA values for RP2 earthquakes (return period of 975 years) and the latter are higher than PGA values for RP1 earthquakes (return period of 475 years).

Figure 3-39 shows the amplification factors ($PGA_{surface}/PGA_{bedrock}$) for the 38 points. Amplification factors for RP1 earthquakes (return period of 475 years) are higher than one in most points, which means that the bedrock earthquake was amplified by the soil deposit. For the higher return periods (975 and 2475 years) the bedrock earthquake was de-amplified by the soil deposit.

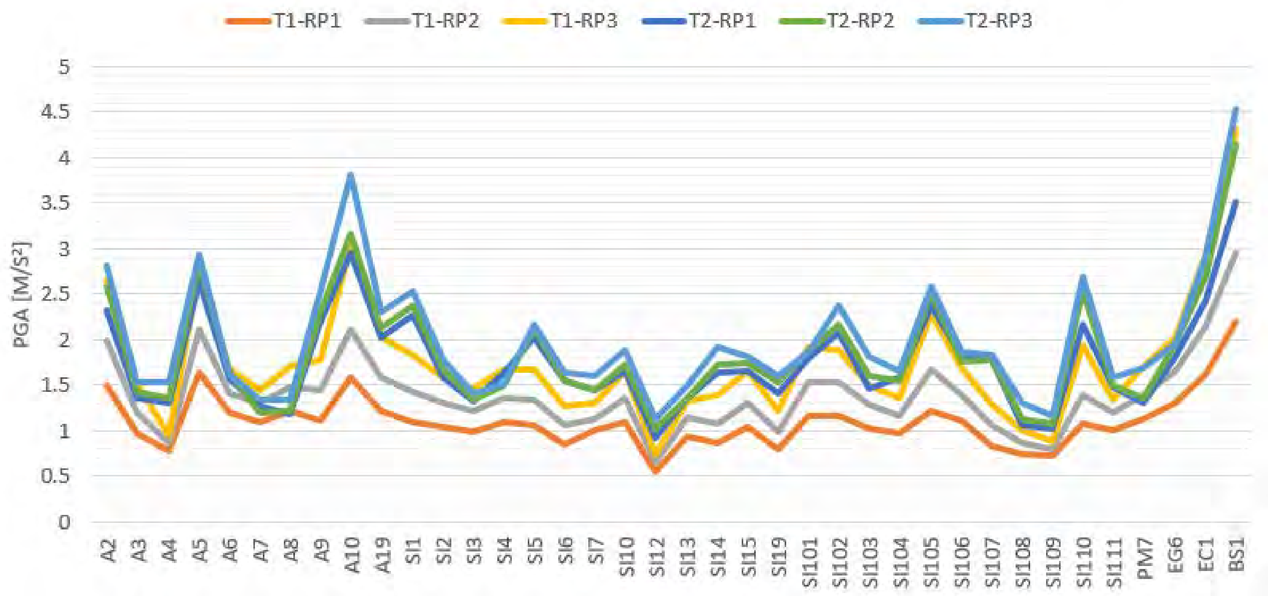

Figure 3-38 PGA values at surface from ELA (α equal to 0.65)

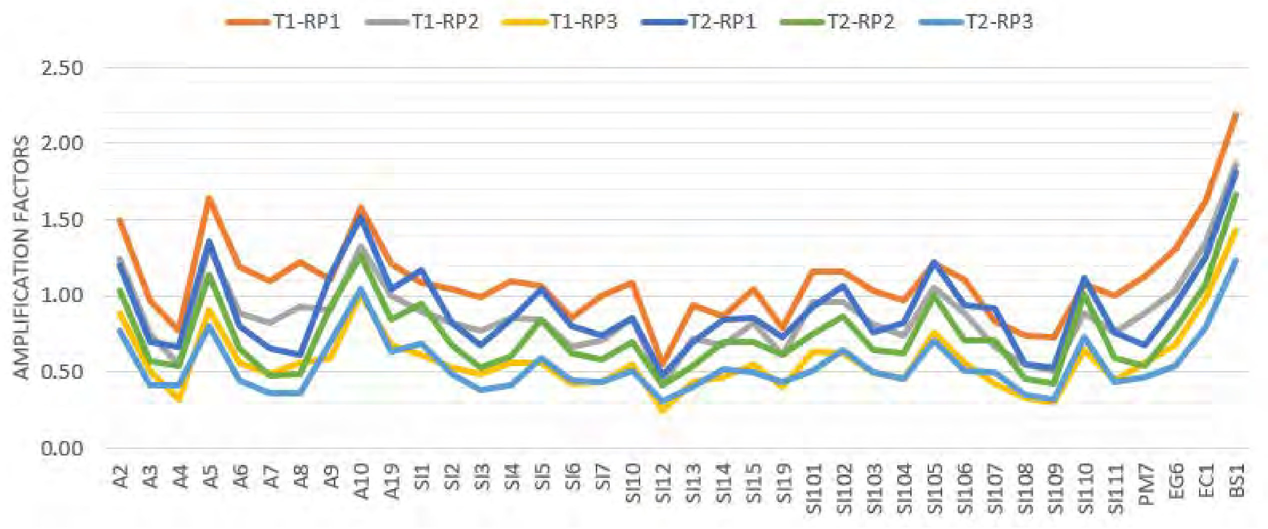

Figure 3-39 Amplification factors ($PGA_{surface}/PGA_{bedrock}$)

3.4.4 Site response considering liquefaction

Bouckovalas et al (2017) developed an adapted method called the "Spectral Envelope Method", where an equivalent linear analyses is performed for the pre and post liquefaction segments of the ground motion, with the pre liquefaction segment using non-liquefied properties and the post-liquefaction segment using liquefied properties similar to Miwa & Ikeda (2006). Bouckovalas et al. (2017) provided further guidance on the choice of post-liquefaction damping ratios, and validated the proposed method against numerical analyses and recorded ground motions in the field.

A recent method developed by Millen et al. (2019b) called the equivalent linear Stockwell analysis method, was used in this project to consider liquefaction in the Low Taggus River Pilot-Site response analysis. This method extends the work by Bouckovalas et al. (2017) and performs it in the time-frequency domain to obtain a surface acceleration time series. It creates a time-frequency transfer function between the upward propagating and surface motion to identify liquefaction triggering using the Stockwell transform. The upward propagating motion is first converted into the Stockwell transform in the time-frequency domain and then a series of excess pore pressure (time) dependent base-to-surface transfer functions are applied along the frequency axis before performing the inverse Stockwell transform to obtain the surface motion in the time domain.

The same three points selected in section 3.4.2 (A2, A19 and BS1) were used to obtain the surface motion using this method. The CPTu data was interpreted using CPeT-IT®, a software package for the interpretation of Cone Penetration Test (CPT) data based on the Robertson (2009) methodology, to calculate some parameters of the soil. Table 3-9 contain a summary with all the parameters.

The strain energy based method (SEBM) presented recently by Millen et al. (2019c), was used to estimate the pore pressure time series.

Table 3-9 Soil parameters for the A2, A19 and BS1 points

Parameter/Point	**A2**	**A19**	**BS1**
Properties of layer 1			
Height, H1 [m]	7.8	4.8	3.0
Unit weight, γ_{dry} [kN/m^3]	15.6	15.1	15.1
Specific gravity, Gs	2.7	2.7	2.7
Poisson ratio, v	0.35	0.35	0.35
Initial shear modulus, G_{max} [MPa]	31.2	17.4	12.6
Undrained strength, Su [kPa]	58.2	34.5	33.9
Permeability, k_1[m/s]	1.25e-05	5.43e-08	3.97E-07
Properties of layer 2			

Height, H2 [m]	4.3	1.9	9.0
Unit weight, γ_{dry} [kN/m^3]	17.2	17.1	17.0
CSR_n15	0.137	0.139	0.600
Poisson ratio, v	0.3	0.3	0.3
Relative density, Dr [%]	40.2	48.7	50.8
Constant volume friction angle, ϕ_{cv} [°]	33.0	33.0	33.0
Initial shear modulus, G_{max} [MPa]	62.8	58.3	46.7
Minimum void ratio, e_{min}	0.5	0.5	0.5
Maximum void ratio, e_{max}	0.8	0.8	0.8
Permeability, k_2[m/s]	1.28e-05	4.66e-05	9.53E-05
PM4Sand hpo factor	$h_{po} = \dfrac{CSR_{target} \cdot (2.05 - (2.4 * D_r))}{1 - CSR_{target} \cdot (12.0 - (12.5 * D_r))}$		
Normalised shear modulus, G_0	$G_0 = 167\sqrt{(N_1)_{60} + 2.5} \cdot [0.7 - 1.5]$		

Properties of layer 3			
Height, H3 [m]	17.9	23.3	18.0
Unit weight, γ_{dry} [kN/m^3]	15.2	16.4	16.0
Specific gravity, Gs	2.7	2.7	2.7
Poisson ratio, v	0.35	0.35	0.35
Initial shear modulus, G_{max} [MPa]	32.2	50.8	40.5
Undrained strength, Su [kPa]	41.5	81.3	53.4
Permeability, k_3[m/s]	2.43e-09	4.02e-06	5.06E-09

Profile A19 presented liquefaction when the highest return period (2475 years) was used. Figure 3-40 shows the surface acceleration time series for the three points selected when an earthquake type 1 and return period of 2475 years is used. Figure 3-41 shows the PGA values and amplification factors ($PGA_{surface}/PGA_{bedrock}$) calculated for the 3 points.

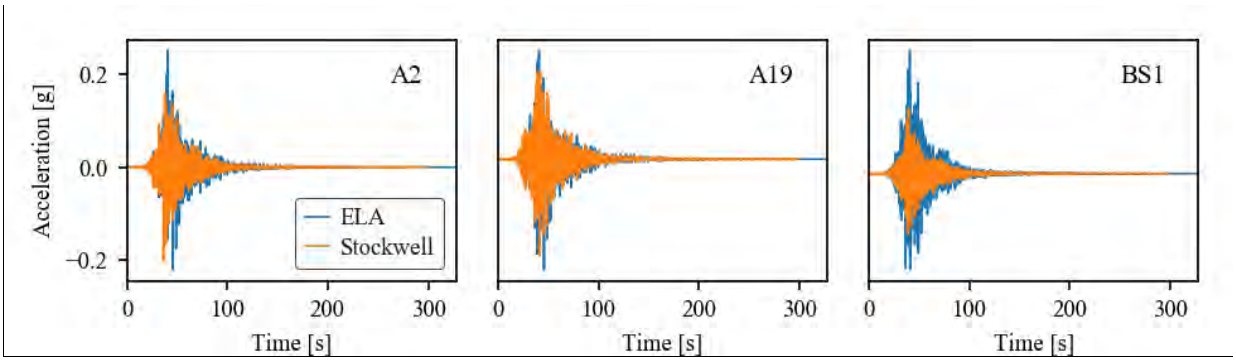

Figure 3-40 Surface acceleration time series considering liquefaction using Stockwell transfer function.

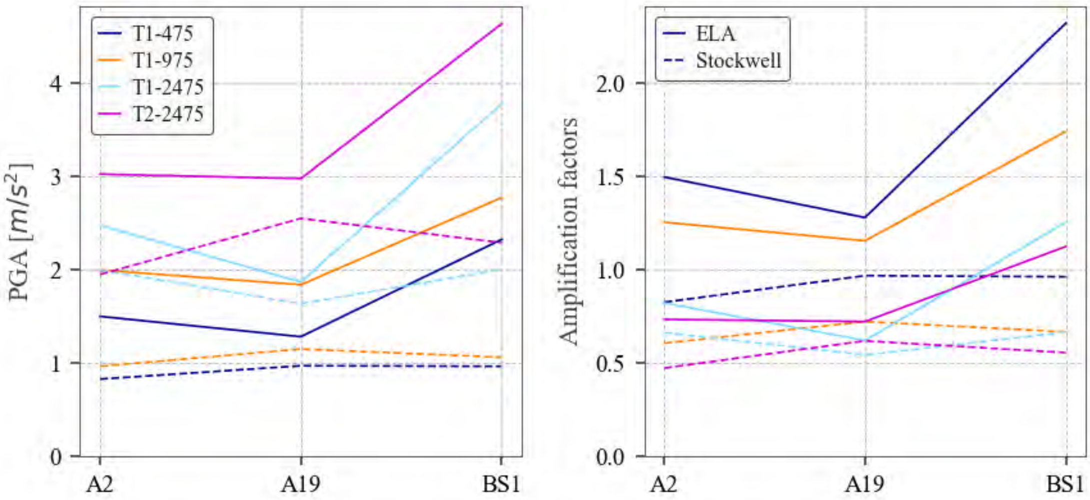

Figure 3-41 Surface acceleration time series considering liquefaction using Stockwell transfer function.

As expected, the values of PGA expressed in Figure 3-41 change significantly when the effect of the increase in pore pressure is taken into account, which was thoroughly discussed in Deliverable 3.2 (Viana da Fonseca et al. 2018a). For the purpose of the elaboration of seismic hazard maps in microzonation for risk assessment of infra and superstructures laying in soil profiles with liquefiable layers, these values should be taken into account.

Naturally, the expected decrease in the PGA values on the ground surface in such profiles or areas (at local or regional level) is not necessarily a favourable factor. In fact, being the amplification factors expressed in Figure 3-41 lower than one (others would have similar trends depending on the earthquake ground motion at the rock – this depending on the magnitude and distance to the epicentre), it shall not be dissociated to the other factors that are responsible for EILD (Earthquake Induced Liquefaction Damages), like the induced vertical settlements due to the increase of pore pressure in contractible soils when loaded cyclically, specially due to the increase in shear strains.

Soil deformations (vertical settlements – total and differential - and horizontal displacements – lateral spreading) largely condition soil-liquefaction-foundation-structure interaction (SLFSI) and, while the new ground motion at the surface has lower values of PGA, the vulnerability analysis has to congregate these two demands (shaking and settlements). This substructuring was developed in Deliverable 3.2 for modelling differential settlements and soil-foundation-structure interaction, overcoming some of the issues of superposition by considering rates of deformation rather than loads and forces. A loss assessment procedure developed in Deliverable 3.3 (Viana da Fonseca et al. 2018b) has effectively taken this into account.

To cope with this complexity, in future works maps should consider not only peak ground acceleration (PGA), but other parameters that can integrate the energy transmitted to the structures, but also the damages induced by settlements (facing vulnerability). Some indices can be envisaged, like, peak spectral acceleration at the effective period of 0.654 s (Sa_t,eff between 0.26 and 17.15 m/s^2), and the average of the spectral acceleration (Sa_av) from the shortest possible first mode period of 0.248 s (which represent intact infills and no liquefaction) to the longest possible period of 1.060 s (which represent no infills yielding structure and liquefaction). Besides, other intensity measures that represent cumulative energy, like Cumulative Absolute Velocity (CAV), Arias Intensity (I_a), and Unit Kinetic Energy (UKE), would be more representative of the input demand to evaluate EILD, the main purpose of the Microzonation for Liquefaction Risk, presented in what follows. The intensity measures should be calculated for two times the upward propagating motion, and therefore compatible with ground motion prediction equations for surface quantities, except for in the case of soft soil on very shallow bedrock (Viana da Fonseca et al., 2018a).

3.4.5 Final microzonation maps

From the ground motion analyses previously described, the following microzonation maps have been produced, in terms of surface peak acceleration (m/s^2) and factor of amplification (computed in relation with the PGA at the rock). These maps are presented for the six different seismic scenarios in Figure 3-42 (Type 1, return period 1) to Figure 3-47 (Type 2, return period 3).

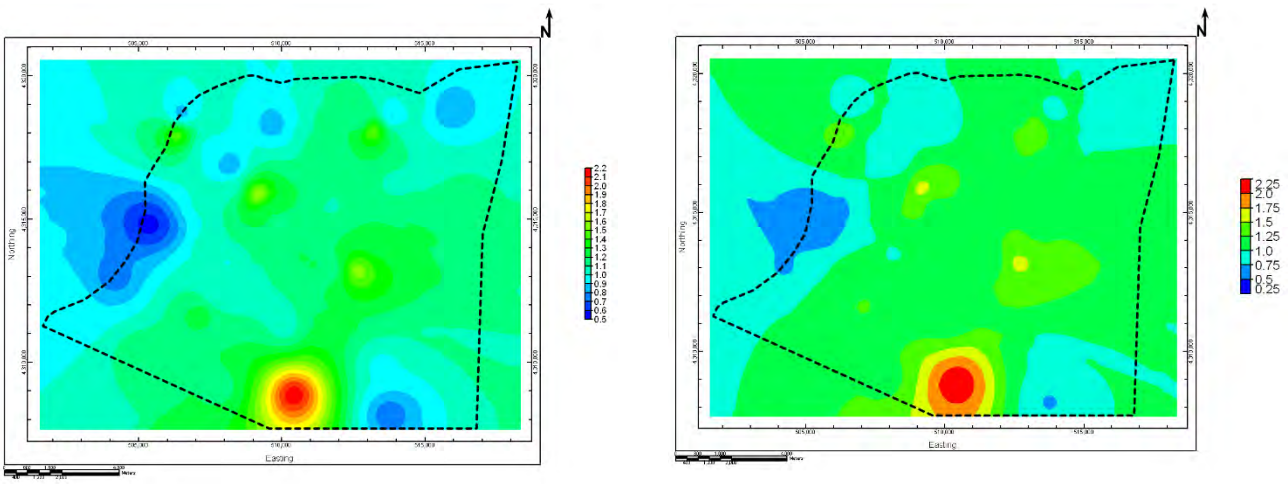

Figure 3-42 Site response analysis results for seismic action T1-RP1 (475 y): a) PGA; b) FA

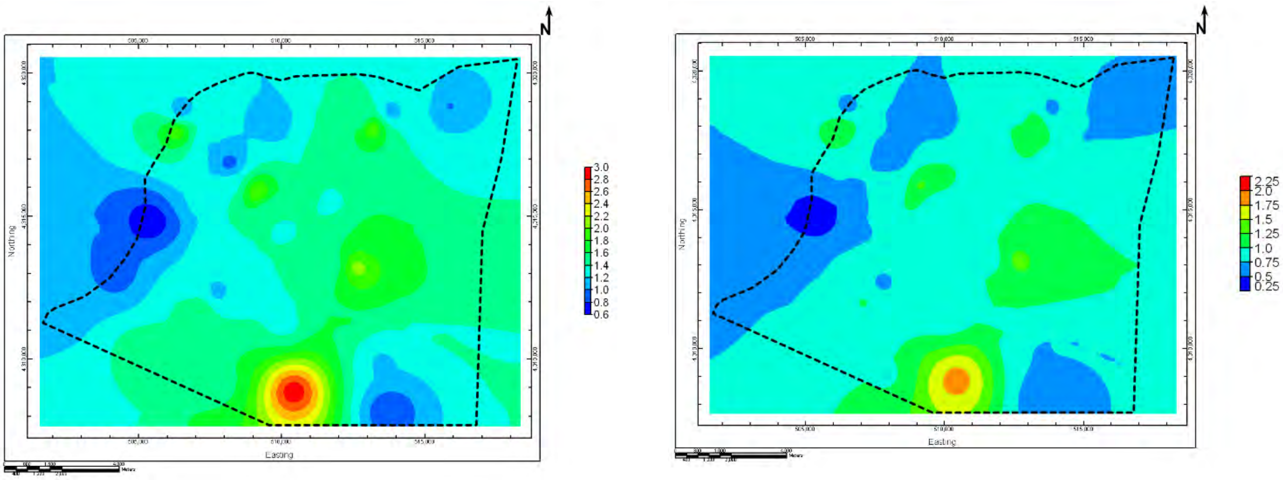

Figure 3-43 Site response analysis results for seismic action T1-RP2 (975 y): a) PGA; b) FA

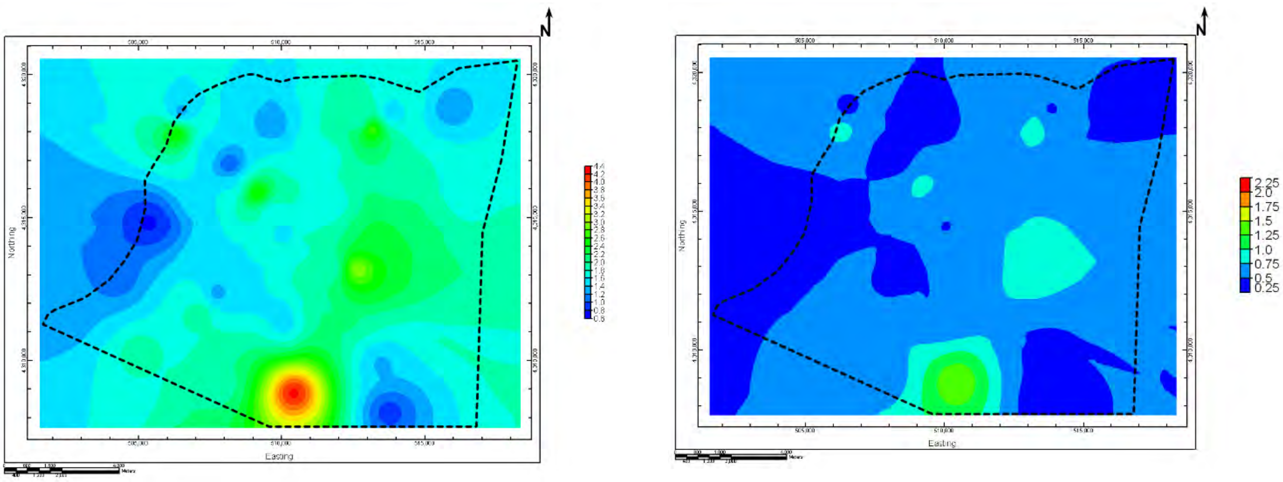

Figure 3-44 Site response analysis results for seismic action T1-RP3 (2475 y): a) PGA; b) FA

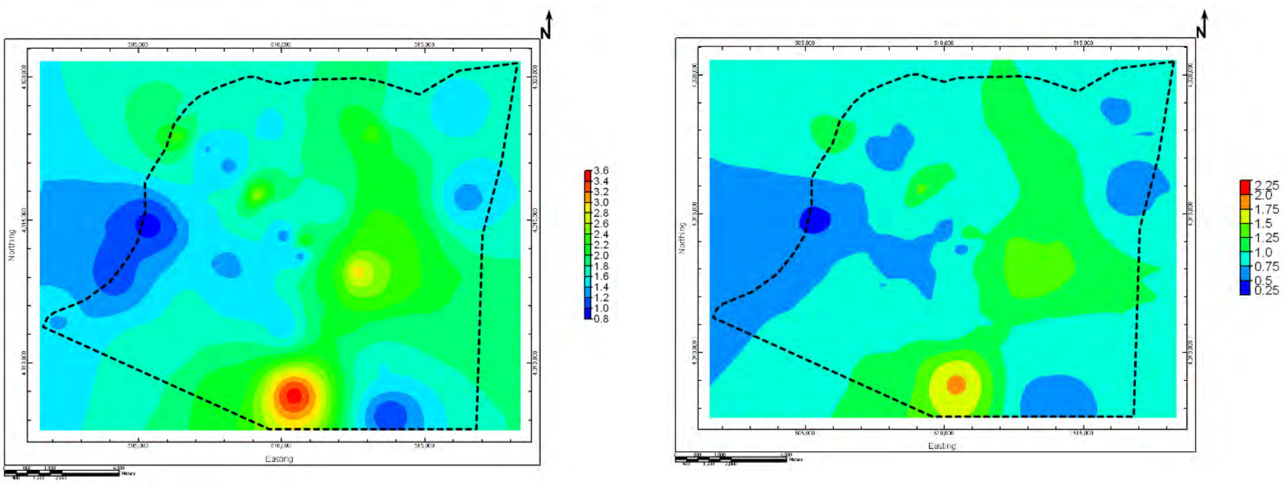

Figure 3-45 Site response analysis results for seismic action T2-RP1 (475 y): a) PGA; b) FA

This project has received funding from the European Union's Horizon 2020 research and innovation programme under grant agreement No. 700748

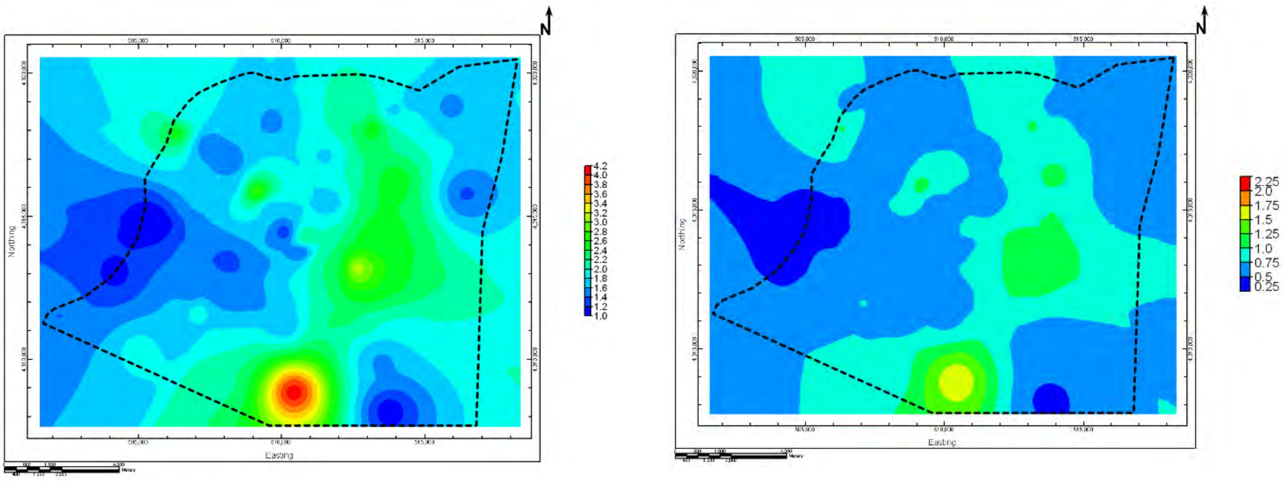

Figure 3-46 Site response analysis results for seismic action T2-RP2 (975 y): a) PGA; b) FA

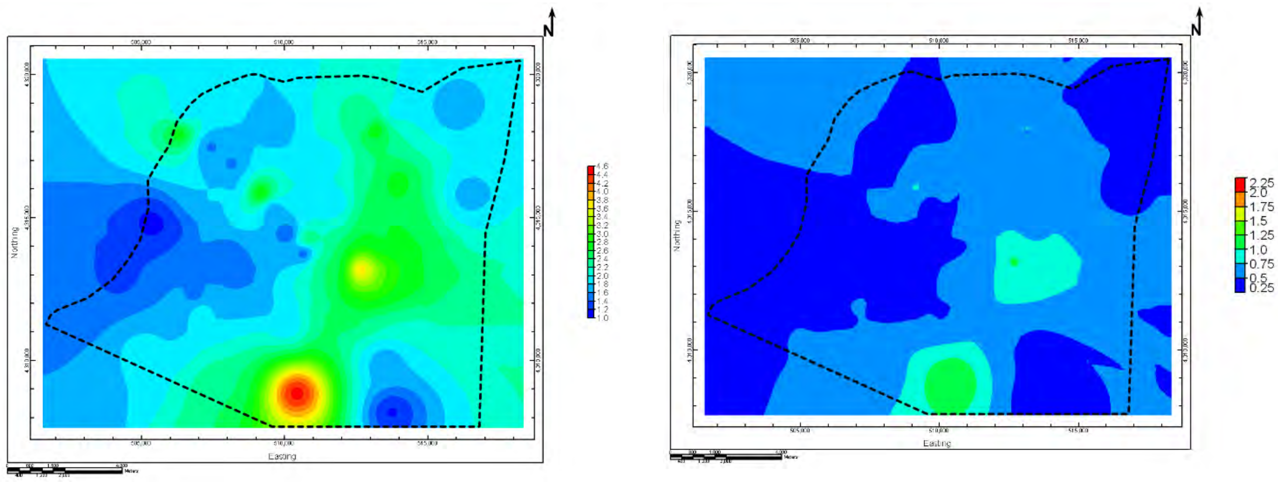

Figure 3-47 Site response analysis results for seismic action T2-RP3 (2475 y): a) PGA; b) FA

3.5 Microzonation for liquefaction risk

3.5.1 Microzonation 3D models of CRR

The microzonation for liquefaction risk has initiated, based on the numerous in situ SPT and CPT results, from which the cyclic resistance ratio (CRR) of the soils was computed in depth.

For the purpose of illustrating the hazard-independent liquefaction resistance of the soils of the pilot site, 3D models of the cyclic resistance ratio have been produced from the SPT (Figure 3-48) and CPT (Figure 3-49) results. Since both figures show considerable differences, the two sets of data were combined in a similar 3D model, as shown in Figure 3-50, and using fences, for a number of selected cross-sections, as shown in Figure 3-51.

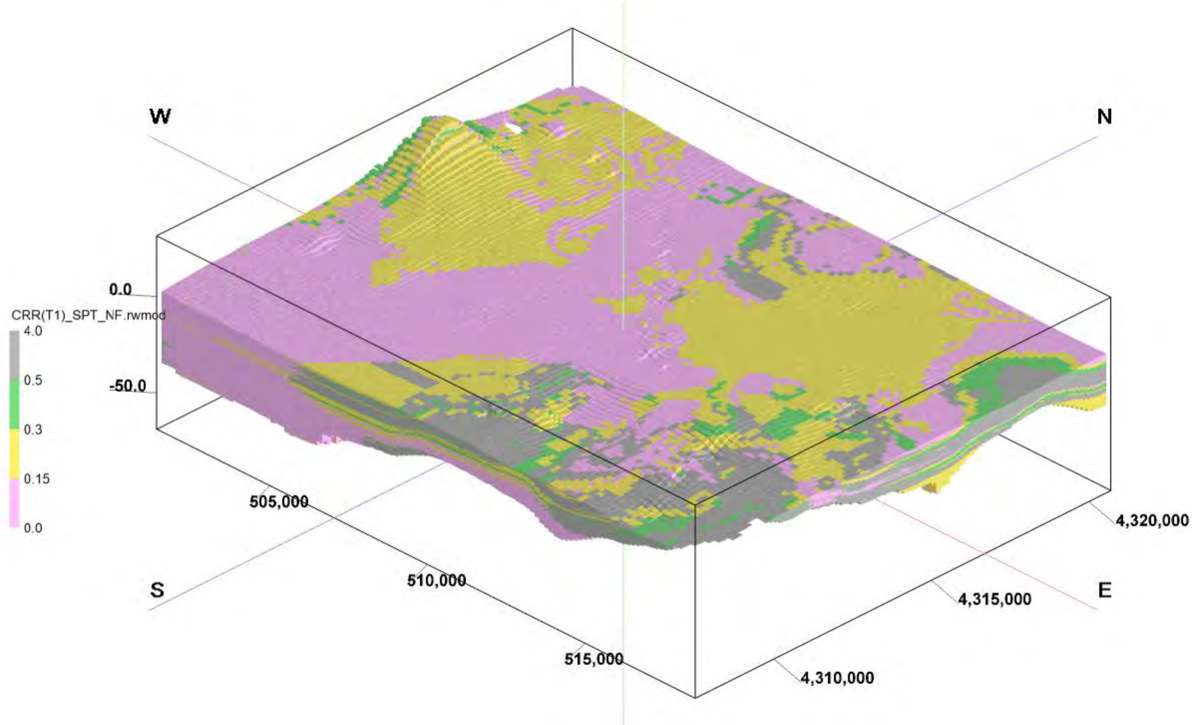

Figure 3-48 CRR 3D model obtained from the analysis of SPT results

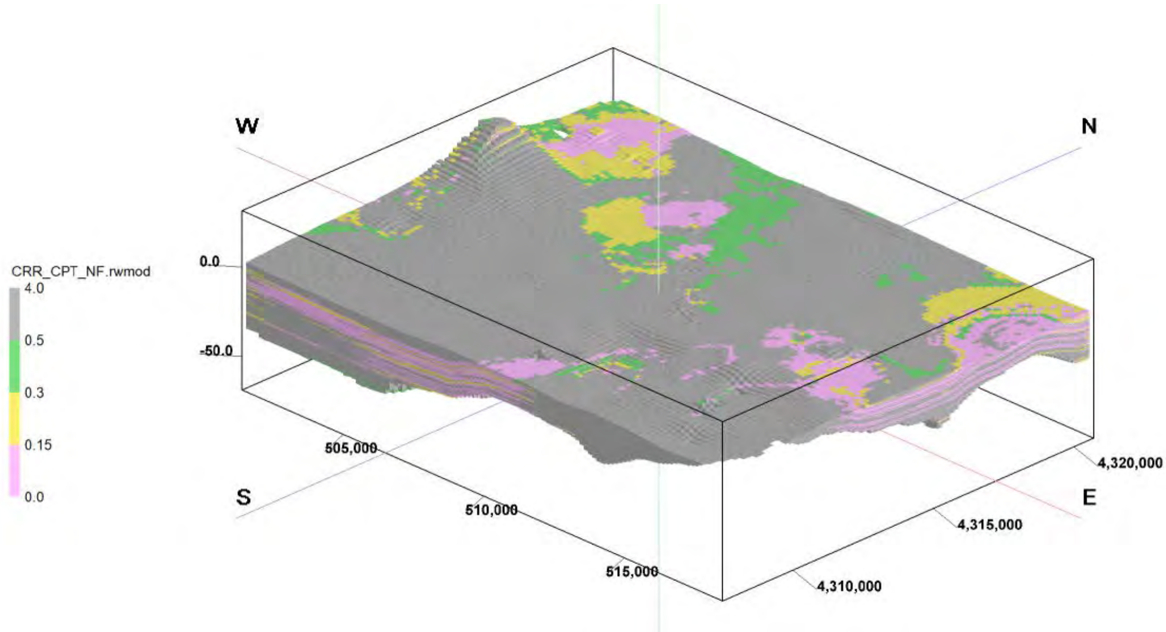

Figure 3-49 CRR 3D model obtained from the analysis of CPT results

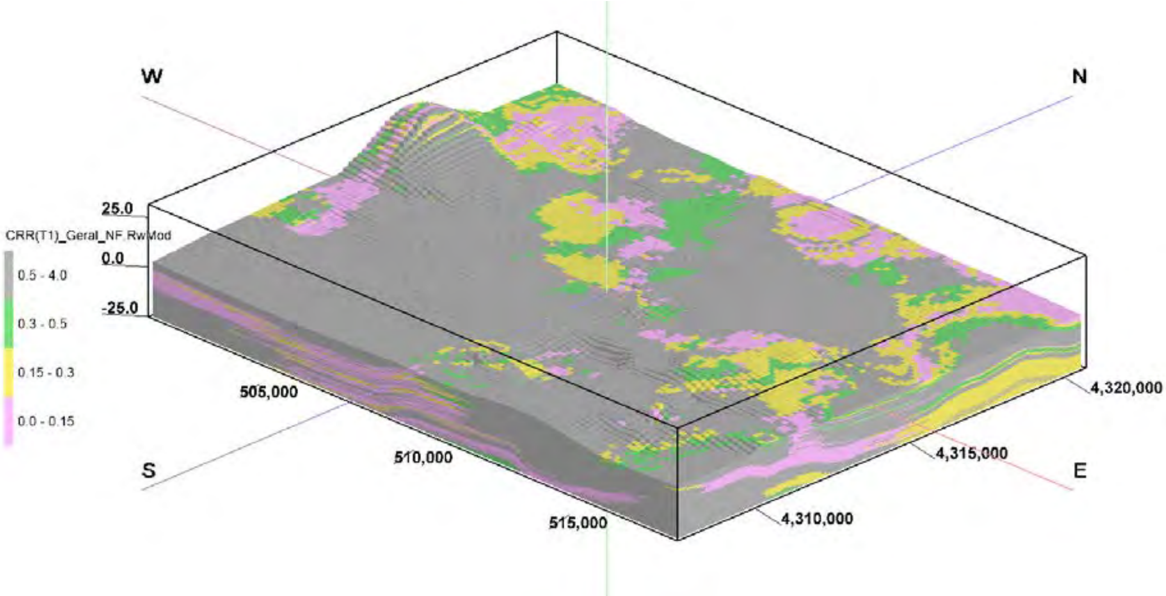

Figure 3-50 Combined CRR 3D model obtained from the analysis of SPT and CPT results

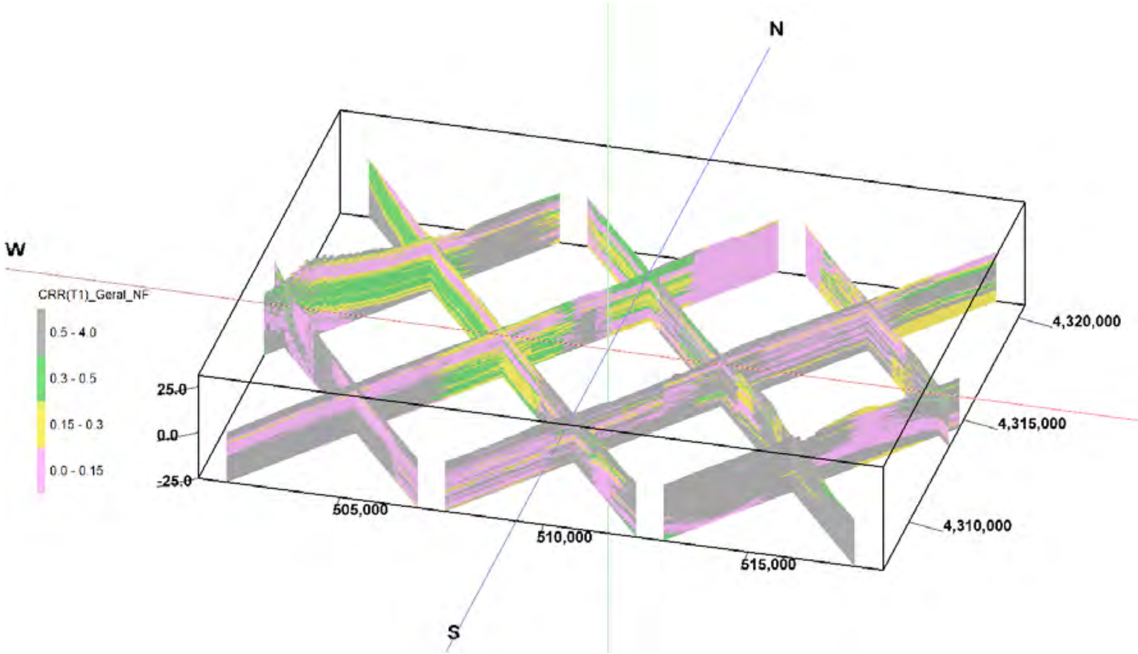

Figure 3-51 Fences (cross-sections) of the 3D-model of the combined CRR obtained from the analysis of SPT and CPT results

The differences in the independent calculation of CRR from SPT and CPT, evidenced in the comparison between Figure 3-48 and Figure 3-49, are a consequence of the type and nature of the tests. While the SPT provides one data point every 1 to 1.5 meters, the CPT data points are usually acquired every 1 to 2 cm. In addition, the methods for calculating CRR for the SPT and the CPT differ, since more parameters are registering with depth from the CPT acquisition. In effect, the CPT provides reliable quantitative indication of the type of soil at each depth, through the calculation of SBT and Ic, instead of the generic and qualitative lithological description of the SPT. This is particularly relevant to liquefaction assessment, given the impact of the soil type and, especially, the fines content in the analysis. For this reason, it was decided to use SPT-based liquefaction analysis only at a preliminary stage, for a general overview of the region. For the final stage of microzonation of the pilot site, only CPT(u)-based liquefaction assessment analysis were considered, to ensure an adequate level of confidence and reliability of the results.

3.5.2 Microzonation 3D models of the factors of safety

The microzonation for liquefaction risk has initiated considering the standard seismic type actions of Eurocode 8 (Type 1 – large distant earthquake; Type 2 – medium near earthquake), prior to the implementation of the ground response analyses and the respective microzonation for ground shaking.

Subsequently to the CRR calculations, the factors of safety against liquefaction (FS) have been computed, considering the Eurocode 8 seismic actions, designated EC8-T1 and EC8-T2. Since the factor of safety changes in depth, the visualization of the results requires 3D modelling of the site, as provided in Figure 3-52 and Figure 3-53.

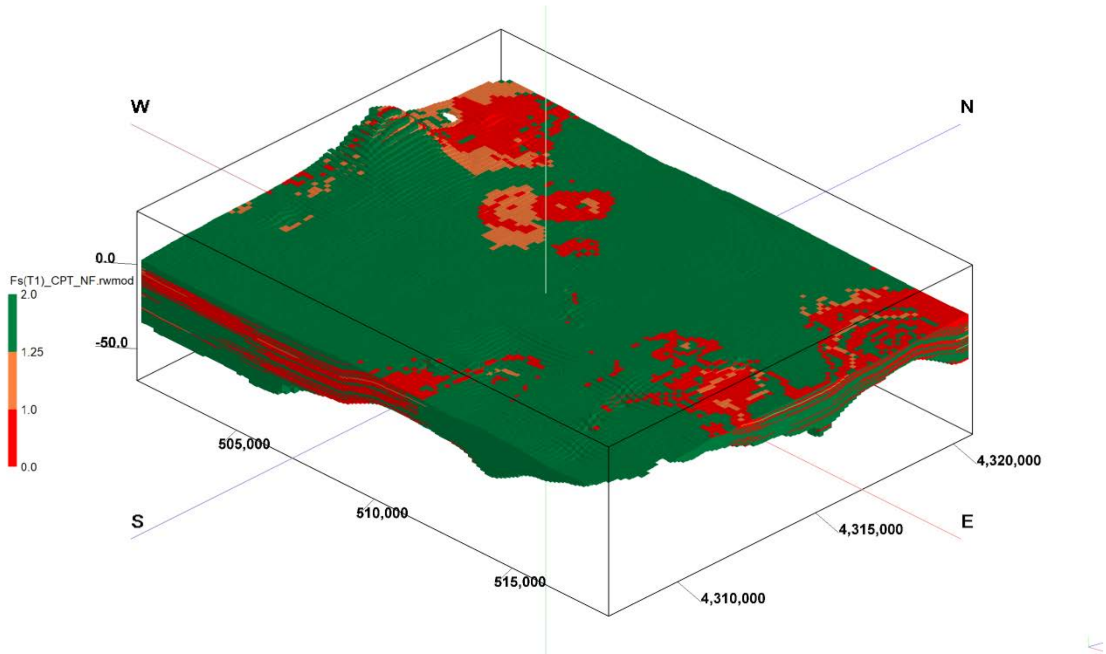

Figure 3-52 Factor of safety 3D model for seismic action EC8-T1 based on CPT tests

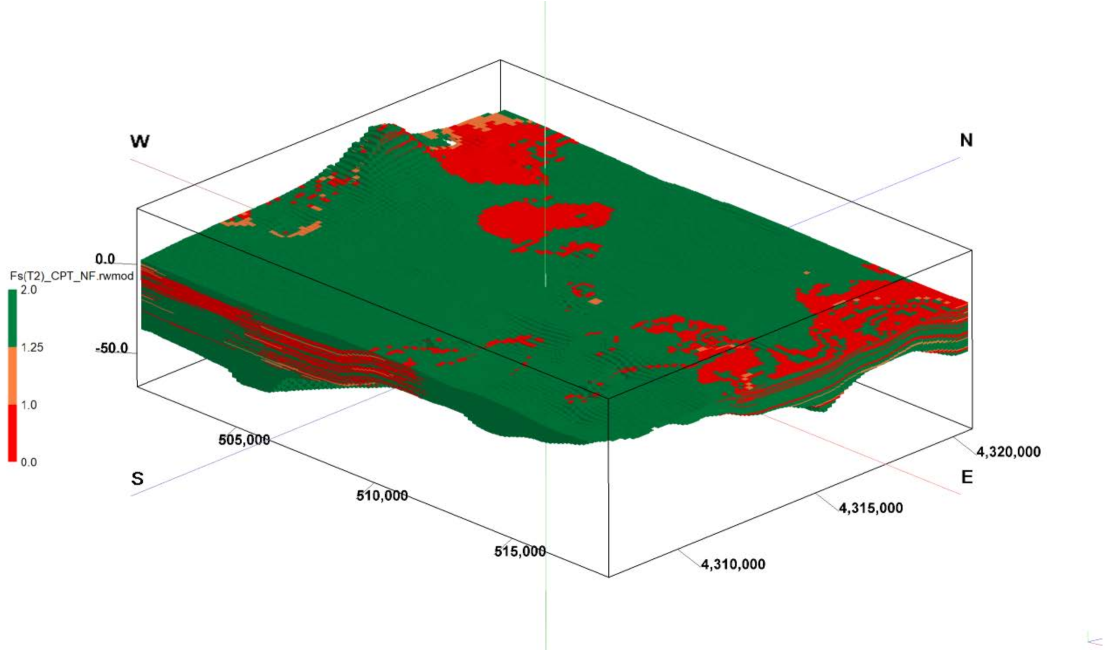

Figure 3-53 Factor of safety 3D model for seismic action EC8-T2 based on CPT tests

Following the implementation of the ground response analyses, the liquefaction assessment analyses were conducted and the respective factors of safety were computed in depth, for the two types of seismic action (T1 and T2) and three return periods (RP1, RP2 and RP3), as previously described in sections 3.3 and 3.4.

The factors of safety 3D models for the seismic action T1 resulting from the analyses of CPT results are illustrated in the following figures, from Figure 3-54 to Figure 3-59.

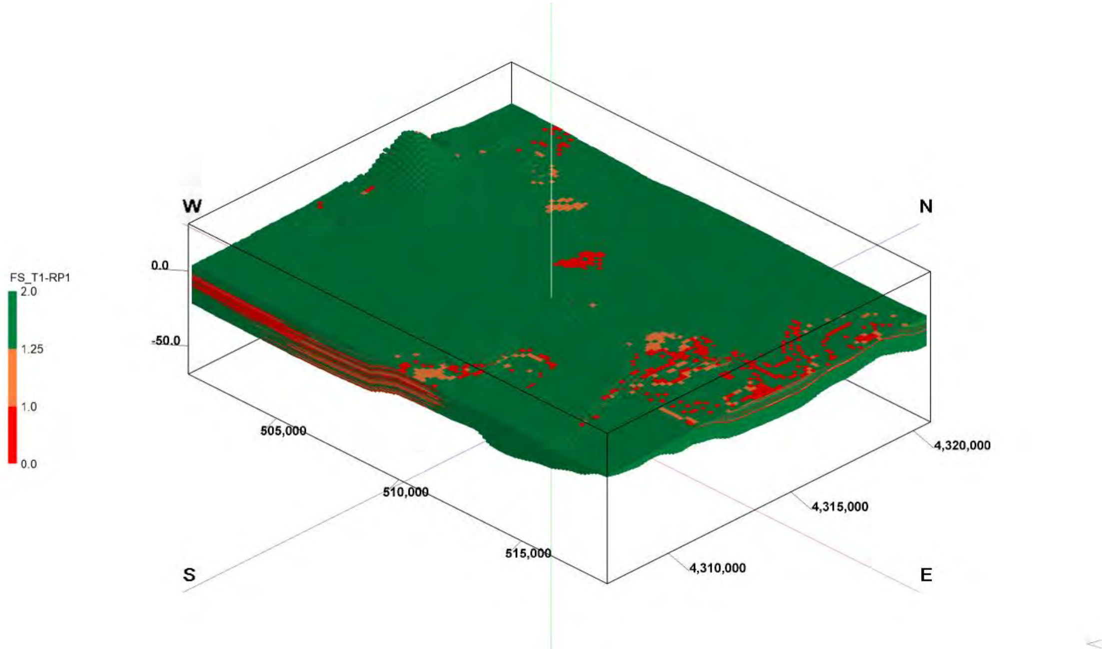

Figure 3-54 Factor of safety 3D model for seismic action T1-RP1 based on CPT tests

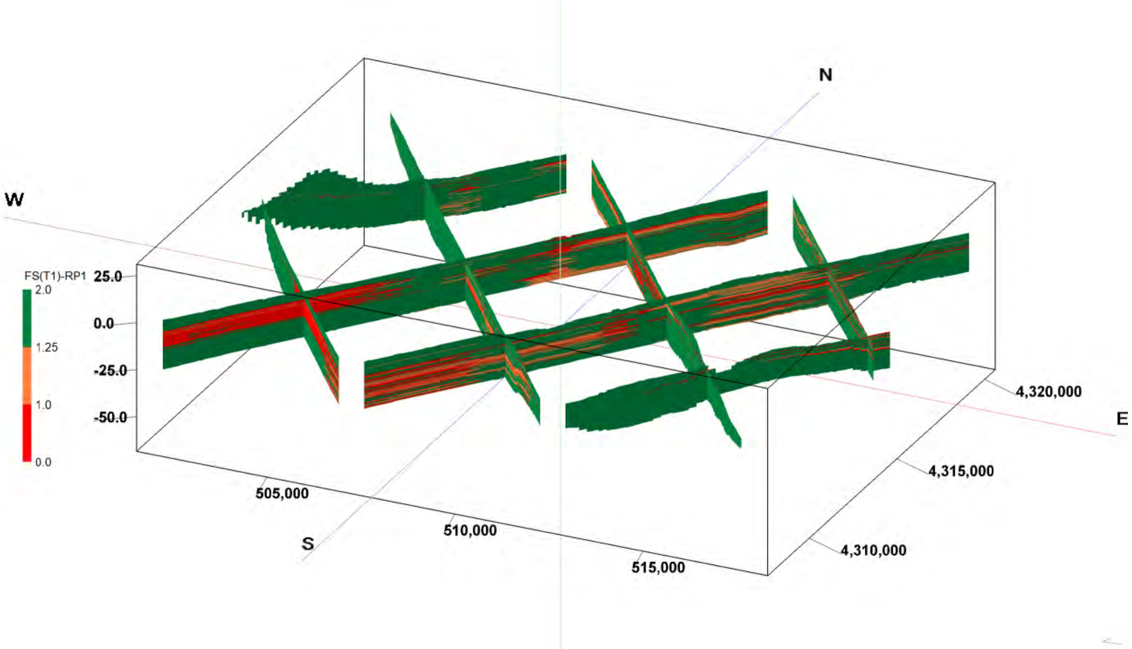

Figure 3-55 Fences of the factor of safety 3D model for seismic action T1-RP1 based on CPT tests

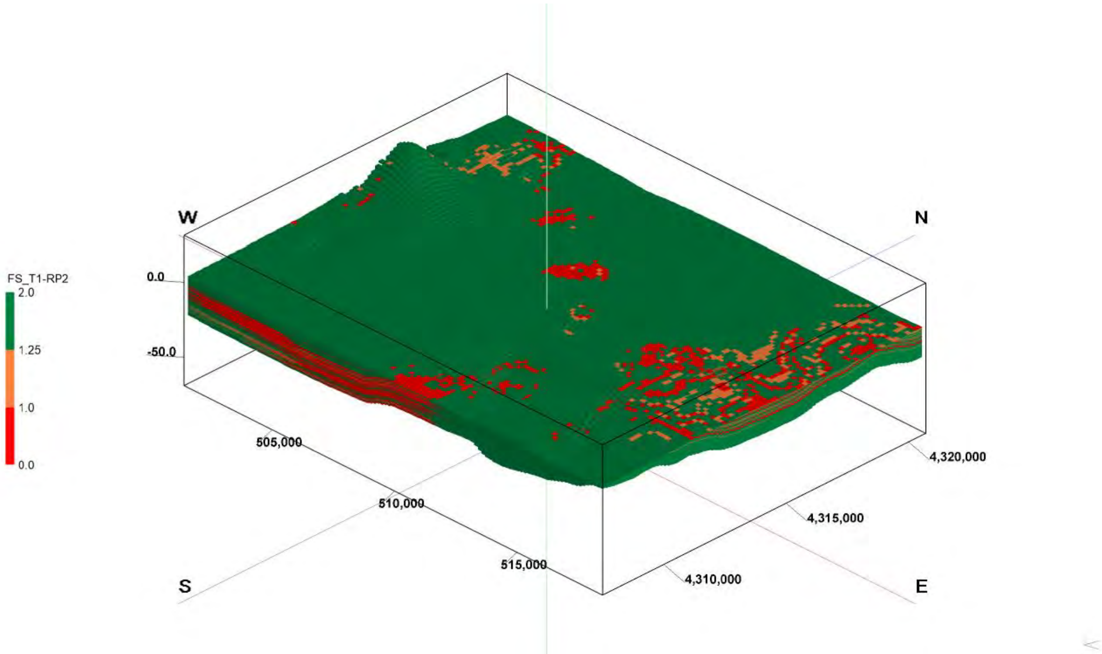

Figure 3-56 Factor of safety 3D model for seismic action T1-RP2 based on CPT tests

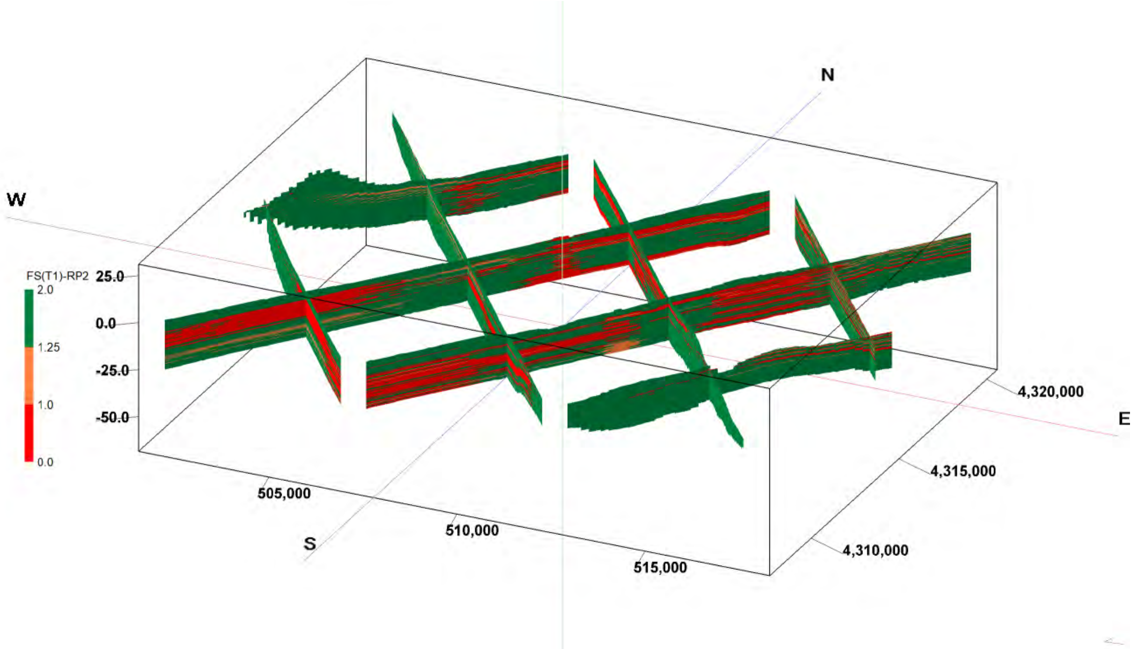

Figure 3-57 Fences of the factor of safety 3D model for seismic action T1-RP2 based on CPT tests

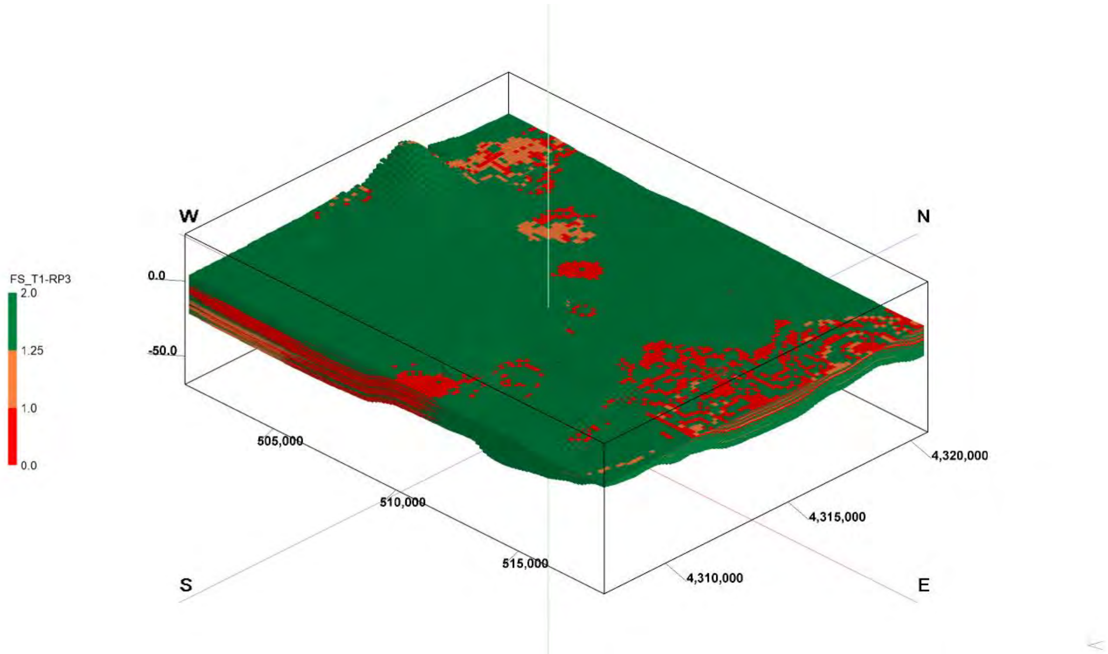

Figure 3-58 Factor of safety 3D model for seismic action T1-RP3 based on CPT tests

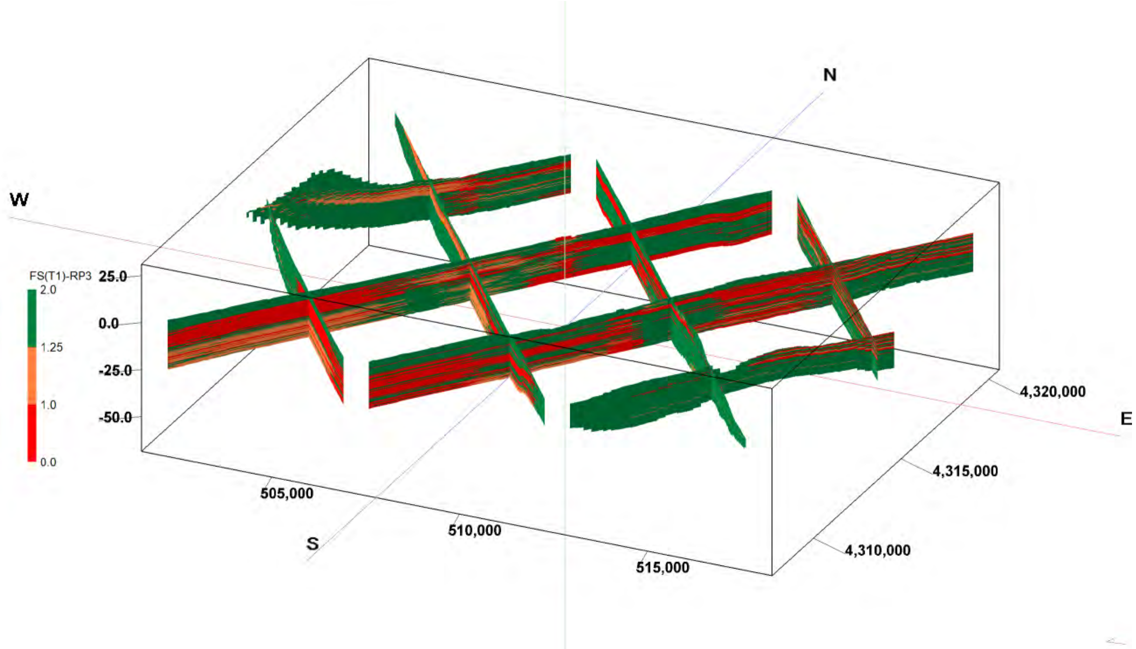

Figure 3-59 Fences of the factor of safety 3D model for seismic action T1-RP3 based on CPT tests

For seismic action T2, the factors of safety 3D models resulting from the analyses of CPT results are illustrated in Figure 3-60 to Figure 3-65.

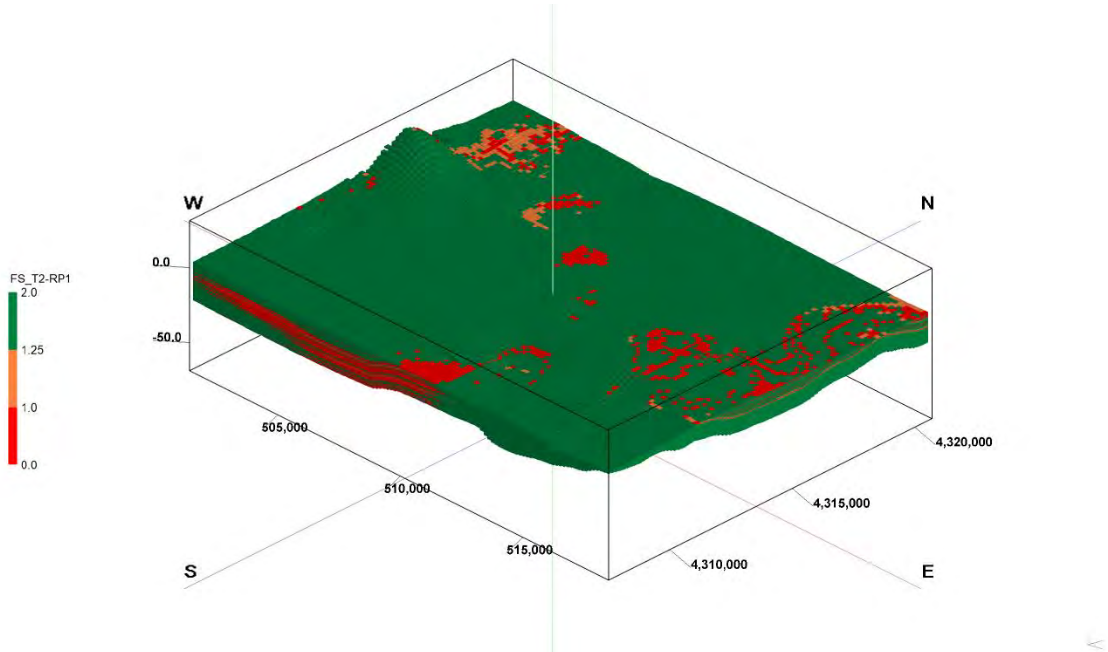

Figure 3-60 Factor of safety 3D model for seismic action T2-RP1 based on CPT tests

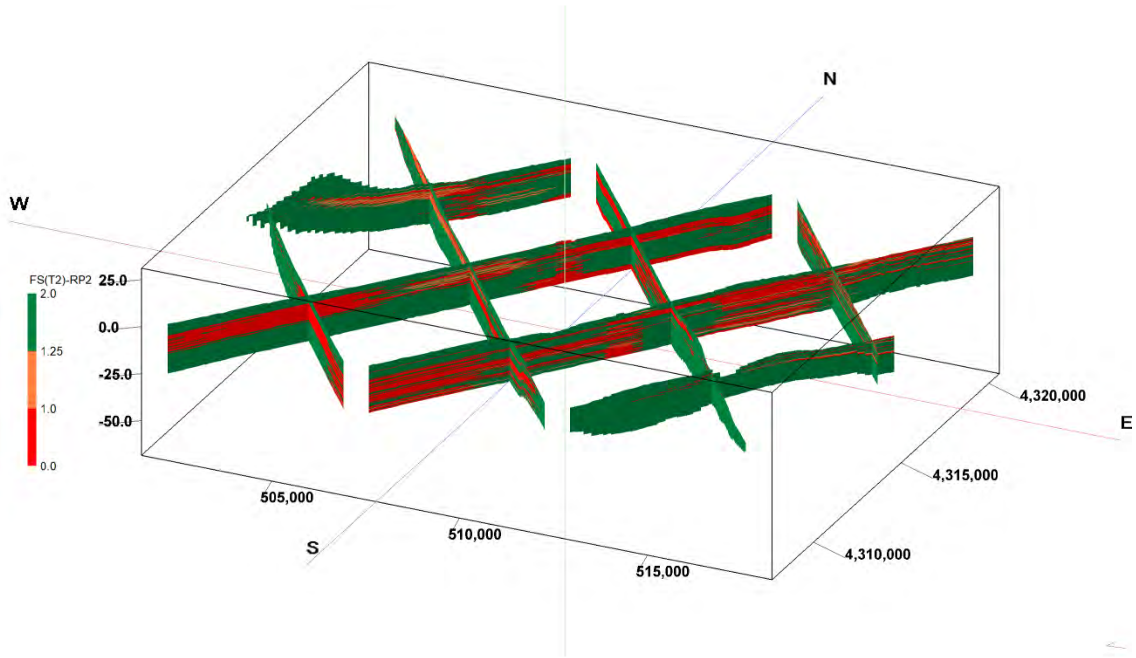

Figure 3-61 Fences of the factor of safety 3D model for seismic action T2-RP1 based on CPT tests

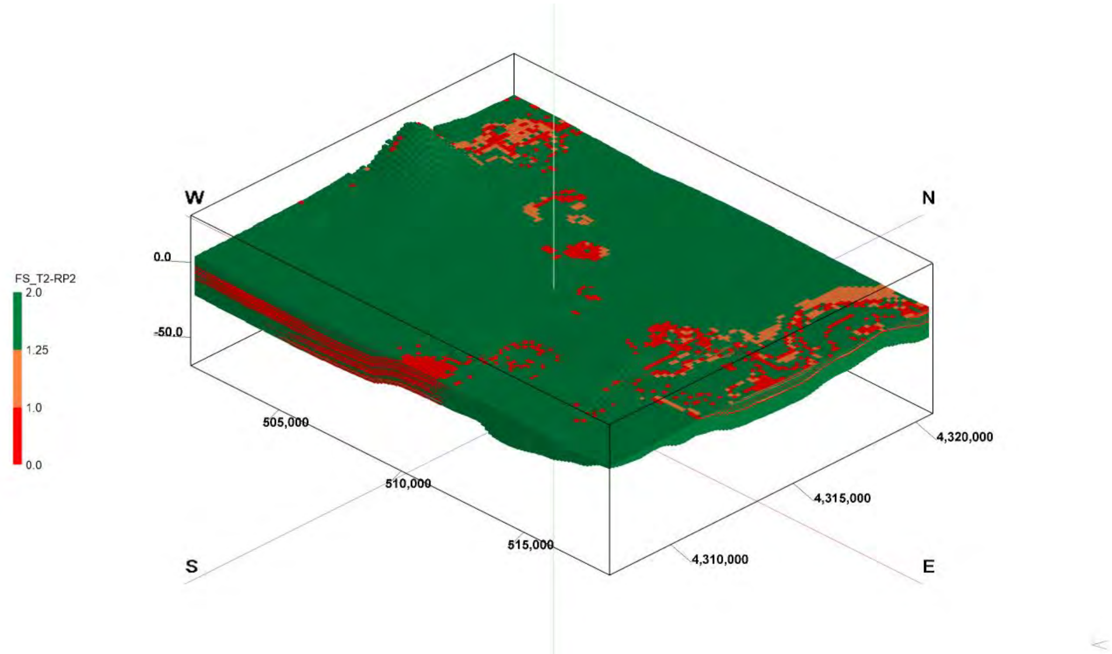

Figure 3-62 Factor of safety 3D model for seismic action T2-RP2 based on CPT tests

This project has received funding from the European Union's Horizon 2020 research and innovation programme under grant agreement No. 700748

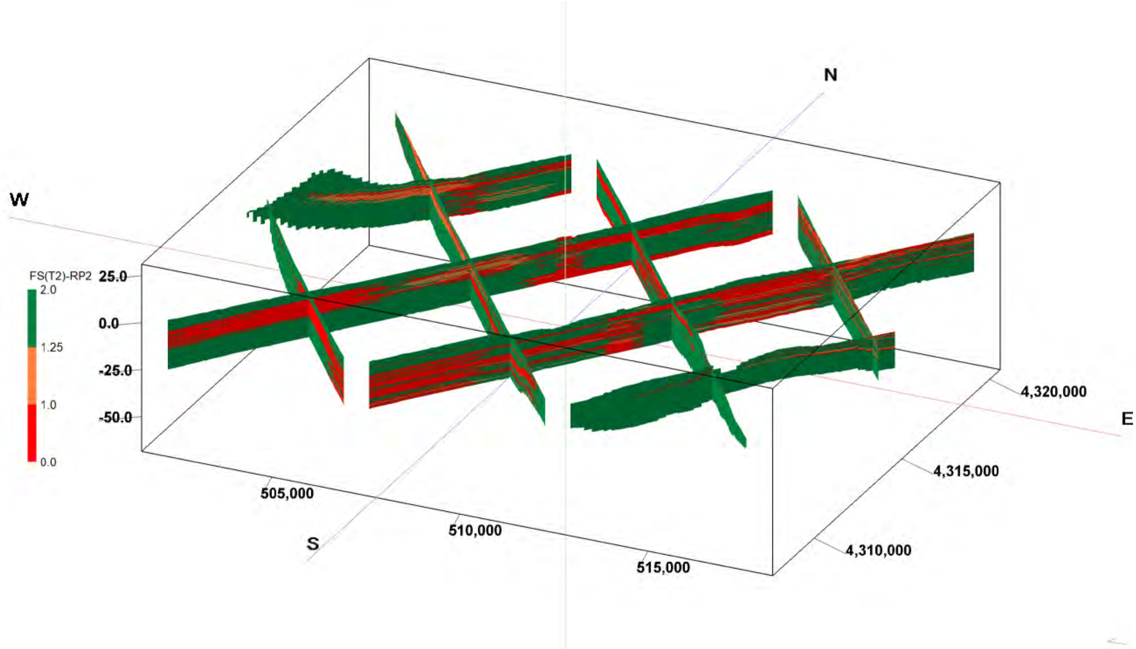

Figure 3-63 Fences of the factor of safety 3D model for seismic action T2-RP2 based on CPT tests

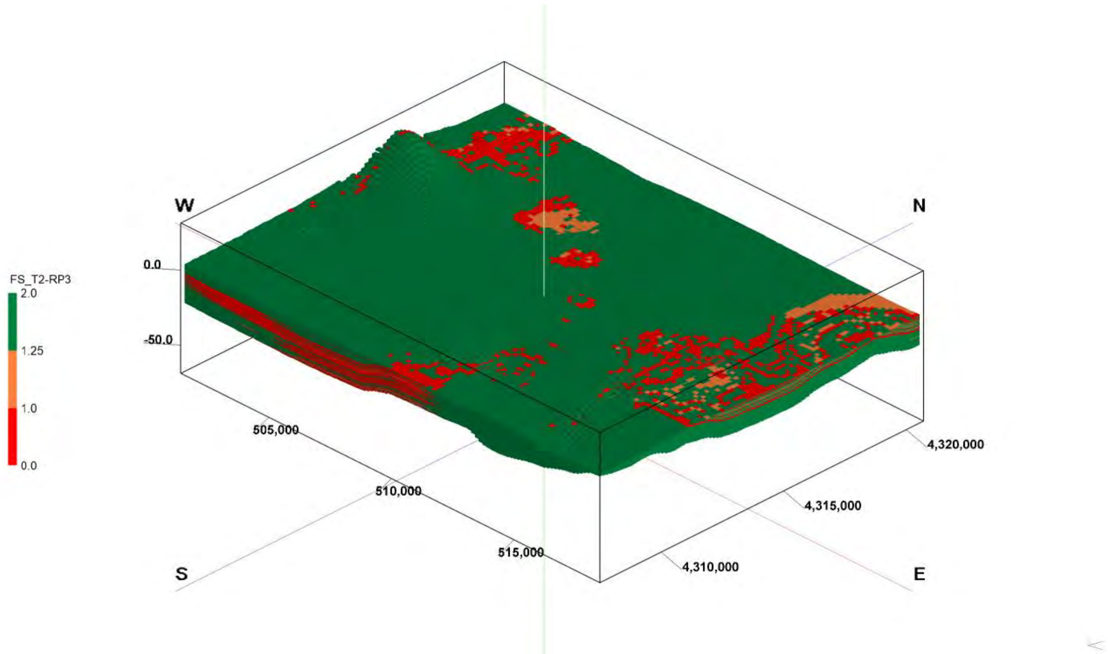

Figure 3-64 Factor of safety 3D model for seismic action T2-RP3 based on CPT tests

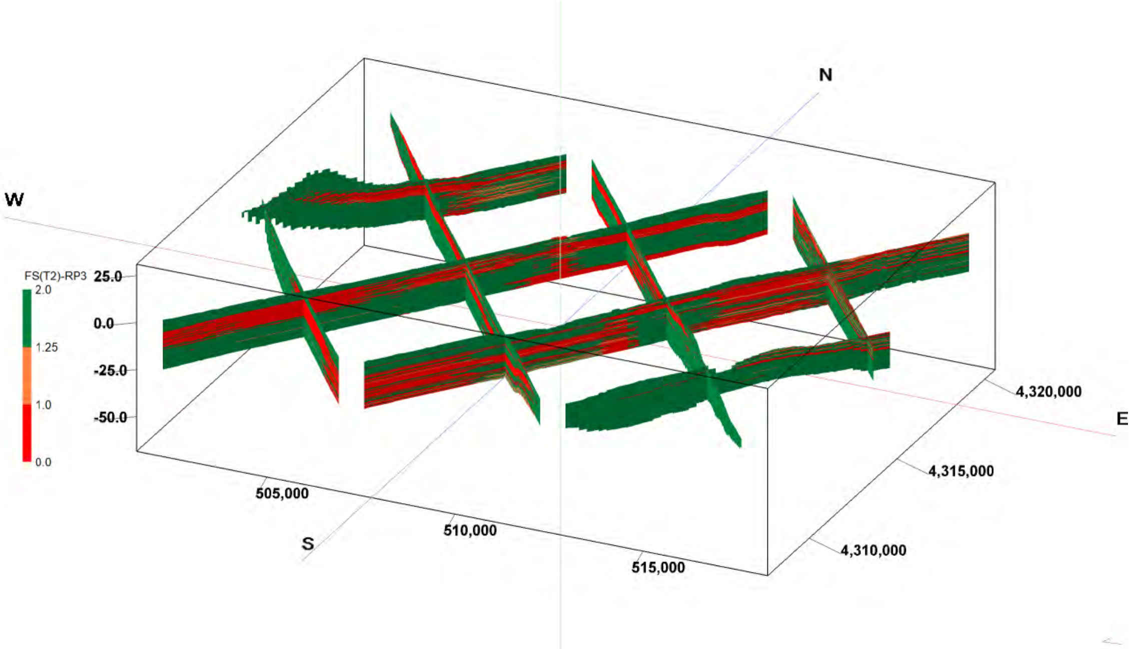

Figure 3-65 Fences of the factor of safety 3D model for seismic action T2-RP3 based on CPT tests

3.5.3 Microzonation maps of liquefaction indexes: LPI, LSN and LDI

The estimation of liquefaction-induced damages, based on quantitative liquefaction risk indexes, namely the Liquefaction Potential Index (LPI) and the Liquefaction Severity Number (LSN) is particularly convenient for the production of microzonation maps. Originally developed by Iwasaki et al. (1978), LPI combines the safety factor with depth, *z*, down to 20 m:

$$LPI = \int_0^{20m} F \cdot w(z)dz \tag{3.12}$$

where $F = 1 - FS_{liq}$, if $FS_{liq} \leq 1$ and $F = 0$, if $FS_{liq} > 1$ (3.13)

and $w(z) = 10 - 0.5z$ (3.14)

By comparing estimated LPI values with field observations of liquefaction-induced damages, different classifications of surface liquefaction severity have been proposed, namely by Iwasaki et al. (1982, 1984), Lee et al. (2003), Sonmez (2003) and Wotherspoon et al. (2014). Iwasaki et al. (1982) classification was adopted, as indicated in Table 3-10, since it is also implemented in CLiq® and the differences with other classifications are minor. The adopted colour code relative to each LPI class is also included in the table.

Table 3-10 Classification of liquefaction potential based on LPI (after Iwasaki et al., 1982)

LPI		Liquefaction potential
0	⬜	Very low
0 <LPI <5	🟩	Low
5 <LPI <15	🟨	High
15> LPI	🟥	Very high

Tonkin and Taylor (2013) developed another quantitative indicator of the liquefaction-induced damages, the Liquefaction Severity Number (LSN). This index represents the expected damage effects of shallow liquefaction on direct foundations, based on post-liquefaction volumetric deformations, associated with reconsolidation settlements, and it is defined as:

$$LSN = 1000 \cdot \int \frac{\varepsilon_v}{z} dz \tag{3.15}$$

Where ε_v is the volumetric densification strain due to post-liquefaction consolidation of soil layer *i*, according to Zhang et al. (2002), and *z* is the depth of the soil layer in metres, below the ground surface. Idriss and Boulanger (2008) procedure for the assessment of FS_{liq} was used in the development of LSN, which should refer only to the top 10 m of the soil profile. Using this approach, the liquefaction severity can be classified in terms of expected damage, according to Tonkin and Taylor (2013), as shown in Table 3-11, which also includes the adopted colour scheme.

Table 3-11 Liquefaction severity and damage based on LSN (Tonkin and Taylor, 2013)

LSN range		Typical performance
0 – 10	🟦	Little to no expression of liquefaction
10 – 20	🟩	Minor expression of liquefaction, some sand boils
20 – 30	🟨	Moderate expression of liquefaction, sand boils and some structural damage
30 – 40	🟧	Moderate to severe liquefaction, settlement can cause structural damage
40 – 50	🟫	Major expression of liquefaction, damage ground surface, severe total and differential settlements
> 50	🟥	Severe damage, extensive evidence of liquefaction, severe total and differential settlements affecting structures, damage to services

For the purpose of microzonation for liquefaction risk, these liquefaction indexes were calculated considering the ground water level (GWL) as measured in situ at the time of the test. However, a short sensitivity study was conducted to assess the impact of the fluctuation of GWL, for a pessimist scenario of a constant depth of 1m. The obtained maps of LPI and LSN are provided in Figure 3-66 to Figure 3-69. A specific liquefaction assessment analysis was carried out considering the extreme case of a constant ground water level at 1m depth, as illustrated in Figure 3-70 to Figure 3-73.

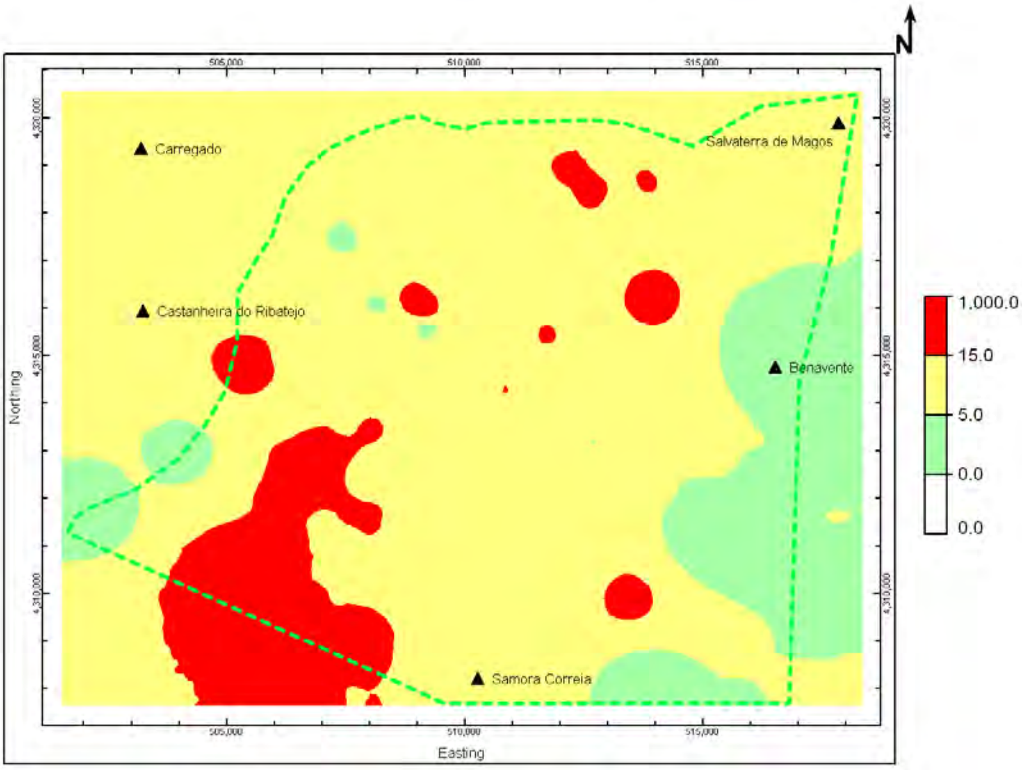

Figure 3-66 Map of LPI for seismic action EC8-T1 based on CPT tests

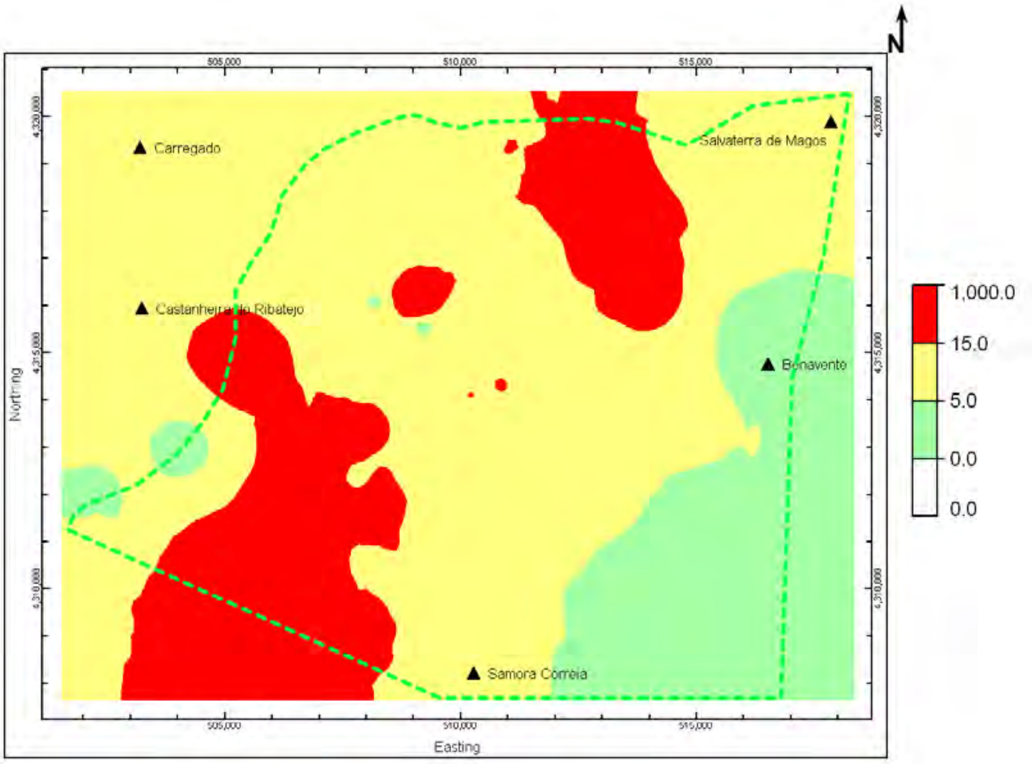

Figure 3-67 Map of LPI for seismic action EC8-T2 based on CPT tests

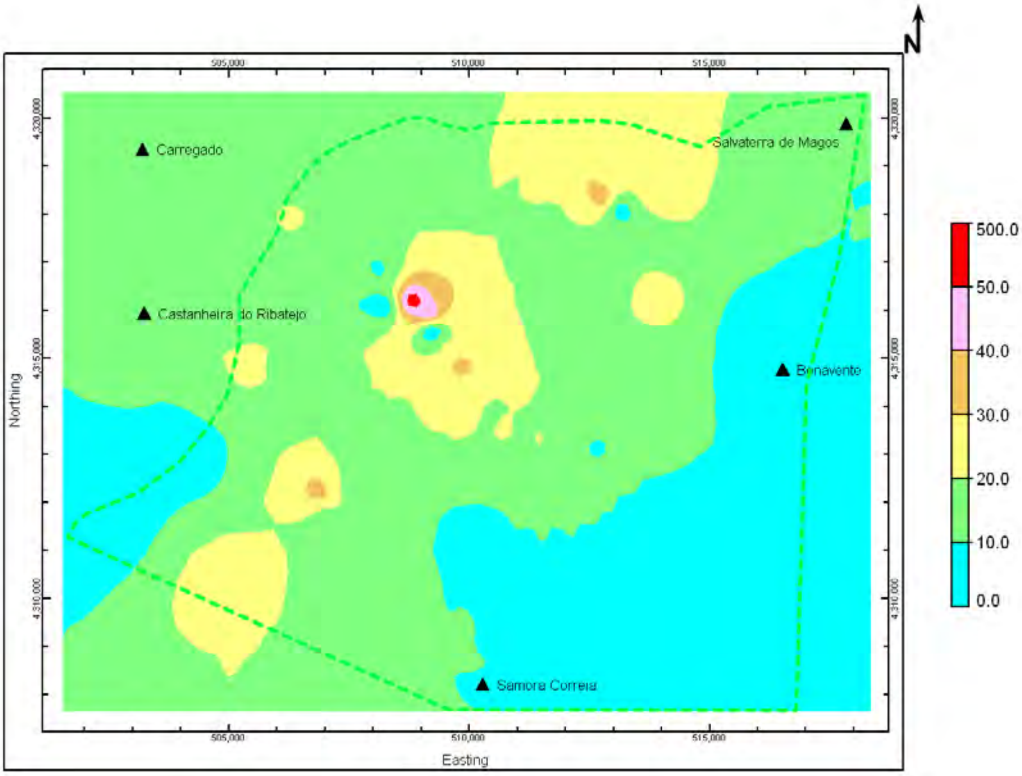

Figure 3-68 Map of LSN for seismic action EC8-T1 based on CPT tests

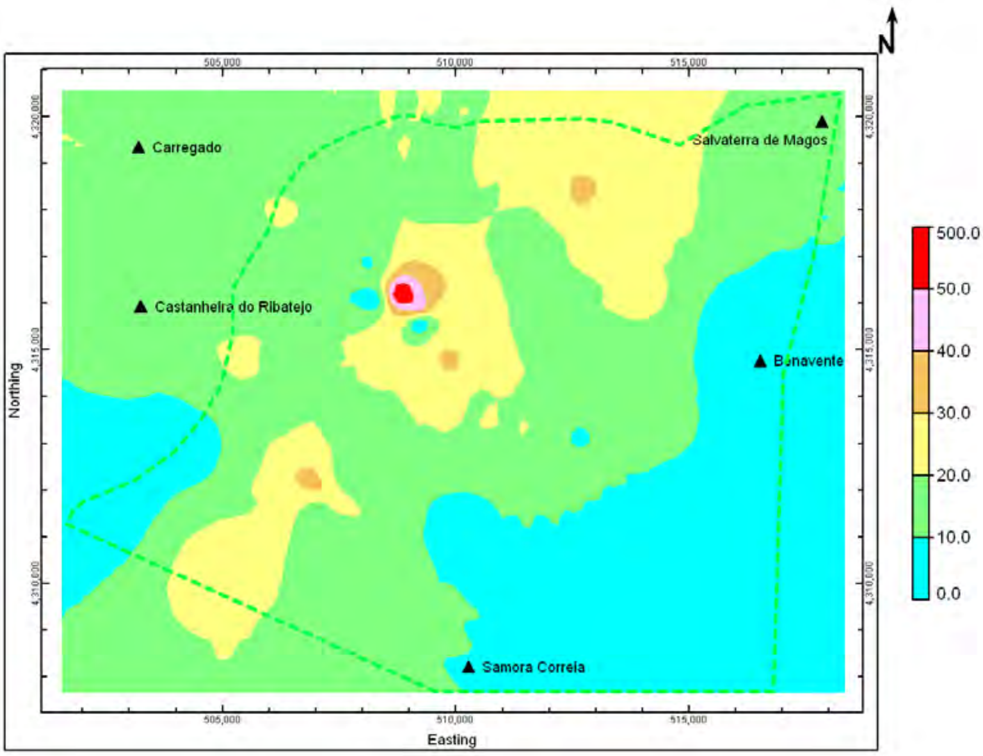

Figure 3-69 Map of LSN for seismic action EC8-T2 based on CPT tests

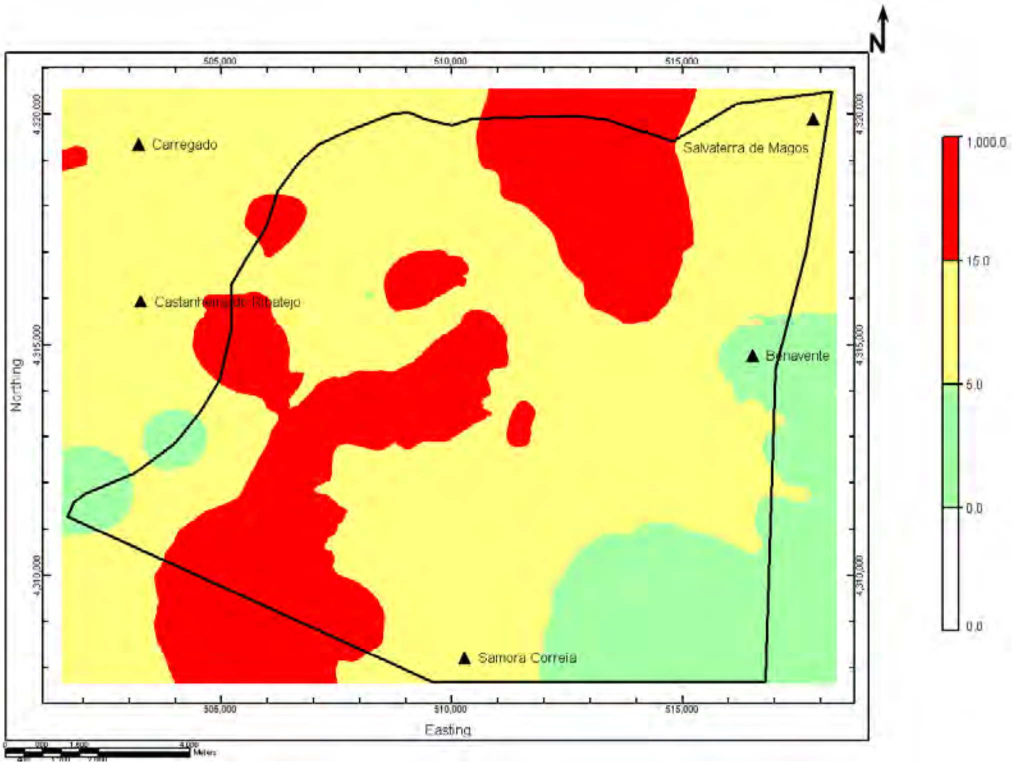

Figure 3-70 Map of LPI for seismic action EC8-T1, for a constant GWL depth of 1m, based on CPT tests

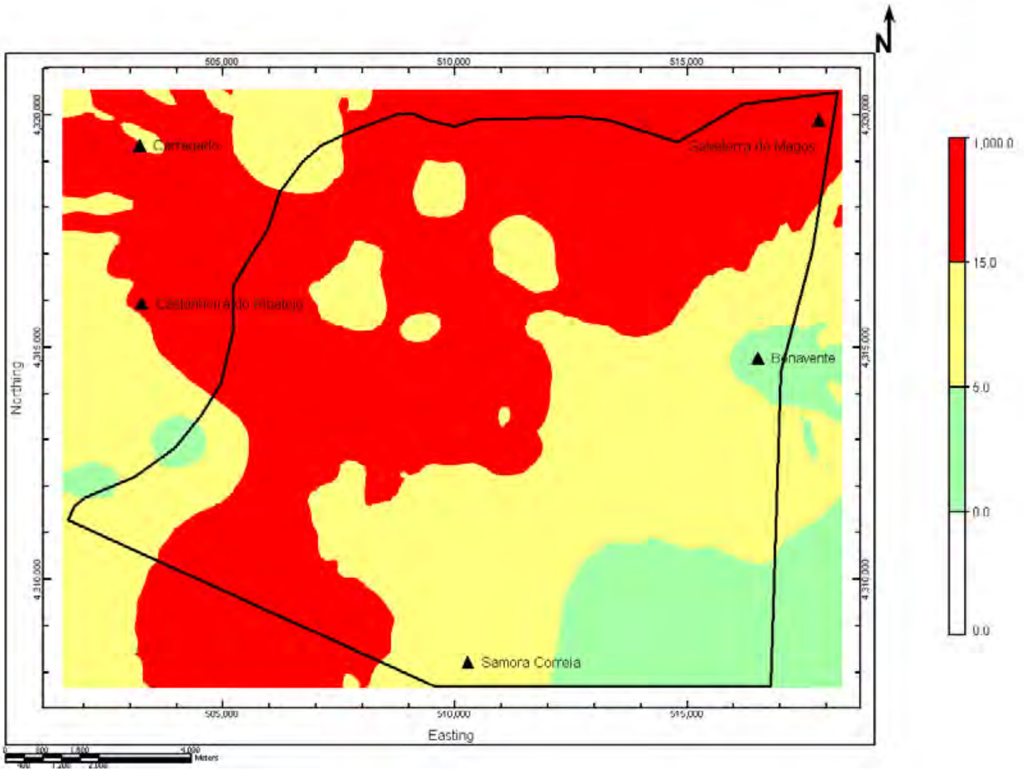

Figure 3-71 Map of LPI for seismic action EC8-T2, for a constant GWL depth of 1m, based on CPT tests

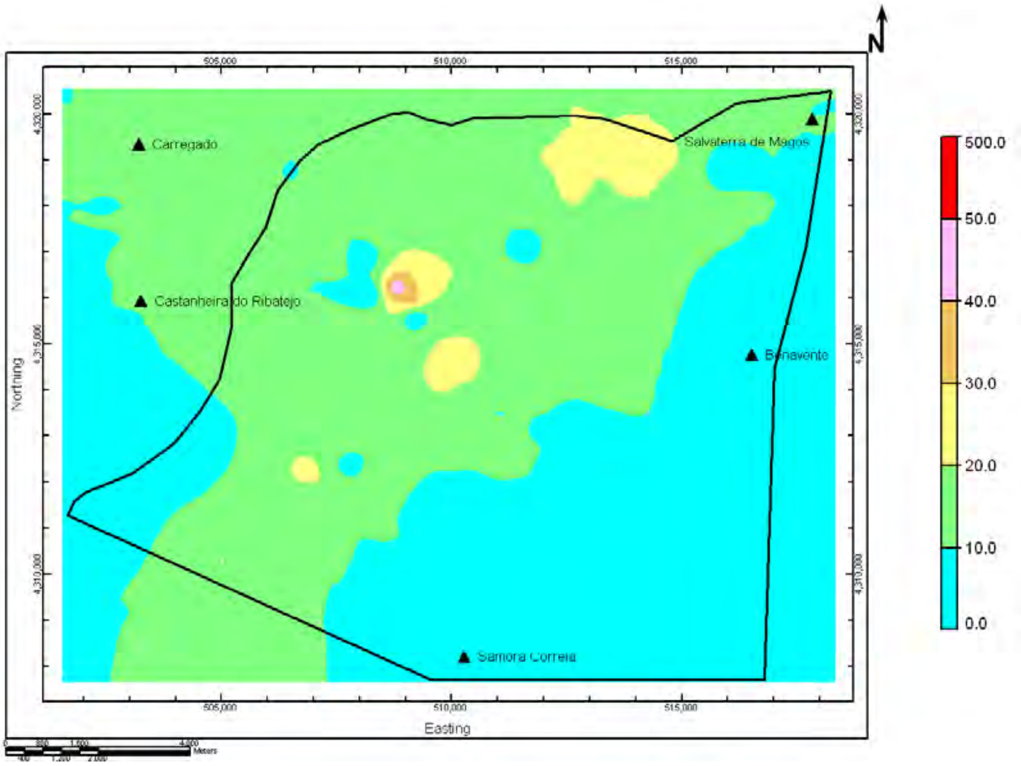

Figure 3-72 Map of LSN for seismic action EC8-T1, for a constant GWL depth of 1m, based on CPT tests

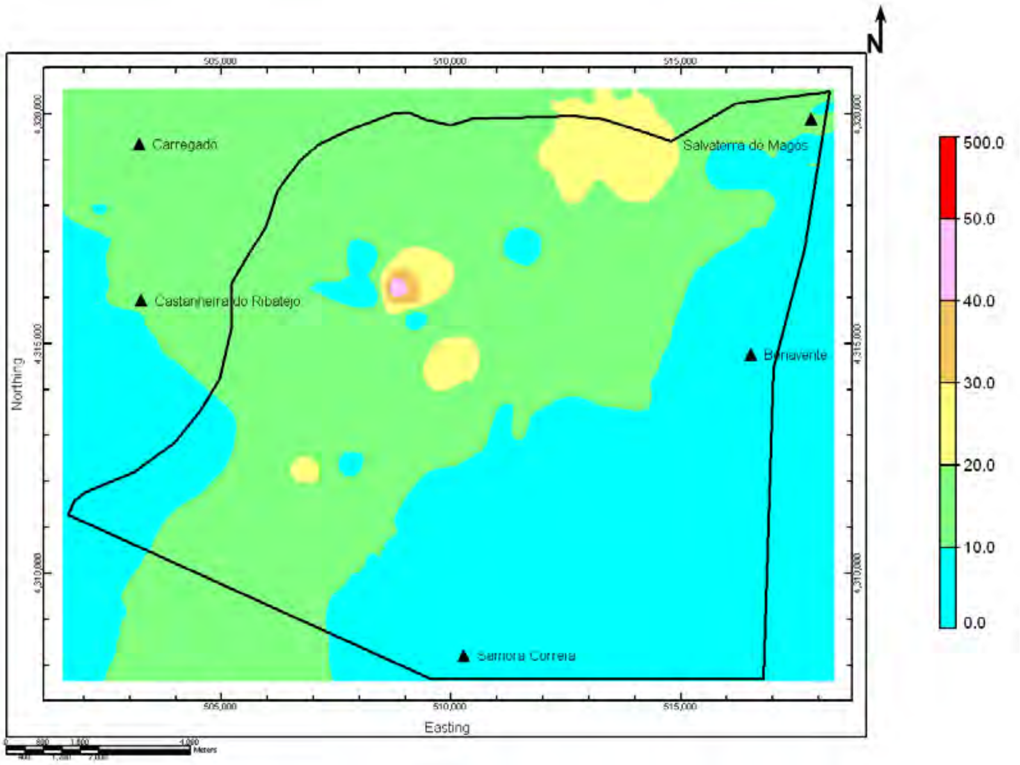

Figure 3-73 Map of LSN for seismic action EC8-T2, for a constant GWL depth of 1m, based on CPT tests

The quantitative liquefaction indices were also computed for the six seismic scenarios resulting from the site-specific ground response analyses, as previously shown for the case of the factor of safety. The obtained microzonation maps of LPI for the different seismic scenarios are provided in Figure 3-74 to Figure 3-79.

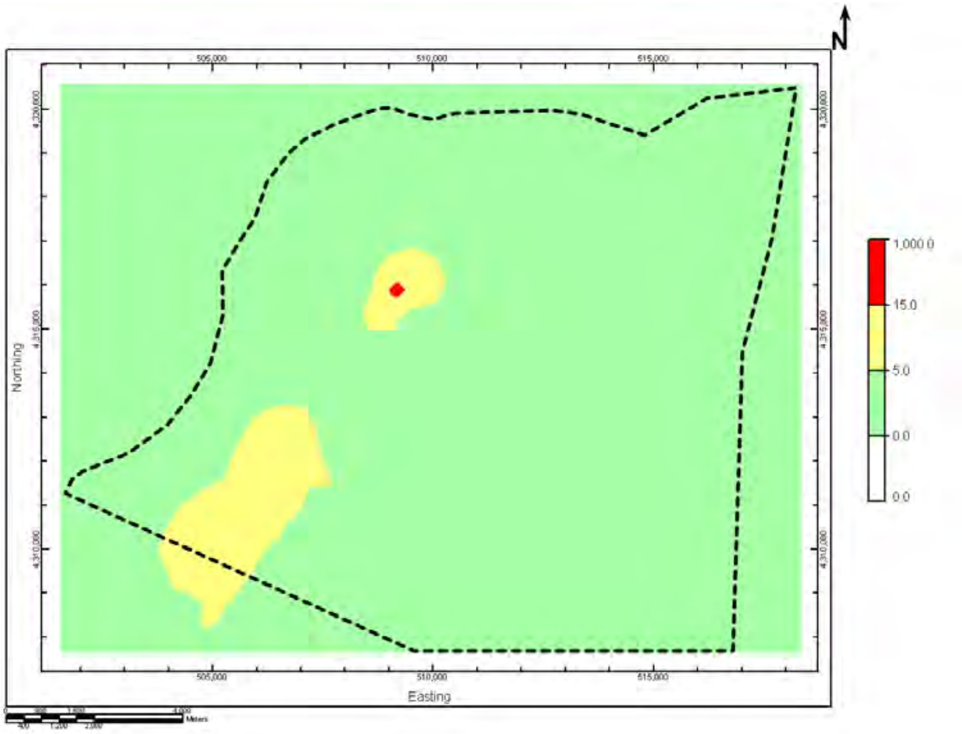

Figure 3-74 Map of LPI for seismic action T1-RP1 based on CPT tests

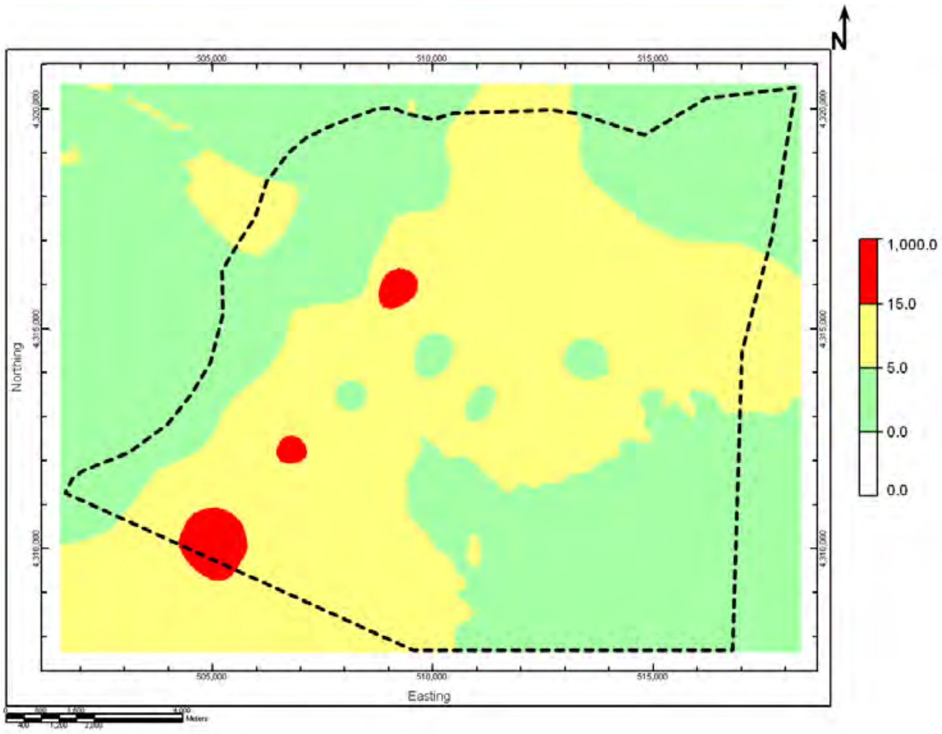

Figure 3-75 Map of LPI for seismic action T1-RP2 based on CPT tests

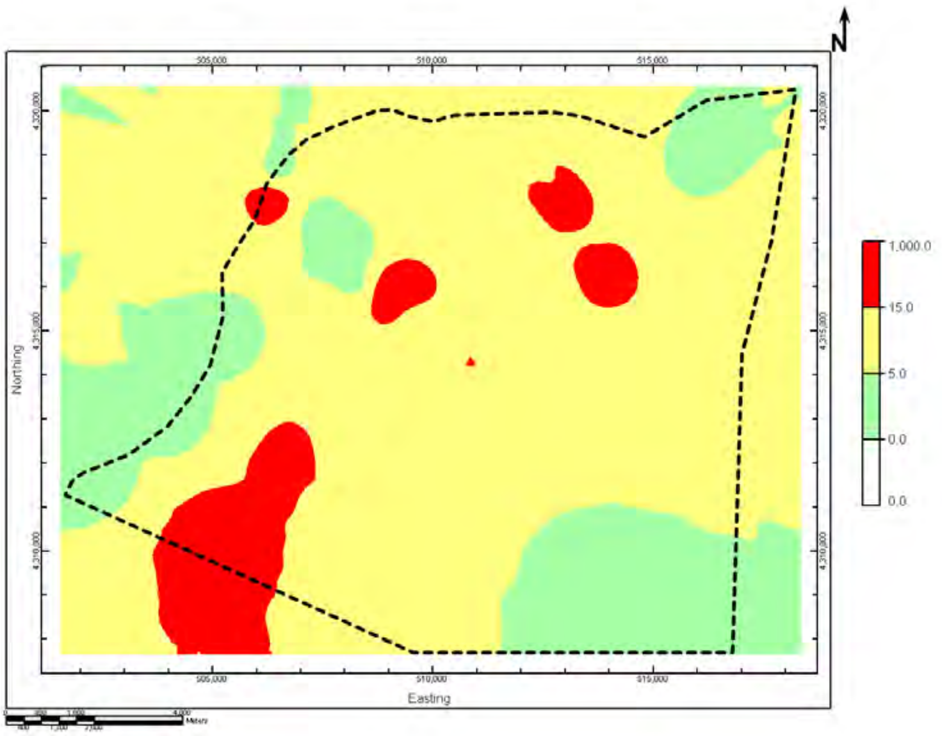

Figure 3-76 Map of LPI for seismic action T1-RP3 based on CPT tests

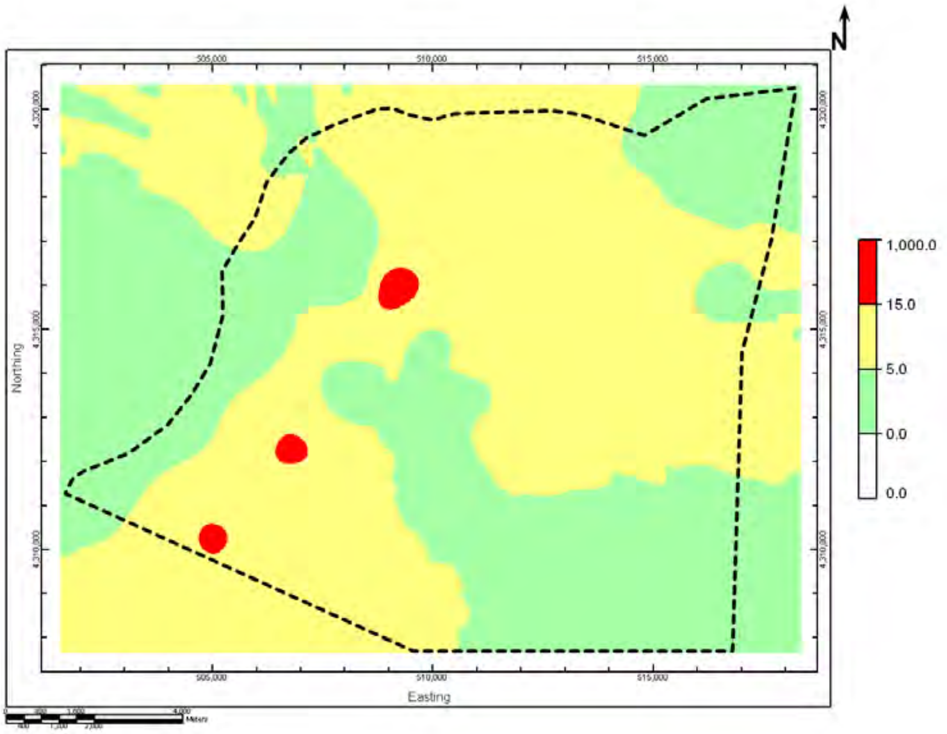

Figure 3-77 Map of LPI for seismic action T2-RP1 based on CPT tests

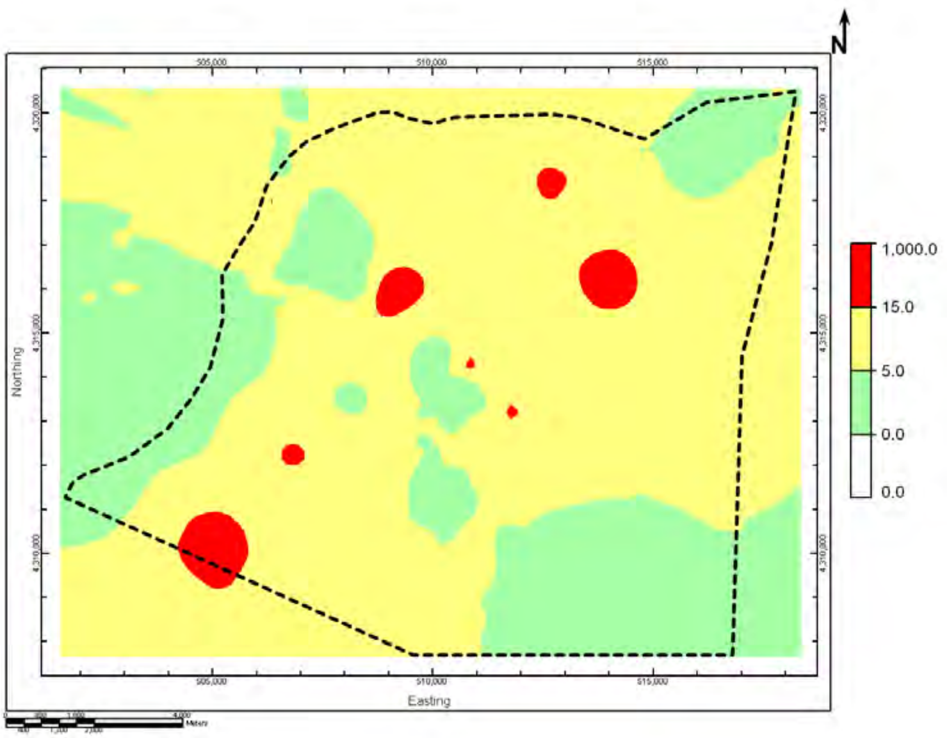

Figure 3-78 Map of LPI for seismic action T2-RP2 based on CPT tests

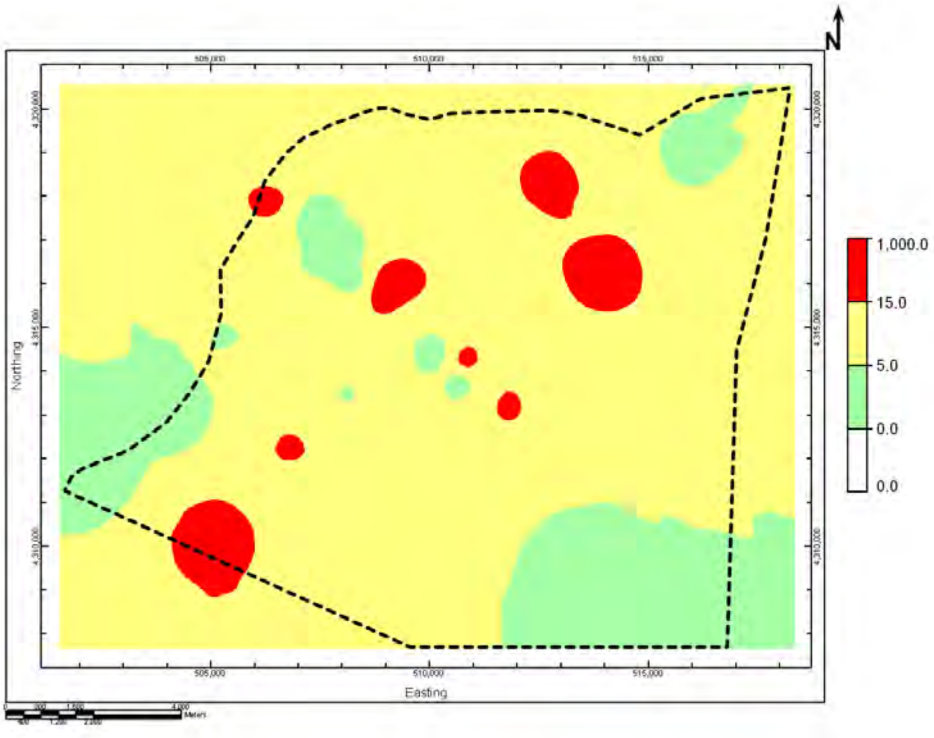

Figure 3-79 Map of LPI for seismic action T2-RP3 based on CPT tests

The microzonation maps of LSN for the six seismic scenarios are provided in Figure 3-80 to Figure 3-85**.**

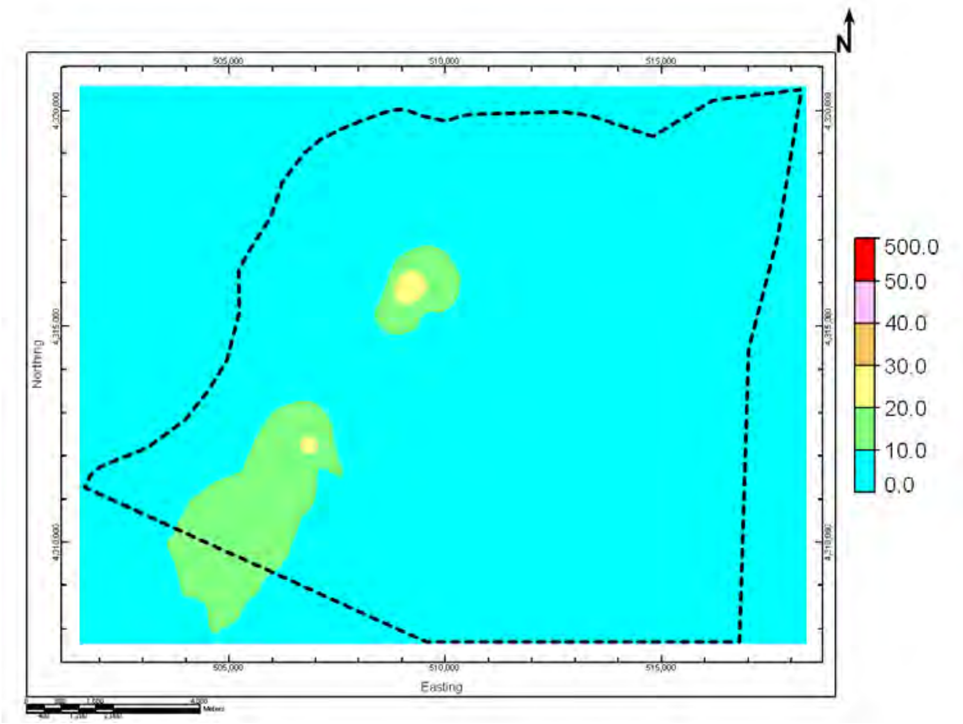

Figure 3-80 Map of LSN for seismic action T1-RP1 based on CPT tests

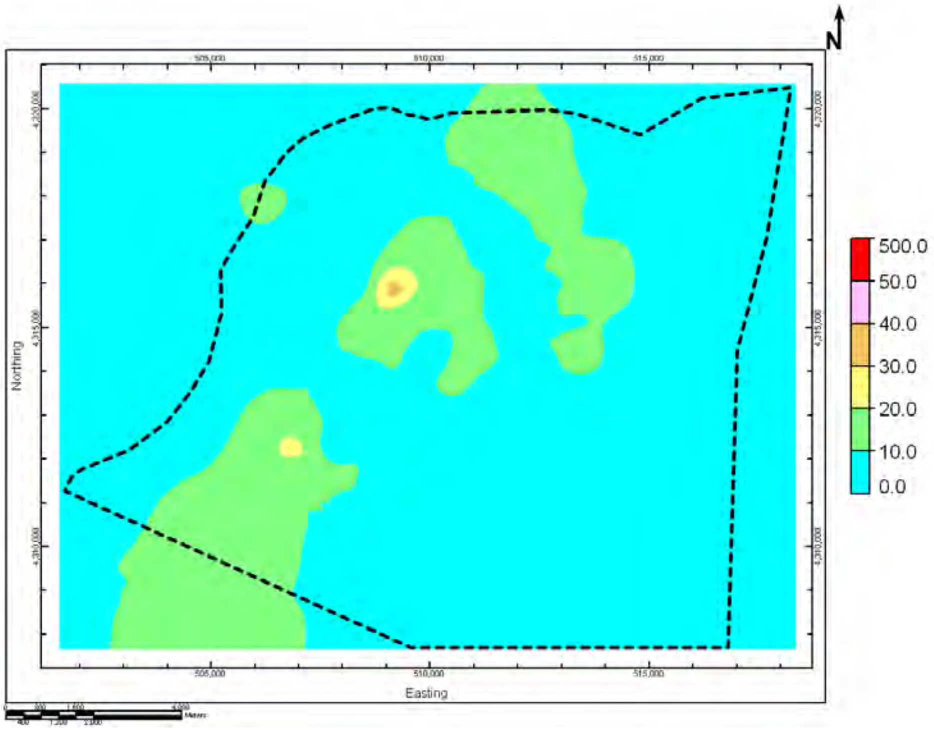

Figure 3-81 Map of LSN for seismic action T1-RP2 based on CPT tests

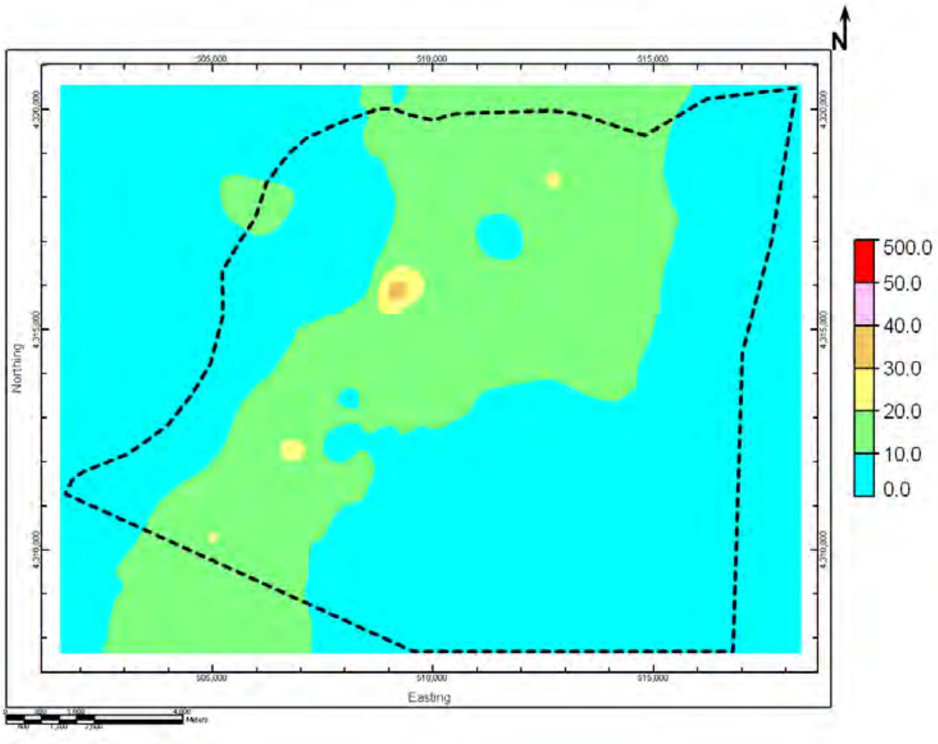

Figure 3-82 Map of LSN for seismic action T1-RP3 based on CPT tests

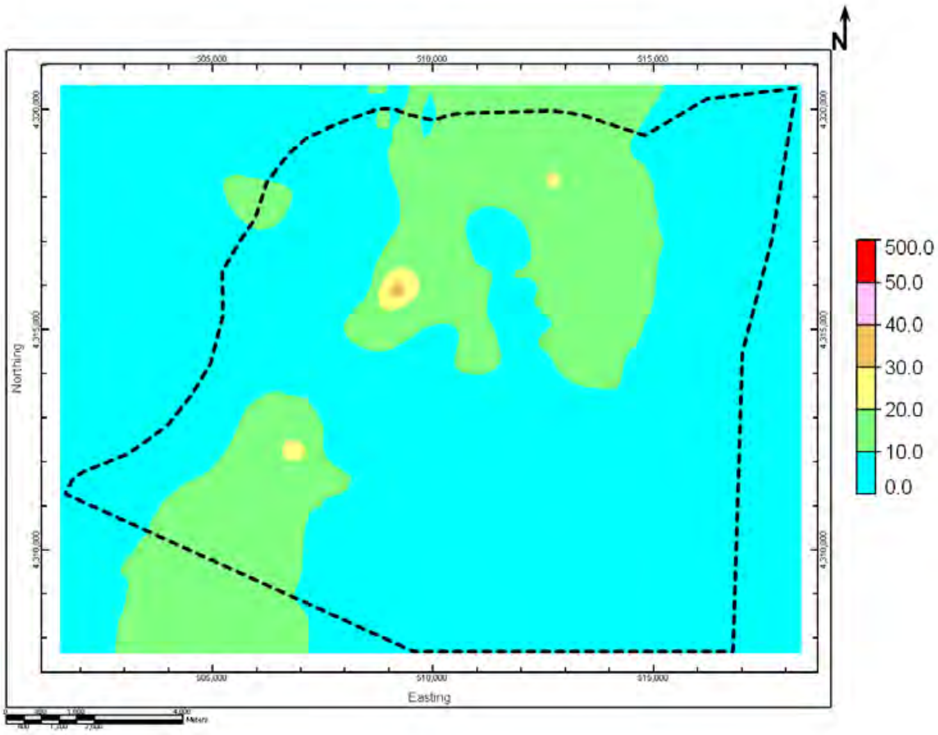

Figure 3-83 Map of LSN for seismic action T2-RP1 based on CPT tests

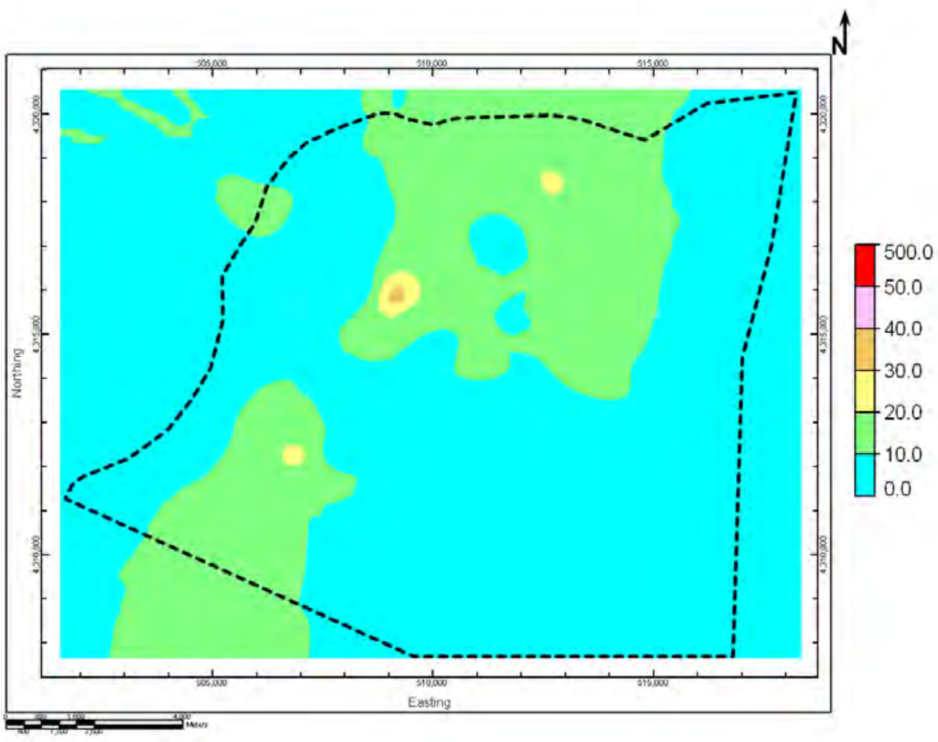

Figure 3-84 Map of LSN for seismic action T2-RP2 based on CPT tests

This project has received funding from the European Union's Horizon 2020 research and innovation programme under grant agreement No. 700748

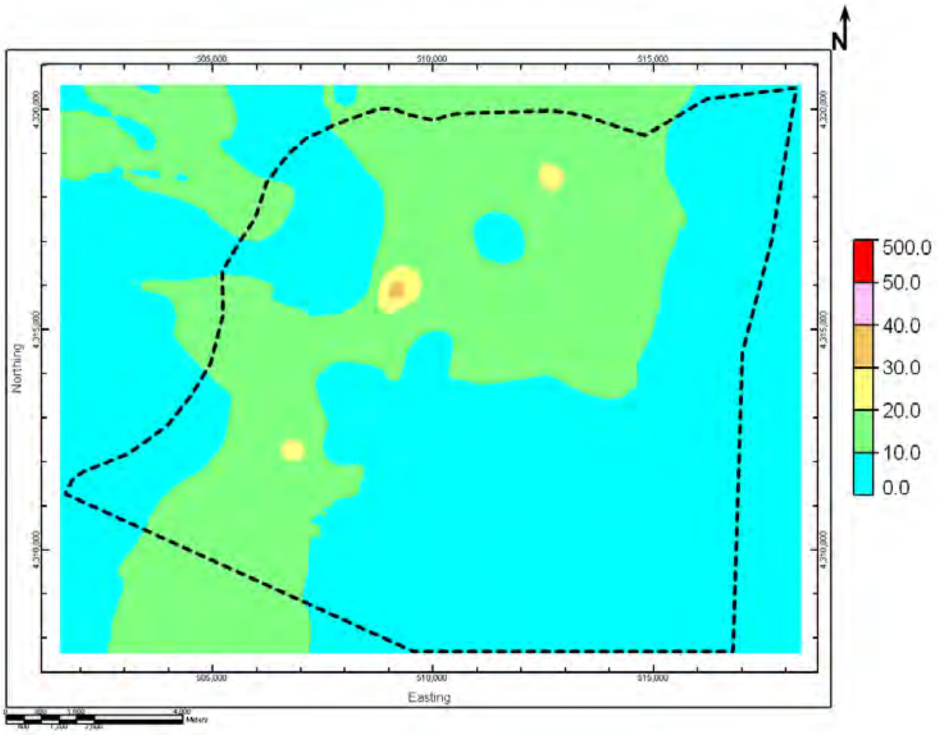

Figure 3-85 Map of LSN for seismic action T2-RP3 based on CPT tests

In order to estimate the magnitude of lateral displacements associated with a liquefaction-induced lateral spreading, a preliminary approach was applied to the Low Taggus River Pilot-Case, in the municipalities of Benavente and Vila Franca de Xira, using the cone penetration test (CPT) data. Lateral spreading is defined as the finite, lateral displacement of gently sloping ground or for nearly level (or gently inclined) ground with a free face (e.g. river banks, road embankments, dykes and levees), as a result of pore pressure build-up or liquefaction in a shallow underlying deposit during an earthquake.

In this area, this damage is mostly probable, due to the significant extension of dikes and levees, protecting the territory from the floads of the Taggus River and regulating the extensive system of channels for water supply regulation, as well roads embankments connecting populations who depend on them for mobility.

Zang et al. (2004) defines the lateral displacement index (LDI) as the integrated value of the maximum cyclic shear strains ($\Upsilon_{máx}$) at the ground surface as shown in the following equation.

$$LDI = \int_0^{Z_{máx}} \gamma_{máx} \, dz \qquad (3.16)$$

LDI only provides an index to quantify potential lateral displacements for a given soil profile, soil properties, and earthquake characteristics. The actual magnitude of lateral displacement depends on both LDI and geometric parameters characterizing ground geometry.

Zang et al. (2004) defined three ground geometries that enhance lateral spreadings: (a) gently sloping ground without a free face, (b) level ground with a free face, and (c) gently sloping ground with a free face. Regarding real case histories, the LDI and LD plots versus the ground geometry enable the correlation between the 3 parameters, which are presented in Table 3-12.

Table 3-12 Different ground geometries for liquefaction-induced lateral spreading (Zang et al., 2004)

gently sloping ground without a free face (a)	level ground with a free face (b)	gently sloping ground with a free face (c)
	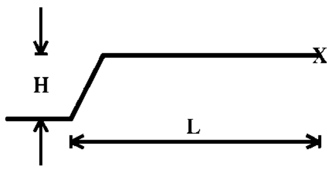	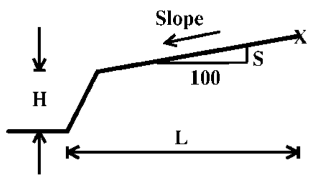
$\frac{LD}{LDI} = S + 0.2$ $(for\ \ 0.2\% < S < 3.5\%)$	$\frac{LD}{LDI} = 6 * \left(\frac{L}{H}\right)^{-0.8}$ $(for\ \ 4 < L/H < 40)$	$\frac{LD}{LDI} = 6 * \left(\frac{L}{H}\right)^{-0.8}$ $(for\ \ 4 < L/H < 40)$

For this case study, the estimate of lateral displacements associated with liquefaction-induced lateral spreading using cone penetration test data was carried out according to the following steps:

1. <u>Identification of critical points</u>

From all the CPT performed in this pilot site, there were only chosen for analysis those locations where the ground geometry could lead to lateral spreading, namely river banks, road embankments, dykes and levees, and landfills.

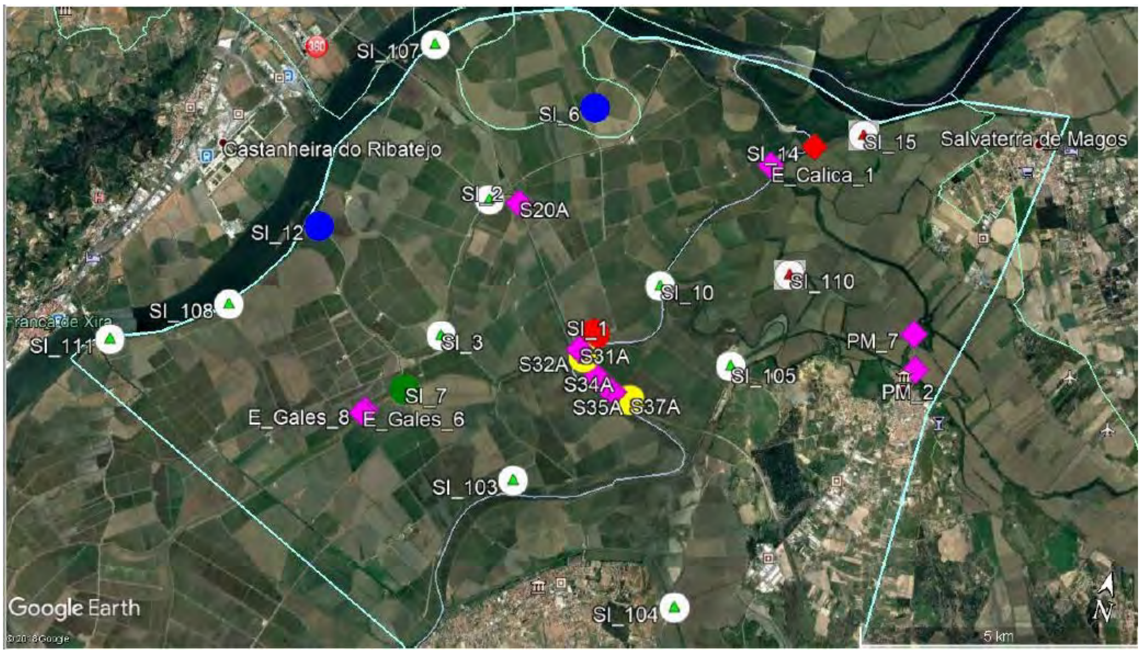

Figure 3-86 Map of the selected points for LDI calculation

2. Liquefaction potential assessment, using CPT based methods

In order to calculate LDI, it is necessary to estimate the maximum cyclic shear strain (γ_{max}). Ishihara & Yoshimine (1992) and Seed (1979) established the relationship between the γ_{max} and the factor of safety (FS) against liquefaction for different relative densities (D_r), as shown in the expressions below.

The values of FS and D_r were estimated from correlations with the CPT data. The calculation method used was based on Boulanger & Idriss (2014), assuming a clay-like behaviour and this analysis was performed using the CLiq software.

$$
\begin{array}{ll}
\text{if } D_r=90\%, \quad \gamma_{max}=3.26(\text{FS})^{-1.80} \quad \text{for } 0.7\leq \text{FS}\leq 2.0 & (8)\\
\text{if } D_r=90\%, \quad \gamma_{max}=6.2 \quad \text{for } \text{FS}\leq 0.7 & (9)\\
\text{if } D_r=80\%, \quad \gamma_{max}=3.22\cdot(\text{FS})^{-2.08} \quad \text{for } 0.56\leq \text{FS}\leq 2.0 & (10)\\
\text{if } D_r=80\%, \quad \gamma_{max}=10 \quad \text{for } \text{FS}\leq 0.56 & (11)\\
\text{if } D_r=70\%, \quad \gamma_{max}=3.20\cdot(\text{FS})^{-2.89} \quad \text{for } 0.59\leq \text{FS}\leq 2.0 & (12)\\
\text{if } D_r=70\%, \quad \gamma_{max}=14.5 \quad \text{for } \text{FS}\leq 0.59 & (13)\\
\text{if } D_r=60\%, \quad \gamma_{max}=3.58\cdot(\text{FS})^{-4.42} \quad \text{for } 0.66\leq \text{FS}\leq 2.0 & (14)\\
\text{if } D_r=60\%, \quad \gamma_{max}=22.7 \quad \text{for } \text{FS}\leq 0.66 & (15)\\
\text{if } D_r=50\%, \quad \gamma_{max}=4.22\cdot(\text{FS})^{-6.39} \quad \text{for } 0.72\leq \text{FS}\leq 2.0 & (16)\\
\text{if } D_r=50\%, \quad \gamma_{max}=34.1 \quad \text{for } \text{FS}\leq 0.72 & (17)\\
\text{if } D_r=40\%, \quad \gamma_{max}=3.31\cdot(\text{FS})^{-7.97} \quad \text{for } 1.0\leq \text{FS}\leq 2.0 & (18)\\
\text{if } D_r=40\%, \quad \gamma_{max}=250\cdot(1.0-\text{FS})+3.5 \quad \text{for } 0.81\leq \text{FS}\leq 1.0 & (19)\\
\text{if } D_r=40\%, \quad \gamma_{max}=51.2 \quad \text{for } \text{FS}\leq 0.81 & (20)
\end{array}
\tag{3.17}
$$

3. <u>Calculation of lateral displacement index (LDI)</u>

LDI was calculated using equation (3.16), where Z_{max} is the maximum depth below all the potential liquefiable layers with a calculated FS <2.0.

4. <u>Estimation the lateral displacement (LD)</u>

With information on the ground slope (S) or/and free face height (H) and the distance to a free face (L), it is possible to calculate the lateral displacements for gently sloping ground with and/or without a free face or level ground with a free face.

Different geometries were tested and the results showed that the lateral spreads are most significant when the ground geometry has a free face and when the relation between the distance to the free face and the free face height is minimum. Therefore, the estimation of liquefaction-induced lateral displacements using the cone penetration test data, was done considering the worst-case scenario (level ground with a free face and L/H=4).

The computation of LDI in specific locations, along the waterlines, resulted in the following microzonation maps of lateral displacement index, LDI, shown in Figure 3-87 and Figure 3-88.

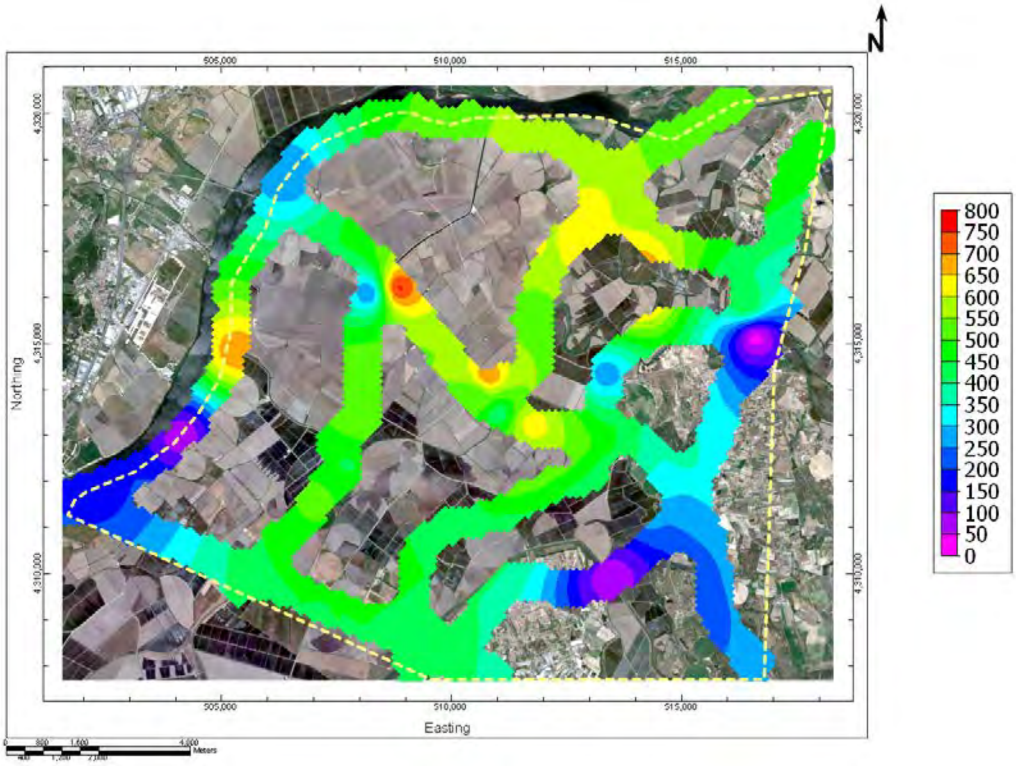

Figure 3-87 Map of LDI for seismic action EC8-T2 based on CPT tests

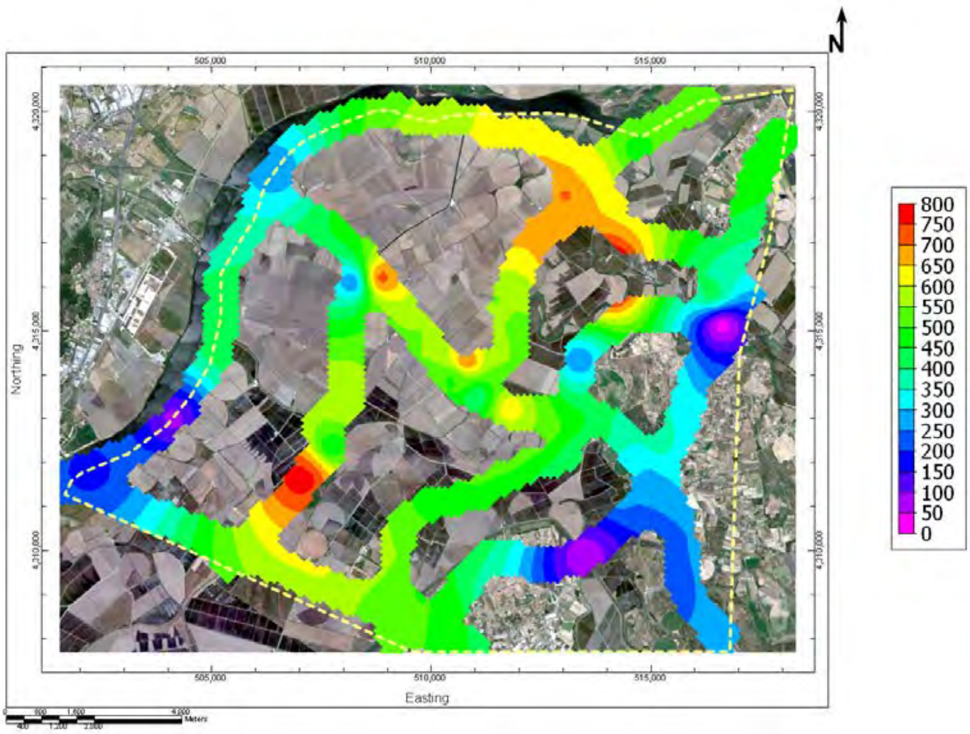

Figure 3-88 Map of LDI for seismic action EC8-T2 based on CPT tests

This project has received funding from the European Union's Horizon 2020 research and innovation programme under grant agreement No. 700748

3.5.4 Microzonation of selected cross-sections of the pilot site

In order to better visualise the liquefaction susceptibility in depth, three specific cross-section alignments were selected, where the vulnerability is expected to be higher and the consequences of liquefaction would most likely affect the community. These sections follow important alignments within the pilot site, as is clearly identified in Figure 3-89. The label A10 corresponds to the alignment along the A10 motorway, including a bridge and viaducts, while N10 refers to the main national road (N10) in the area. Finally, the third alignment (labelled "Cidades") is more irregular and corresponds to secondary roads connecting the town centres of the area, namely of Samora Correia and Benavente.

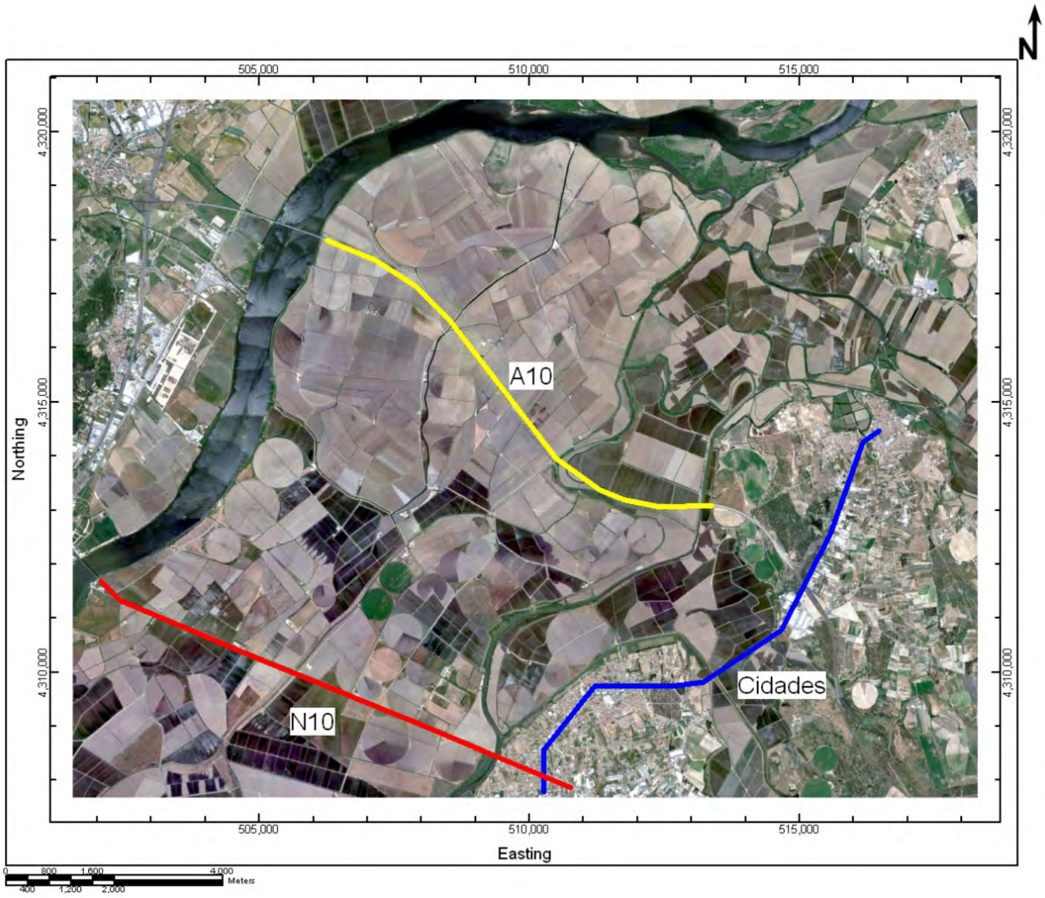

Figure 3-89 Map of the location of the three selected cross-section alignments

For these three alignments, the following cross-section models have been produced, and are provided in Appendix 3D, in terms of lithology, FS against liquefaction based on CPT tests, for EC8-T1 and EC8-T2 and FS against liquefaction based on CPT tests, for the six seismic scenarios.

3.6 Final considerations: main achievements with discussion

New geological and geotechnical models were developed for areas of the municipalities of Vila Franca de Xira and Benavente located in the Greater Lisbon region, more precisely the ones on the left bank of the river Tagus, covering a total area of 146.9 km^2. A georeferenced database was created in SQLite with data obtained from lithological surveys and geotechnical and geophysical tests. The database used in this work consisted of geological, geotechnical and geophysical information in two extensive campaigns (a total borehole depth of 6136.86 m sampling is as good example of effort made for this purpose). A special attention was due to the definition of the map with the groundwater level depth in the pilot site, as well as the definition of the geological bedrock, which was derived from more than one hypothesis.

The geotechnical model enabled to produce site-specific liquefaction risk maps and more complete 3D models, for the final goal of microzonation of the pilot site. Indeed, being this area inside a highly seismic region, with well documented historical descriptions of previous very strong Earthquakes Induced Liquefaction Damages (EILD), the definition of well-fundamented solid model for the microzonation was pursued. This risk map will help to cope with the daily implications of the life of hundreds of thousands inhabitants of the two municipalities surrounding the highly populated Lisbon metropolitan area, where the mobility of the populations is very high. The most relevant historical earthquakes-induced soil liquefaction occurred in 1755 (Lisbon) and 1909 (Benavente). After the destruction of the city of Benavente and its neighbourhood, with spread areas of liquefied grounds, new infrastructures were built during the 20th century, like embankments for roads and railways, bridges (connecting the two margins of the river Taggus where big cities are interdependent) with abutments, as well as several critical buildings for public institutions, like schools, hospitals and health centers, fire departments and police and civil protection services buildings, connected by these linear transportation infrastructures. In case of their collapse (partial or total) populations would be isolated, while private companies that operate in some industrial zones (and largely dependent on these insfrastructures to keep their activity) would loose their business. A vast area of very productive agriculture is supported by associations that regulate the water supply, relying on a system of dikes that regulate channels in connection with the Taggus river and effluents, complemented by a modern system of pumping stations, and small to medium dams. The collapse of these dikes, stations and dams, would put in danger this activity. These and the villages are also served by pipelines (gas, water and sewage) highly sensitive to the ground shakings and the ground deformation (vertical subsidence and lateral spreading) due to liquefaction of the holocene and of recent granular hydraulic fills (which have been constructed to connect the small islands of this deltaic area) would be destroyed in case EILD.

As in Emilia, Italy, from the results of ground amplification analyses it is readily apparent the correlation between the spatial variability of surface ground motion within Benavente and Vila Franca de Xira municipalities. Also here, the characteristics of the adopted seismic-geotechnical and seismo-stratigraphic models, which were developed in tight connection with the partners responsible for the Italian pilot-case, confirmed that correlation. That was emphasized in chapter 2 in view of the interplay and complementarity among different methodological approaches and spatial resolution scales characterizing a seismic microzonation study when tackled from a geological, geophysical, seismological and geotechnical prospective. The subsoil model developed in UPorto has harmonized coherently the different scales at which it can be visualized and this was possible because there was a fair spatial variation of the subsoil properties over the territory. When that was more difficult, additional site investigations were conducted to solve any inconsistency. Two earthquake types and three return periods identified in Eurocode 8 (475 years, 975 years, and 2475 years) were used to perform the analyses. Type 1 seismic action corresponds to a "far" earthquake, with epicentre in the Atlantic Ocean. Type 2 corresponds to a "near" earthquake, with epicentre in Continental Portugal. For each return period of type 1, six motions were selected, while for type 2 seven motions were adopted for each return period, giving 39 different motions. The ground motion accelerograms were then used for the analyses of EILD.

Conventional liquefaction assessment focuses only on triggering; however, earthquake-induced liquefaction is also responsible for considerable structural damage. For this reason, a new hazard-independent liquefaction classification was proposed in Liquefact – created and developed in UPorto - where the interested ground profile is defined as an equivalent 3-layered soil profile. The classification consists of only three features, taking into account the performance of shallow-founded buildings: the depth of the non-liquefying crust, and the thickness and liquefaction resistance of the potentially liquefiable layer. A procedure to obtain the 3-layered soil profile from CPT data was developed and a set of soil profile classes are generated for rapid loss assessment purposes.

In case of evident 2D/3D response, the use of more advanced numerical models will be unavoidable. H/V spectral ratio variability across the area was defined, in order to justify the increased investment required for such advanced methodology but that implies very long time computational analysis. Still, and for the purpose of the "big-data" recoiled for this vast region selected for the microzonation in Portugal, three ground response models were adopted for estimation of the representative seismic motion: linear approach, equivalent linear approach and non-linear approach. A calibration of the α value to be used in the equivalent linear approach was made, cross-checking with more complete non-linear numerical analysis, starting from the lower boundary of this coefficient, with the value of 0.2, corresponding to the most conservative PGA, to the most current value of 0.65. The comparative analyses allowed us to conclude that the value of 0.65 was very much appropriate to the microzonation purpose and finally adopted. Site-factor sensitivity study was performed, and even for the steep ancient geological beds in borders of the Low Taggus Valley, this area had a sufficiently large plateau of sediments to allow 1D analyses for this purpose.

A specific study of the site response considering liquefaction was done by adopting a method developed in Liquefact, called the equivalent linear Stockwell analysis method (details in the Deliverable 3.2 - Viana da Fonseca et al. 2018a). By creating a time-frequency transfer function between the upward propagating and surface motion to identify liquefaction triggering using the Stockwell transform, a series of excess pore pressure (time) dependent base-to-surface transfer functions are applied along the frequency axis before performing the inverse Stockwell transform to obtain the surface motion in the time domain. The strain energy based method (SEBM) also created and developed in UPorto was used to estimate the pore pressure time series (details in the Deliverable 3.2). Soil deformations (vertical settlements – total and differential - and horizontal displacements – lateral spreading) largely condition soil-liquefaction-foundation-structure interaction (SLFSI) and, while the new ground motion at the surface has lower values of PGA, the vulnerability analysis has to congregate these two demands (shaking and settlements). This substructuring was developed in Deliverable 3.2 for modelling differential settlements and soil-foundation-structure interaction.

Following all the works above, the final following microzonation maps have been produced, in terms of surface peak acceleration (m/s2) and factor of amplification (computed in relation with the PGA at the rock). These maps were presented for six different seismic scenarios Type 1, with return periods of 475, 957 and 2475 years, and Type 2, with the same return periods.

For the purpose of illustrating the hazard-independent liquefaction resistance of the soils at the pilot site, 3D models of the cyclic resistance ratio (CRR) have been produced from the SPT and CPT results. The differences in the results resulting from these alternative in situ tests were analysed and it was concluded that the CPT provide reliable quantitative indication of the type of soil at each depth, while the SPT revealed being very generic and qualitative.

The microzonation for liquefaction risk considered both the standard seismic type actions of Eurocode 8 (Type 1 – large distant earthquake; Type 2 – medium near earthquake), but also the implementation of the ground response analyses and the respective microzonation for ground shaking. The corresponding maps, with cross-sections were presented and the files with the data were uploaded in Zenodo.

The same was done for the estimation of liquefaction-induced damages, based on quantitative liquefaction risk indexes, namely the Liquefaction Potential Index (LPI) and the Liquefaction Severity Number (LSN), being these particularly convenient for the production of microzonation maps. These liquefaction indexes were calculated considering the ground water level (GWL) as measured in situ at the time of the test, without a prior calculation of these indices with a short sensitivity study to assess the impact of the fluctuation of GWL. The extreme case of a constant ground water level at 1m depth was concluded to be adequate.

Finally, in order to estimate the magnitude of lateral displacements associated with a liquefaction-induced lateral spreading, an index very relevant to identify risk losses in the many dykes and abutments in operation in this area was considered. In fact, this damage is mostly probable in this area due to the significant extension of dikes and levees, protecting the territory from the floods of the Taggus River and regulating the extensive system of channels for water supply regulation, as well as embankments for transportation networks. The critical points were chosen where the ground geometry could lead to lateral spreading. Maps of the Lateral Displacement Indices (LDI) were created along the waterlines and along the main roads.

3.7 Acknowlegments

This work was made possible with the collaboration of the following institutions and persons: 'Instituto Superior Técnico' of the University of Lisbon, represented by Doctor Rui Carrilho Gomes, Doctor Fátima Gouveia and Eng. André Ramos; the Faculty of Sciences of the University of Lisbon, represented by Dr. Paula Teves-Costa; the National Laboratory of Energy and Geology (LNEG), represented by Doctor João Carvalho and Doctor Ruben Dias, for the geological expertise and support on the acquisition of the geological charts of the region; the Association of the Beneficiaries of 'Lezíria Grande de Vila Franca de Xira', represented by Eng. Rui Paixão, for the facilities granted in the access to the pilot site and the support in obtaining owner's permissions; the Municipality of Montijo, represented by the Mayor, Eng. Nuno Canta; the Municipality of Benavente, represented by the Mayor, Dr. Carlos Coutinho; the Civil Protection Service of Benavente, represented by Dr. Nuno Rolo and Commander Miguel Cardia; the Polytechnic Institute of Guarda (IPG), represented by Doctor Carlos Rodrigues; Doctor Sara Amoroso from the INGV and Doctor Luca Minarelli from GEOTEMA, Univ. Ferrara, for their knowledge and collaboration in risk microzonation and its application; the construction company, 'Teixeira Duarte – Engenharia and Construções, S.A.', represented by Geologists Dr. Costa Vilar and Dr. Pedro Nunes; the geotechnical survey company SLP, namely Dr. Gorazd Strniša, Eng. Matevž Lesjak and Eng. Ivan Lesjak; National Laboratory of Civil Engineering (LNEC), represented by Dr. Alexandra Carvalho, for providing the seismic characteristics of the region; BRISA, Engenharia e Gestão (Engineering and Management), represented by Eng. Paulo Lima Barros; ENMC - Entidade Nacional para o Mercado de Combustíveis, E.P.E. (National Authority for Fuel Market), represented by Dr. Rita Silva; the consulting companies: COBA, SA, represented by Doctor Ricardo Oliveira; CENOR Consulting Engineering, represented by Eng. Gonçalo Tavares; JETsj, represented by Eng. Alexandre Pinto; Geocontrole, represented by Eng. Jorge Correia; and, the colleagues in the from University of Porto (FEUP), the MSc student, Carlos Maria Azerêdo for the early works on equivalent linear Stockwell analysis method, the PhD Students Fausto Molina Goméz and Catarina Ramos for the collaboration in situ tests campaigns and Doctor Pedro Alves Costa and his PhD students Aires Colaço and Alexandre Pinto for the SASW tests.

3.8 References

- Andreotti, G., Famà, A., & Lai, G. (2018). Hazard-dependent soil factors for site-specific elastic acceleration response spectra of Italian and European seismic building codes. Bulletin of Earthquake Engineering, 16, 5769-5800.
- Bardet, J.P and Tobita, T. (2001). NERA - A Computer Program for Nonlinear Earthquake site Response Analyses of Layered Soil Deposits. Department of Civil Engineering. University of Southern California.
- Bouckovalas, G. D., Tsiapas, Y. Z., Zontanou, V. A., & Kalogeraki, C. G. (2017). Equivalent linear computation of response spectra for liquefiable sites: The spectral envelope method. Journal of geotechnical and geoenvironmental engineering, 143(4), 04016115-12.
- Boulanger, R. W., & Idriss, I. M. (2014). CPT AND SPT Based Liquefaction Triggering Procedures. University of California at Davis, Department of civil & environmental engineering, college of engineering. Davis: University of California.
- Boulanger, R. W., & Idriss, I. M. (2016). CPT-Based Liquefaction Triggering Procedure. Journal of Geotechnical and Geoenvironmental Engineering, 142(2), 04015065. https://doi.org/10.1061/(ASCE)GT.1943-5606.0001388
- Bowden, A., 2003. Presentation and discussion of evidence support logic (ESL). A note to the British Geological Survey (Unpublished).
- Carlton, B.D. & Tokimatsu, K. (2016). Comparison of Equivalent Linear and Nonlinear Site Response Analysis Results and Model to Estimate Maximum Shear Strain. Earthquake Spectra, 32(3), p 1867–1887.

- Carvalho, J., Cabral, J., Gonçalves, R., Torres, L., Mendes-Victor, L., 2006. Geophysical methods applied to fault characterization and earthquake potential assessment in the Lower Tagus Valley, Portugal. Tectonophysics 418, 277–297 doi:10.1016/j.tecto.2006.02.010
- Clarke, S., 2004. Confidence in geological interpretation. A methodology for evaluating uncertainty in common two and three-dimensional representations of subsurface geology. British Geological Survey - Internal Report IR/04/164.
- Cooley, & Tukey. (1965). An algorithm for the machine computation of complex Fourier series. Mathematics of Computation, 19(4), 297-301.
- Cubrinovski, M., Rhodes, A. Ntritsos, N. & van Ballegooy, S. (2017). System response of liquefiable deposits. In 3rd International Conference on Performance-based Design in Earthquake Geotechnical Engineering, pp. 1–18.
- Darendeli, M. B. (2001). Development of a new family of normalized modulus reduction and material damping curves. University of Texas at Austin, Austin.
- Davidenkov, N.N. (1938): Energy dissipation in vibrations. Journal of Technical Physics, 8(6) (in Russian).
- Groholski, D.R., Hashash, Y.M.A., Musgrove, M.I., Harmon, J.A. & Kim, B. (2015): Evaluation of 1-D non-linear site response analysis using a general quadratic/hyperbolic strength-controlled constitutive model. 6th International Conference on Earthquake Geotechnical Engineering, 1-4 Nov, Christchurch, New Zealand.
- Hardin, B.O. & Drnevich, V.P. (1972): Shear modulus and damping in soils: design equations and curves. J. of the Soil Mechanics and Foundations Div., ASCE, 98 (SM7), 667-692.
- Hashash, Y.M.A., Musgrove, M.I., Harmon, J.A., Groholski, D.R., Phillips, C.A., & Park, D. (2015): DEEPSOIL 6.1 User Manual.
- Idriss, I.M. & Sun, J.I. (1992). "Shake91: a computer program for conducting equivalent linear seismic response analysis of horizontally layered soil deposits", User's Guide, University of California, Davis, 13 pp.
- Iwasaki, T., Tatsuoka, F., Tokida, K. & Yasuda, S. 1978. A practical method for assessing soil liquefaction potential based on case studies at various sites in Japan. Proceedings of the 2nd International Conference on Microzonation. San Francisco, CA, USA, pp. 885–896.
- Iwasaki, T., Tokida, K., Tatsuoka, F., Watanabe, S., Yasuda, S., Sato, H (1982). Microzonation for soil liquefaction potential using simplified methods, In: Proceedings of the 3th International Conference on microzonation, Seattle, USA, 3: 1319–1330
- Iwasaki T, Arakawa T, Tokida K (1984) Simplified Procedures for Assesing Soil Liquefaction During Earthquakes. Soil Dynamics and Earthquake Engineering, 3(1):49–58.
- Kaynia, A.M. (2012): QUIVER_site – numerical code for nonlinear seismic site response analyses. NGI Report 20071851-00-82-R, 8 June.
- Kausel, E., & Assimaki, D. (2002). Seismic simulation of inelastic soils via frequency-dependent moduli and damping. J Eng Mech, 128(1), 34-47.
- Kramer, S. (1996). Geotechnical earthquake engineering. New Jersey: Prentice Hall.
- Lee, D.H., C.S. Ku, & H. Yuan. (2003). A study of liquefaction risk potential at Yuanlin, Taiwan. Engineering Geology 71: 97–117.

- Manupella, G., Ferreira, A.B., Dinis, J., Callapez, P., Ribeiro, M.L., Pais, J., Rebêlo, L., Cabral, J., Moniz, C., Baptista, R. Henriques, P., Falé, P. Lourenço, C., Sampaio, J., Midões, C. & Zbyszewski, G., 2011. Notícia explicativa da folha 34-B, Loures da Carta Geológica de Portugal, 1/50000. Laboratório Nacional de Energia e Geologia, Lisboa, 57 pp; ISBN: 978-989-675-014-5.
- Millen, M., Ferreira, C., Gerace, A., & Viana da Fonseca, A. (2019a). Simplified equivalent soil profiles based on liquefaction performance. 7th International Conference on Earthquake Geotechnical Engineering. Rome, Italy.
- Millen, M., Azeredo, C., & Viana da Fonseca, A. (2019b). Time-frequency filter for computation of surface acceleration for liquefiable sites: the equivalent linear Stockwell analysis method. Journal of Geotechnical and Geoenvironmental Engineering (submitted).
- Millen, M., Rios, S., Quintero, J., & Viana da Fonseca, A. (2019c). Prediction of time of liquefaction using kinetic and strain energy. Soil dynamics and Earthquake engineering (submitted).
- Miwa, S., & Ikeda, T. (2006). Shear modulus and strain of liquefied ground and their application to evaluation of the response of foundation structures. Structural engineering / earthquake engineering, 23(1), 167s–179s.
- Pyke, RM (1979): Nonlinear soil models for irregular cyclic loadings. Journal of Geotechnical and Geoenvironmental Engineering, ASCE, 105(GT6), 715-726.
- Robertson, P. K. (2009). Interpretation of Cone Penetration Test - A unified approach. Can Geotech J, 27(1), 151-158.
- Rockworks 17 (2017). Help Files. Rockware Inc, Colorado, 2017.
- Sonmez, H. (2003). Modification of the liquefaction potential index and liquefaction susceptibility mapping for a liquefaction-prone area (Inegol, Turkey). Environmental Geology 44:862–871.
- Tonkin & Taylor Ltd. 2013. Liquefaction Vulnerability Study. Report to the Earthquake Commission, by S. van Ballegooy and P. Malan. T&T Ref: 52020.0200/v1.0. Available and accessed in 6 July 2019 at: http://www.eqc.govt.nz/sites/public_files/documents/liquefaction-vulnerability-study-final.pdf;
- Viana da Fonseca, A., Millen, M., Romão, X., Quintero, J., Rios, S., Ferreira, C., Panico, F., Azeredo, C., Pereira, N., Logar, J., Oblak, A., Dolšek, M., Kosič, M., Kuder, S., Logar, M., Oztoprak, S., Kelesoglu, M. K., Sargin, S., Oser, C., Bozbey, I., Flora, A., Billota, E., Prota, A., Di Ludovico, M., Chiaradonna, A., Modoni, G., Paolella, L., Spacagna, R., Lai, C.G., Shinde, S. and Bozzoni, F. (2018a). Methodology for the liquefaction fragility analysis of critical structures and infrastructures: description and case studies. DELIVERABLE 3.2 of LIQUEFACT project "Assessment and mitigation of liquefaction potential across Europe: a holistic approach to protect structures / infrastructures for improved resilience to earthquake-induced liquefaction disasters" (www.liquefact.eu)
- Viana da Fonseca, A., Millen, M., Romão, X., Quintero, J., Rios, S. and Meslem, A. (2018b). Design guidelines for the application of soil characterisation and liquefaction risk assessment protocols. DELIVERABLE 3.3 of LIQUEFACT project "Assessment and mitigation of liquefaction potential across Europe: a holistic approach to protect structures / infrastructures for improved resilience to earthquake-induced liquefaction disasters" (www.liquefact.eu)

- Viana da Fonseca, A., Ferreira, C., Ramos, C., Saldanha, S., Amoroso, S. & Rodrigues, C. (2019). Liquefaction susceptibility assessment based on in situ geotechnical and geophysical characterisation of a pilot site in the greater Lisbon area. Bulletin of Earthquake Engineering (submitted)
- Wotherspoon, L.M., R.P. Orense, M. Jacka, R.A. Green, B.R. Cox, & C.M. Wood. 2014. Seismic performance of improved ground sites during the 2010-2011 Canterbury earthquake sequence. Earthquake Spectra 30(1): 111–119.
- Vis, G., Kasse, C. & Vandenberghe, J., 2008. Late Pleistocene and Holocene palaeogeography of the Lower Tagus Valley (Portugal): effects of relative sea level, valley morphology and sediment supply. Quaternary Science Reviews 27, 1682–1709. doi:10.1016/j.quascirev.2008.07.003.
- Yoshida, N., Kobayashi, S., Suetomi, I., & Miura, K. (2002). Equivalent linear method considering frequency dependent characteristics of stiffness and damping. Soil Dyn Earthq Eng, 22(3), 205-222.
- Zhang, G., Robertson, P.K. & Brachman, R.W.I. (2002). Estimating Liquefaction induced ground settlements from CPT for level ground. Canadian Geotechnical Journal. 39(5): 1168–1180. doi: 10.1139/t02-047.
- Zhang, G., P.K. Robertson, and R.W.I. Brachman. 2004. Estimating liquefaction-induced lateral displacements using the standard penetration test or cone penetration test. Journal of Geotechnical and Geoenvironmental Engineering. 130(8): 861–871. Doi: 10.1061/(ASCE)1090-0241(2004)130:8(861)
- Zbyszewski, G., Torre de Assunção, C., 1965. Notícia Explicativa da folha 30-D, Alenquer da Carta Geológica de Portugal, 1/50000. Serviços Geológicos de Portugal.
- Zbyszewski, G., Veiga Ferreira, O., 1968. Notícia Explicativa da folha 31-C, Coruche da Carta Geológica de Portugal, 1/50000. Serviços Geológicos de Portugal.

APPENDICES

APPENDIX 3A Tools, Methods, Algorithms and Modelling Options

Software tools

The software application selected for this work was Rockworks17 from Rockware ®. All the information was georeferenced and inserted into a SQLite database, from which all the results presented in this report were generated. Other applications used in this project included:

- ArcGis (ArcMap 10.6) ® for the treatment of existing data in shapefile format (geological charts and topographic data);
- PaintNet® for image processing and editing;
- GoogleEarth® for coordinate collection and as an output viewer;
- http://www.igeoe.pt/coordenadas/ for coordinate transformation.

Methods

In order to enable data usage, which are spatially dispersed and discontinuous by nature, it was necessary to follow a gridding process, in which data are transformed into regular networks of numerical values. It was based on these networks that calculations were performed and 2D and 3D graphical representations were created.

The network model consists of a grid of imaginary lines that overlap the original data. The dimensions of this grid are defined according to the area of study, the average spacing of the data and their variability.

The gridding process consists of assigning values to the intersections of the network lines - the nodes. Accordingly, there are several methods (algorithms) that can be used to interpolate the data. Each algorithm has both positive and negative aspects.

A network file consists of a computer file that contains the results of the gridding process. This file contains a list of X and Y location coordinates of network nodes spaced regularly (X, Y and Z in 3D) and the value of the Z variable (G in 3D) extrapolated to each node.

Networks can be mathematically operated between each other, node to node (numerical and boolean) and graphically represented in 2D and 3D in vector format. The results can be exported to raster (jpg, png, tiff, for example), arcview (shapefile), autocad (dxf) and google earth (kmz).

The geological entities (lithological and stratigraphic) are identified through univocal numerical values called lithocodes assigned at the beginning of the project.

Project Dimensions

The coordinate system used in this project is the WGS84 / UTM zone 29T (EPGS: 32629). It was necessary to convert the coordinates of the existing data since they were in several systems used in Portugal: ETRS89 / PT-TM06 (EPGS: 3763); Datum 73 / Hayford-Gauss (EPGS: 27493).

Taking into account the spatial distribution of the data, a spacing grid of 150m x 150m corresponding to 113x87 nodes was established for X and Y, respectively. The vertical resolution was defined based on the minimum sand thickness in the boreholes. For this, a spacing of 0.25m was defined for Z, corresponding to 333 nodules.

Algorithms and Modelling Options

(adapted from *Help Files, Rockworks17*)

Distance to Point: Each node is assigned a value that represents its distance, in your X, Y, Z coordinate units, to the closest control point.

Inverse-Distance: The value assigned to a node is a weighted average of either all of the data points or a number of directionally distributed neighbors. The value of each of the data points is weighted according to the inverse of its distance from the grid node, taken to a user-selected power.

IDW Anisotropic (Inverse Distance Anisotropic): This method is one of the "flavors" of the Inverse-Distance algorithm. Using Inverse-Distance in general, a voxel node value is assigned based on the weighted average of neighboring data points, and the value of each data point is weighted according the inverse of its distance from the voxel node, taken to a power.

Lateral Blending: The Lateral Blending method looks outward horizontally from each data point, in search circles of ever-increasing diameter. It first assigns the voxels immediately surrounding each borehole the closest lithology or real number value. It then moves out by a voxel, and assigns the next "circle" of voxels the closest lithology value. It continues in this manner until it reaches a point about a third of the way to neighboring data points. Then, in the center areas, it applies a randomizing algorithm to minimize the abrupt changes between material types.

Interpolate Outliers: Permits to assign all model voxels a G value. If not selected the "outlying" nodes, positioned either in the center zones between points or in outer zones beyond a cutoff distance or, will be assigned the Undefined value (e.g. null), thus making them invisible in the output model. The cutoff distance is defined as the distance between a well and its closest neighboring well.

Resample at Regularly-Spaced Intervals: Resample the data to regular depth intervals, with a variety of methods.

Superface: Nodes above a grid surface will be assigned the Undefined value (e.g. null).

Warping: Biases a solid model with a grid model. This feature works like this: (a) The control point elevations are vertically shifted, based on the corresponding elevations within the reference grid. (b) The solid model is interpolated (based on the vertically shifted coordinates). (c) The corresponding nodes within the model are then shifted back to their proper elevations based on the corresponding elevations within the reference grid. Why? Algorithms such as the horizontal lithoblending strongly bias the interpolation in a horizontal fashion. The "warp" option introduces structure while still allowing the modeling to be horizontally biased.

Database

Figure A3.1 illustrates a screenshot of the Rockworks17 borehole manager interface tab. For each data point (whether lithological, geotechnical or geophysical) its location is created by inserting its horizontal coordinates (Easting and Northing) and the vertical coordinates (elevation, collar elevation and total depth).

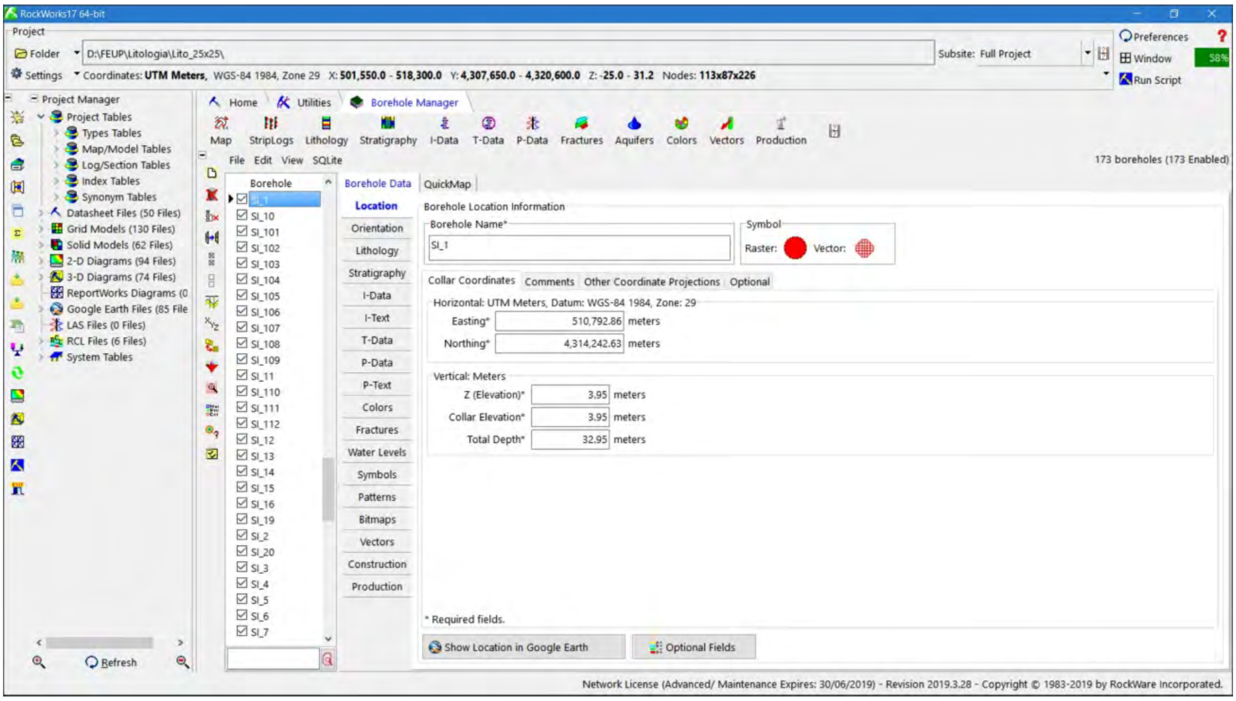

Figure A3.1 Rockworks17 screenshot: Borehole Manager tab

According to the existing data for each point, these were inserted in the specific table according to the depth at which they occurred. In this database, the following database tables were defined: stratigraphy (Figure A3.2a), lithology (Figure A3.2b), water levels and P-data (Figure A3.3).

a) b)

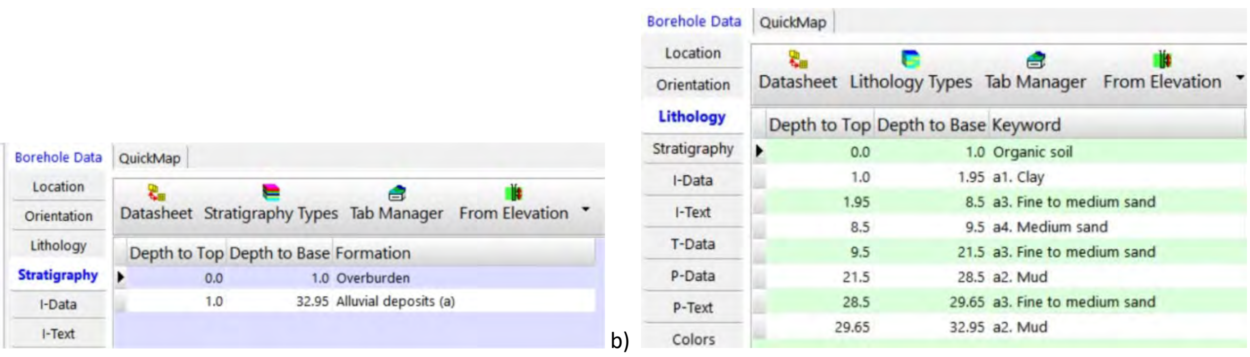

Figure A3.2 Rockworks17 screenshots: a) stratigraphy tab; b) lithology tab

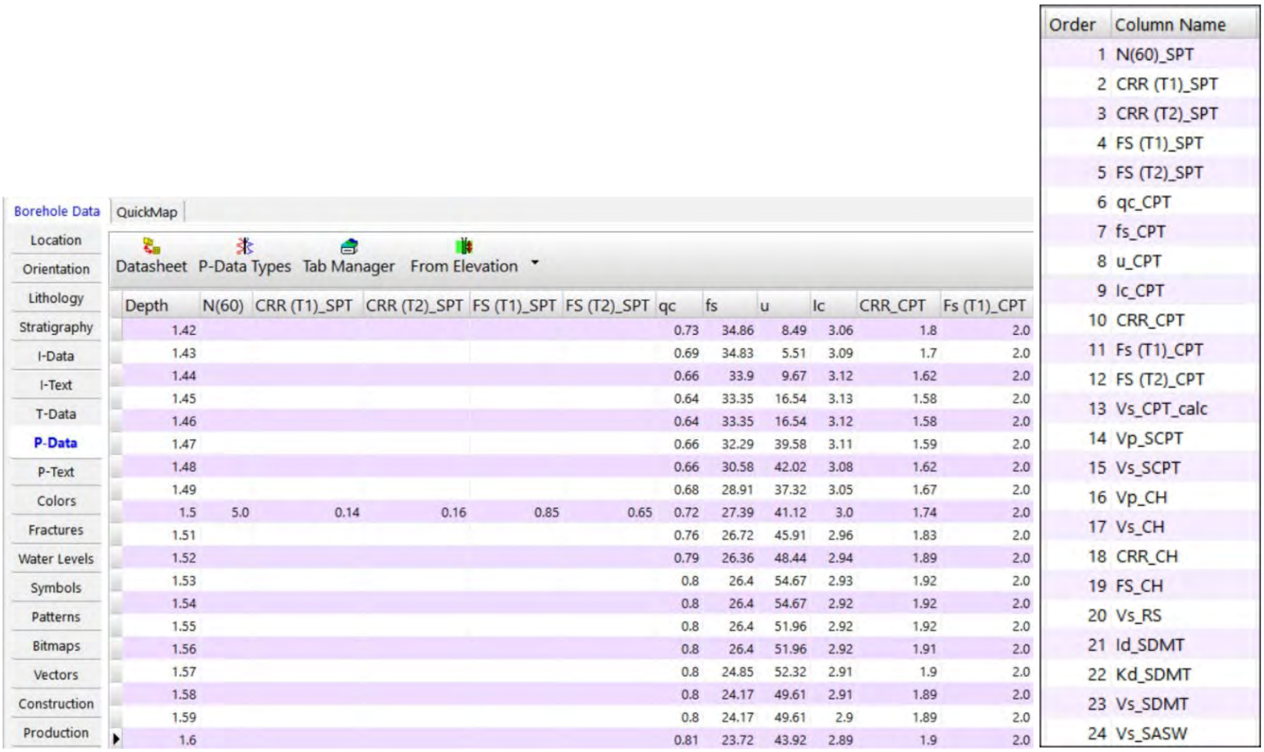

Depth	N(60)	CRR (T1)_SPT	CRR (T2)_SPT	FS (T1)_SPT	FS (T2)_SPT	qc	fs	u	Ic	CRR_CPT	Fs (T1)_CPT
1.42						0.73	34.86	8.49	3.06	1.8	2.0
1.43						0.69	34.83	5.51	3.09	1.7	2.0
1.44						0.66	33.9	9.67	3.12	1.62	2.0
1.45						0.64	33.35	16.54	3.13	1.58	2.0
1.46						0.64	33.35	16.54	3.12	1.58	2.0
1.47						0.66	32.29	39.58	3.11	1.59	2.0
1.48						0.66	30.58	42.02	3.08	1.62	2.0
1.49						0.68	28.91	37.32	3.05	1.67	2.0
1.5	5.0	0.14	0.16	0.85	0.65	0.72	27.39	41.12	3.0	1.74	2.0
1.51						0.76	26.72	45.91	2.96	1.83	2.0
1.52						0.79	26.36	48.44	2.94	1.89	2.0
1.53						0.8	26.4	54.67	2.93	1.92	2.0
1.54						0.8	26.4	54.67	2.92	1.92	2.0
1.55						0.8	26.4	51.96	2.92	1.92	2.0
1.56						0.8	26.4	51.96	2.92	1.91	2.0
1.57						0.8	24.85	52.32	2.91	1.9	2.0
1.58						0.8	24.17	49.61	2.91	1.89	2.0
1.59						0.8	24.17	49.61	2.9	1.89	2.0
1.6						0.81	23.72	43.92	2.89	1.9	2.0

Order	Column Name
1	N(60)_SPT
2	CRR (T1)_SPT
3	CRR (T2)_SPT
4	FS (T1)_SPT
5	FS (T2)_SPT
6	qc_CPT
7	fs_CPT
8	u_CPT
9	Ic_CPT
10	CRR_CPT
11	Fs (T1)_CPT
12	FS (T2)_CPT
13	Vs_CPT_calc
14	Vp_SCPT
15	Vs_SCPT
16	Vp_CH
17	Vs_CH
18	CRR_CH
19	FS_CH
20	Vs_RS
21	Id_SDMT
22	Kd_SDMT
23	Vs_SDMT
24	Vs_SASW

Figure A3.3 Rockworks17 screenshots: P-data

The P-data table (Figure A3.3) includes all measured values in geotechnical and/or geophysical tests and the computed values for CRR and FS for the different return periods.

In this table were also inserted the test results with measurements in depth: SPT; CPT; CH; SR; SDMT and SASW. The tests and / or calculations with point measurement (for 2D mapping) are not included in this table. For these, individual data sheets were generated, namely for: HVSR; Vs30; LPI; LSN and LDI.

Outputs

The complete output database is available in SQLite, xlsx, odf and txt formats. The maps were generated in Rw2D and PNG format, with georreferencing file in pgW. The 3D models were generated in Rw3D and PNG formats.

APPENDIX 3B Pilot site area (polygon coordinates)

Table A3.1 Pilot site polygon coordinates

X (Easting)	Y (Northing)
518230.57	4320495.89
516199.97	4320239.39
514788.87	4319405.71
513338.09	4319881.85
512691.05	4319965.52
510467.48	4319900.97
509988.65	4319760.13
509421.86	4319890.65
509071.88	4320031.30
508730.45	4320006.78
507763.94	4319651.02
507111.37	4319336.26
506708.59	4318996.53
506215.56	4318338.30
506063.25	4317856.33
505953.19	4317534.10
505586.88	4316965.20
505218.22	4316316.39
505220.02	4315337.88
504952.46	4314227.74
504525.49	4313523.31
503964.51	4312838.85
503099.50	4312198.01
502031.01	4311770.85
501808.19	4311591.16
501648.98	4311278.89
509557.44	4307698.41
516794.44	4307692.44
517014.29	4314473.11
517685.14	4317065.12

This project has received funding from the European Union's Horizon 2020 research and innovation programme under grant agreement No. 700748

APPENDIX 3C Confidence levels of the model

As a rule of thumb, for representative sampling, data spacing must be equal to or less than the range of the spacing interval identified in Figure A3.4 to Figure A3.6. For example, for the case of CPT data, a minimum range of 2691 m and a minimum average distance (DMM) of 1108 m were determined. These values enabled to classify the CPT sampling density as good.

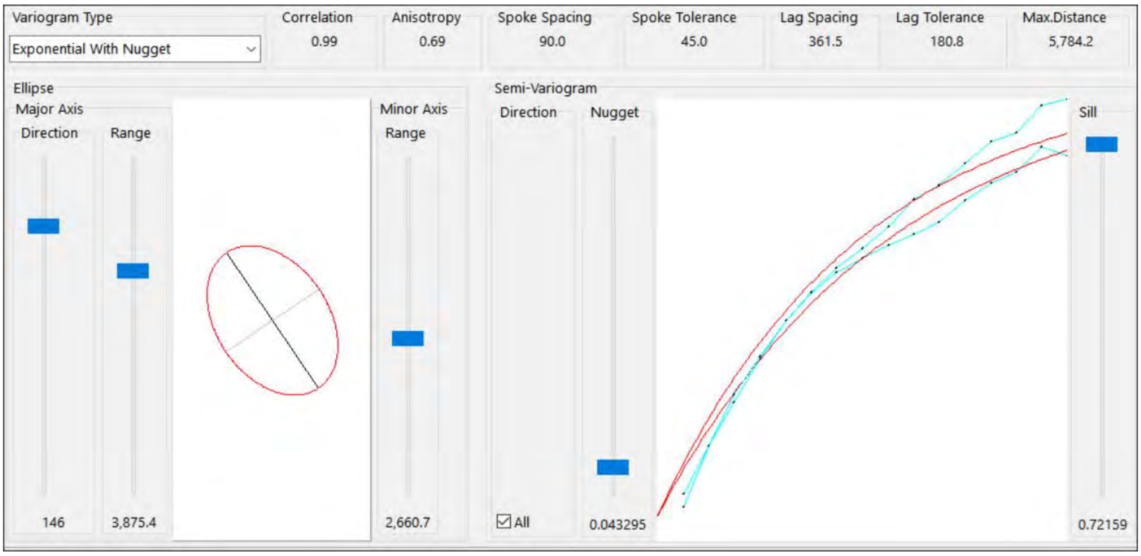

Figure A3.4 Half-variogram of lithological sampling

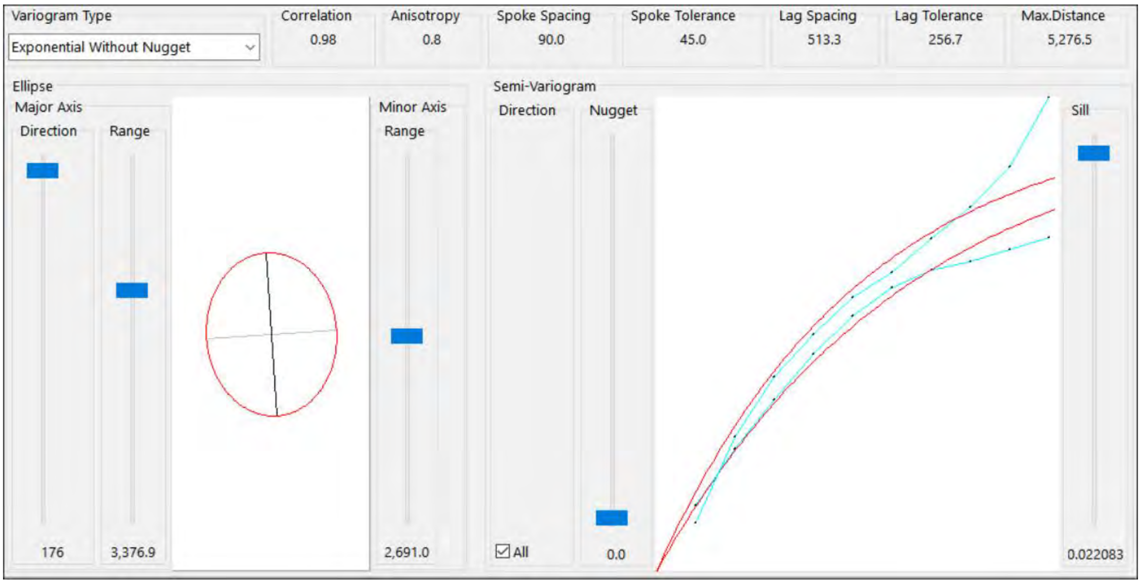

Figure A3.5 Half-variogram of CPT sampling

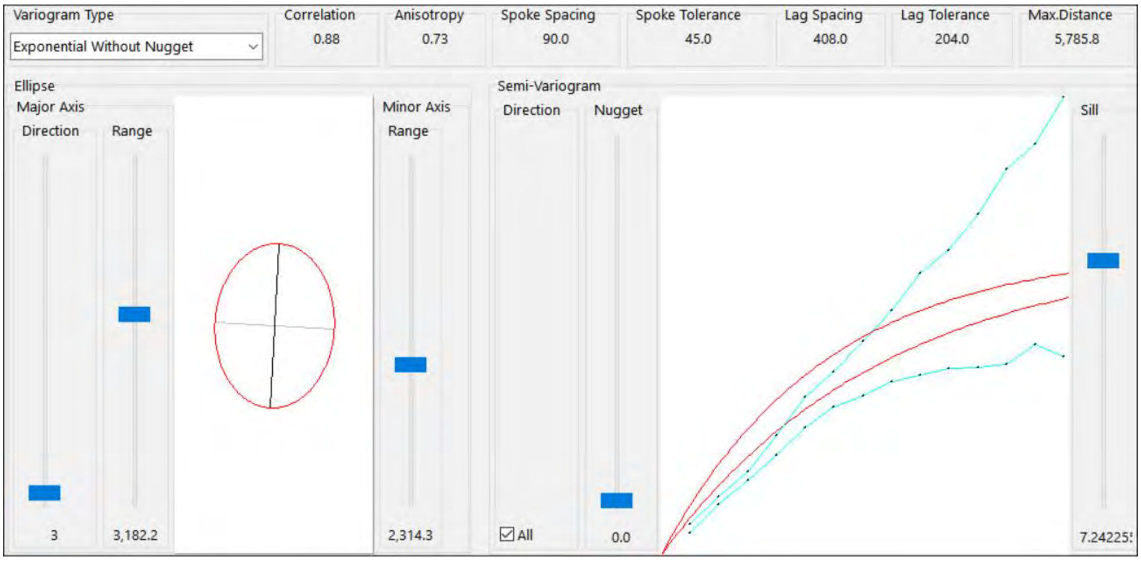

Figure A3.6 Half-variogram of SPT sampling

According to Clarke (2004), sampling confidence can be determined from a combination of the quantity and quality scores. Based on this concept, CPT sampling quantity would score between 80 to 90% (CQT), as shown in Figure A3.7. Taking into account the CPT procedures, its sampling quality can be scored at 80%. Consequenty, a confidence or certainty score of 0.87 (from 0 to 1) has been atributted to CPT data, corresponding to high-very high.

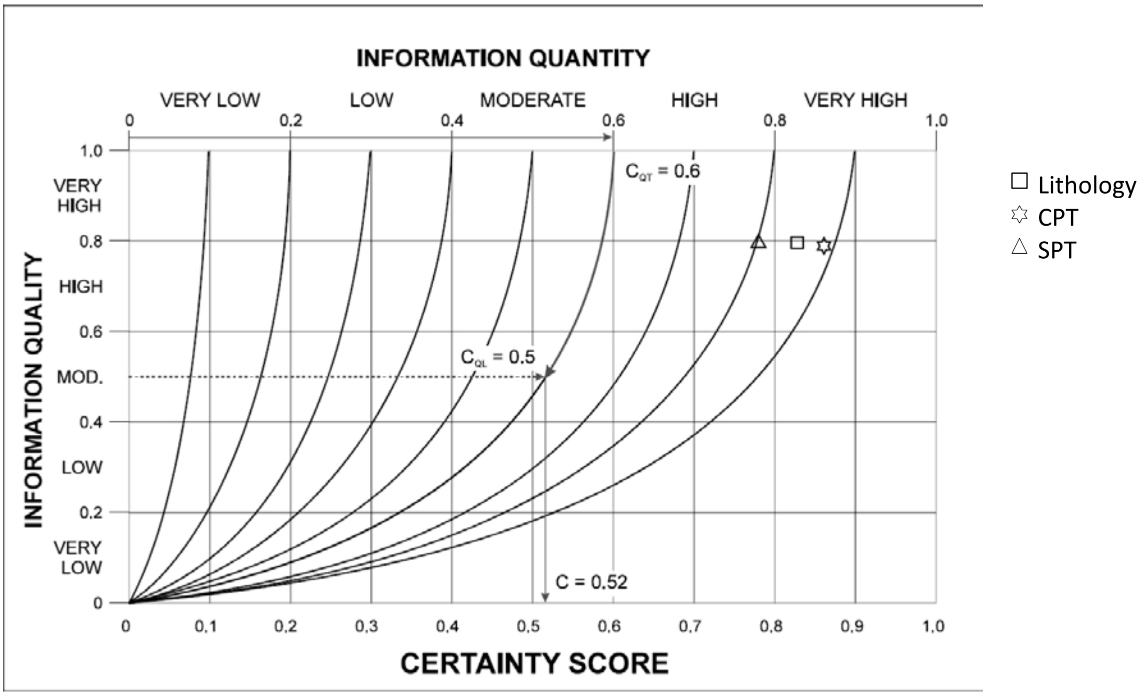

Figure A3.7 Determination of the certainty score as a combination of quantity and quality scores. The quantity score moves along the appropriate curve to a value of the quality score (adapted from Bowden, 2003).

Table A3.2 summarises the main confidence scores (0 to 19 of the datasets of this pilot site.

Table A3.2 Summary of the confidence scores of the lithology, CPT and SPT datasets

Type	R	DMM	C_{QL}	C_{QT}	Confidence
Lithology	2660	762	80%	80-90%	0.82
CPT	2691	1108	80%	80-90%	0.87
SPT	2314	840	80%	80%	0.78

R = Minimum range, DMM = Minimum average distance, C_{QL} = Quality score, C_{QT} = Quantity score

The computed confidence scores refer to the minimum average distance (DMM). However, these scores do not reflect geographical variability. This can be assessed by mapping the distances from the sampled data points to the closest grid nodes. Such variability is illustrated in Figure A3.8 to Figure A3.10, which was prepared according to the following process:

- For each dataset type, a network was created translating the distance of each sampling point to the nearest node of the project network;
- This network was standardised, so that the Z value of each point would translate the previous distance relative to half the minimum range of the respective half-variogram (R/2), expressed in the number of standard deviations of the initial distance network . That is, the Z value of each point corresponds to [X - (R/2)]/S where X is the value of the distance in the first network, R/2 represents half of the range and S is the corresponding standard deviation.

As such, maps of distance anomalies in relation to R/2, expressed in number of standard deviations were created. A value of zero represents a distance equal to R/2, negative values represent points with a distance lower than R / 2 (that is, of confidence) and positive values represent points with a distance greater than R/2 (thus, without confidence), all expressed in the number of standard deviations.

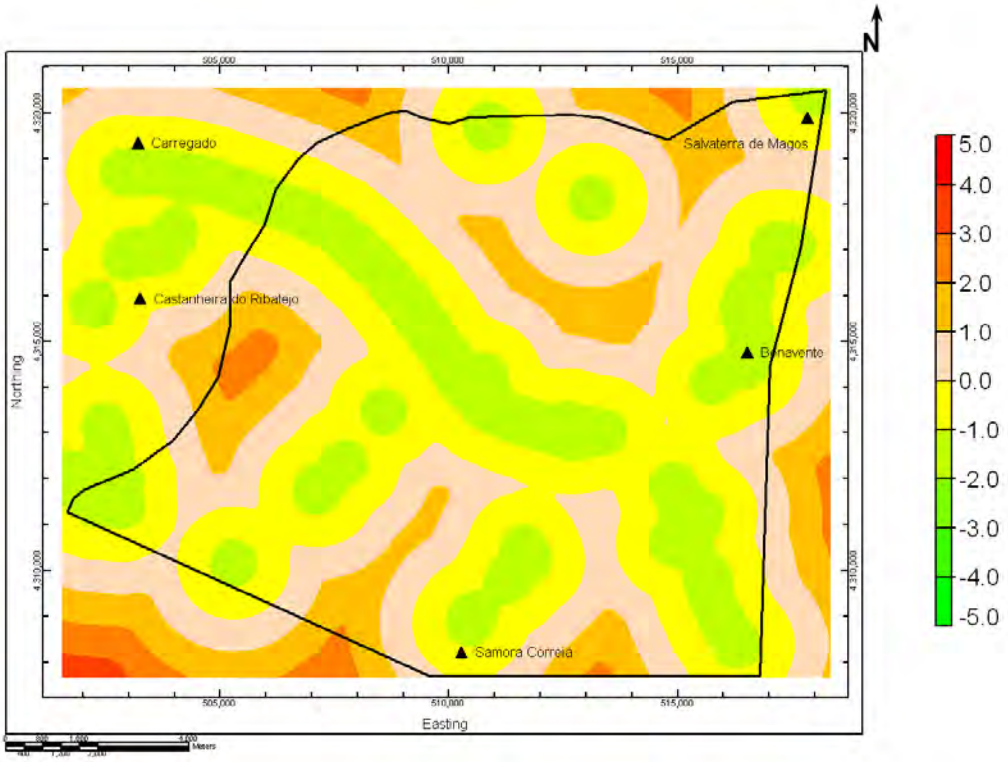

Figure A3.8 Distribution map of lithology confidence in the pilot site area. Positive values correspond to regions with a distance greater than R/2.

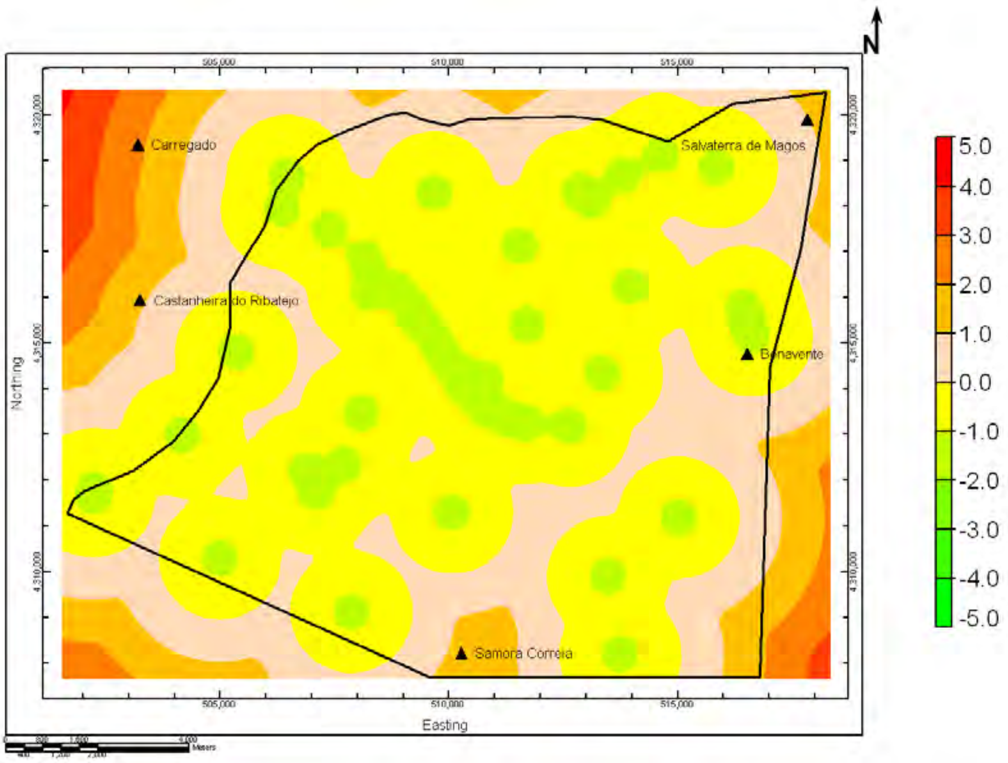

Figure A3.9 Distribution map of CPT confidence in the pilot site area. Positive values correspond to regions with a distance greater than R/2.

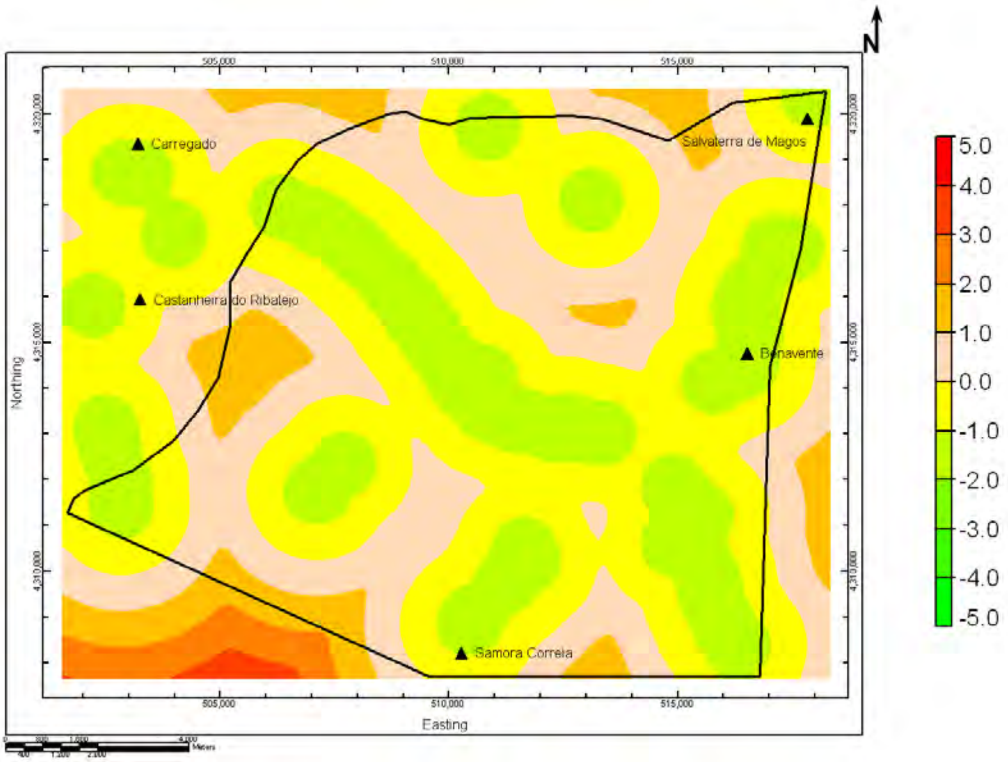

Figure A3.10 Distribution map of SPT confidence in the pilot site area. Positive values correspond to regions with a distance greater than R/2.

APPENDIX 3D Microzonation of selected cross-sections of the pilot site

Cross-section models in terms of lithology, FS against liquefaction based on CPT tests, for EC8-T1 and EC8-T2 and FS against liquefaction based on CPT tests, for the six seismic scenarios.

A10 alignment

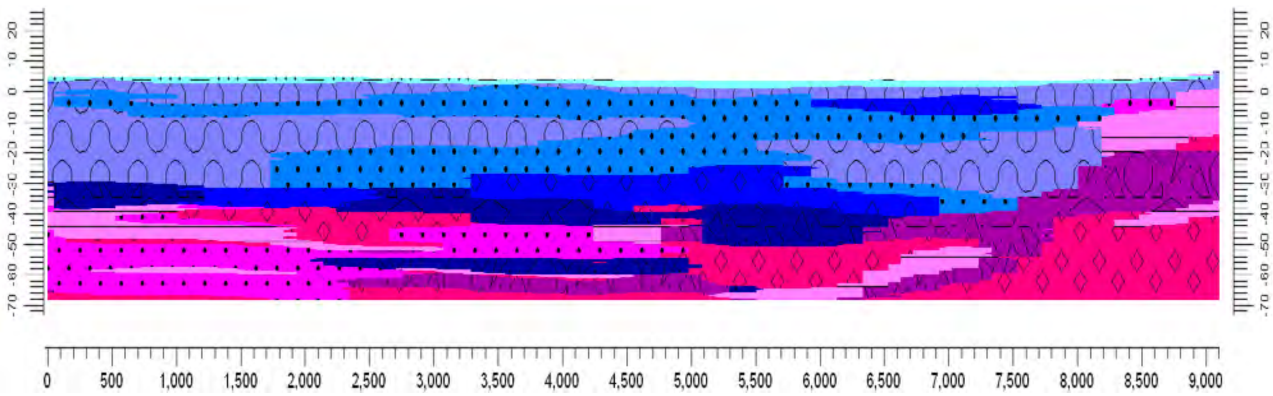

Figure A3.11 Lithological cross-section of A10 alignment

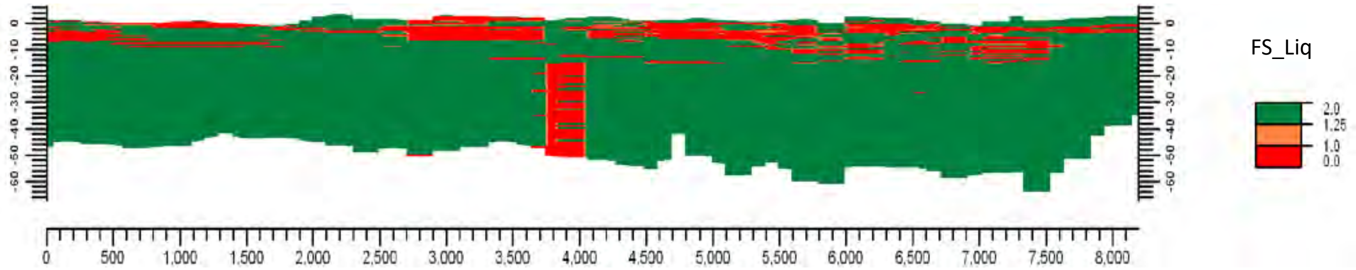

Figure A3.12 Cross-section of FS for the A10 alignment, considering EC8-T1

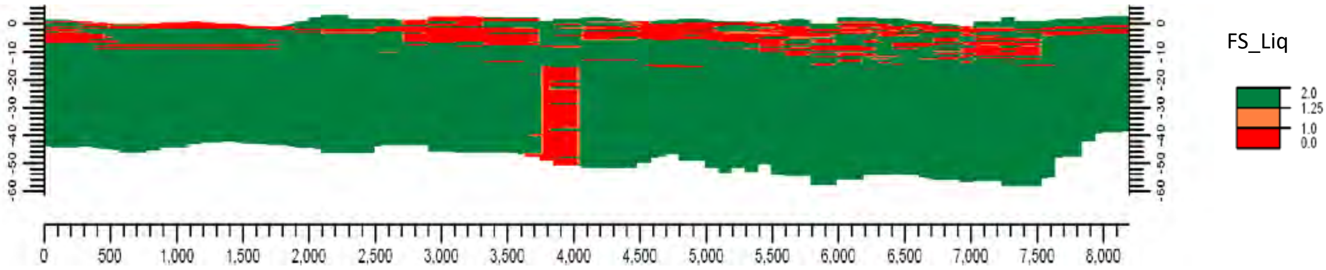

Figure A3.13 Cross-section of FS for the A10 alignment, considering EC8-T2

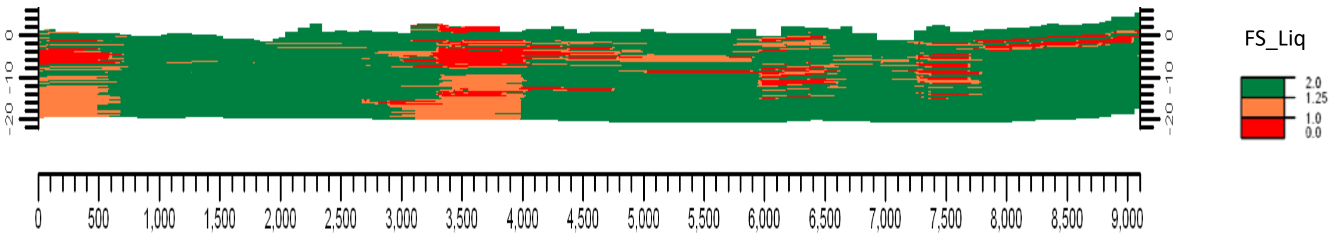

Figure A3.14 Cross-section of FS for the A10 alignment, considering T1-RP1

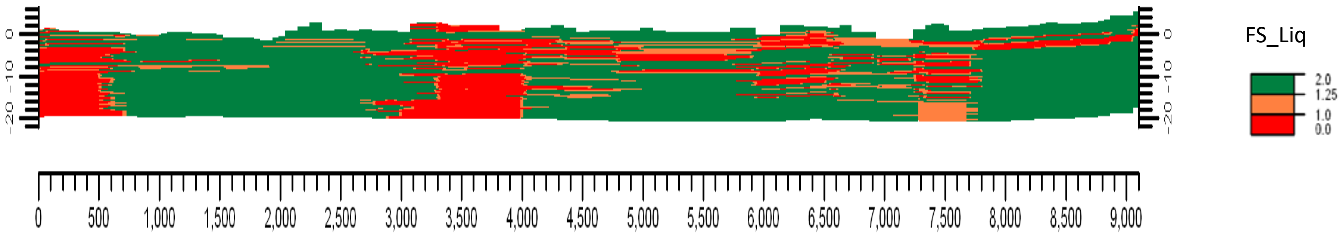

Figure A3.15 Cross-section of FS for the A10 alignment, considering T1-RP2

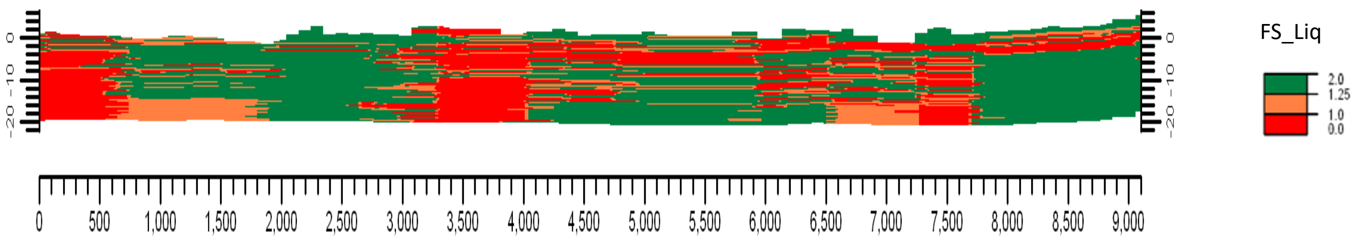

Figure A3.16 Cross-section of FS for the A10 alignment, considering T1-RP3

This project has received funding from the European Union's Horizon 2020 research and innovation programme under grant agreement No. 700748

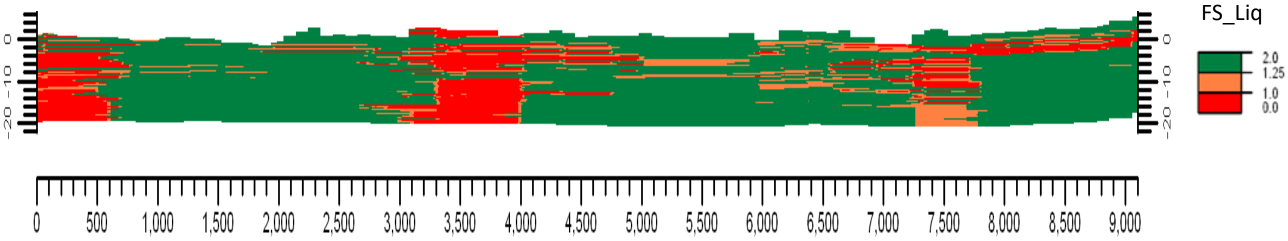

Figure A3.17 Cross-section of FS for the A10 alignment, considering T2-RP1

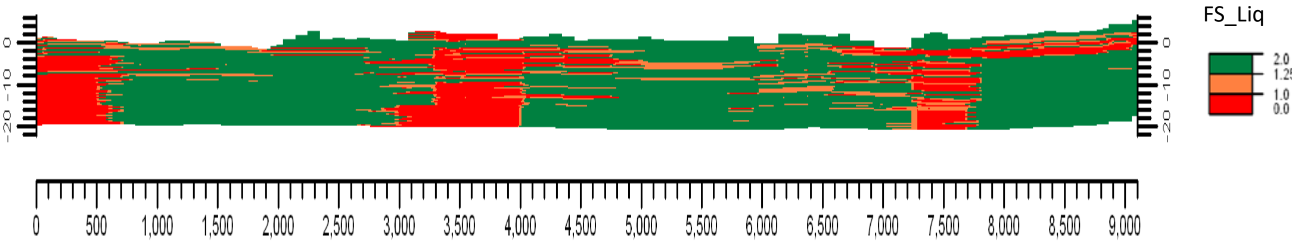

Figure A3.18 Cross-section of FS for the A10 alignment, considering T2-RP2

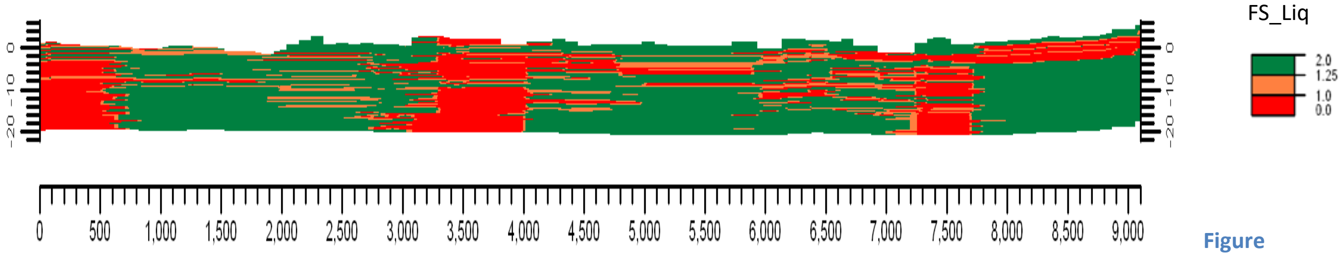

Figure A3.19 Cross-section of FS for the A10 alignment, considering T2-RP3

N10 alignment

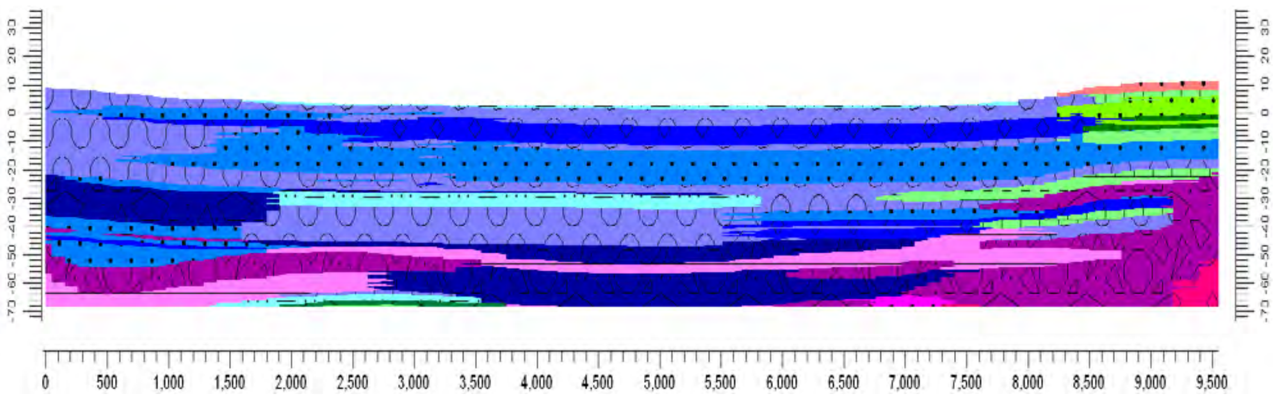

Figure A3.20 Lithological cross-section of N10 alignment

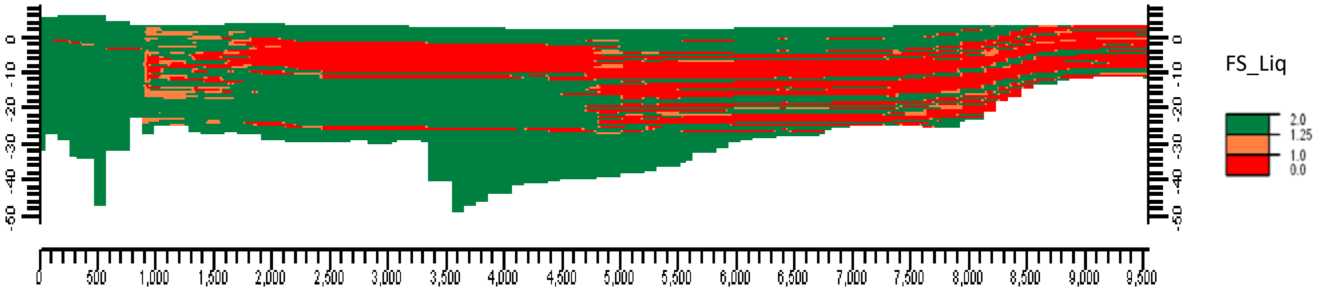

Figure A3.21 Cross-section of FS for the N10 alignment, considering EC8-T1

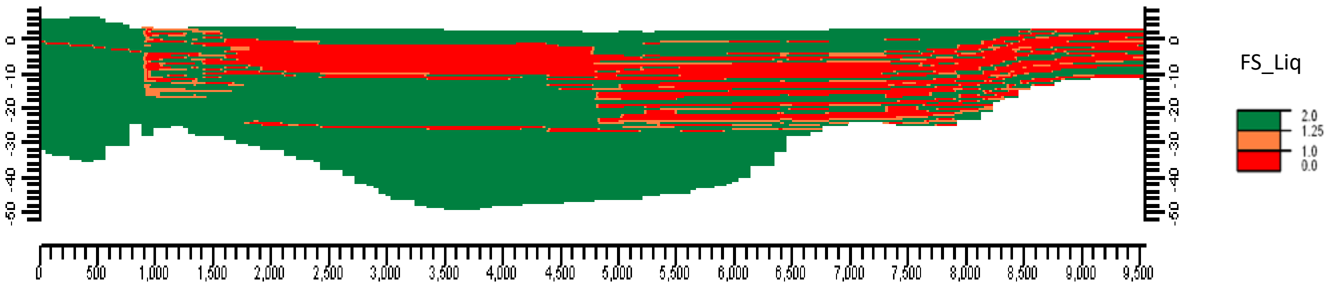

Figure A3.22 Cross-section of FS for the N10 alignment, considering EC8-T2

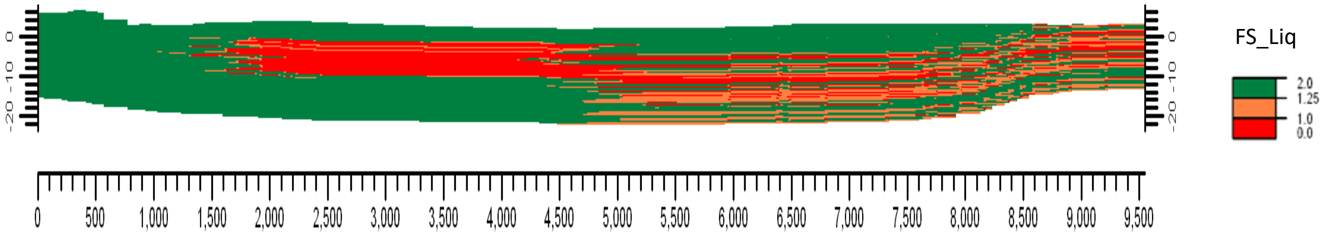

Figure A3.23 Cross-section of FS for the N10 alignment, considering T1-RP1

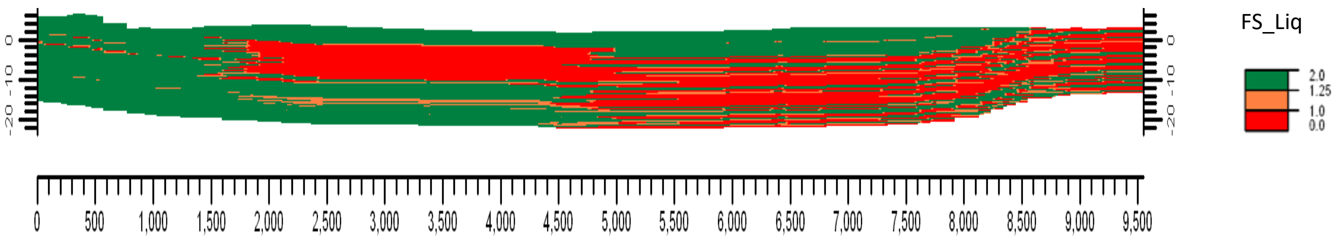

Figure A3.24 Cross-section of FS for the N10 alignment, considering T1-RP2

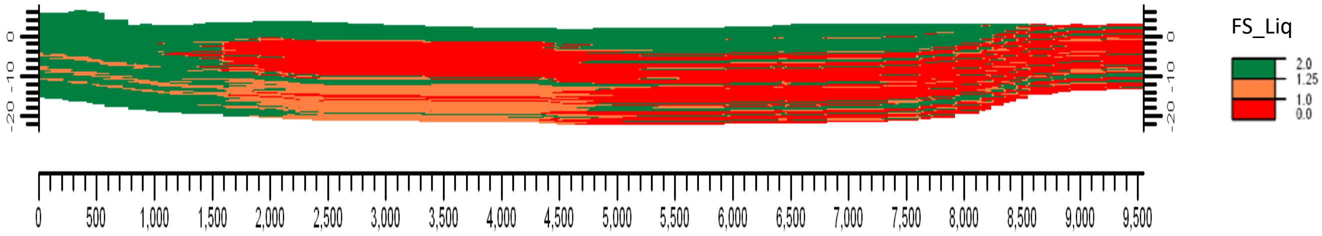

Figure A3.25 Cross-section of FS for the N10 alignment, considering T1-RP3

Figura 1: Perfil N10 do modelo de FS T2 resultante da junção dos ensaios de SPT e CPT.

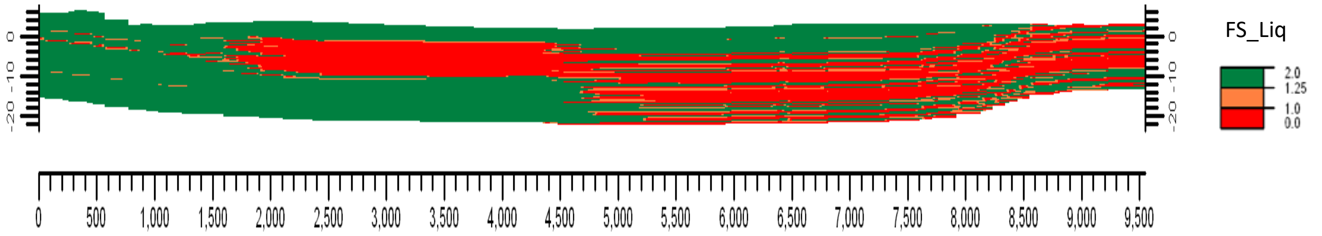

Figure A3.26 Cross-section of FS for the N10 alignment, considering T2-RP1

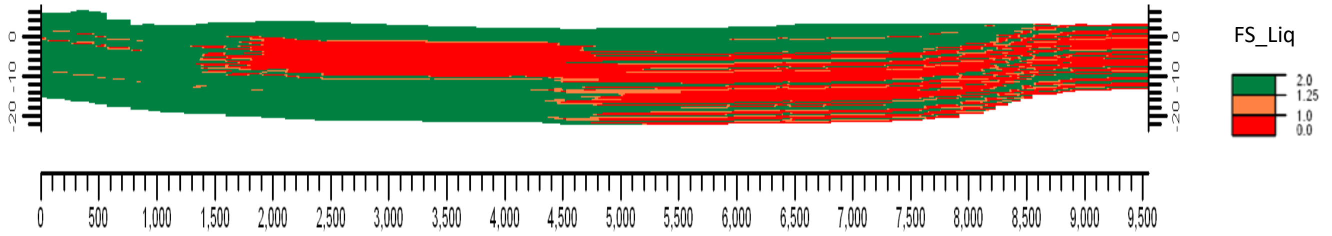

Figure A3.27 Cross-section of FS for the N10 alignment, considering T2-RP2

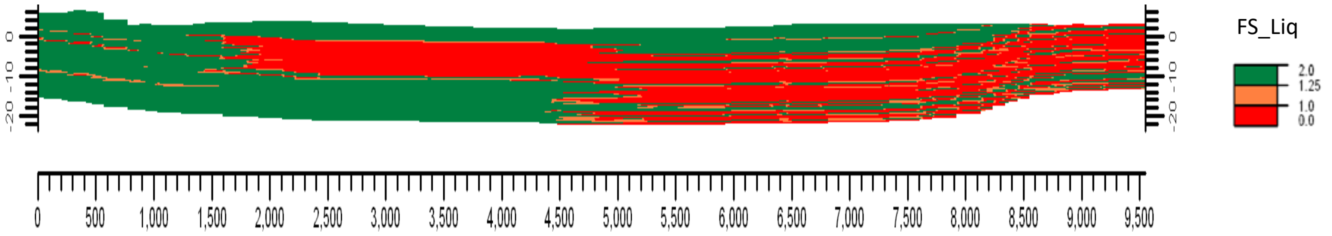

Figure A3.28 Cross-section of FS for the N10 alignment, considering T2-RP3

Cities alignment

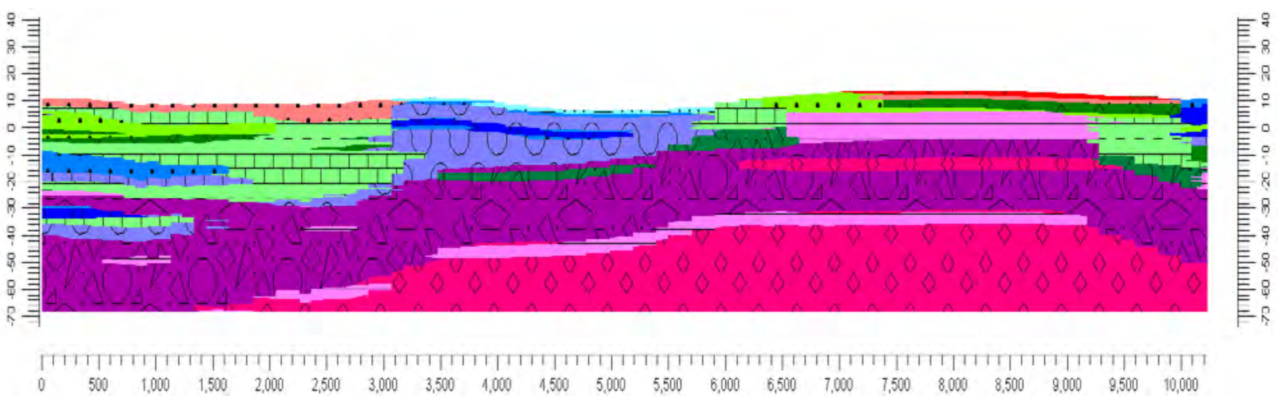

Figure A3.29 Lithological cross-section of "Cidades" alignment

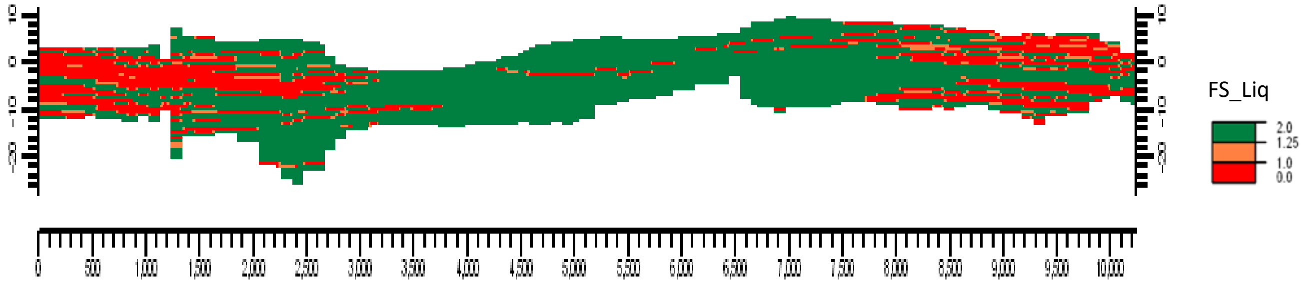

Figure A3.30 Cross-section of FS for the Cidades alignment, considering EC8-T1

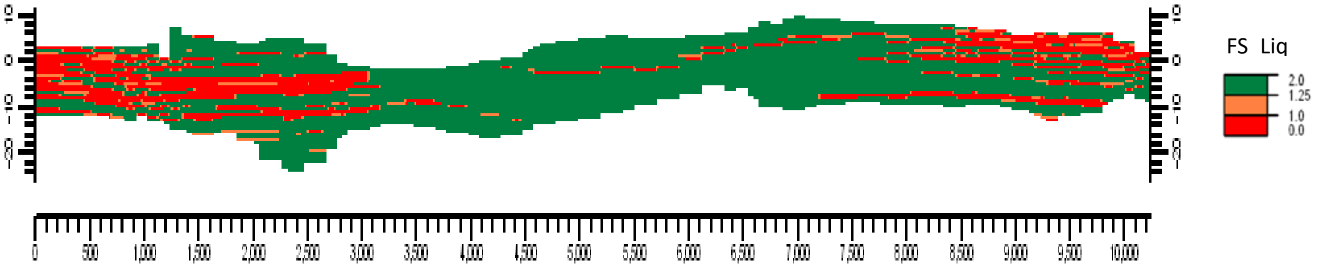

Figure A3.31 Cross-section of FS for the Cidades alignment, considering EC8-T2

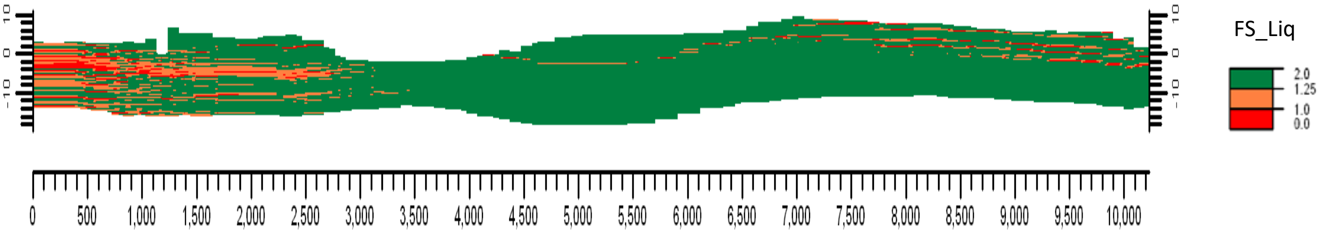

Figure A3.32 Cross-section of FS for the Cidades alignment, considering T1-RP1

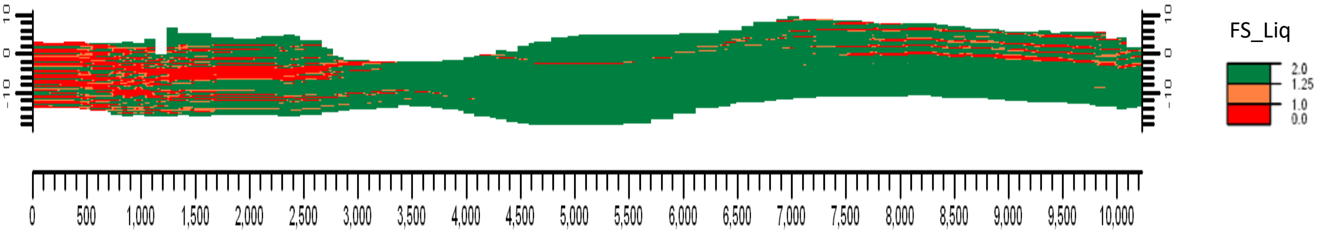

Figure A3.33 Cross-section of FS for the Cidades alignment, considering T1-RP2

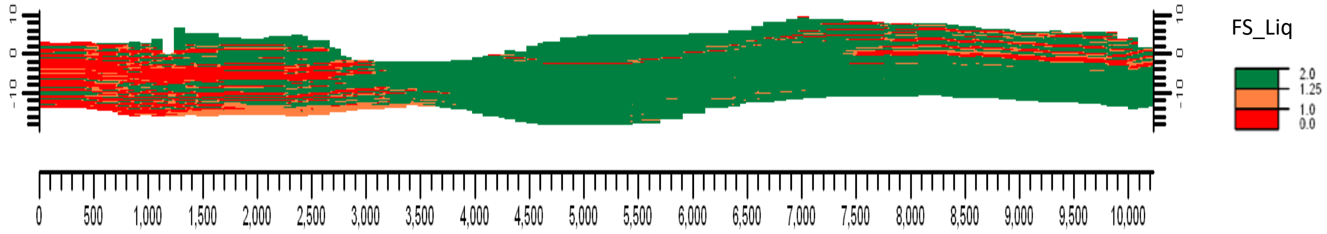

Figure A3.34 Cross-section of FS for the Cidades alignment, considering T1-RP3

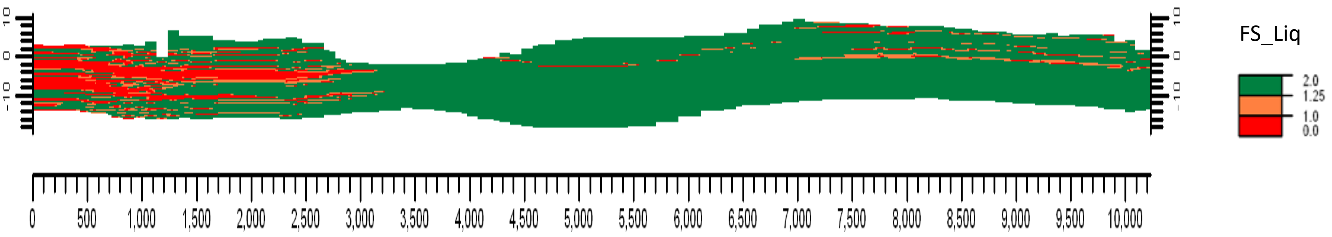

Figure A3.35 Cross-section of FS for the Cidades alignment, considering T2-RP1

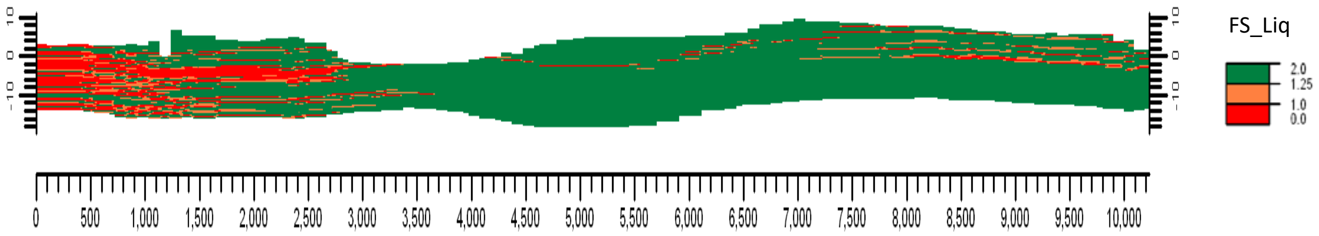

Figure A3.36 Cross-section of FS for the Cidades alignment, considering T2-RP2

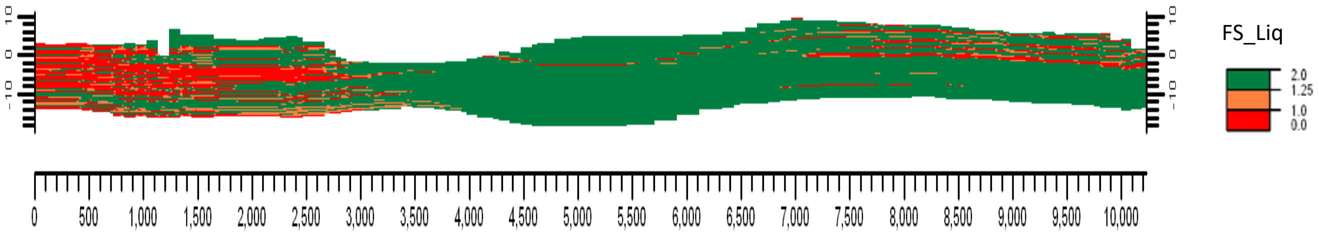

Figure A3.37 Cross-section of FS for the Cidades alignment, considering T2-RP3

This project has received funding from the European Union's Horizon 2020 research and innovation programme under grant agreement No. 700748

4. MICROZONATION OF THE LJUBLJANA AREA IN SLOVENIA

4.1 Introduction

The case study involves the area upstream of the newly built hydropower plant (HPP) Brežice in SE Slovenia and is presented in Figure Figure 4-1. The area is located on alluvial plain on the left and right banks of river Sava. This area is very well investigated in geological and geotechnical terms also due to the nearby Krško nuclear power plant.

This site has been selected as Slovenian testing site due to the following reasons:

- Occurrence of liquefaction 20 km downstream on the ground of the same origin (Veinović et al., 2007, Herak and Herak, 2010)
- No documented occurrence of past liquefaction events in Slovenia
- High expected seismicity in the area (SHARE project, 2013)
- Available ground data due to the design and construction of HPP Brežice (Vukadin, 2014)
- The construction of HPP Brežice affected the groundwater level and increased the liquefaction risk

Hydropower plant (HPP) Brežice has been recently completed and put in operation (October 2017). The water reservoir for HPP Brežice extends 7 km upstream and is made of levees along left and right banks of the river Sava. For the design of HPP Brežice and all corresponding structures and facilities but also other infrastructural projects in the area, large number of ground investigations were carried out in the past. These investigations have shown the presence of loose Holocene sands and silts immediately below the ground surface in variable thickness (0 to 6.5 m). Before the construction of accumulation basin for HPP Brežice the loose sandy and silty layer was mostly above groundwater table and was saturated only rarely during flood events. With the rise of water level within the water reservoir for HPP also the groundwater in the surrounding is expected to rise. Combining these facts with high seismicity of the area, liquefaction phenomenon has been considered seriously. The loose sandy/silty layer was found to be highly susceptible to liquefaction in saturated conditions (Smolar et al, 2012). During the design of HPP Brežice, mitigation measures against liquefaction were sought. In order to study the effect of compaction on the properties of loose sandy/silty layer, a number of test sites were made to study the possibilities of application of ground improvement techniques. The influence of roller compaction, the rapid impact compaction and soil mixing were studied on site (Vukadin, 2013; Petkovšek et al, 2016). Finally, for the construction of HPP the decision was adopted to remove and replace the sandy/silty layer beneath all structures. Within this study, original ground will be considered and analysed.

The main scope of this study is to use the methodology for localized assessment of liquefaction potential on the particular site in SE Slovenia (Brežice) in proposed step-by-step procedure: collection of geological, hydrogeological, geophysical and geotechnical data, establishing geological, hydrogeological, geotechnical and geophysical models, definition of seismic input, seismic microzonation for ground motion and finally, seismic microzonation for liquefaction risk.

4.2 Definition of geological model

4.2.1 Study area

Our study area is located along the river Sava on its left and right bank upstream of the hydro-power plant Brežice in the length of 6 km and width 1 to 2 km. Within this area enough geological and geotechnical data exist in order to perform the microzonation study. The limits of the study area are selected in such a way that the interpolation of data between individual investigation points gave reliable results, i.e. some investigation points were left out of the study area. All available investigation points and the study area are presented in Figure 4-1.

This project has received funding from the European Union's Horizon 2020 research and innovation programme under grant agreement No. 700748

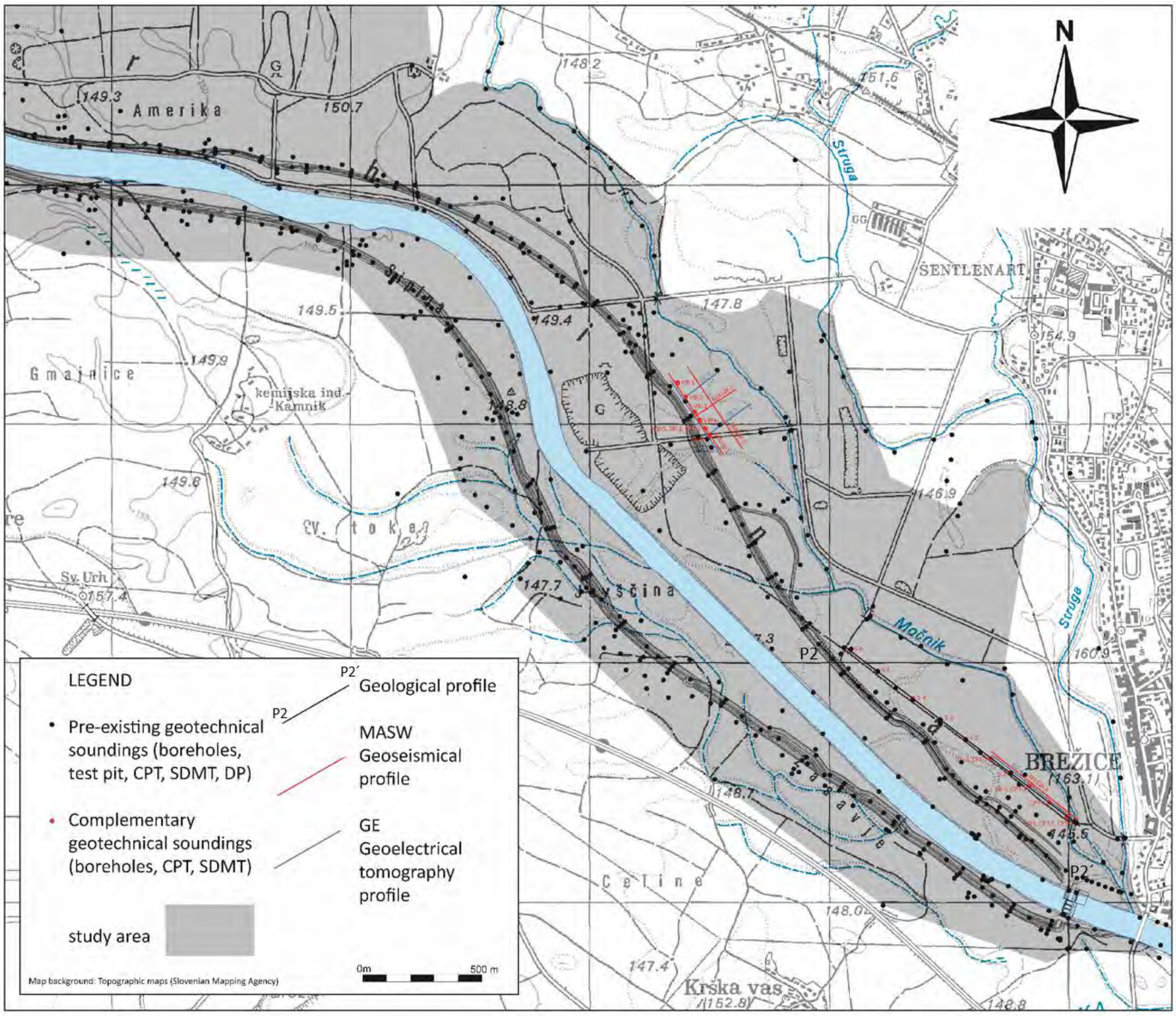

Figure 4-1: Study area upstream of Hydro power plant Brežice.

4.2.2 Geological data – ground investigation campaigns

The wider location was investigated for geological and geotechnical properties several times in recent history. In 1960's first geological investigations were made for the national geological map. In 1970's very detailed investigations were performed for the design of nearby nuclear power plant Krško. In 1980's emphasize was on the hydrogeological investigations for water supply purposes. In the same decade, investigations started for hydro power plants Brežice and Mokrice and continued with increasing level of detail until recent years (Vukadin, 2014). The broader area is therefore geologically well known.

The plain area along river Sava between hill ridges Gorjanci on the south and Bohor on the north is a tectonic syncline. In Miocene, it was filled with silty and sandy sediments, which presently form an over 100 m thick deposit of hard soil to soft rock. Later tectonic sinking in Pliocene and Quaternary allowed the deposition of alluvial gravel, sand, silt and occasionally clay on the top of geological sequence. Deep-seated bedrock is found at a depth over 500 m and is formed predominantly by Triassic limestone and dolomite (Vukadin, 2014). The stratigraphic sequence on HPP Brežice site is presented in Table 4-1.

Table 4-1: Stratigraphic units at HPP Brežice site (IZIIS, 2008).

Layer	Thickness	Liquefiable
Quaternary (Holocene) silty sand, loose	0 to 6.5 m	Yes
Quaternary gravel, dense	4 to 40 m	No
Miocene stiff overconsolidated silts and sands (marls)	>300 m	No
Cretaceous limestone and marl	200-300 m	No
Triassic limestone and dolomite	at >700 m depth	No

Extensive ground investigations for HPP Brežice included borehole drilling, excavation of trial pits, dynamic probing, CPT and DMT testing, MASW, seismic refraction and electrical resistivity profiles. Some additional testing was performed within Liquefact project. Overview of performed number of tests is presented in Table 4-2, while the position of all test points is given in Figure 4-1. These investigations revealed the high liquefaction risk within the surface layer of loose silty sand if this layer becomes saturated with water.

During Liquefact project, additional in-situ tests were made in two locations that were accessible during the investigation campaign, which coincided with intensive construction works for HPP Brežice. The aim was to obtain more CPT, SDMT and MASW data on locations with greater thickness of silty sand layer. In this respect, we were only partly successful. Most of locations with relatively thick sandy layer were within the construction site. Hence, we were not able to assure the even distribution of investigation CPT and SDMT points over the entire study area. However, over 500 dynamic probing tests spread over the site showed that the critical sandy layer is fairly homogeneous.

Table 4-2: Number of investigation points.

Type	Quantity	
	For HPP Brežice	Liquefact
Boreholes	260	11
Dynamic probing	>500	3
Trial pits	>100	6
MASW and seismic refraction	9 km	1.5 km
Electrical resistivity	-	1.2 km
CPT	4	6
DMT	2	3

Since 2009 extensive field and laboratory investigations were made on loose silty sands from Brežice basin in order to identify their liquefaction susceptibility. A detailed overview of all collected data was presented by Petkovšek (2010, 2016), Smolar et al (2012, 2018, 2019). The index data as well as the performance related data showed that Quaternary silty sands exhibit high potential to liquefaction at given seismic excitation.

4.2.3 Geological model

For the study of liquefaction susceptibility, the Quaternary silty sand is of primary interest. The vast number of boreholes, dynamic probing tests and some CPT and DMT tests allowed to build a reliable geological model for near surface conditions. The thickness of loose silty sand layer over the study area was of particular importance. For the analysis of ground motion at the surface, also the distribution of the thickness of dense Quaternary gravel over the study area was analysed. The stiff Miocene silts and sands have to be considered in the ground motion analyses. However, due to its properties (high and increasing shear wave velocity) and huge thickness, a seismic bedrock was modelled within this layer. Our geological model for microzonation of liquefaction risk therefore consists of three layers: (1) loose Quaternary silty sand, (2) dense Quaternary gravel and (3) Miocene stiff silts and sands. These three layers are shown below (Figure 4-2 and Figure 4-3) on the two characteristic cross sections (Lai, 2017) showing that the thickness of the upper two layers changes gently over the area and consequently the position of contact with stiff Miocene layer varies accordingly. Note that the scale is different in horizontal and vertical direction (10:1).

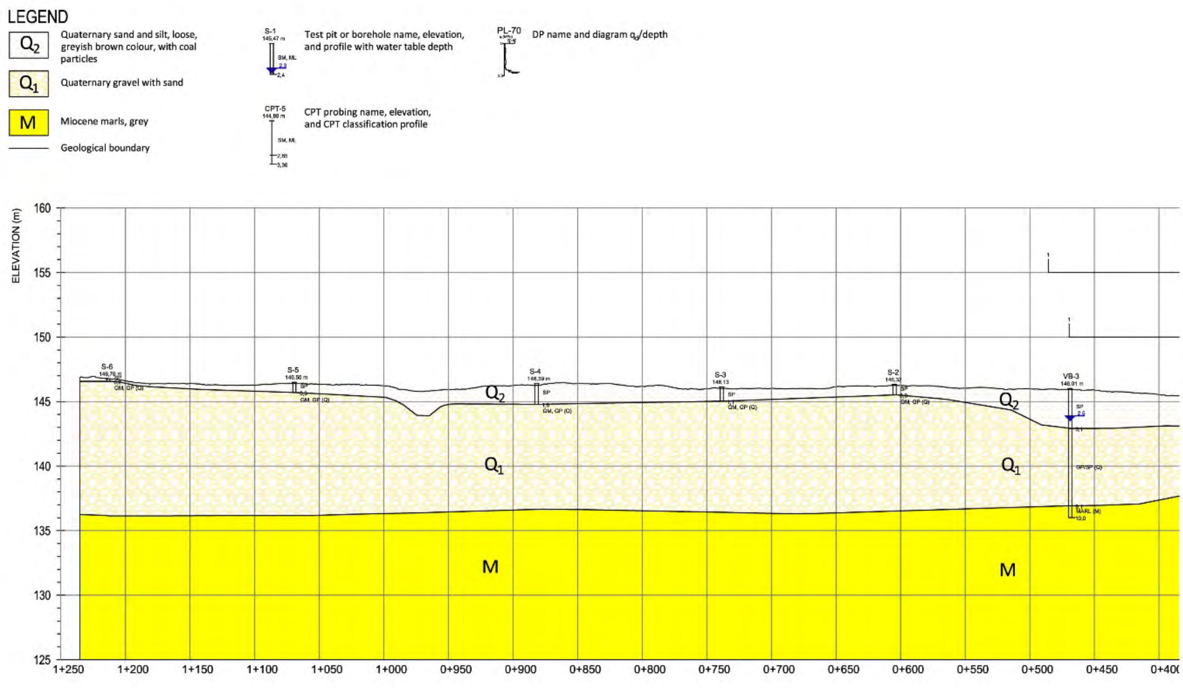

Figure 4-2: HPP Brežice site. Geotechnical section P2 along the left bank of the river Sava – part 1.

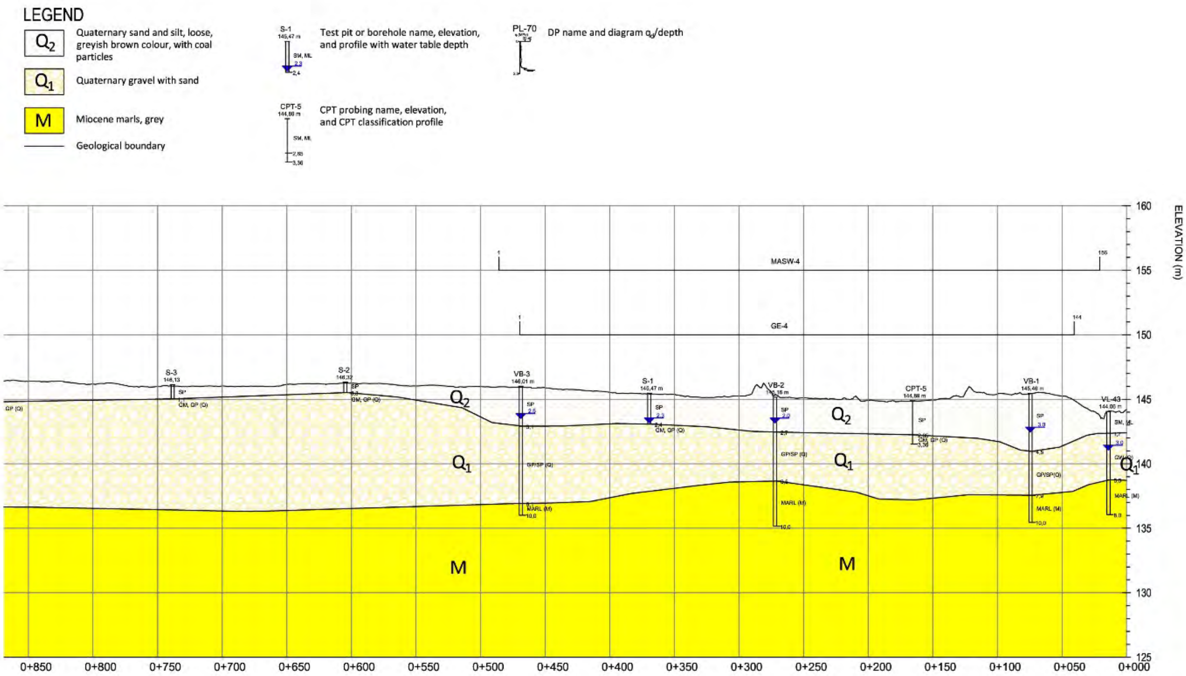

Figure 4-3: HPP Brežice site. Geotechnical section P2 along the left bank of the river Sava – part 2.

The database of thicknesses of upper two layers was formed from all available investigation points. Using the nearest-neighbour interpolation method, the maps of thickness of loose silty sand layer was obtained (Figure 4-4) and map of thickness of dense gravel (Figure 4-5).

This project has received funding from the European Union's Horizon 2020 research and innovation programme under grant agreement No. 700748

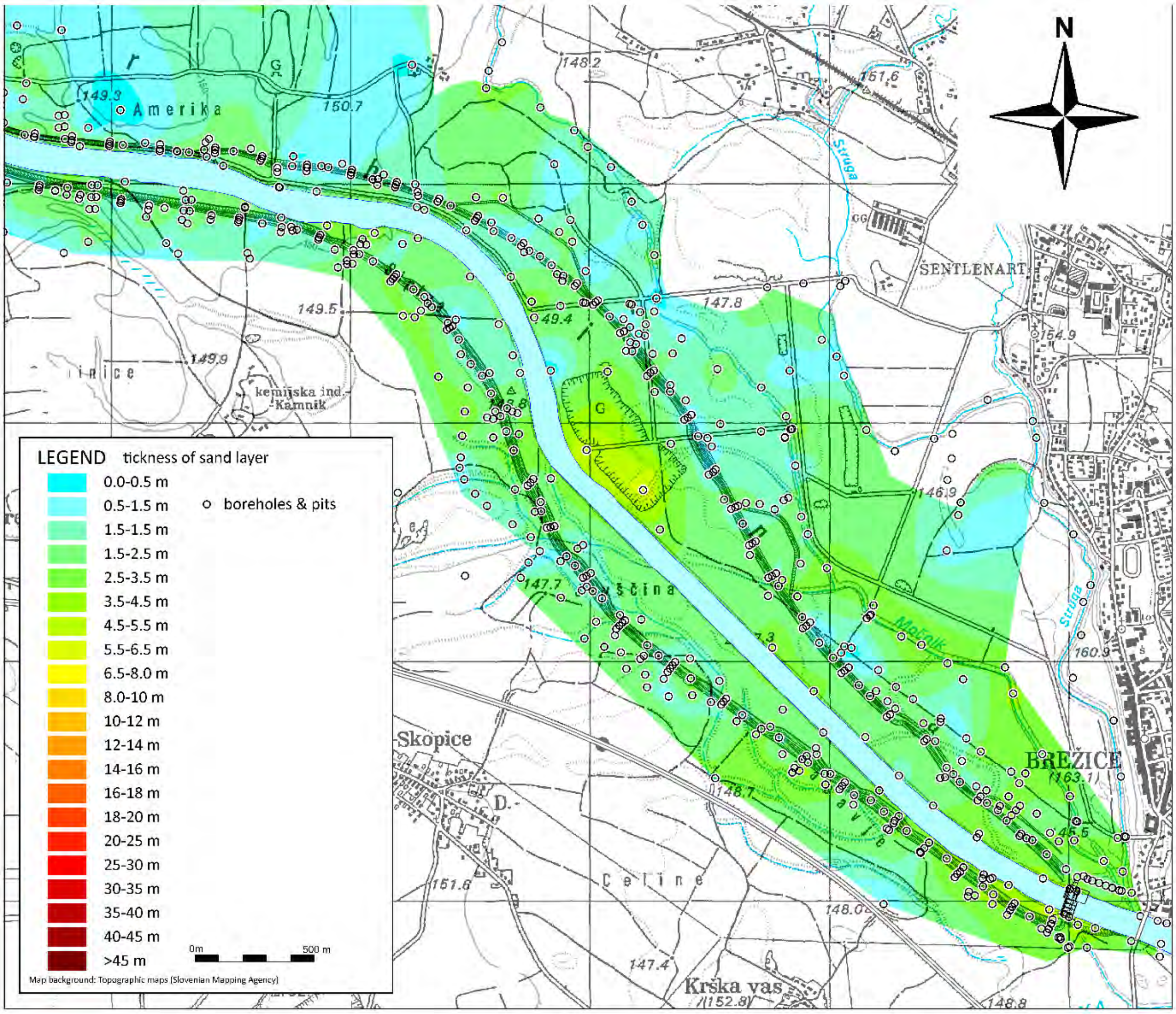

Figure 4-4: Thickness of the silty sand layer over the study area varies between 0 and 6.5 m.

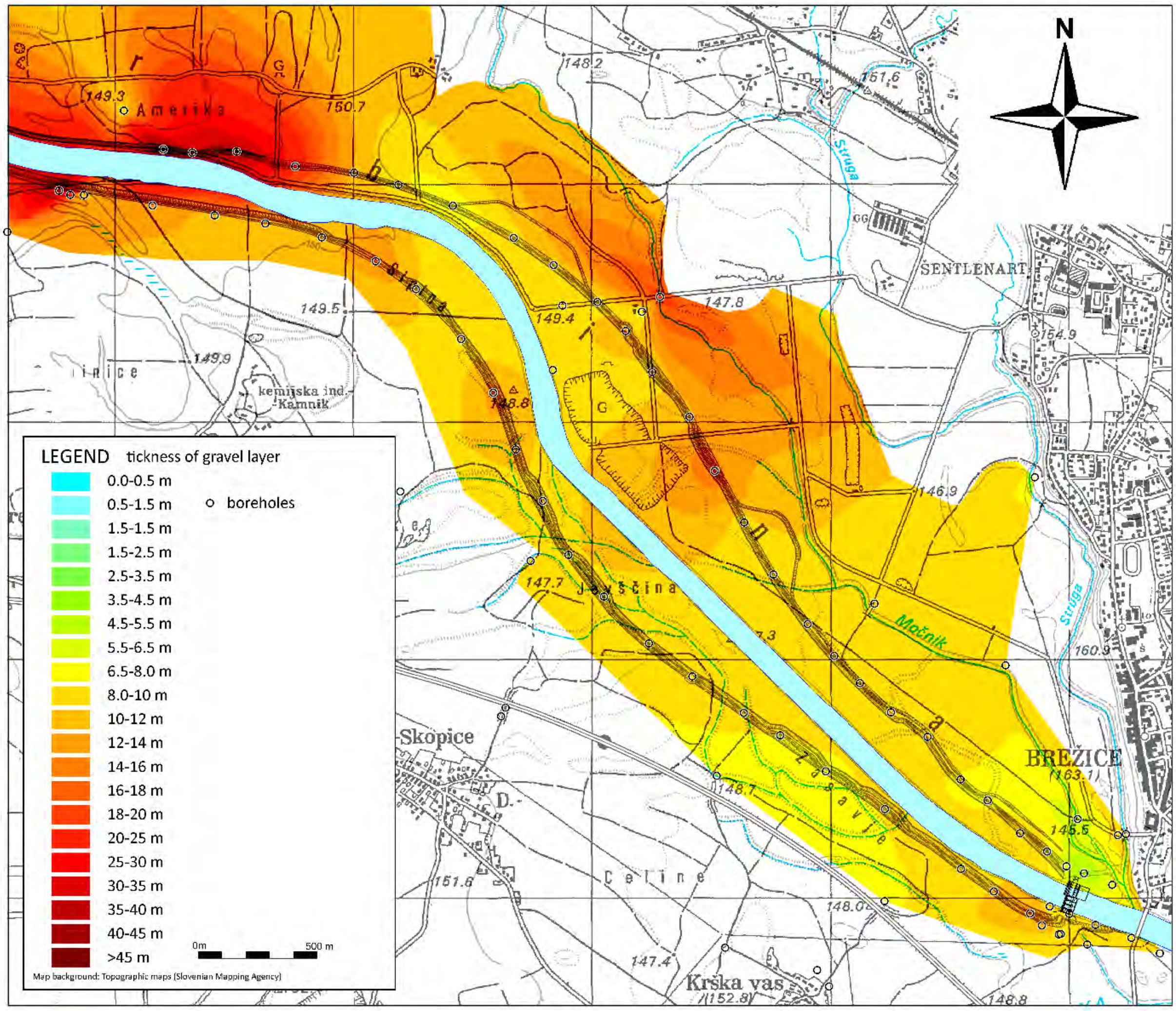

Figure 4-5: Thickness of the gravel layer over the study area varies between 4 and 55 m.

From these maps, one can observe that within the study area the thickness of silty sand varies from 0 to 6.0 m but is predominantly less than 2 m thick. The gravel layer has a mean thickness of 11 m but the thickness varies from 4 to 53 m. The maximum thickness of gravel layer is found in the area of local fault zone.

4.2.4 Groundwater table

The groundwater level before the construction of HPP Brežice depended on the free water level in river Sava and on groundwater flow from the nearby hills. The groundwater level was measured during drilling in several boreholes at different time. The differences in observed groundwater levels over the study area are partly due to different locations with respect to the river and partly due to temporal variations of groundwater level. The result of these measurements is presented in Figure 4-6 as a plot of groundwater depth below surface. Within the study area, the minimum and maximum depth of the groundwater level is 1.0 and 9.0 m respectively with the mean value of 4.3 m.

However, due to the presence of newly built HPP Brežice, ground water level is expected to increase.

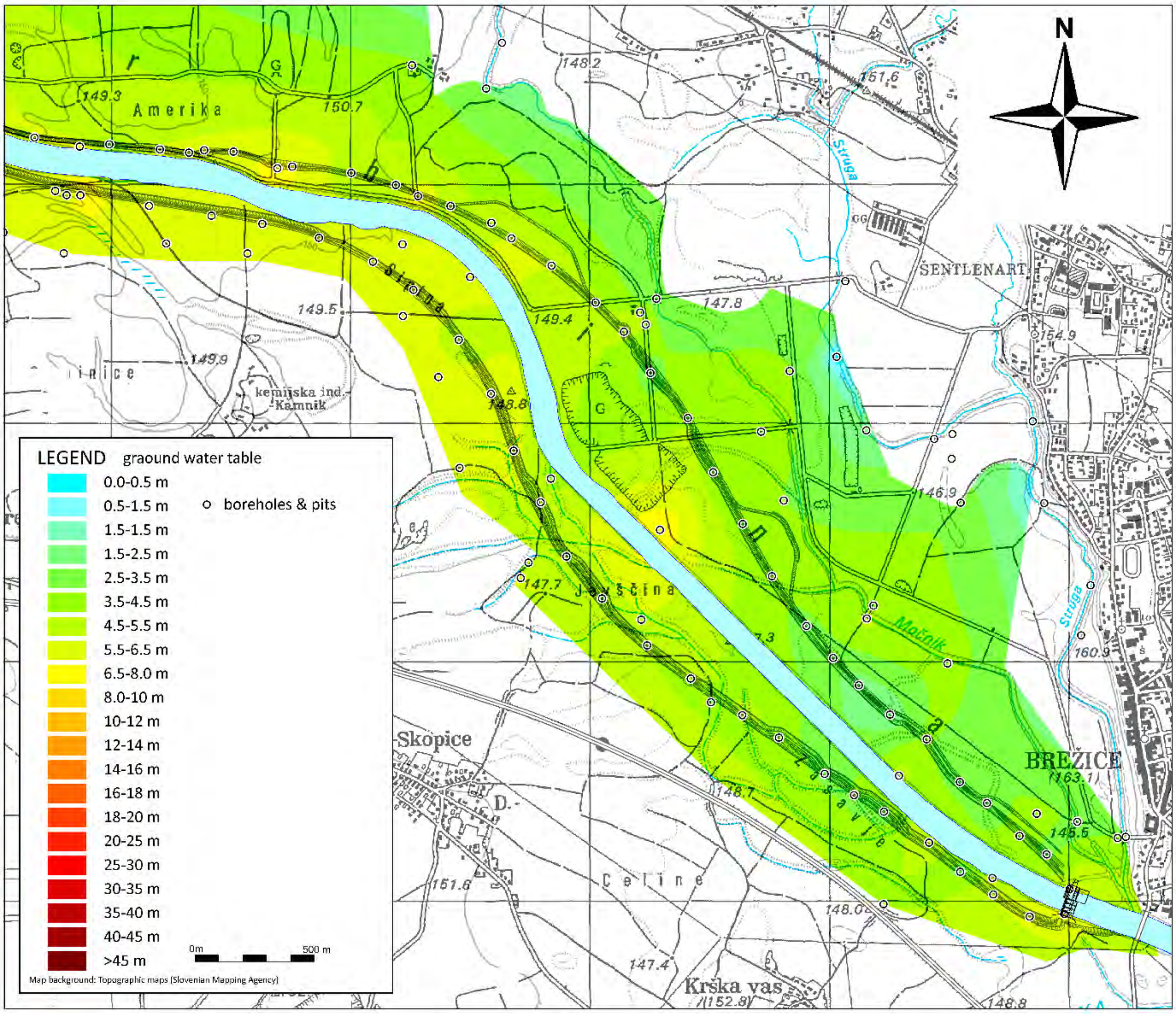

Figure 4-6: Depth of groundwater level over the study area varies between 1 and 9 m.

4.2.5 Topography

Topographically the study area may be considered flat. The maximum height difference is 10 m over 6 km length.

4.3 Geotechnical and geophysical data

The extensive representation on the collected geotechnical and geophysical data from HPP Brežice site was given in the report D2.1 - Report on ground characterization of the four areas selected as testing sites by using novel technique and advances methodologies to perform in situ and laboratory tests (Lai et al, 2017). This is the source of geotechnical and geophysical data for the derivation of the geotechnical and geoseismic ground model.

The main concern is the Quaternary silty sand layer on the top of geological sequence, which is considered susceptible for liquefaction due to its loose state and measured particle size distribution shown in Figure 4-7 together with boundaries for potentially liquefiable and most liquefiable soils according to Ishihara et al (1980). The measured bulk densities for silty sand in its natural unsaturated state varied between 1.23 and 1.61 t/m^3 with median value 1.4 t/m^3. Figure 4-8 presents the results of cyclic simple shear tests on the local silty sand layer.

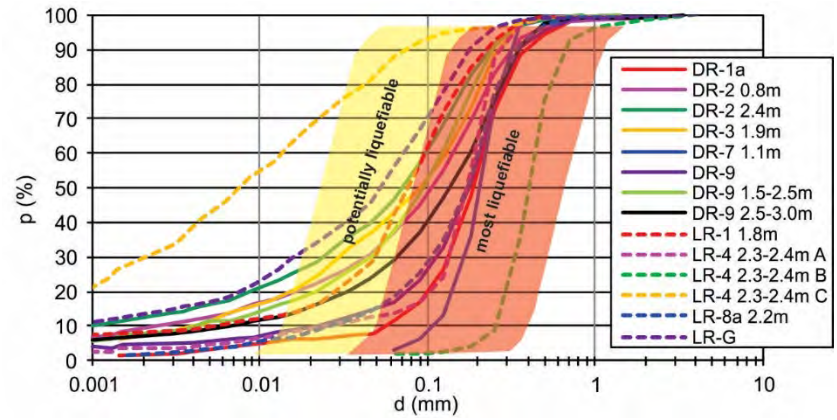

Figure 4-7: Particle size distribution for upper silty sand layer together with the boundaries for potentially liquefiable and most liquefiable soils after Ishihara et al (1980).

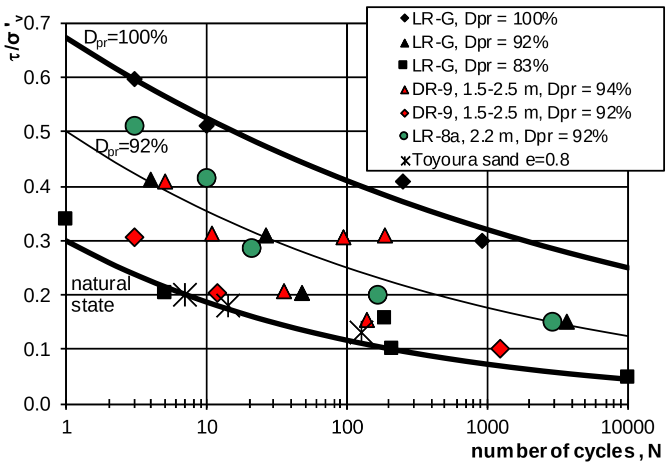

Figure 4-8: Results of cyclic simple shear tests for all investigated samples of silty sand from study area Brežice in comparison with literature data for Toyoura sand.

The calculation of cyclic resistance ratio (CRR) will be mainly based on the in-situ test results (SDMT and CPT). Since the number of these measurements is low, we used the numerous dynamic probing tests to confirm that the liquefiable silty sand layer is sufficiently homogeneous over the study area. Figure 4-10 and Figure 4-11 present CPT and SDMT results used in further analyses. Based on these in-situ test results, the silty sand layer was considered sufficiently homogeneous for the analysis of the propagation of ground motion using unique soil parameters over the entire study area.

This project has received funding
from the European Union's
Horizon 2020 research and
innovation programme under
grant agreement No. 700748

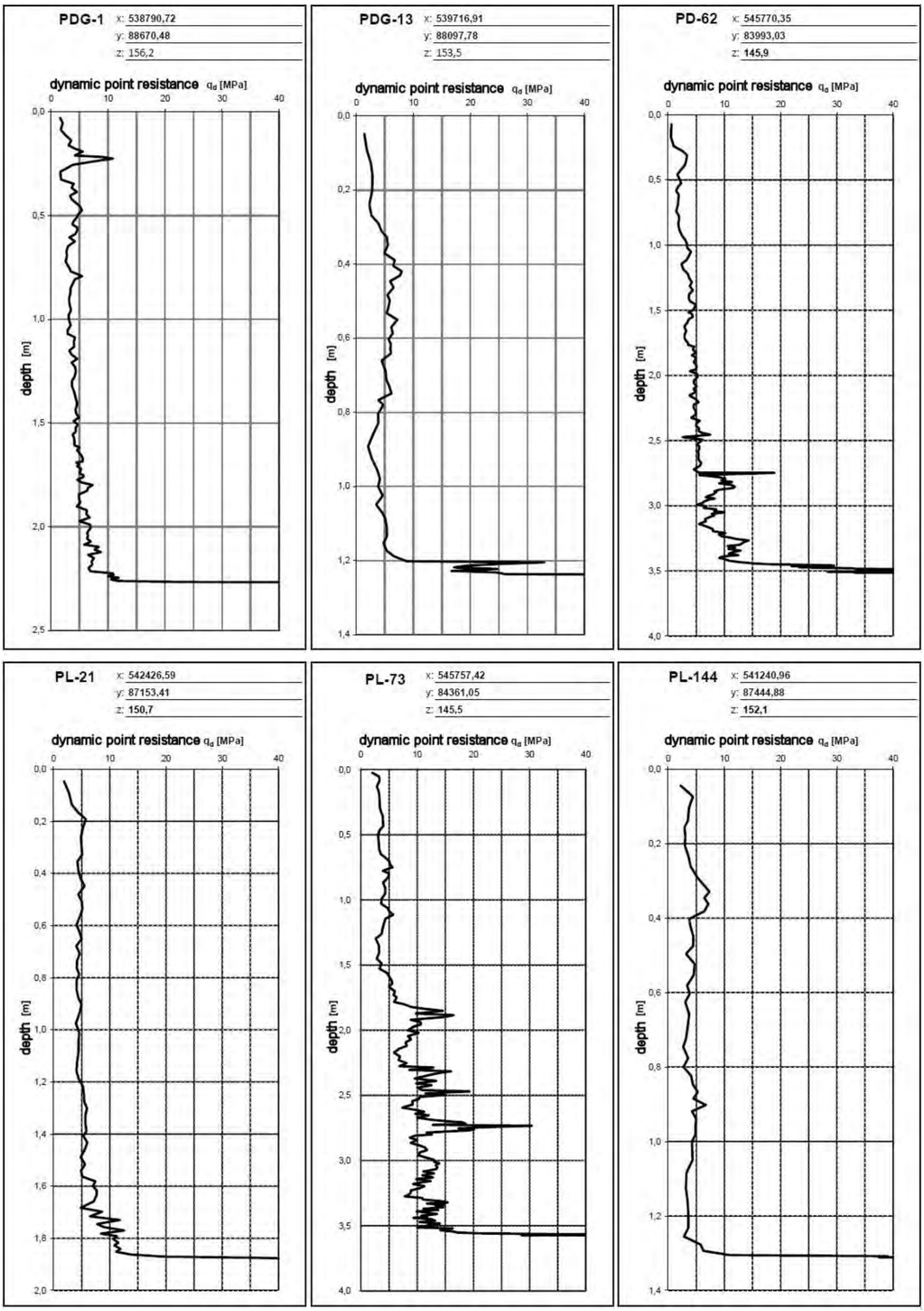

Figure 4-9: Results of 6 selected DP-L dynamic probing tests from the broader study area of HPP Brežice site: dynamic point resistance vs. depth.

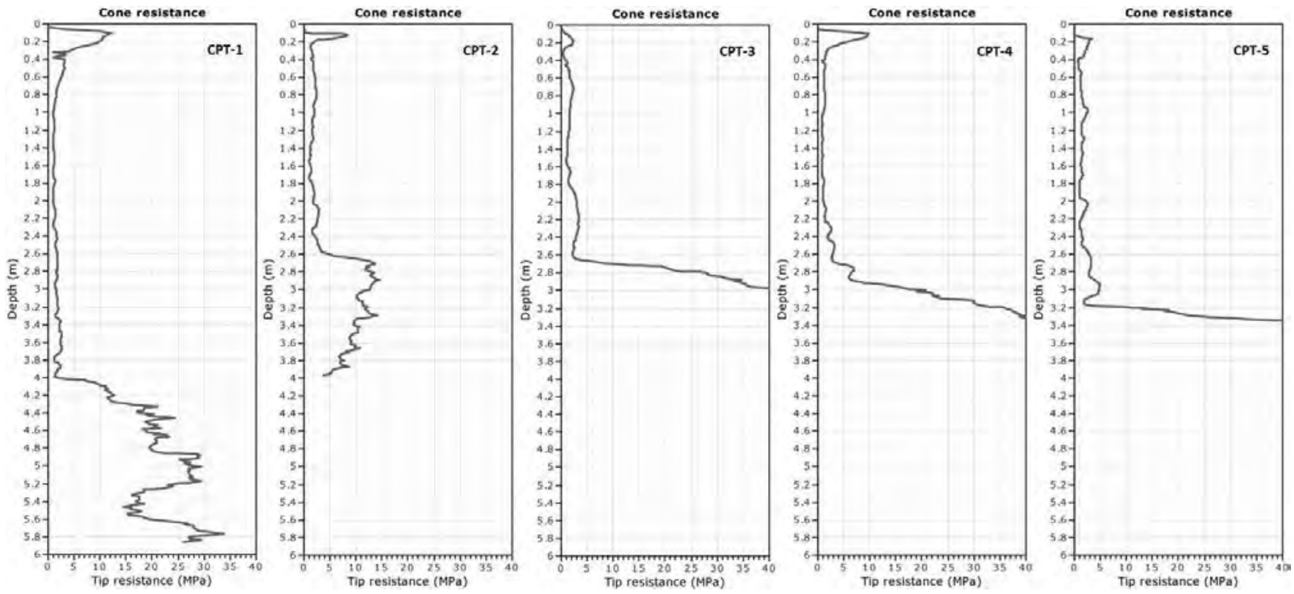

Figure 4-10: Results of 5 CPT tests from the study area of HPP Brežice site: tip resistance vs. depth.

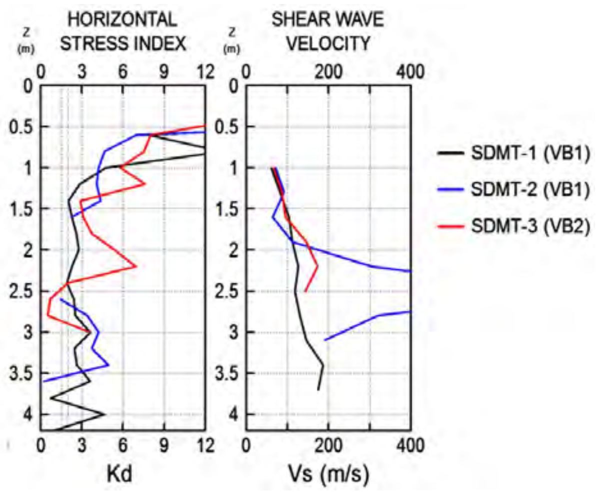

Figure 4-11: Results of 3 SDMT tests from the study area of HPP Brežice site: horizontal stress index and shear wave velocity vs. depth.

4.4 Ground model

4.4.1 Lythostatigraphic model

The simplified geotechnical model showing the three relevant soil layers and the levels of river Sava before and after the construction of HPP Brežice is graphically presented in Figure 4-12.

This project has received funding from the European Union's Horizon 2020 research and innovation programme under grant agreement No. 700748

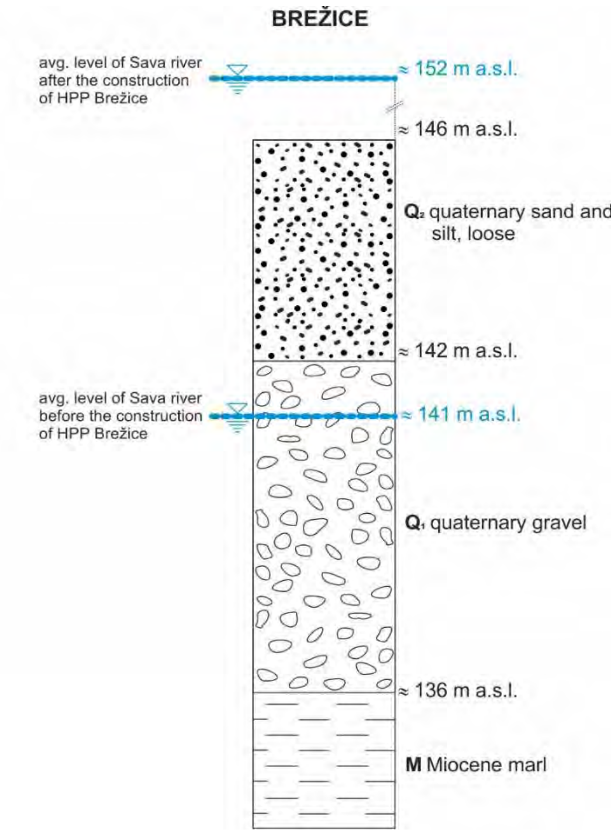

Figure 4-12: The simplified geotechnical model with three relevant soil layers. The levels of river Sava before and after the construction of HPP Brežice are also presented.

Since ground stratigraphy at Brežice test site area consists of non-horizontal layers as a consequence of gradual deposition of sediments and past geologic activities, various thicknesses of sandy and gravelly layers were taken into account within numerical simulations. According to the derived geological model, the following matrix of combinations of thicknesses of silty sand (SM) and gravel (GP) layer was selected for ground motion analyses and is presented in Table 4-3, where the check mark represents the performed analyses and the cross sign the combinations that were not considered/needed. These combinations of layer thicknesses resulted in small variations of calculated PGA at the surface that enabled smooth and reliable interpolation for intermediate values of thicknesses of silty sand and gravel layers (see calculated PGA values in Table 4-8).

On the other hand, constant thickness was assigned to a Miocene layer included in the model (78 m). Due to an increase of shear wave velocity within this Miocene layer it was further divided into two sublayers having thickness of 19 m and 59 m for upper and lower part, respectively.

Table 4-3: Variations of thicknesses of alluvial layers (analysed combinations are denoted by green check mark).

SM Thickness of sandy layer [m]	**GP** – Thickness of gravel layer [m]										
	4	**5.5**	**7**	**8.5**	**10**	**13**	**16**	**19**	**31**	**43**	**55**
0	✓	X	✓	✓	✓	✓	✓	✓	✓	✓	✓
1.5	✓	✓	✓	✓	✓	✓	✓	✓	✓	✓	✓
2	X	✓	X	X	X	X	X	X	X	X	X
2.5	✓	X	✓	✓	✓	✓	✓	✓	✓	✓	✓
3.5	✓	X	✓	✓	✓	✓	✓	✓	✓	✓	X
4.5	✓	X	✓	✓	✓	✓	X	X	X	X	X
5.5	✓	X	✓	✓	✓	✓	X	X	X	X	X
6.5	X	X	✓	X	✓	✓	X	X	X	X	X

4.4.2 Seismic bedrock

Beneath Miocene layers, elastic halfspace was placed, representing seismic bedrock, where shear wave velocity exceeds 1000 m/s. These parameters were derived from the results of geoseismic measurements.

4.4.3 Groundwater table

The groundwater level within the study area was mostly over 4 m deep before the construction of HPP Brežice (see Figure 4-6). Occasionally during floods, the water level rose above ground surface. After the construction of HPP Brežice the general groundwater level is slightly higher but the flood risk is reduced.

For the study of liquefaction susceptibility over the test area, two groundwater levels will be used:

- 3 m below ground surface (this value was selected as representative and slightly conservative groundwater level before the construction of HPP Brežice but also because the liquefiable silty sand layer only locally exceeds the thickness of 3 m).
- At the ground surface (this is the worst case scenario for the unlikely coincidence of flood and seismic event but also the scenario for severe rise in groundwater level after the construction of HPP Brežice in case that the cut-off walls and drainage systems fail to operate satisfactory).

4.4.4 Geotechnical model

The selected geotechnical parameters, relevant for the analysis of the propagation of ground motion are given in Table 4-4 and were determined using the compilation of all available data from laboratory and in-situ geotechnical and geophysical investigations referred to in previous chapters.

Table 4-4: Material properties for the ground motion propagation analyses.

Layer ID	Unit Weight	Shear Wave Velocity	Layer thickness
	[kN/m^3]	[m/s]	[m]
SM unsaturated	14.4	150	varies
SM saturated	17.7	150	varies
GP	21	300	varies
Miocene (upper)	20	450	19
Miocene (lower)	20	750	59
Seismic bedrock	20	1000	-

Additionally, two different pairs of degradation curves were assigned to materials in ground motion amplification analyses (Figure 4-13). Same curves of shear modulus and damping degradation for sand, gravel and lower Miocene layer were used (blue curves), while the other pair (red curves) was used for the upper Miocene layer. These degradation curves were taken from the detailed numerical study for the nearby site in the same geological setting (Dolšek et al, 2018).

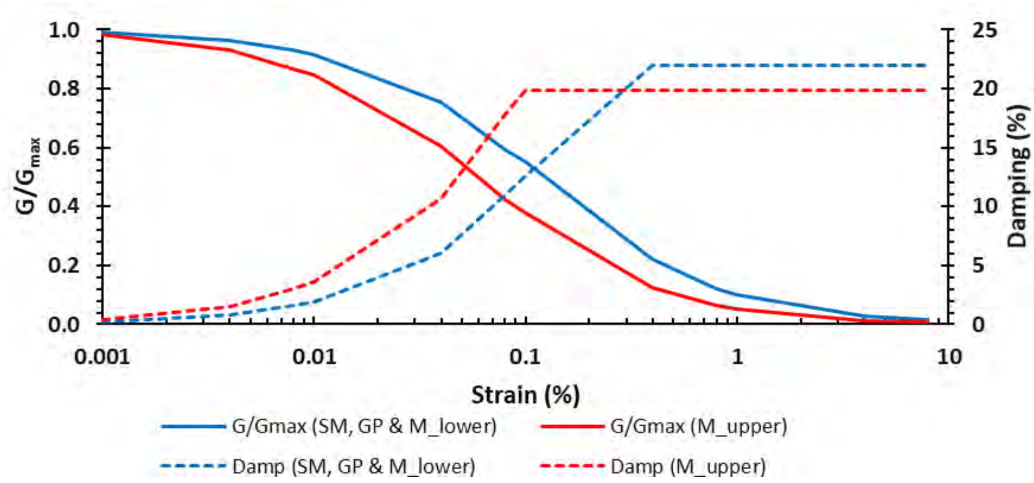

Figure 4-13: Degradation curves.

4.4.5 Geoseismic model – shear wave velocity profile

The representative profile of shear wave velocity with depth was presented in Table 4-4. The map of average shear wave velocity within upper 30 m of ground profile was produced for the presented geological and geotechnical model and is presented in Figure 4-14. Lower values of $v_{s,30}$ correspond to the thicker deposits of alluvial soils.

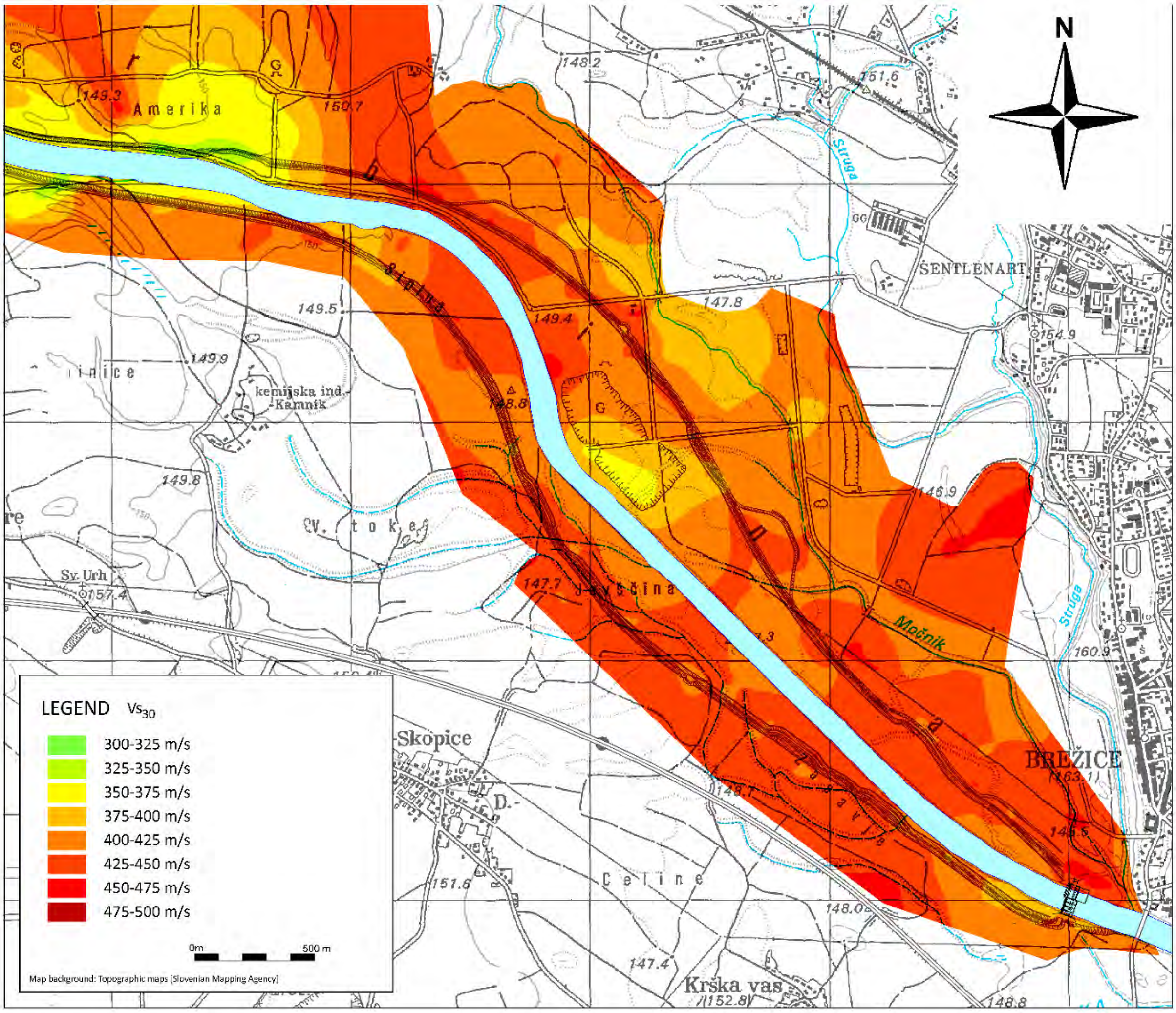

Figure 4-14: Map of $v_{s,30}$.

4.5 Seismic hazard

4.5.1 Seismic hazard data in Slovenia

A detailed description of seismic hazard in Slovenia was given in the Liquefact project report D2.1 (Lai et al, 2017). Here, only the relevant data for microzonation at Brežice test site will be presented.

Two available sources for seismic hazard assessment exist for Slovenian territory: National seismic hazard map for Slovenia (Lapajne et al 2001, 2003) and the more recent European Seismic Hazard Model (SHARE project, 2013). For the nuclear power plant Krško, which is situated near our study site at HPP Brežice, several site specific seismic hazard studies were elaborated (Fajfar et al, 2004; Živčić et al 2015). From comparison of these results with national seismic hazard map and SHARE model, the decision was taken to adopt the seismic hazard parameters from SHARE model. Figure 4-15 and Figure 4-16 present the National hazard map and SHARE model for Slovenia, both for return period 475 years.

This project has received funding from the European Union's Horizon 2020 research and innovation programme under grant agreement No. 700748

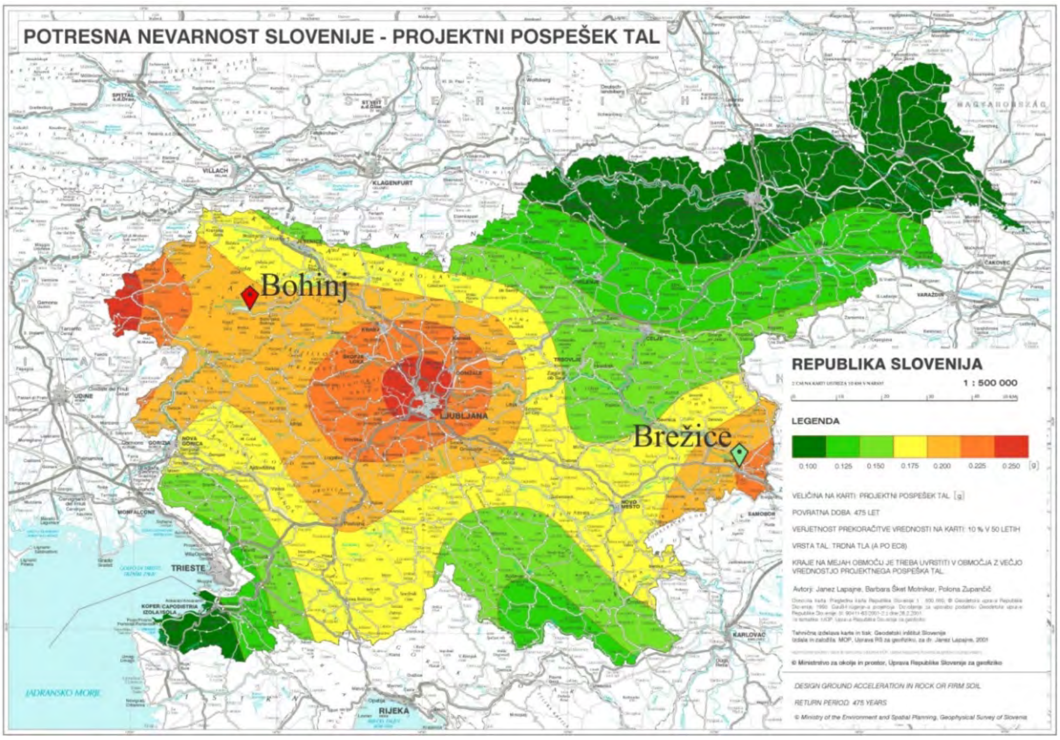

Figure 4-15: National seismic hazard map for Slovenia - Design peak ground acceleration on rock or firm soil corresponding to return period of 475 years (ARSO, 2001).

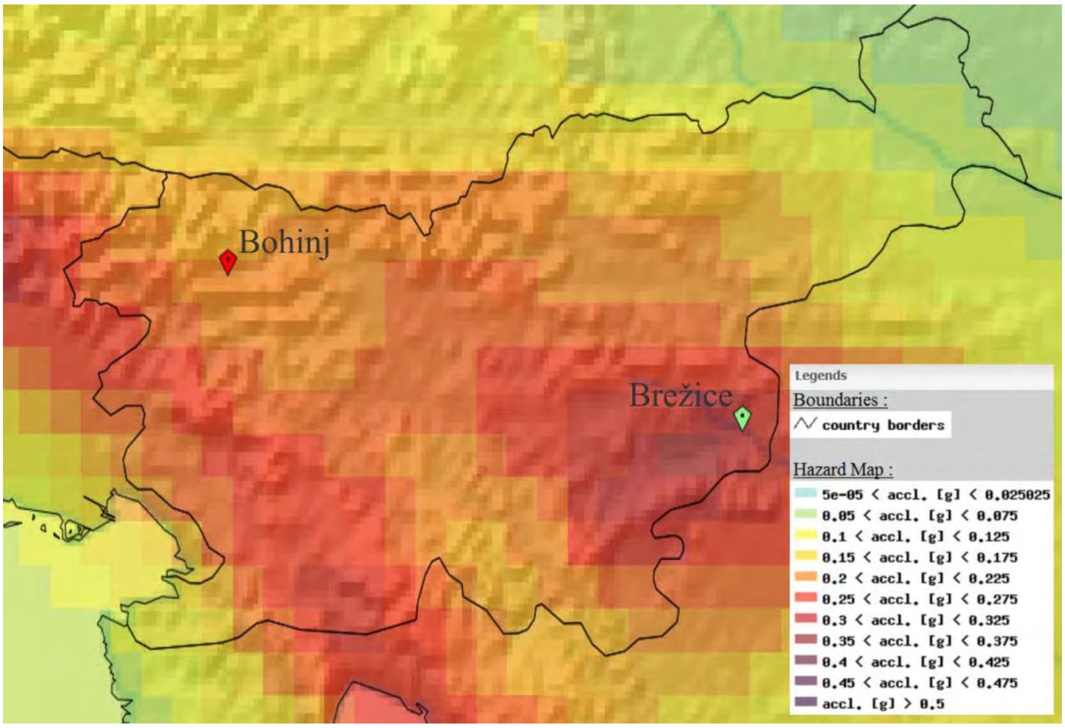

Figure 4-16: Seismic hazard map for Slovenia - Peak ground acceleration on rock or firm soil corresponding to return period of 475 years; SHARE Mean Hazard Model; arithmetic mean (EFEHR 2017).

The results of the SHARE seismic hazard model are also used for computation of the seismic hazard curves for the HPP Brežice site, which represent the probabilities of exceedance of selected peak ground accelerations in a defined period of time (e.g. 50 years, 1 year). The seismic hazard curve for the study area in Brežice is presented in Figure 4-17 by green line and is given in Table 4-5.

Table 4-5: Peak ground accelerations (PGA) and the corresponding probabilities of exceedance in 50 years (H_{50}), mean annual frequencies of exceedance (H) and the corresponding return periods (T_R), for the selected location in Brežice (EFEHR 2017b).

Brežice, SHARE Preferred Mean Hazard Model, rock or firm soil, arithmetic mean

PGA	0.05	0.10	0.15	0.20	0.28	**0.32**	0.40	0.56	0.78
H_{50}	0.78	0.53	0.38	0.24	0.13	**0.10**	0.066	0.029	0.012
H	2.95E-02	1.51E-02	9.42E-03	5.41E-03	2.84E-03	**2.10E-03**	1.36E-03	5.86E-04	2.31E-04
T_R	34	66	106	185	352	**475**	738	1706	4322

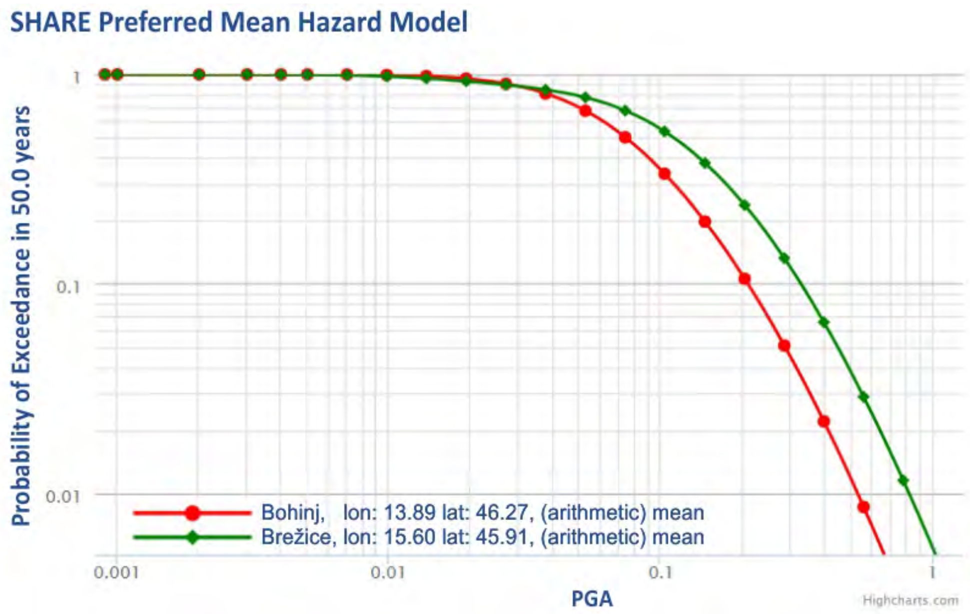

Figure 4-17: Seismic hazard curves for peak ground acceleration (PGA) at the selected locations in Bohinj and Brežice obtained by using the SHARE Preferred Mean Hazard Model, arithmetic mean and the rock or firm soil conditions (EFEHR 2017b).

The microzonation study for liquefaction at HPP Brežice site will be performed for return periods 475, 975 and 2475 years. Respective PGA values on rock and magnitudes are presented in Table 4-6.

Table 4-6: PGA and earthquake magnitude for HPP Brežice according to European Seismic Hazard Model.

Return period (years)	PGA (g)	Magnitude
475	0.32	6.0
975	0.43	6.1
2475	0.63	6.3

4.6 Microzonation for ground motion

4.6.1 Selection of seismic records

Due to the variability of earthquake nature, an attempt was given to a selection of appropriate earthquake records for this study. The purpose was to shake the numerical model with various seismic records, the spectra of which differ greatly, while their average spectrum matches the Eurocode spectrum for soil type A.

A set of 6 ground motions (GM) recorded on rock outcrop was selected from the Strong ground motion database which contains 9188 ground motions obtained from the NGA (Chiou et al, 2008) and the RESORCE (Akkar et al, 2014) database. The selected ground motions correspond to events with magnitudes between 6.2 and 6.7, and source-to-site distances between 6 and 34 km. Due to a lack of records from sites where shear wave velocity in upper 30 meters of soil ($v_{s,30}$) exceeds 800 meters per second (representing soil class A in Eurocodes), less strict criteria was chosen ($v_{s,30}$ > 500 m/s) in selection procedure. Average $v_{s,30}$ of selected GMs is equal to 613 m/s. Ground motions were selected in such a manner that the mean spectrum obtained from selected acceleration time histories coincides well with EC8 spectrum for soil class A related to peak ground acceleration a_g = 0.32 g (Figure 4-24).

More detailed information for all used ground motions is given in Table 4-7, while individual acceleration time histories are presented in Figure 4-18 to Figure 4-23.

Moreover, acceleration time histories were scaled to three different levels regarding peak ground acceleration, namely equal to 0.32 g, 0.43 g and 0.63 g, corresponding to the 475, 975 and 2475 years return periods, respectively. The magnitude of each PGA level was estimated from the SHARE seismic hazard study, as it was, on the basis of a comparison with national seismic hazard map, reflecting higher PGA values at Brežice site.

Table 4-7: Set of used ground motions.

Record Number	id	Earthquake location	Station location	Date	M	Closest distance	Soil_$v_{s,30}$
6	2661	Chi-Chi, Taiwan-03	TCU138	1999-09-20	6.2	22	653
9	1013	Northridge-01	LA Dam	1994-01-17	6.7	6	629

14	1012	Northridge-01	LA 00	1994-01-17	6.7	19	706
23	2703	Chi-Chi, Taiwan-04	CHY028	1999-09-20	6.2	18	543
25	3268	Chi-Chi, Taiwan-06	CHY028	1999-09-25	6.3	34	543
30	1020	Northridge-01	Lake Hughes #12A	1994-01-17	6.7	21	602

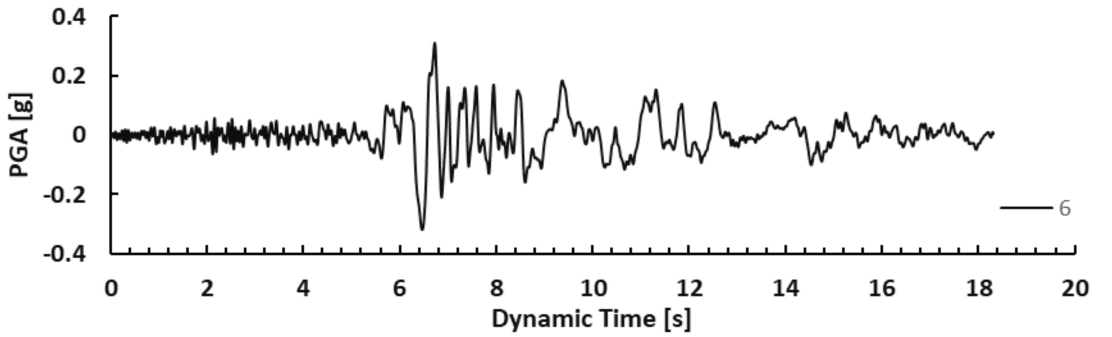

Figure 4-18: Acceleration time history – 6.

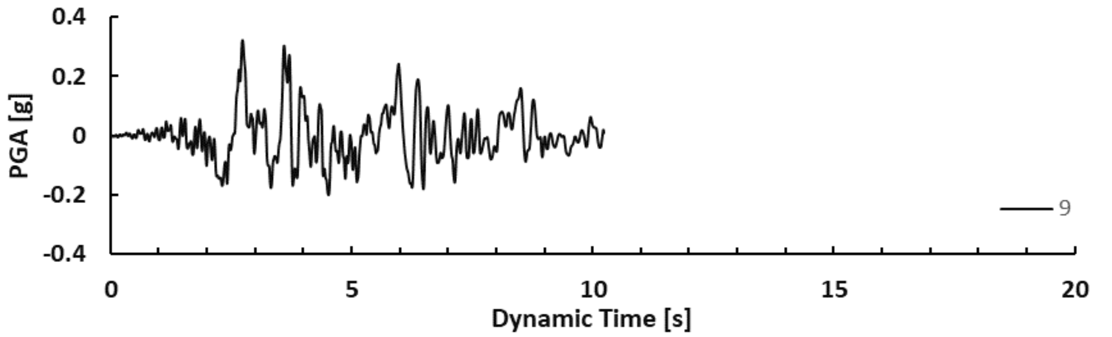

Figure 4-19: Acceleration time history – 9.

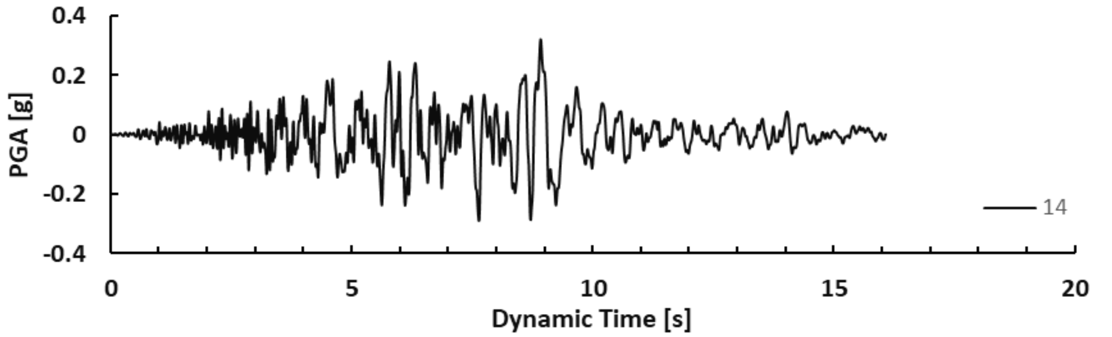

Figure 4-20: Acceleration time history – 14.

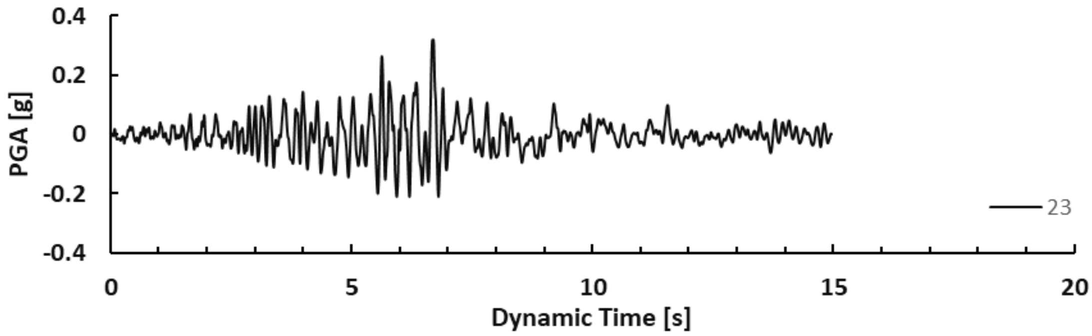

Figure 4-21: Acceleration time history – 23.

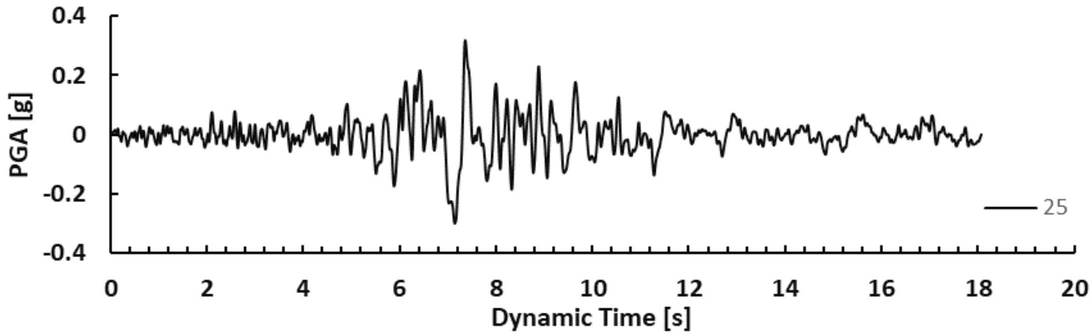

Figure 4-22: Acceleration time history – 25.

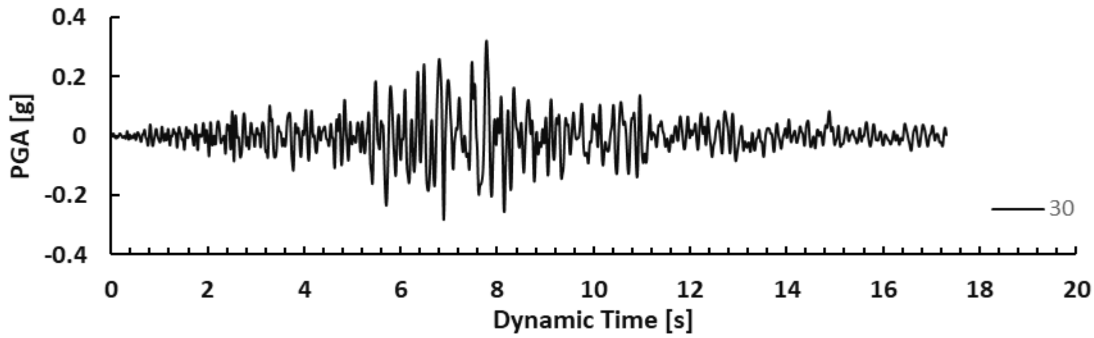

Figure 4-23: Acceleration time history – 30.

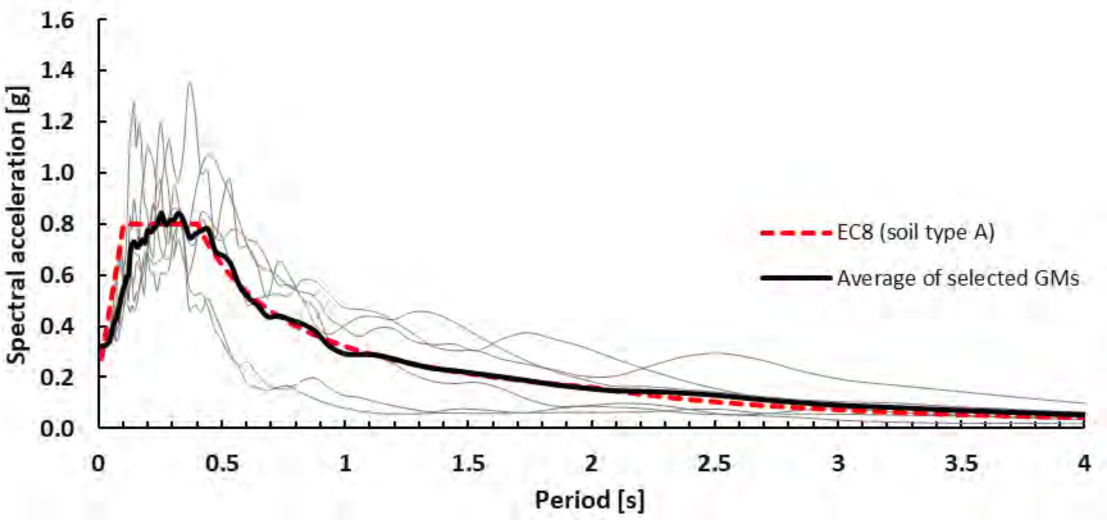

Figure 4-24: Spectra of selected ground motions in comparison with Eurocode 8 spectrum for soil type A.

4.6.2 Ground response analyses

The evaluation of peak ground accelerations at ground surface were carried out using Deepsoil 7.0 (Hashash et al, 2017) software package, where equivalent linear seismic site response of one-dimensional soil column analyses method was used in conjunction with frequency domain solution type.

Initially, ground profile geometry and material properties were assigned to the numerical model, followed by the attribution of the dynamic load, which was applied at the model base. The simplified model was composed of five representative soil layers, including silty sand layer on the top, below it a gravel layer, two layers of Miocene clay and a seismic bedrock (see Table 4-4).

Ground response analysis was performed for 54 variations of ground model (see Table 4-3) which gave close enough pattern of results that allowed the interpolation for any particular combination of layer thicknesses over the study area (see results in Table 4-8).

4.6.3 Results of ground response analyses

Table 4-8 summarizes the results of Deepsoil analyses in terms of PGA at surface for all variations of geometry and three return periods. It is seen that in all analysed cases PGA at bedrock increases through soil medium to the top surface for this particular geometry and combinations of material properties, except for 55 m thick gravel layer and 2475 return period where PGA at surface is lower than a_g = 0.63 g applied at the bottom of the numerical model. Otherwise, it was observed that thicker sandy layer leads to greater PGA amplification, while increasing the thickness of gravel layer reduces the increase of PGA at the surface.

At the outset, models with two different water levels (z_w = 0 m and z_w = 3 m) had been compared for some selected soil profiles and negligible differences had been observed. Therefore, the decision was made that whole geometry combination set would be calculated with the water level at the ground surface only.

Results of PGA amplification study was used for the calculations of cyclic stress ratio (CSR), further needed for the evaluation of safety factor of soil liquefaction.

Spatial distribution of PGA values at the surface over the area around test site Brežice is presented in Figure 4-25 to Figure 4-27 for cases with return period of 475, 975 and 2475 years. These plots are produced for interpolated ground conditions in pattern of 5x5 m.

Table 4-8: Calculated PGA at surface.

T_R Return period [years]	**SM** Thickness of silty sand layer [m]	**GP** - Thickness of gravel layer [m]										
		4.0	**5.5**	**7.0**	**8.5**	**10.0**	**13.0**	**16.0**	**19.0**	**31.0**	**43.0**	**55.0**
475	**0**	0.458	/	0.479	0.493	0.504	0.511	0.498	0.481	0.433	0.402	0.393
	1.5	0.473	0.481	0.495	0.509	0.519	0.526	0.510	0.491	0.440	0.408	0.398
	2	/	0.498	/	/	/	/	/	/	/	/	/
	2.5	0.512	/	0.532	0.546	0.557	0.555	0.539	0.522	0.461	0.424	0.412
	3.5	0.575	/	0.582	0.593	0.601	0.603	0.591	0.565	0.493	0.451	/
	4.5	0.635	/	0.633	0.635	0.633	0.630	/	/	/	/	/
	5.5	0.655	/	0.654	0.657	0.659	0.657	/	/	/	/	/
	6.5	/	/	0.677	/	0.678	0.674	/	/	/	/	/
975	**0**	0.604	/	0.632	0.643	0.648	0.647	0.628	0.604	0.540	0.511	0.482
	1.5	0.620	0.636	0.651	0.662	0.668	0.663	0.641	0.617	0.549	0.518	0.488
	2	/	0.654	/	/	/	/	/	/	/	/	/
	2.5	0.669	/	0.700	0.710	0.712	0.700	0.676	0.648	0.571	0.536	0.504
	3.5	0.749	/	0.761	0.770	0.773	0.760	0.736	0.697	0.607	0.564	/
	4.5	0.810	/	0.812	0.805	0.799	0.783	/	/	/	/	/
	5.5	0.850	/	0.848	0.844	0.840	0.823	/	/	/	/	/
	6.5	/	/	0.881	/	0.870	0.854	/	/	/	/	/
2475	**0**	0.854	/	0.876	0.885	0.890	0.871	0.824	0.773	0.704	0.658	0.583
	1.5	0.876	0.887	0.897	0.906	0.912	0.892	0.841	0.792	0.716	0.670	0.591
	2	/	0.911	/	/	/	/	/	/	/	/	/
	2.5	0.937	/	0.957	0.963	0.965	0.938	0.878	0.825	0.740	0.692	0.608
	3.5	1.031	/	1.044	1.048	1.046	1.016	0.943	0.884	0.781	0.729	/
	4.5	1.090	/	1.091	1.083	1.077	1.056	/	/	/	/	/
	5.5	1.180	/	1.181	1.177	1.167	1.118	/	/	/	/	/
	6.5	/	/	1.300	/	1.293	1.289	/	/	/	/	/

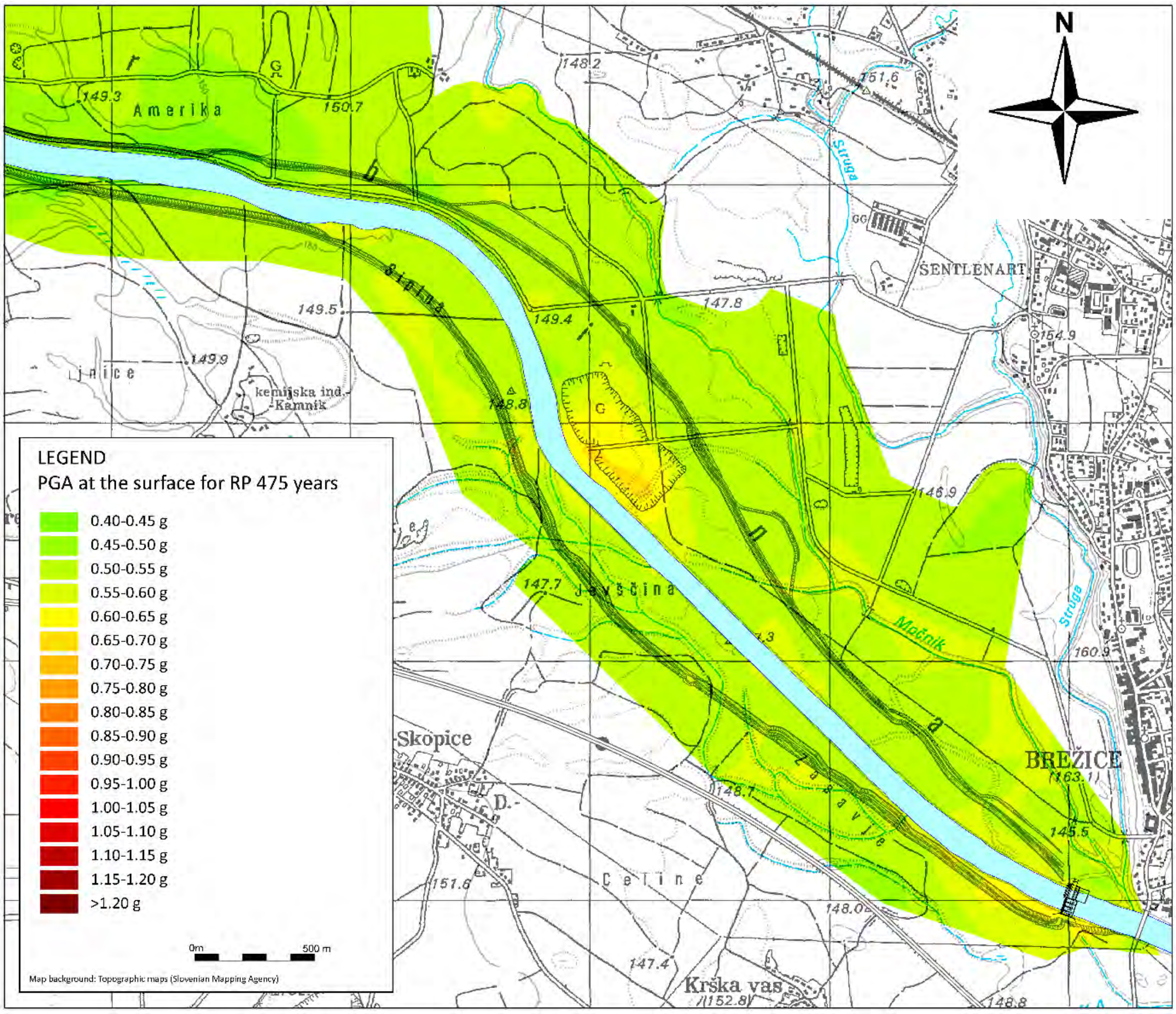

Figure 4-25: Peak ground acceleration at ground surface for return period of 475 years.

This project has received funding from the European Union's Horizon 2020 research and innovation programme under grant agreement No. 700748

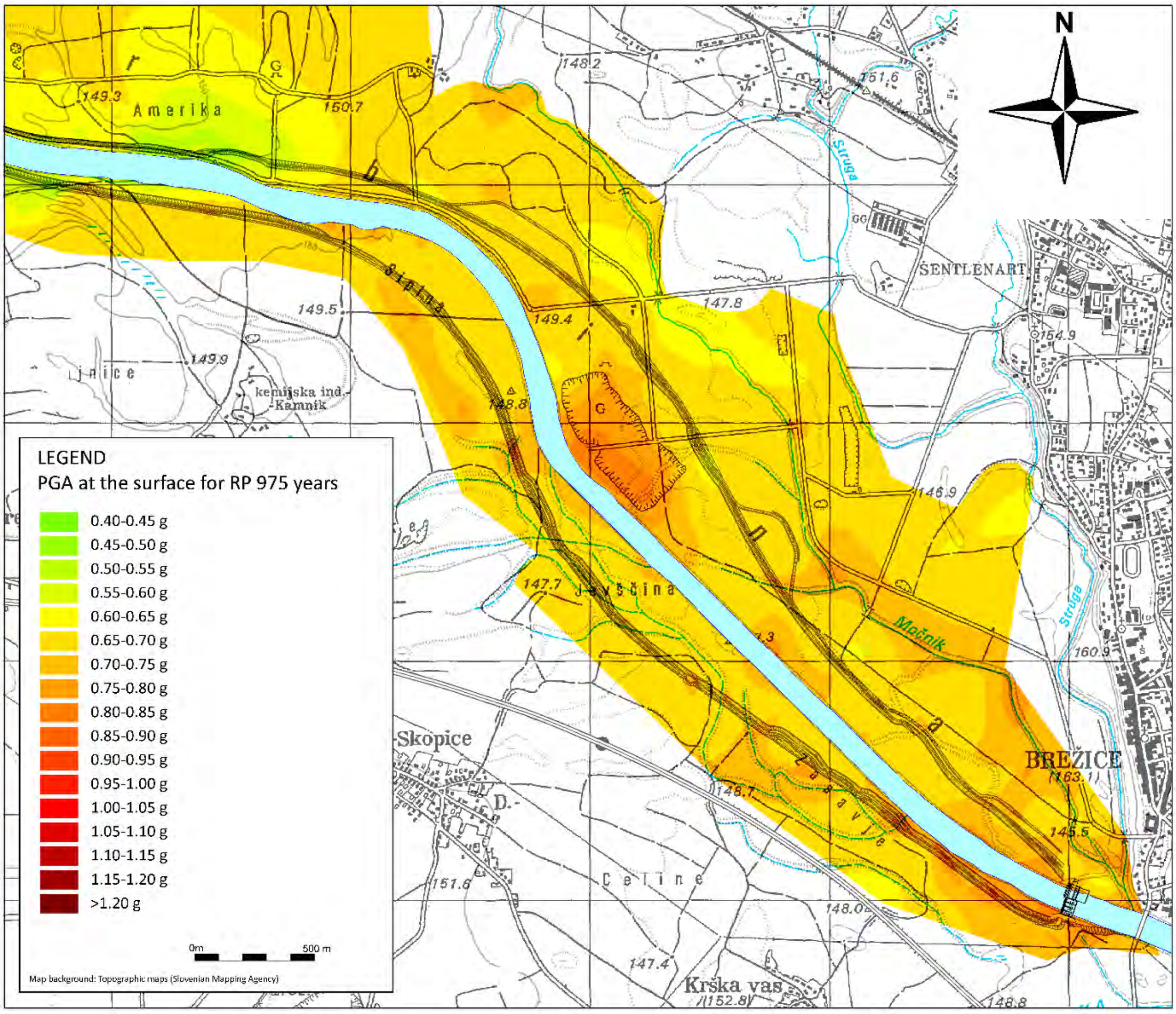

Figure 4-26: Peak ground acceleration at ground surface for return period of 975 years.

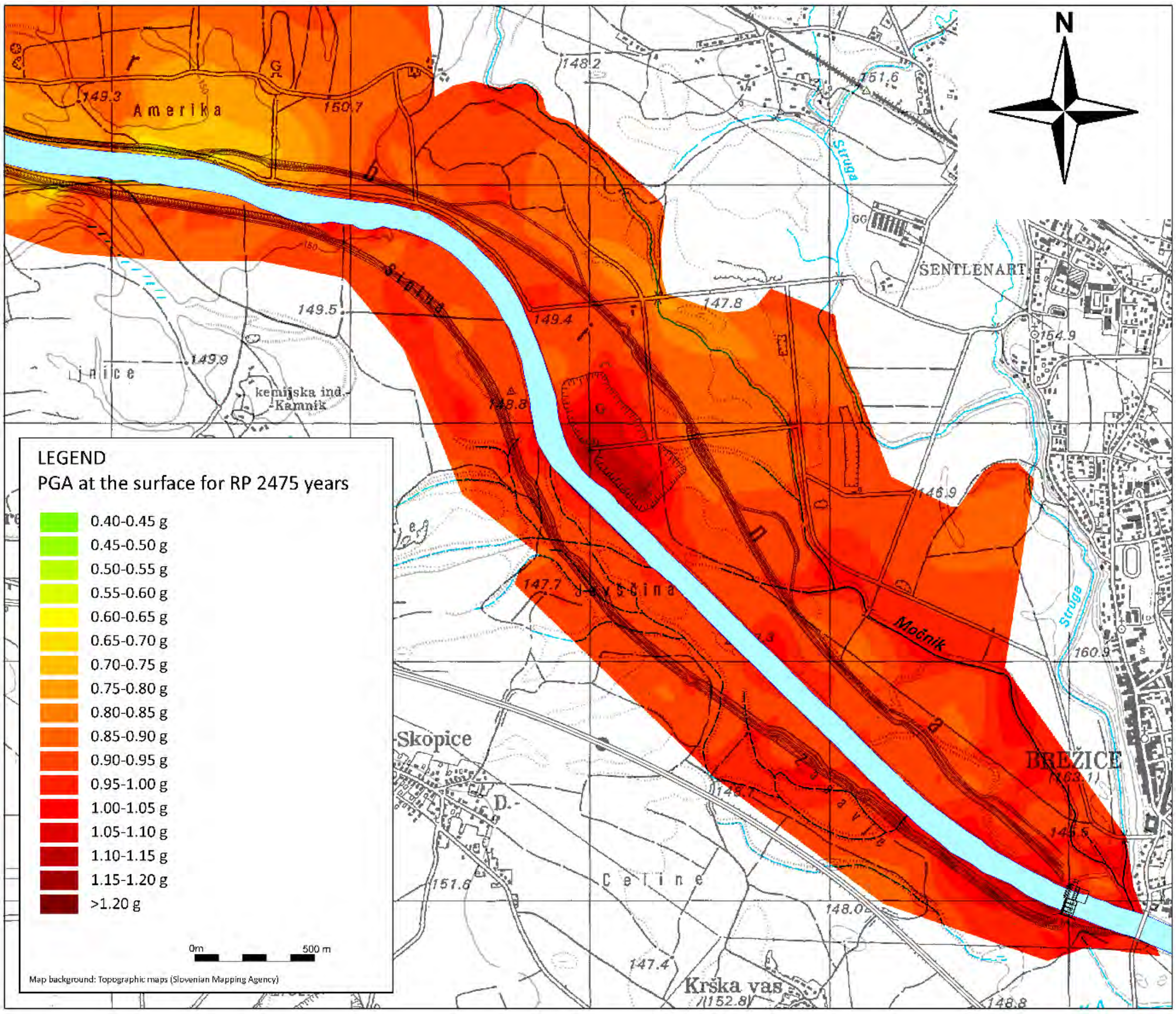

Figure 4-27: Peak ground acceleration at ground surface for return period of 2475 years.

4.7 Microzonation for liquefaction risk

Based on the results of PGA amplification analyses, spatial distribution of the soil profile geometries and material properties in terms of resistivity to cyclic loading, a susceptibility to soil liquefaction study was performed for the area of the HPP Brežice site. Liquefaction resistance of the silty sand layer was assessed through empirical equations using CPT and SDMT in-situ measurements, and is expressed in terms of safety factor and liquefaction potential index (LPI) in the figures below.

Data processing was done using Matlab software package. Firstly, the thicknesses of soil layers from the geological model were implemented in the Matlab model. The nearest-neighbour interpolation method was used to cover the whole range of combinations. The stratigraphy of the soil layers was determined for grid cell size equal to 5x5 m^2 ($\Delta x = \Delta y = 5$ m).

Linear interpolation technique was used to determine PGA values at single grid cell for each return period (Figure 4-25 to Figure 4-27).

4.7.1 Evaluation of cyclic stress ratio (CSR)

On the basis of equations (1 to 5) proposed by original authors in this field (Seed & Idriss, 1982 and Boulanger & Idriss, 2014) the CSR values were calculated to a depth of 6.6 m (the greatest thickness of sandy layer) in steps of 0.2 m, assuming the PGA (=a_{max}/g) is equal to 1. Then, the normalized CSR vector (at PGA = 1) was multiplied by the appropriate PGA value at each grid point (equations 6 and 7), which gave us a CSR distribution with depth over the entire grid mesh.

$$\boldsymbol{CSR_{M=7.5} = 0.65 \cdot \frac{a_{max}}{g} \cdot \frac{\sigma_v}{\sigma'_v} \cdot r_d \cdot \left(\frac{1}{MSF}\right)} \tag{1}$$

$$r_d = e^{\alpha(z)+\beta(z)\cdot M} \tag{2}$$

$$\alpha(z) = -1.012 - 1.126 \cdot \sin\left(\frac{z}{11.73} + 5.133\right) \tag{3}$$

$$\beta(z) = 0.106 + 0.118 \cdot \sin\left(\frac{z}{11.28} + 5.142\right) \tag{4}$$

$$MSF = 6.9 \cdot e^{\left(\frac{-M}{4}\right)} - 0.058 \leq 1.8 \tag{5}$$

$$\boldsymbol{CSR_{M=7.5,PGA=1} = 0.65 \cdot \frac{\sigma_v}{\sigma'_v} \cdot r_d \cdot \left(\frac{1}{MSF}\right)} \tag{6}$$

$$\boldsymbol{CSR_{M=7.5} = PGA\ CSR_{M=7.5,PGA=1}} \tag{7}$$

Figure 4-28 presents the normalized CSR distribution with depth for all six situations considered in the analysis, namely for three return periods and two different ground water levels (z_w = 0 m and z_w = 3 m).

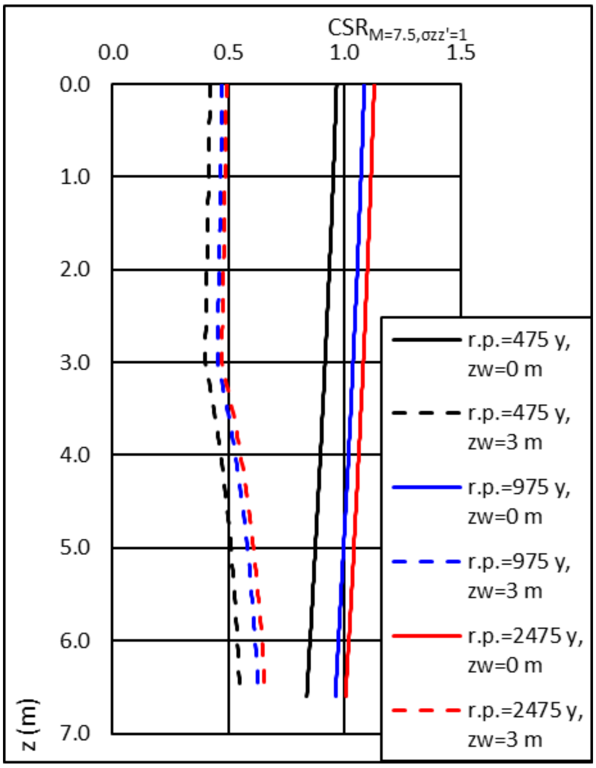

Figure 4-28: Unit CSR (PGA=1) with depth for three return periods and two ground water levels.

4.7.2 Evaluation of cyclic resistance ratio (CRR)

The evaluation of cyclic resistance ratio (CRR) under this study based on the field measurements obtained through CPT and SDMT in-situ tests at the test site Brežice, mentioned in the previous sections. Due to a small number of CPT and SDMT tests available over the study area and due to the differences in individual field measurement results, a reference test concept was applied in the CRR evaluation procedure for microzonation purpose. The reference test was obtained as the sequence of median of all measurements of a single test type at each depth. The reference test was later used to calculate the factor of safety against liquefaction and liquefaction potential indices over the study area. On the maps of safety factor and liquefaction potential index (LPI), the reference test was used to produce the mapped values, while at individual SDMT an CPT points the respective values of SF and LPI for each in-situ test were also calculated and are shown on the maps for comparison.

SDMT based approach

Since different physical and mechanical properties of the soil are measured during the SDMT test, two separate approaches were used for the evaluation of the soil resistance to liquefaction. The CRR was computed using horizontal stress index K_D and shear wave velocity v_s, by the equations 8 (Robertson et al, 2012) and 9 to 10 (Robertson & Wride, 1998 and Robertson, 2015), where P_α is atmospheric pressure (101.3 kPa), σ'_{v0} is effective vertical stress and K_C and α_{vs} factors accounting for the content of fines (*FC*) in the sand. According to the literature, K_C = 3.427 and α_{vs} = 1288.25 were considered for the CRR evaluation, since sandy layer at Brežice test site is reach in silty particles (*FC* can be more than 30 %, see Figure 4-7).

$$CRR_{7.5} = 93 \cdot (0.025 \cdot K_D)^3 + 0.08 \qquad \text{(for } 2 < K_D < 6 \text{ and } I_D > 1.2) \tag{8}$$

$$v_{s1} = v_s \cdot \left(\frac{P_\alpha}{\sigma'_{v0}}\right)^{0.25} \tag{9}$$

$$CRR_{7.5} = 93 \cdot \left[\frac{\left(\frac{K_C}{\alpha_{vs}}\right) \cdot (v_{s1})^2}{1000}\right]^3 + 0.08 \tag{10}$$

In case of SDMT tests, the deepest measurement reached the depth of only 4.2 m, therefore reference test had to be extrapolated to a depth of 6.6 m in order to calculate the SF and LPI over entire study area. Note that only 1.5% of the total study area is covered by silty-sand layer being over 4.2 m thick and is therefore affected by this assumption. Consequently, evaluation of CRR is less reliable in this parts. Figure 4-29 presents CRR values with depth based on horizontal stress index (K_D) and shear wave velocity (v_s), obtained by SDMT tests.

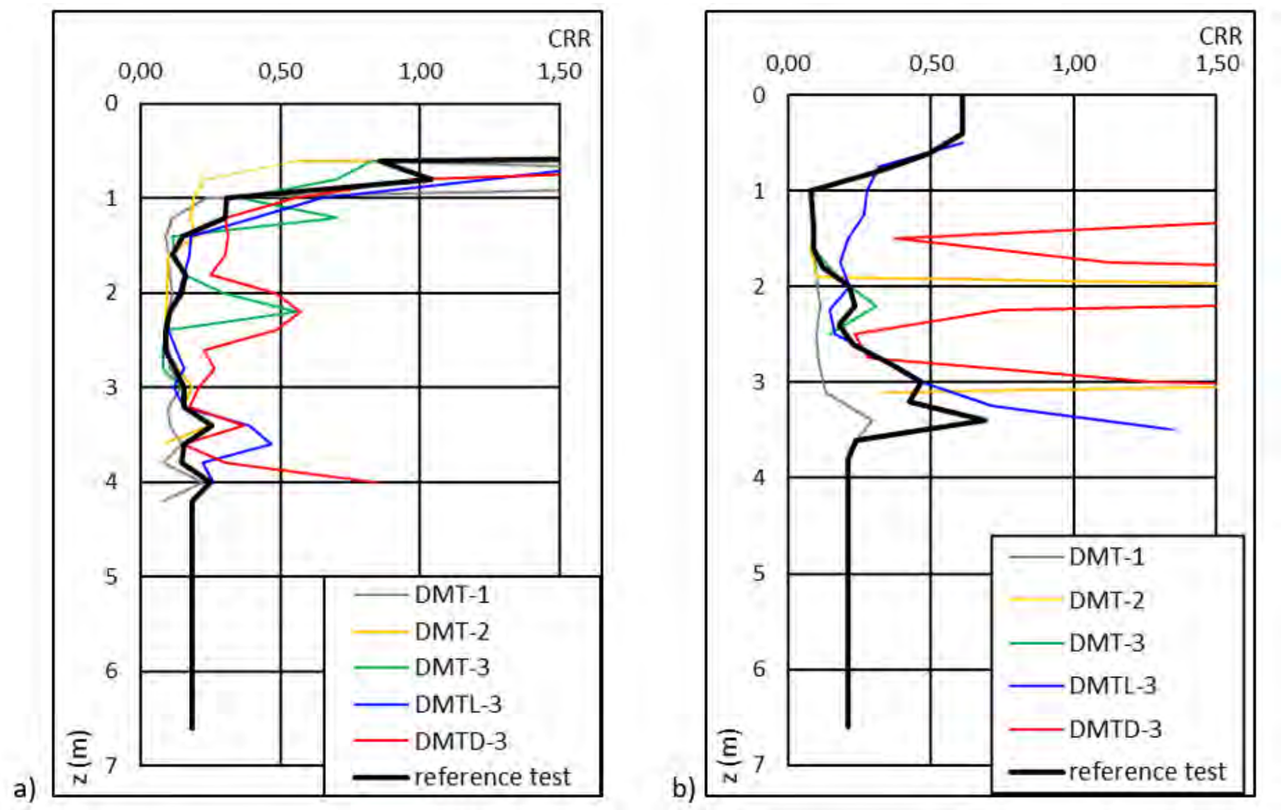

Figure 4-29: CRR evaluation from SDMT measurements - a) based on K_D and b) based on v_s.

CPT based approach

Due to the numerous correlations with liquefaction case histories and the continuity of the measuring with depth, the CPT is considered one of the best in-situ tests for the evaluation of liquefaction susceptibility of a soil. The calculation of the CRR within this study followed the iterative procedure proposed by Robertson in 2009 (Robertson, 2014), developed on the basis of Robertson and Wride (1998) approach for the determination of soil resistance to liquefaction. The used procedure is expressed by the equations (11 to 17) below.

For the initial approximation, stress exponent *n* = 1 was selected, then the procedure was iterated until the change in *n* value was less than 1% (Δn < 0.01).

$$n = 0.381\, I_C + 0.05\left(\frac{\sigma'_{v0}}{p_a}\right) - 0.15 \leq 1 \tag{11}$$

$$Q_{tn} = \left(\frac{q_t - \sigma_{v0}}{p_a}\right)\left(\frac{p_a}{\sigma'_{v0}}\right)^n \tag{12}$$

$$F_r = \left(\frac{f_s}{q_t - \sigma_{v0}}\right) 100\% \tag{13}$$

$$I_c = ((3.47 - \log Q_{tn})^2 + (1.22 + \log F_r)^2)^{0.5} \tag{14}$$

$$\begin{cases} 1 & I_c \leq 1.64 \\ 1 & 1.64 < I_c < 2.36 \text{ and } F_r < 0.5\% \\ 5.581 I_c^3 - 0.403 I_c^4 - 21.63 I_c^2 + 33.75 I_c - 17.88 & 1.64 < I_c \leq 2.5 \\ 6 \cdot 10^{-7} I_c^{16.76} & 2.5 < I_c < 2.7 \\ 1 & I_c \geq 2.7 \end{cases} \tag{15}$$

$$Q_{tn,cs} = K_c Q_{tn} \tag{16}$$

$$CRR_{7.5} = \begin{cases} 0.833\left(\frac{Q_{tn,cs}}{1000}\right) + 0.05 & I_c < 2.7 \text{ and } Q_{tn,cs} < 50 \\ 93\left(\frac{Q_{tn,cs}}{1000}\right)^3 + 0.08 & I_c < 2.7 \text{ and } 50 \leq Q_{tn,cs} \leq 160 \\ 0.053 Q_{tn} K_\alpha & I_c \geq 2.7 \end{cases} \tag{17}$$

The following notation is used in the above equations:
n – stress exponent,
I_c – soil behaviour type index,
σ'_{vo} and σ_{vo} – effective and total vertical stress, respectively,
P_α – reference pressure,
Q_{tn} – normalized CPT penetration resistance,
F_r – normalized friction ratio,

K_c – correction factor,
K_α – correction factor to account for static shear stress (≈1 in our case),
$Q_{tn,cs}$ – equivalent clean sand cone penetration resistance.

Once the $Q_{tn,cs}$ was obtained for each CPT test, the same reference test approach was adopted as described earlier for DMT method. Since the CPT measurement results are available at each 2 cm of depth, the trend of reference test, evaluated at each 0.2 m of depth, follows the line of median values evaluated at every 2 cm of depth obtained from all CPT measurements. The comparison between reference test and curve with median values is shown in Figure 4-30 b), while the results of CRR with depth are presented in Figure 4-30 a). Available CPT tests covered maximum depth of 5.86 m but only 1 test reached the depth greater than 4.2 m. Again, extrapolation from 4.2 m down to the depth of 6.6 m depth was used. As already stated above, this assumption only affected 1.5 % of the total study area.

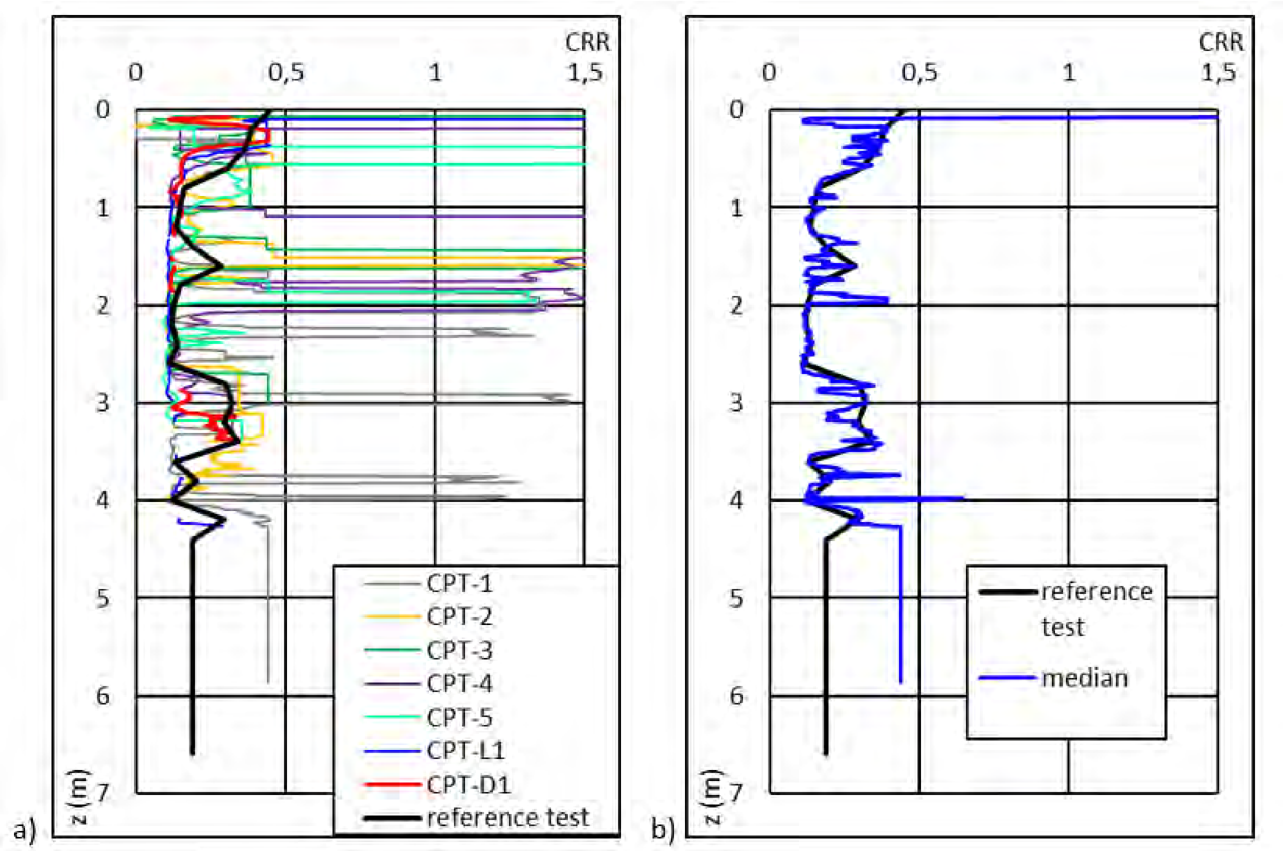

Figure 4-30: CRR evaluation from CPT - a) CRR for single test and reference test, b) CRR for reference test and median values.

From the above results, we can observe that the predominant values of cyclic resistance ratio within critical depths of silty sand layer lie between 0.2 and 0.3. These coincides well with the values obtained from cyclic simple shear tests (Figure 4-8).

4.7.3 Safety Factor (FS) and Liquefaction Potential Index (LPI)

Once the cyclic stress ratios and cyclic resistance ratios were estimated, the factor of safety (equation 18) and liquefaction potential index (equation 19) were calculated for three return periods and two groundwater levels and separately for CPT, DMT and v_s (from SDMT) soil investigation results. The results for all these cases are presented in Figure 4-31 to Figure 4-48 as maps of safety factor and in Figure 4-49 to Figure 4-66 as maps of LPI over the study area. Factor of safety presented on the maps is the minimum value over entire depth of silty sand layer at each point.

$$FS = \frac{CRR}{CSR} \tag{18}$$

$$LPI = \int_0^Z \max(1 - FS(z), 0)\,(10 - 0.5z)\,dz \tag{19}$$

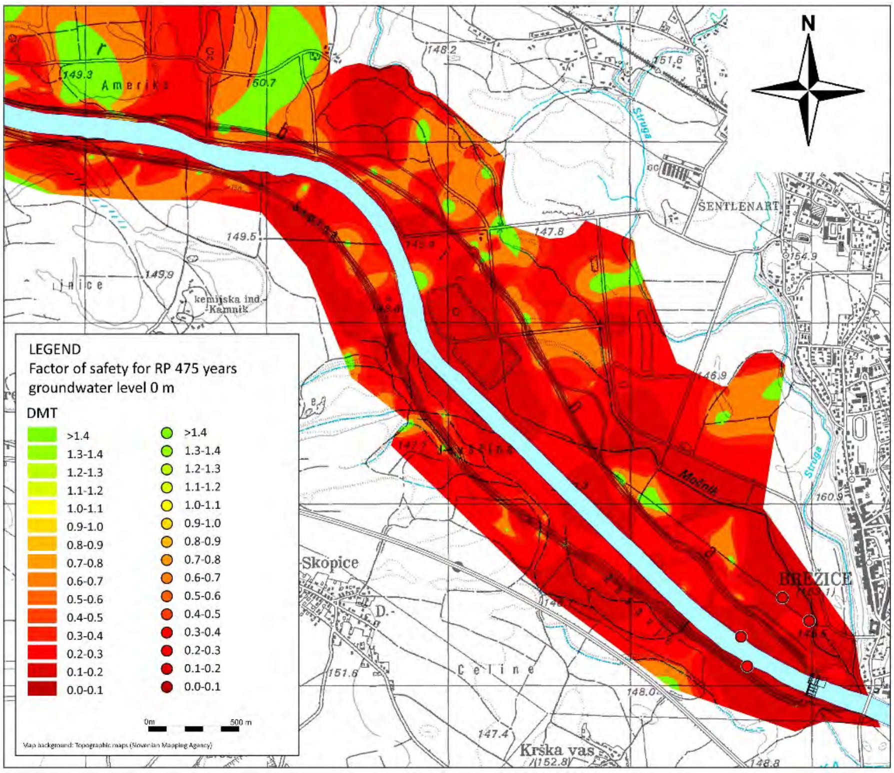

Figure 4-31: Factor of safety - RP = 475 years, z_w = 0 m, K_D from DMT.

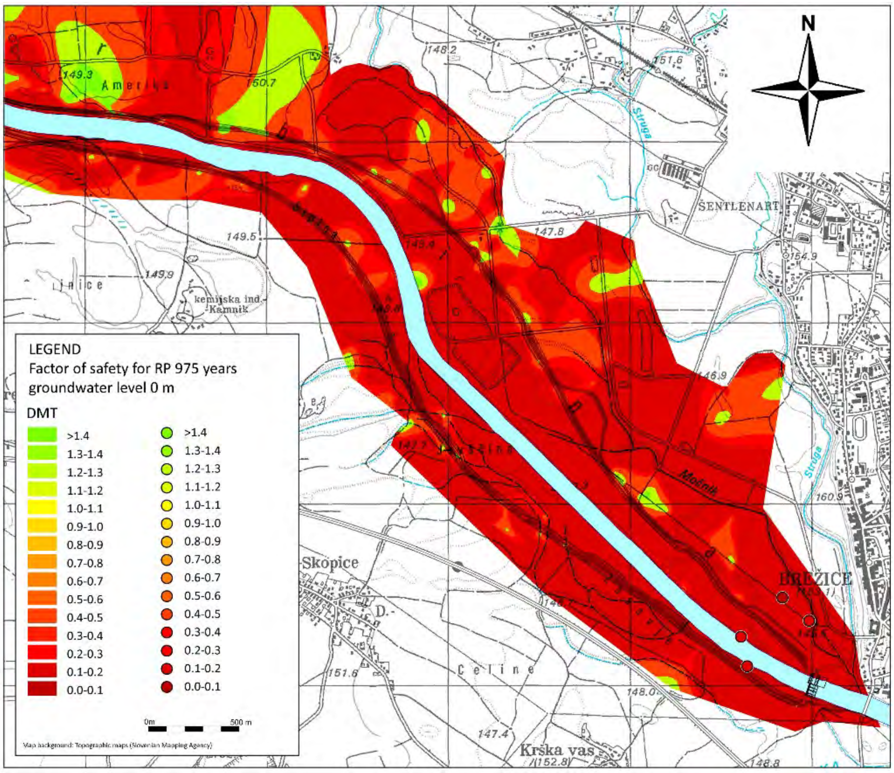

Figure 4-32: Factor of safety - RP = 975 years, z_w = 0 m, K_D from DMT.

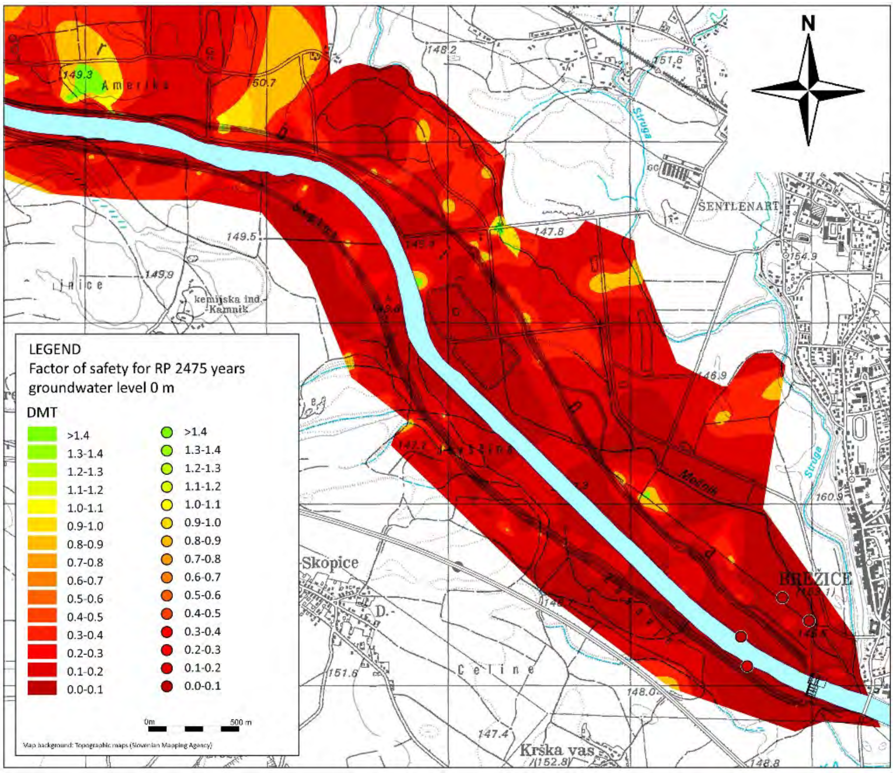

Figure 4-33: Factor of safety - RP = 2475 years, z_w = 0 m, K_D from DMT.

This project has received funding from the European Union's Horizon 2020 research and innovation programme under grant agreement No. 700748

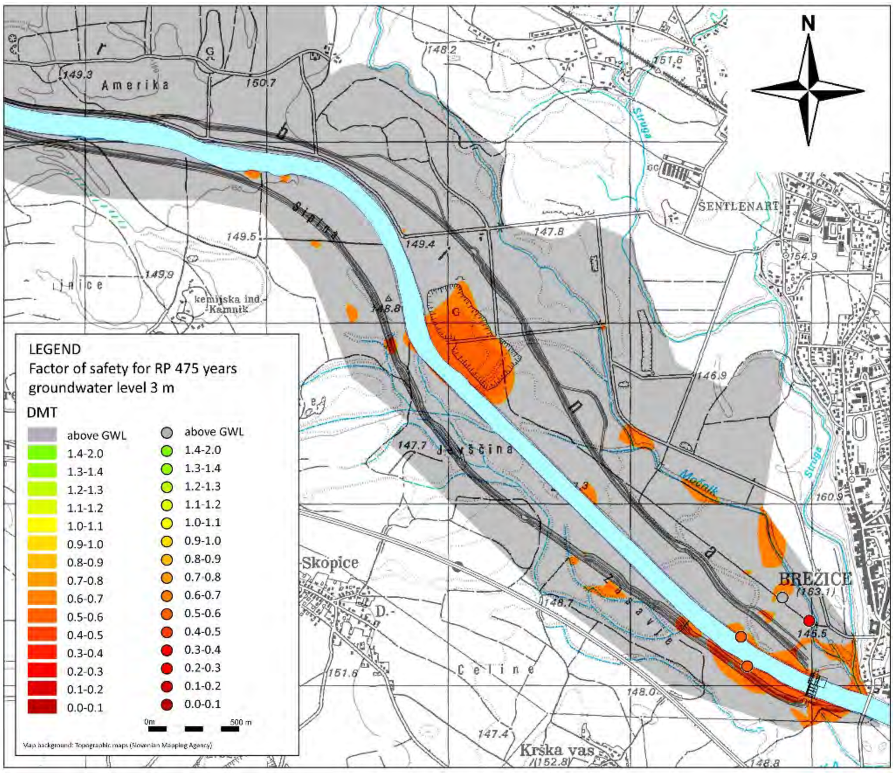

Figure 4-34: Factor of safety - RP = 475 years, zw = 3 m, KD from DMT.

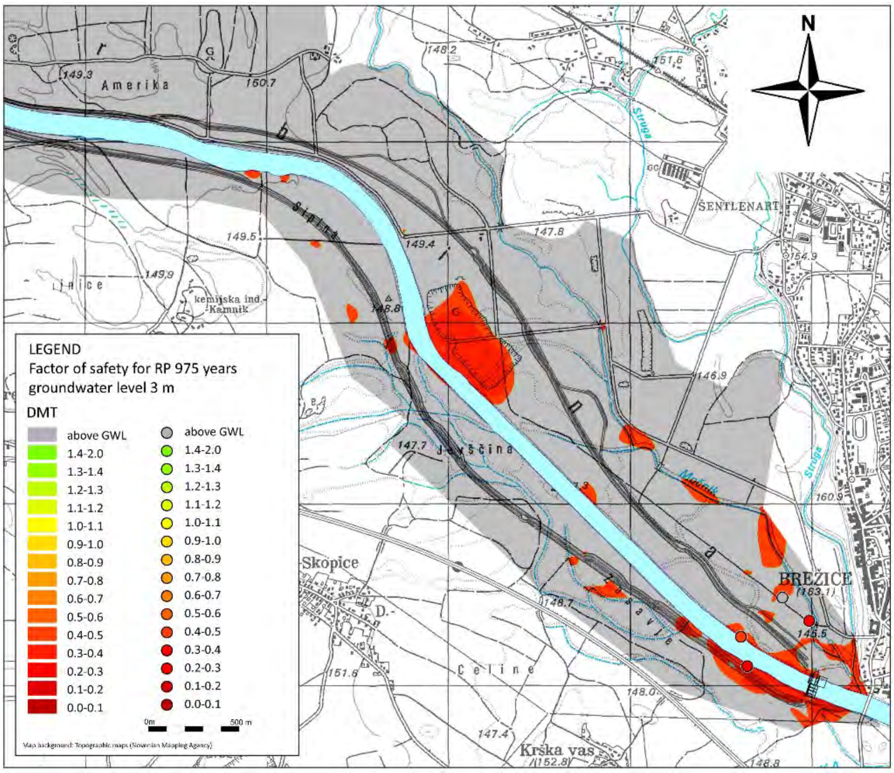

Figure 4-35: Factor of safety - RP = 975 years, zw = 3 m, KD from DMT.

This project has received funding from the European Union's Horizon 2020 research and innovation programme under grant agreement No. 700748

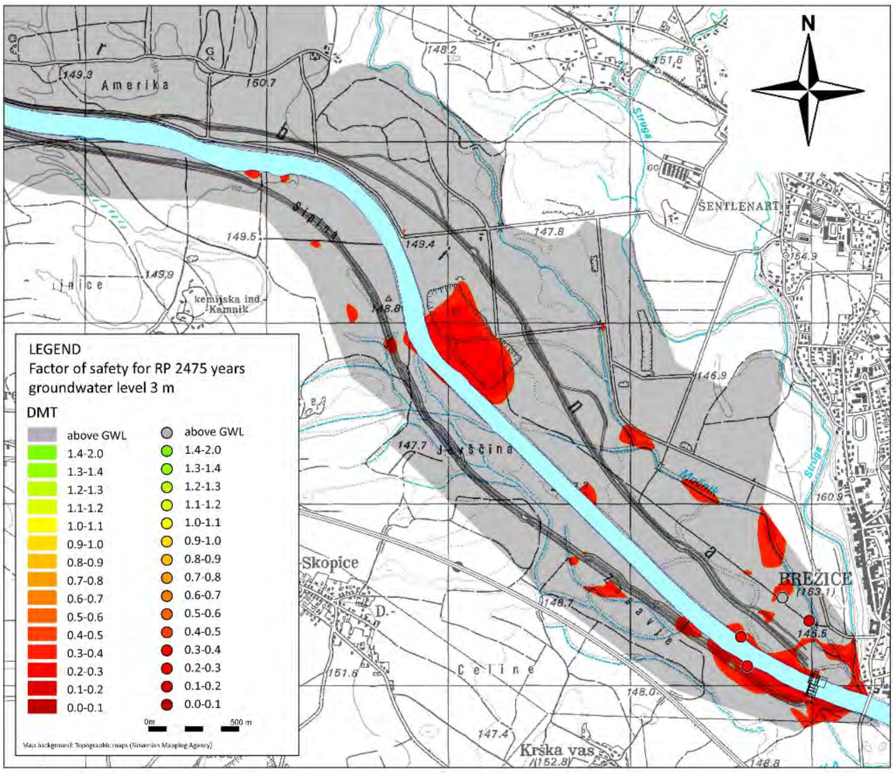

Figure 4-36: Factor of safety - RP = 2475 years, zw = 3 m, KD from DMT.

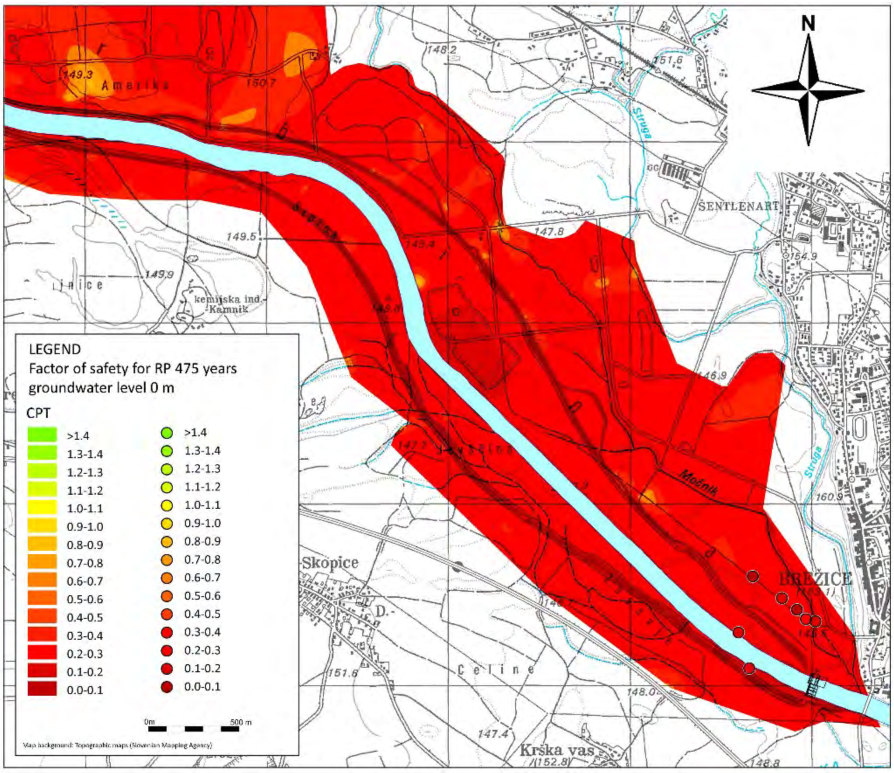

Figure 4-37: Factor of safety - RP = 475 years, z_w = 0 m, CPT.

This project has received funding from the European Union's Horizon 2020 research and innovation programme under grant agreement No. 700748

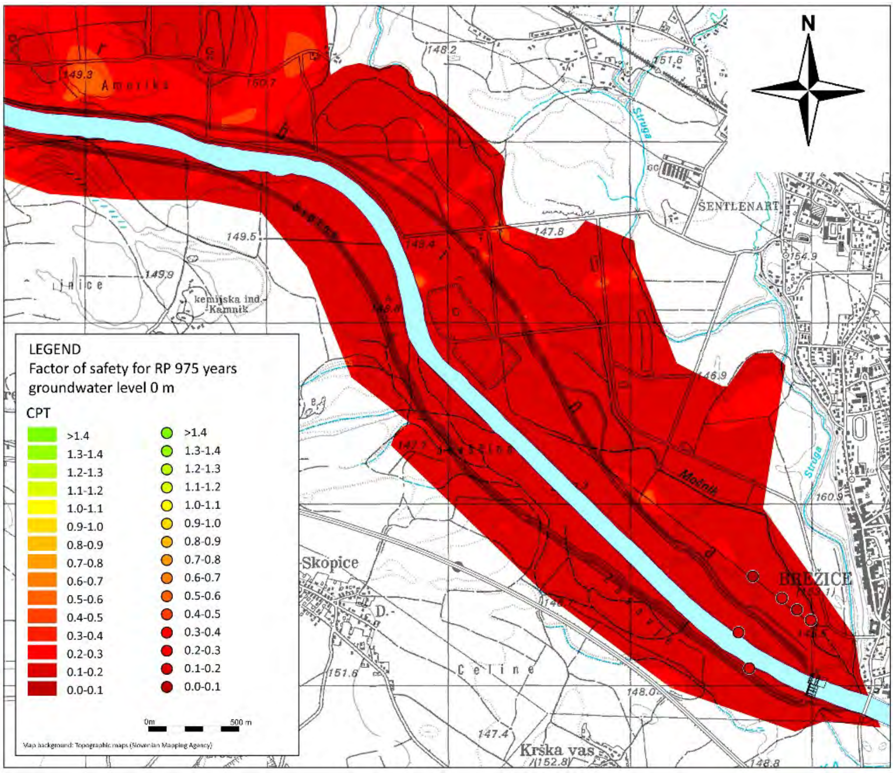

Figure 4-38: Factor of safety - RP = 975 years, zw = 0 m, CPT.

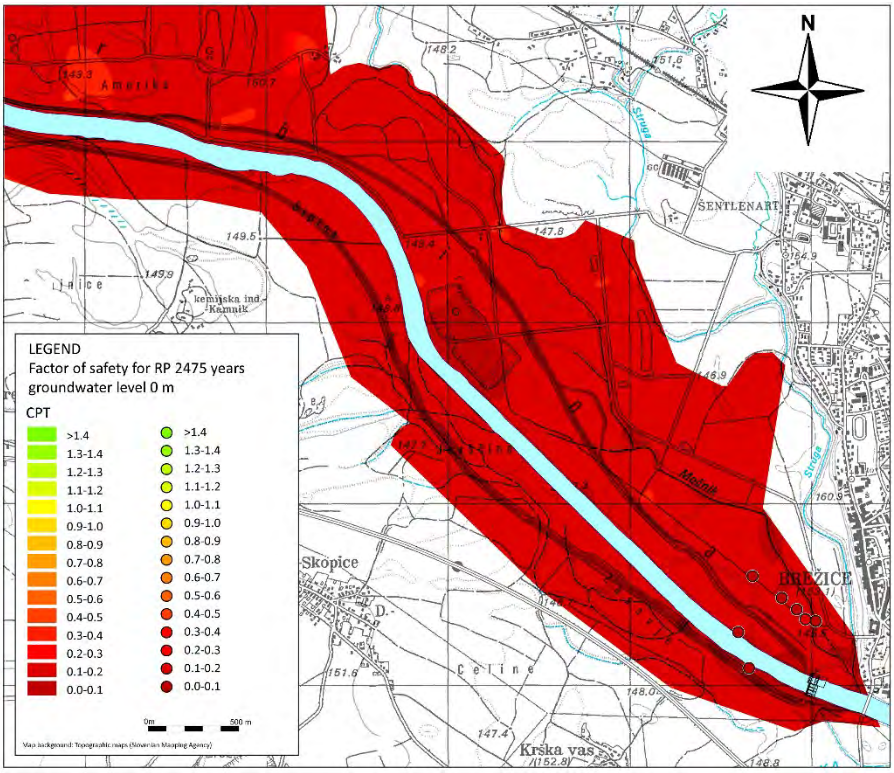

Figure 4-39: Factor of safety – RP = 2475 years, zw = 0 m, CPT.

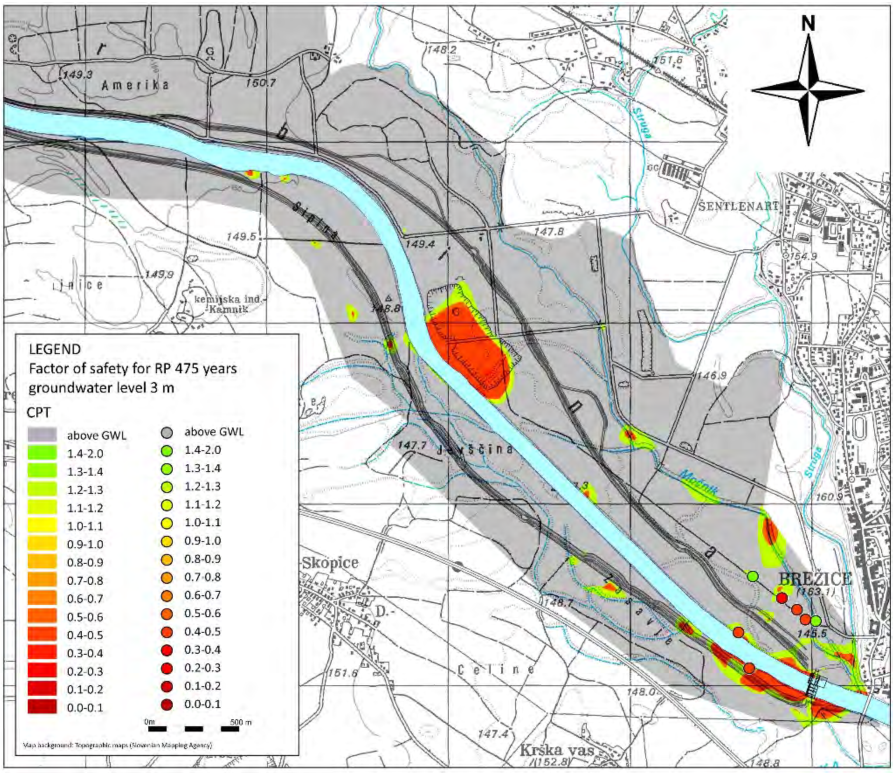

Figure 4-40: Factor of safety - RP = 475 years, zw = 3 m, CPT.

This project has received funding from the European Union's Horizon 2020 research and innovation programme under grant agreement No. 700748

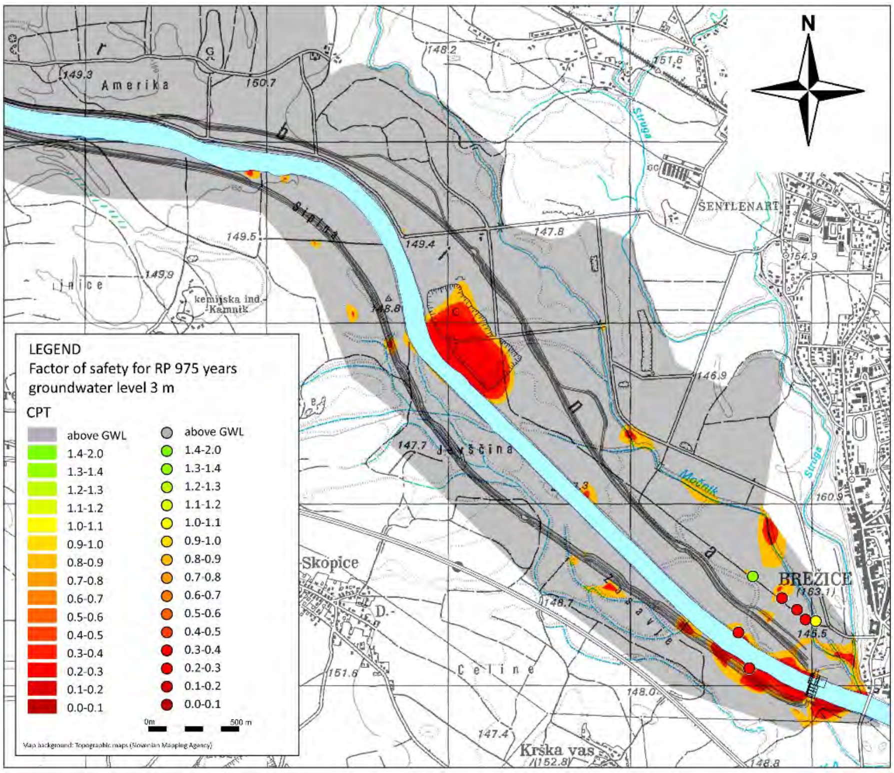

Figure 4-41: Factor of safety - RP = 975 years, zw = 3 m, CPT.

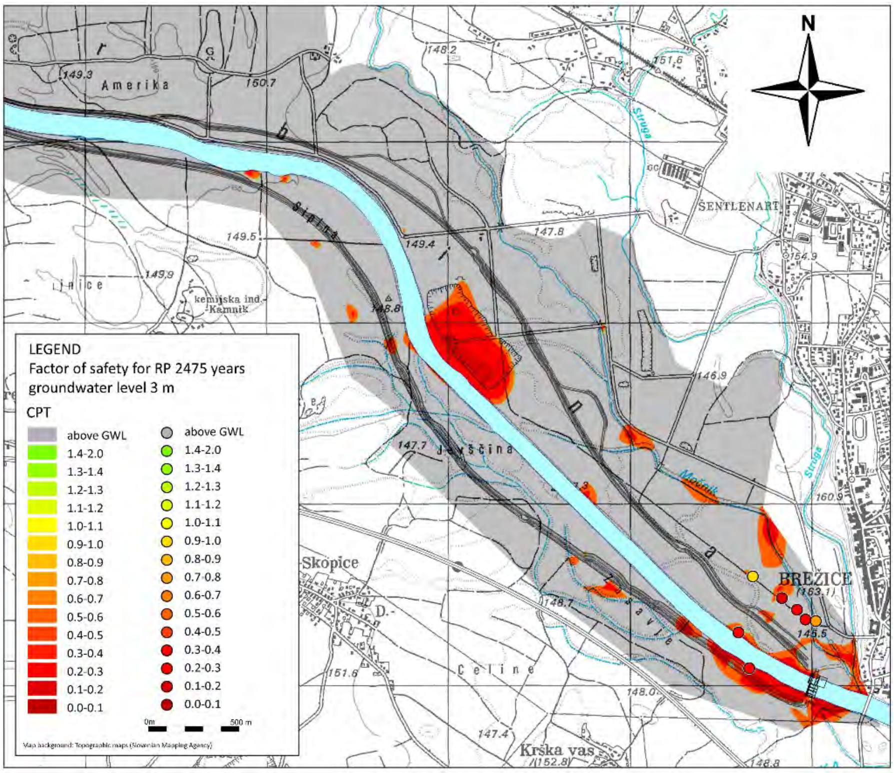

Figure 4-42: Factor of safety - RP = 2475 years, zw = 3 m, CPT.

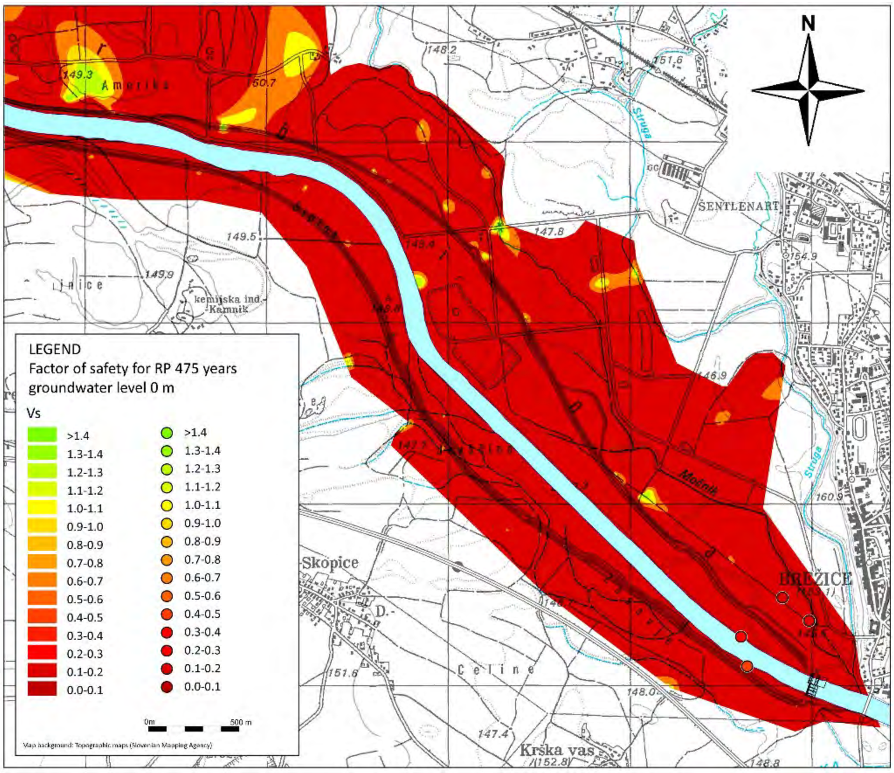

Figure 4-43: Factor of safety - RP = 475 years, zw = 0 m, vs from SDMT.

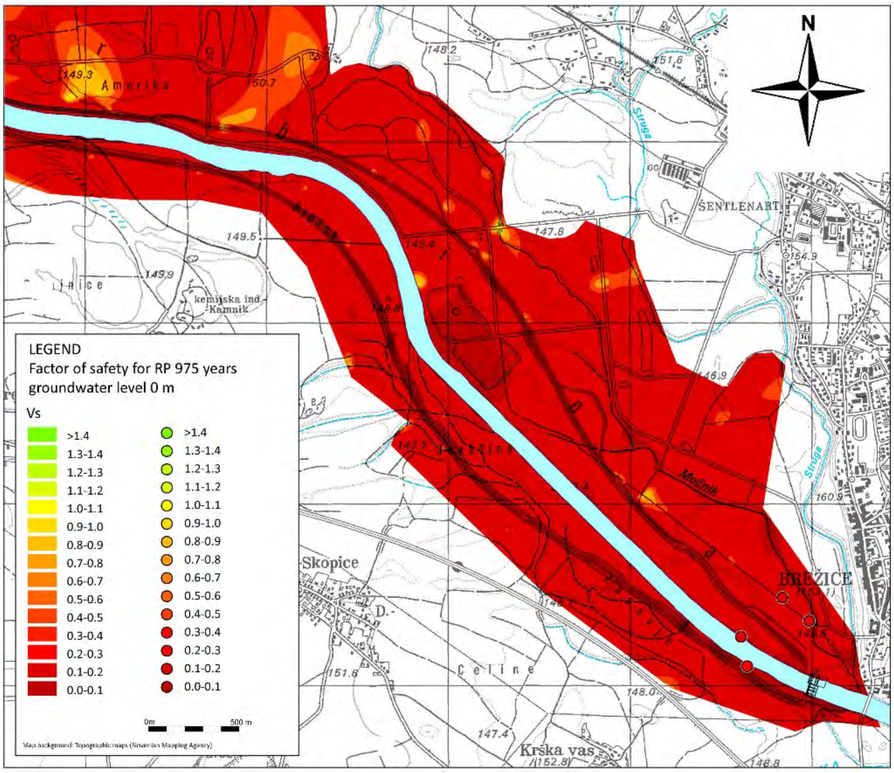

Figure 4-44: Factor of safety - RP = 975 years, zw = 0 m, vs from SDMT.

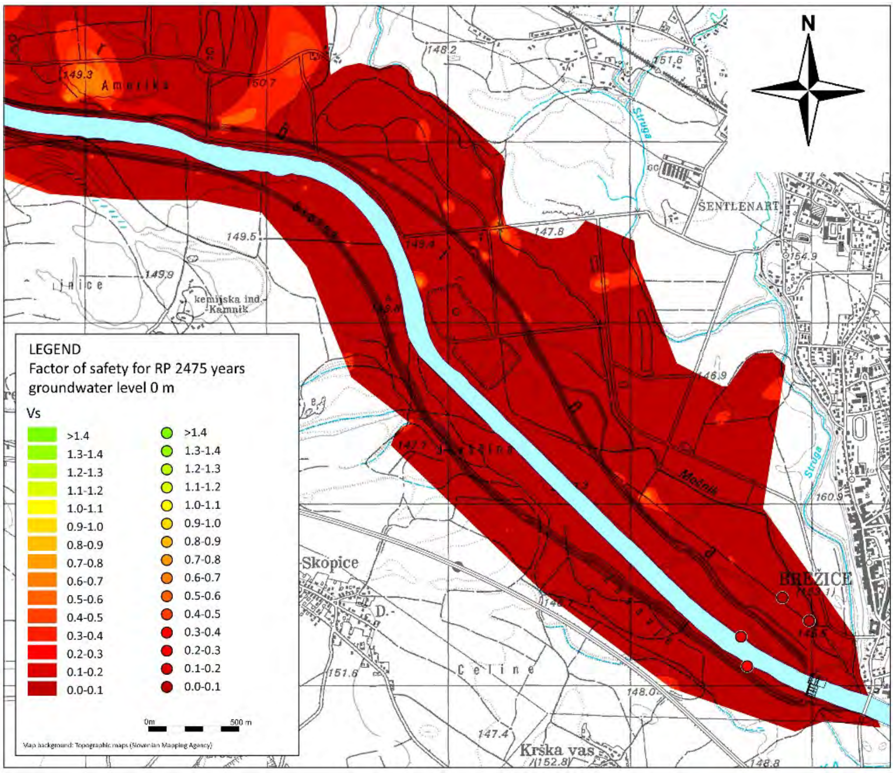

Figure 4-45: Factor of safety - RP = 2475 years, zw = 0 m, vs from SDMT.

This project has received funding from the European Union's Horizon 2020 research and innovation programme under grant agreement No. 700748

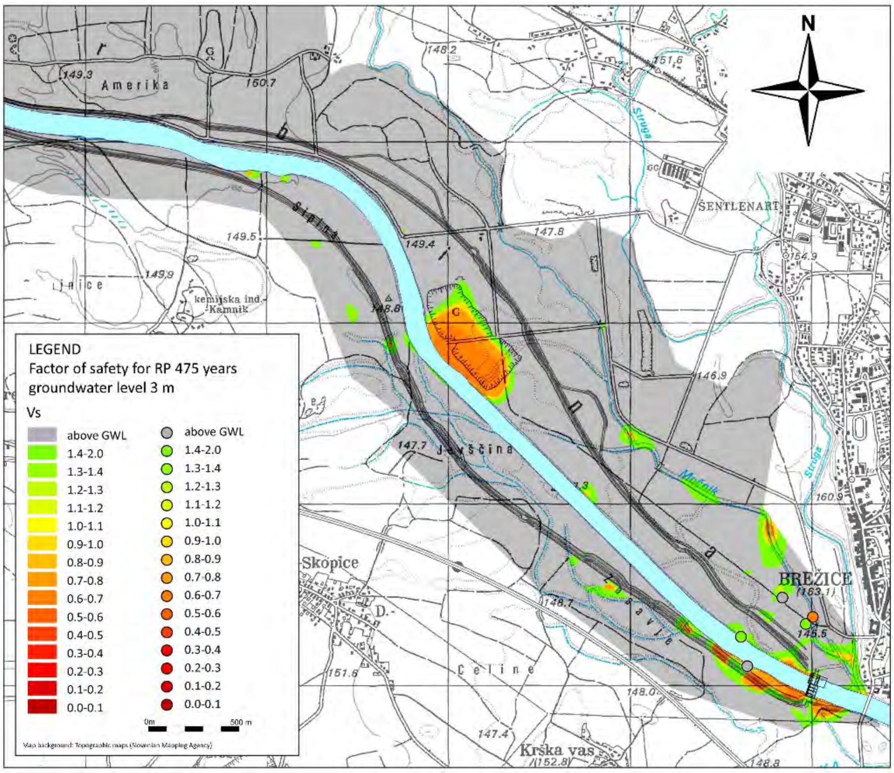

Figure 4-46: Factor of safety - RP = 475 years, zw = 3 m, vs from SDMT.

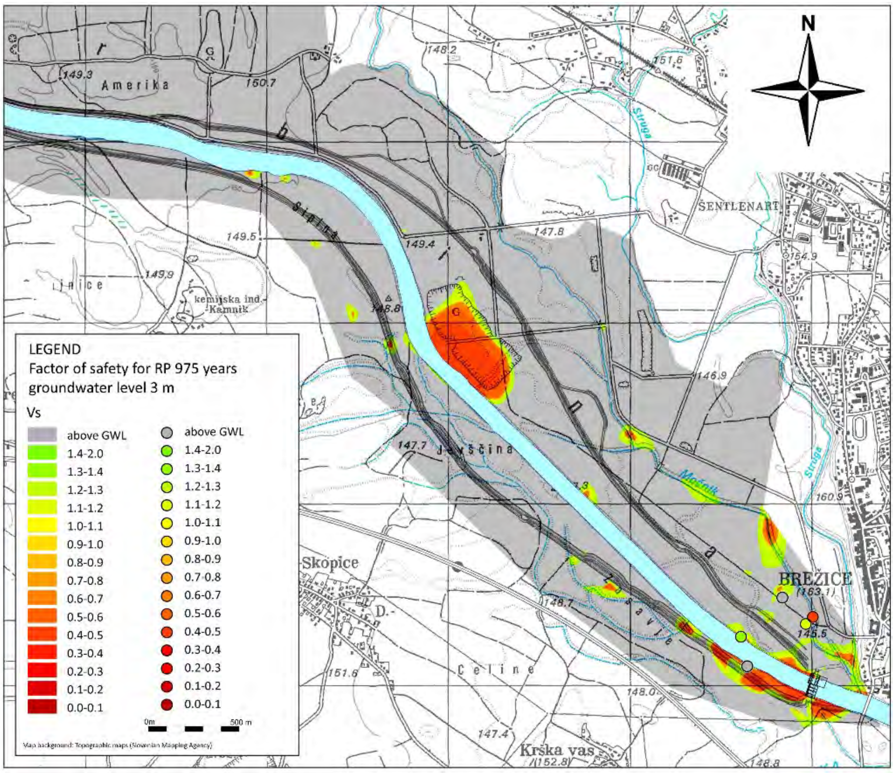

Figure 4-47: Factor of safety - RP = 975 years, zw = 3 m, vs from SDMT.

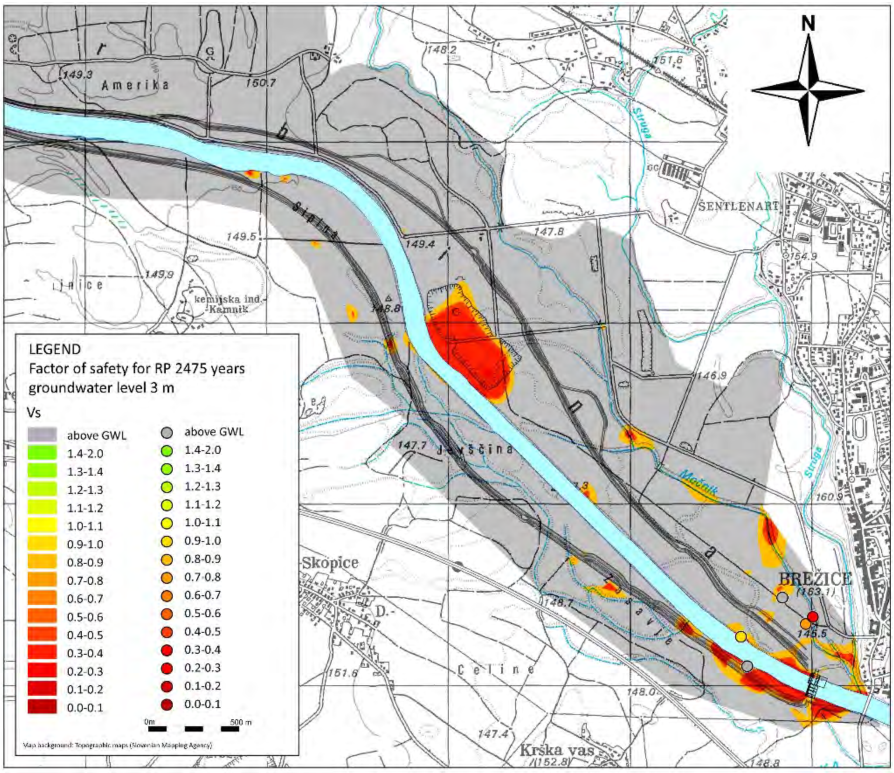

Figure 4-48: Factor of safety - RP = 2475 years, zw = 3 m, vs from SDMT.

This project has received funding from the European Union's Horizon 2020 research and innovation programme under grant agreement No. 700748

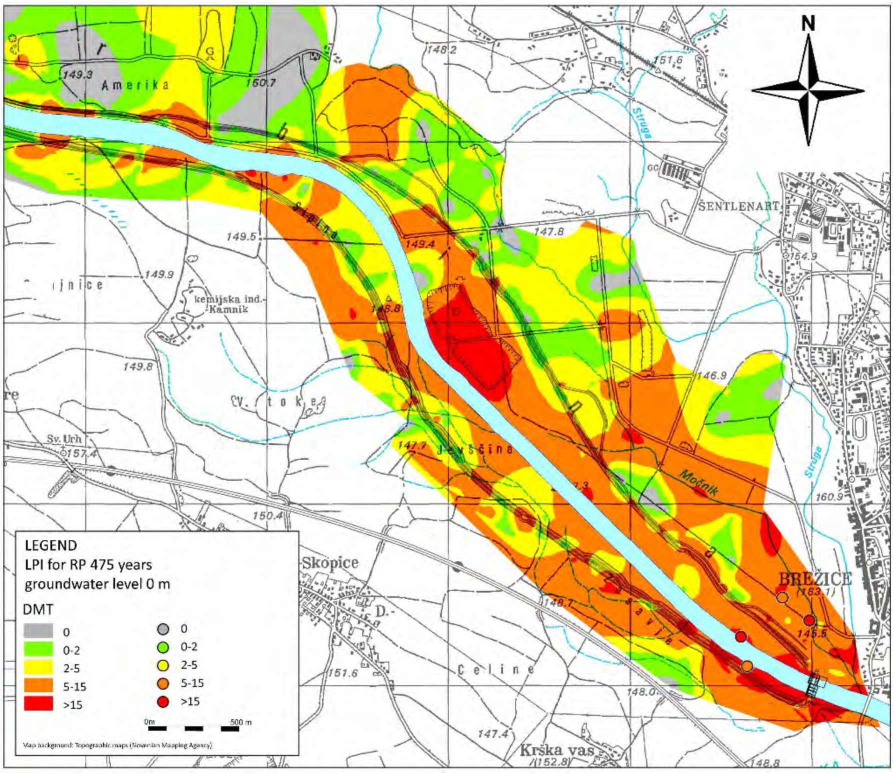

Figure 4-49: Liquefaction potential index - RP = 475 years, zw = 0 m, KD from DMT.

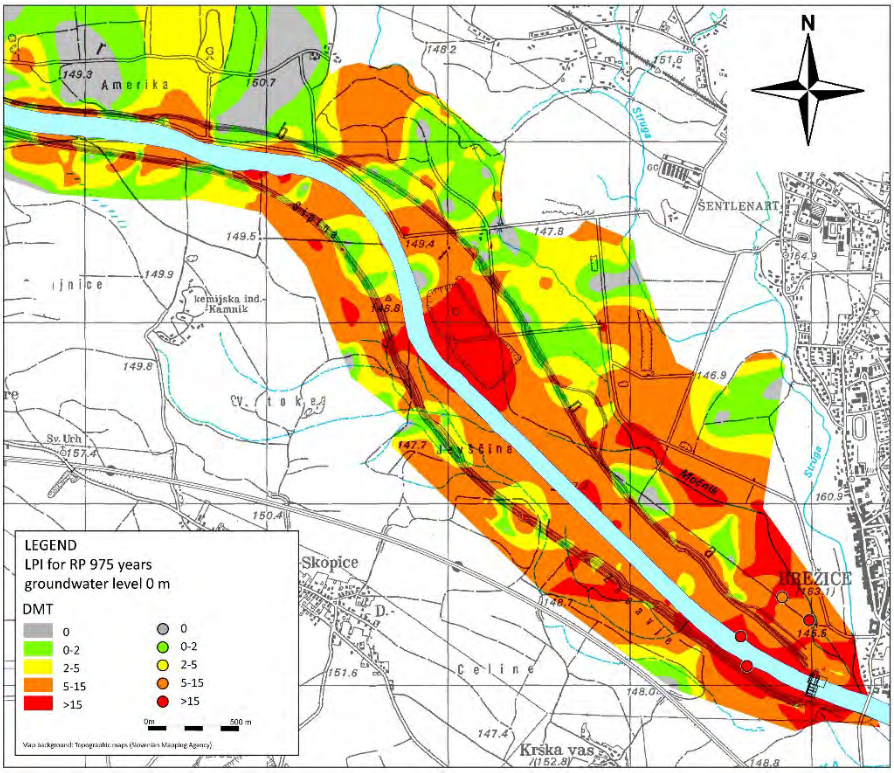

Figure 4-50: Liquefaction potential index - RP = 975 years, zw = 0 m, KD from DMT.

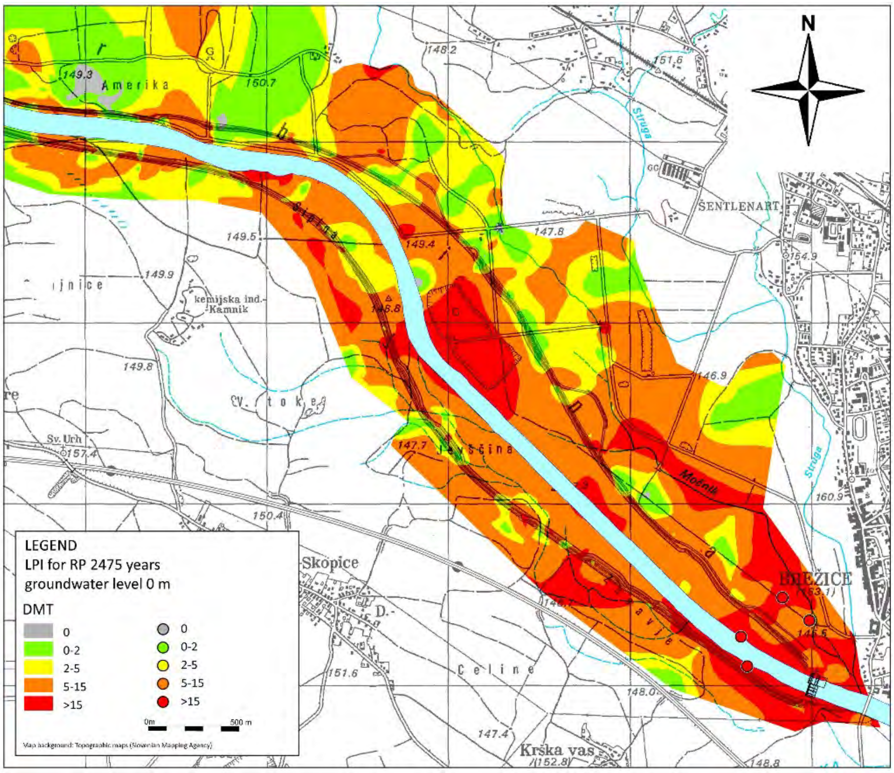

Figure 4-51: Liquefaction potential index - RP = 2475 years, zw = 0 m, KD from DMT.

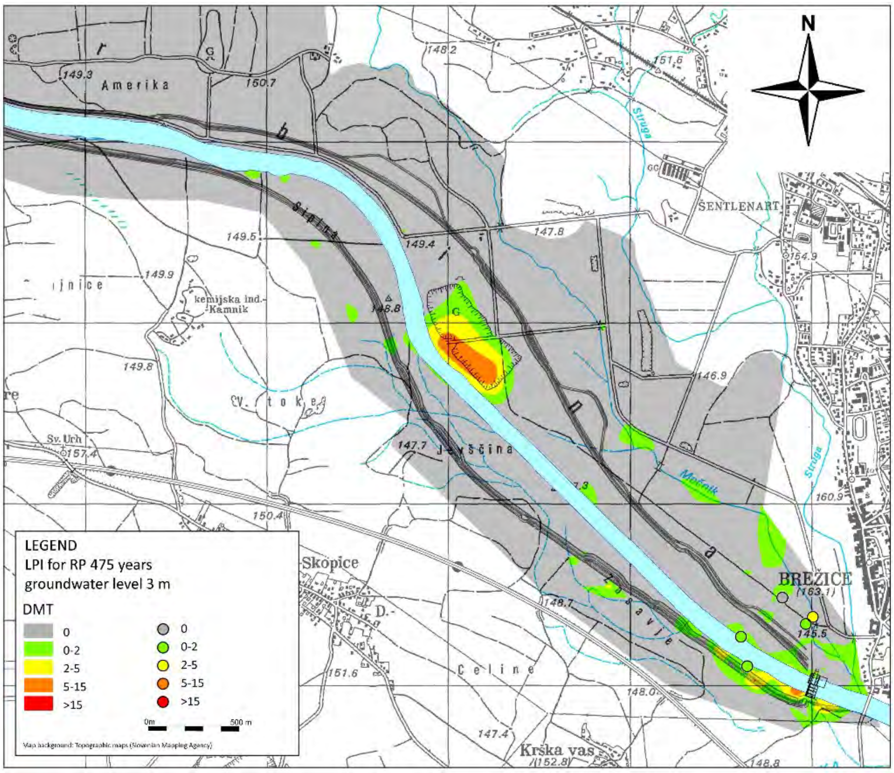

Figure 4-52: Liquefaction potential index - RP = 475 years, z_w = 3 m, K_D from DMT.

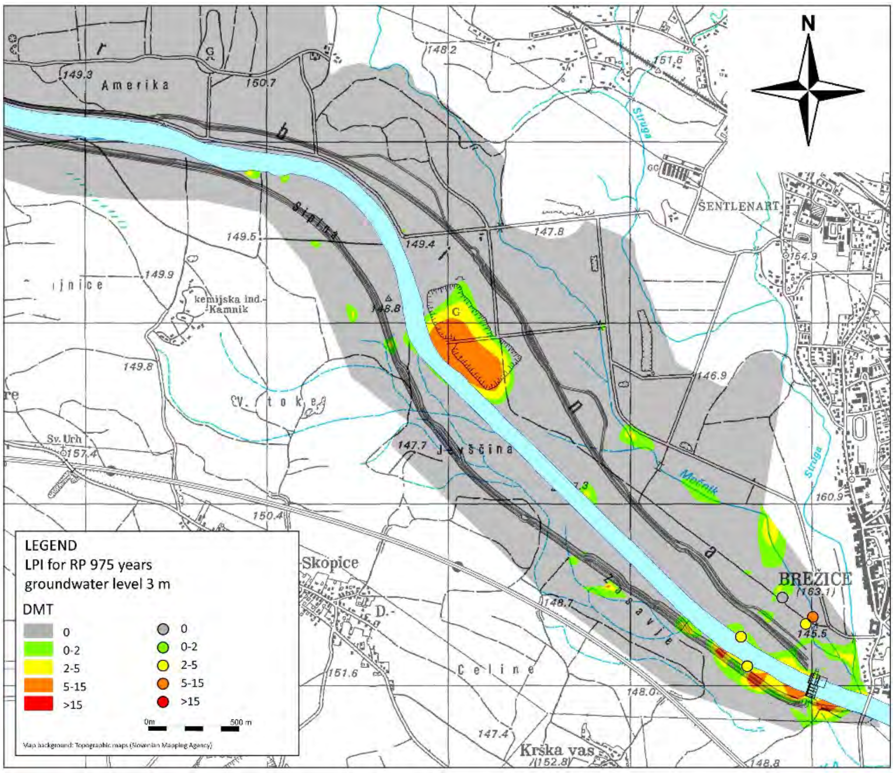

Figure 4-53: Liquefaction potential index - RP = 975 years, z_w = 3 m, K_D from DMT.

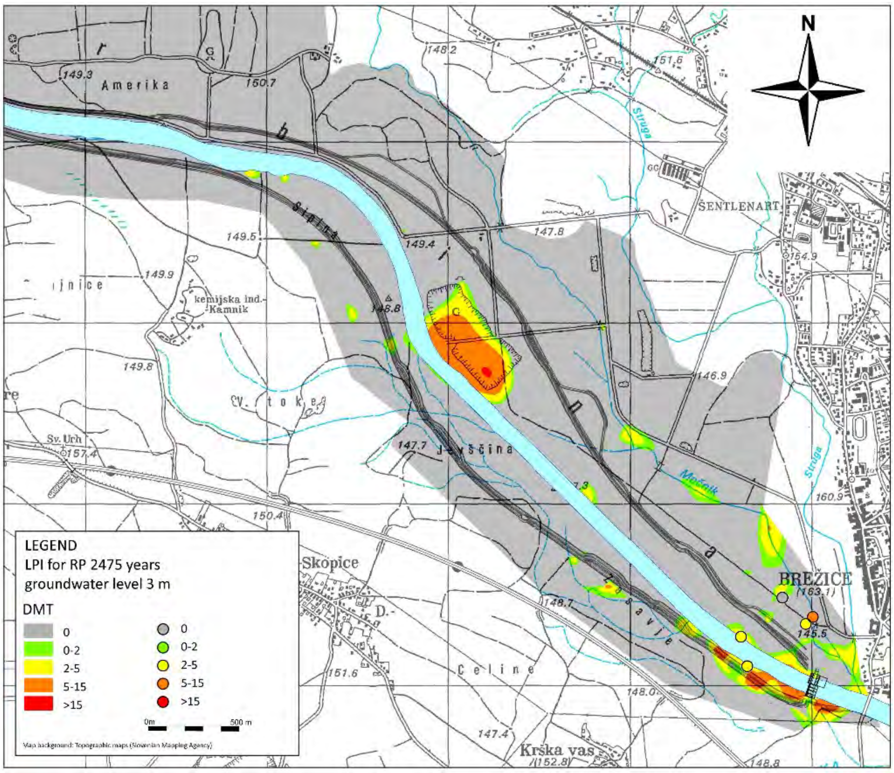

Figure 4-54: Liquefaction potential index - RP = 2475 years, z_w = 3 m, K_D from DMT.

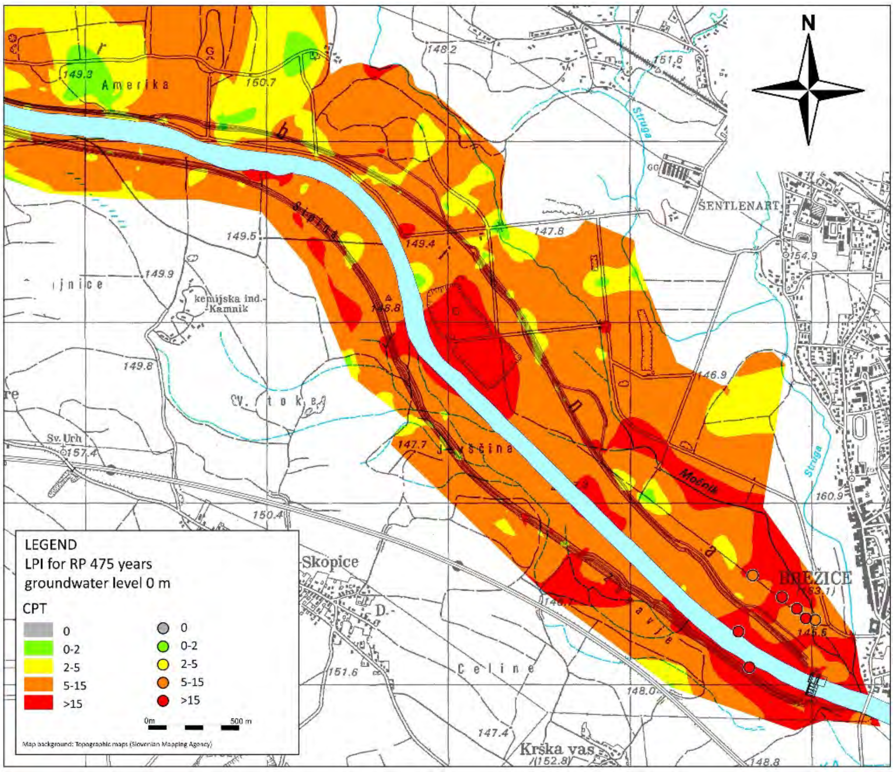

Figure 4-55: Liquefaction potential index - RP = 475 years, z_w = 0 m, CPT.

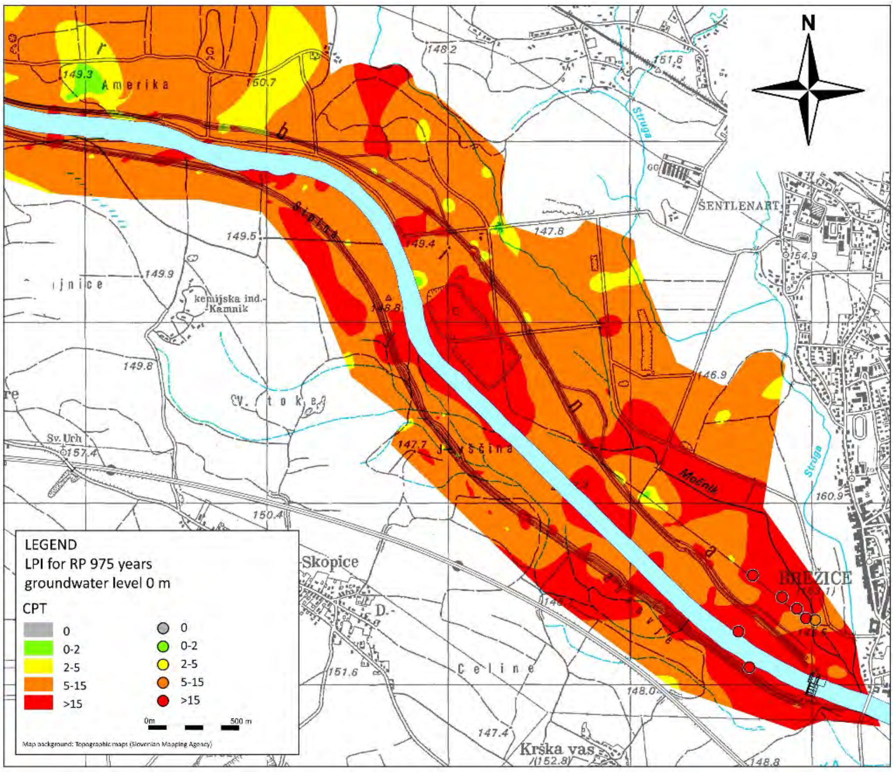

Figure 4-56: Liquefaction potential index - RP = 975 years, z_w = 0 m, CPT.

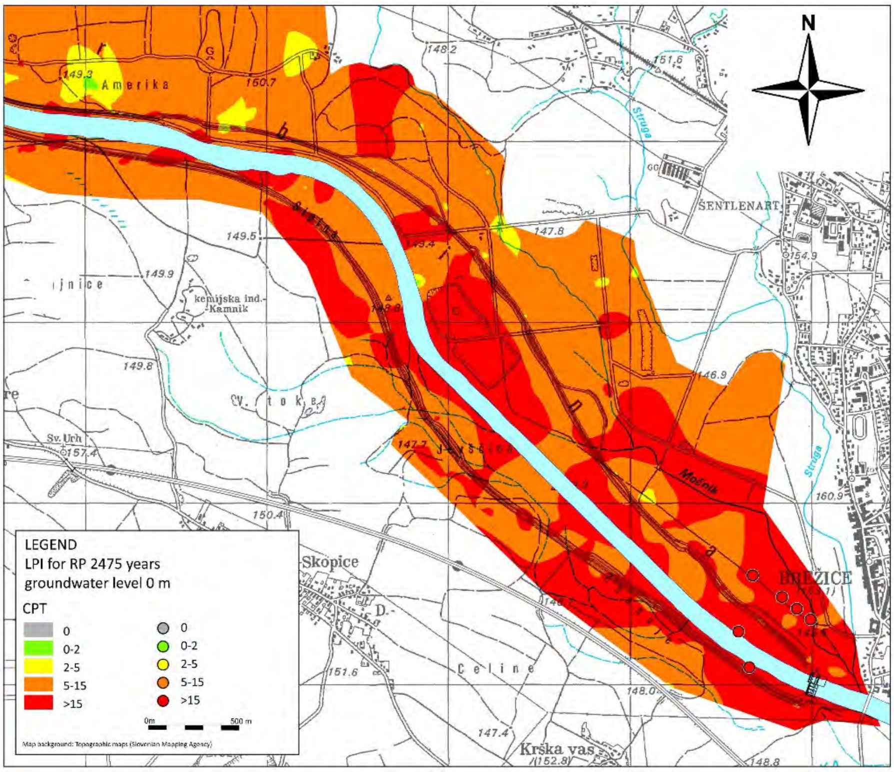

Figure 4-57: Liquefaction potential index – RP = 2475 years, z_w = 0 m, CPT.

This project has received funding from the European Union's Horizon 2020 research and innovation programme under grant agreement No. 700748

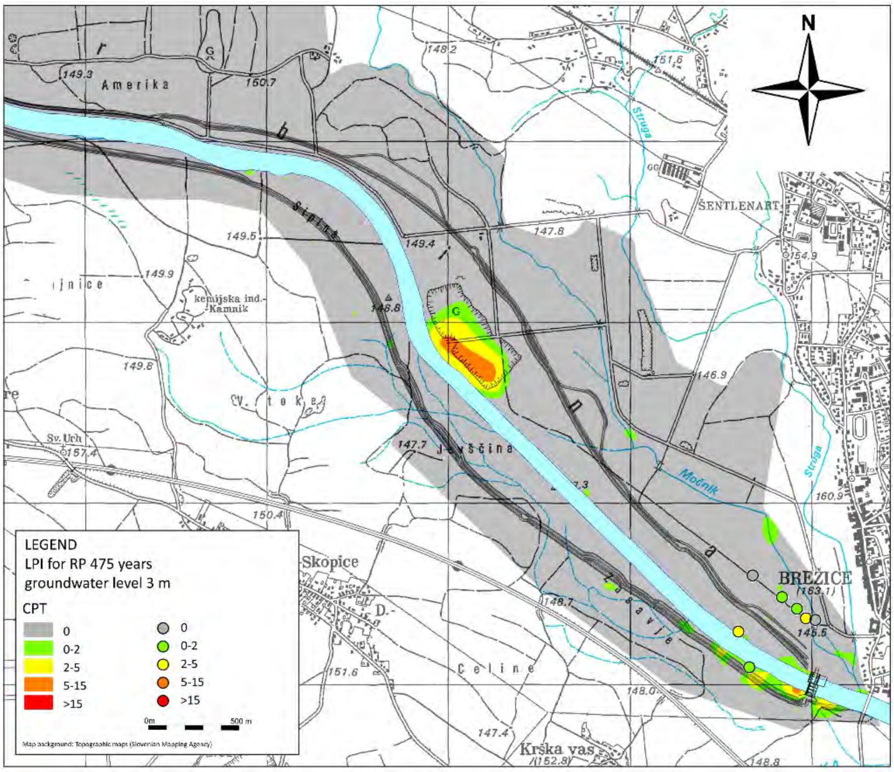

Figure 4-58: Liquefaction potential index - RP = 475 years, z_w = 3 m, CPT.

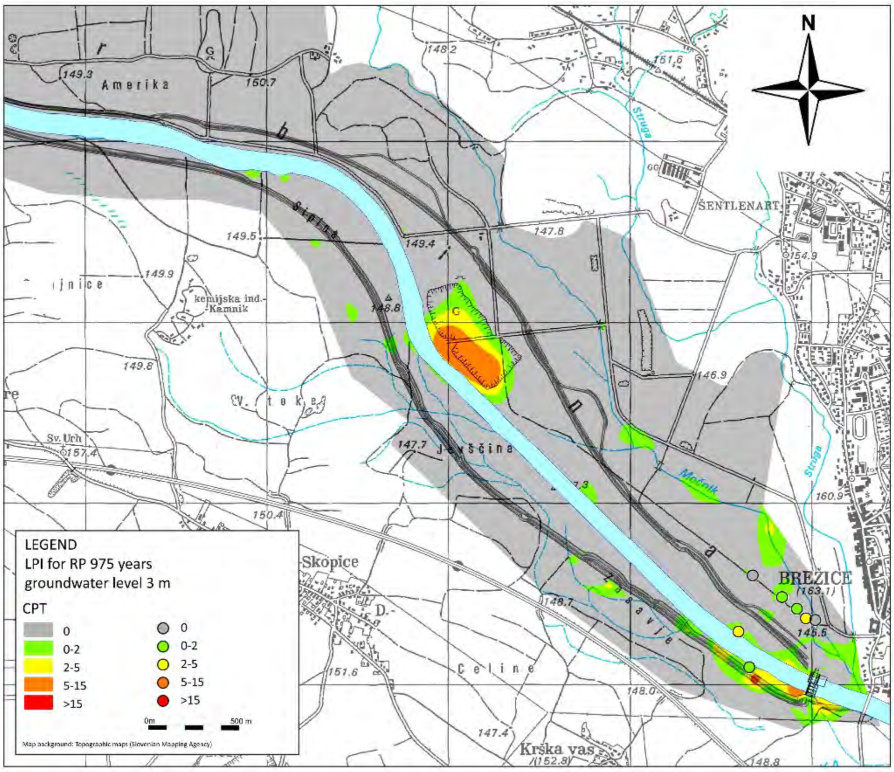

Figure 4-59: Liquefaction potential index - RP = 975 years, z_w = 3 m, CPT.

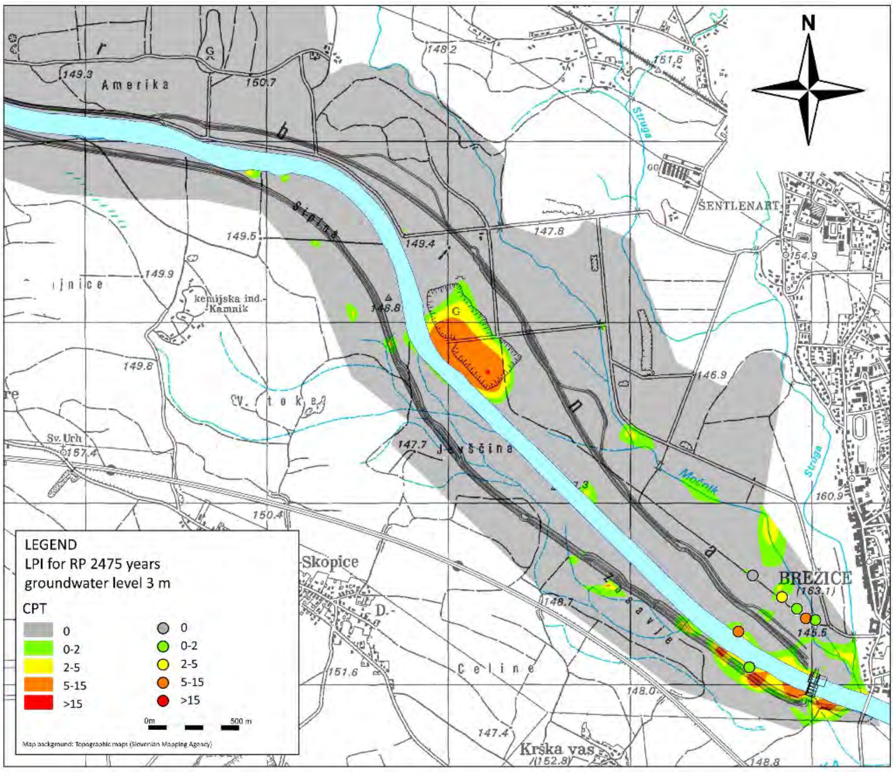

Figure 4-60: Liquefaction potential index - RP = 2475 years, z_w = 3 m, CPT.

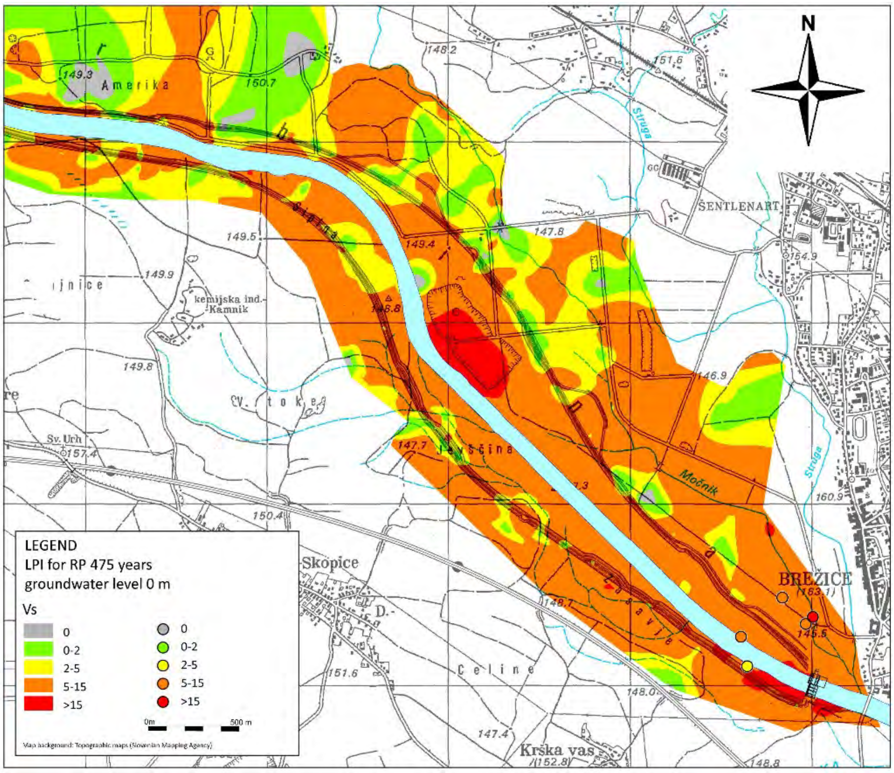

Figure 4-61: Liquefaction potential index - RP = 475 years, z_w = 0 m, v_s from SDMT.

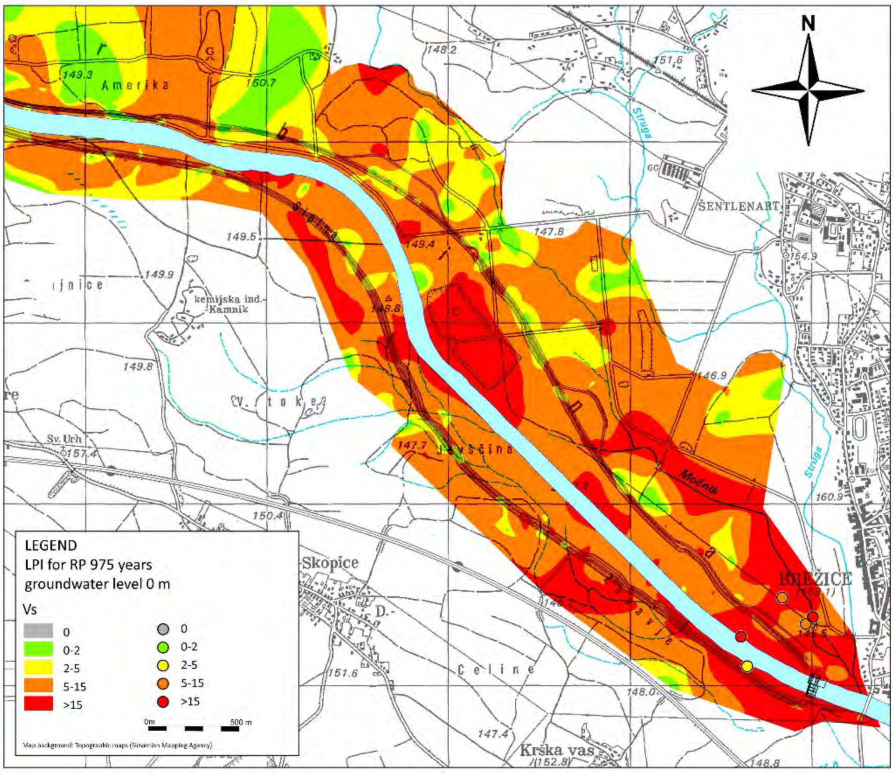

Figure 4-62: Liquefaction potential index - RP = 975 years, z_w = 0 m, v_s from SDMT.

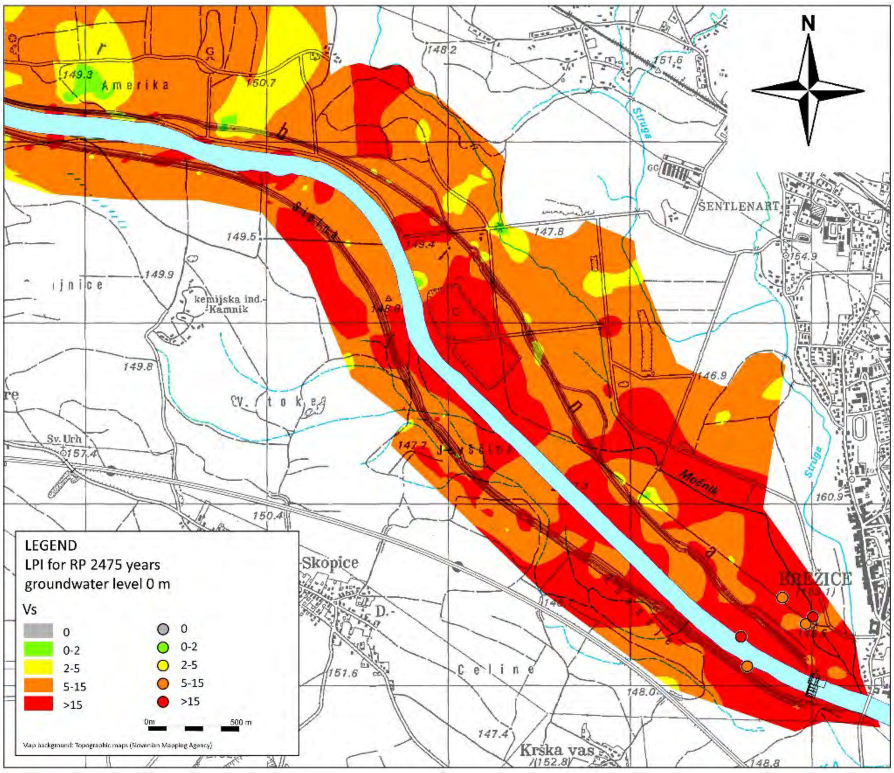

Figure 4-63: Liquefaction potential index - RP = 2475 years, z_w = 0 m, v_s from SDMT.

This project has received funding from the European Union's Horizon 2020 research and innovation programme under grant agreement No. 700748

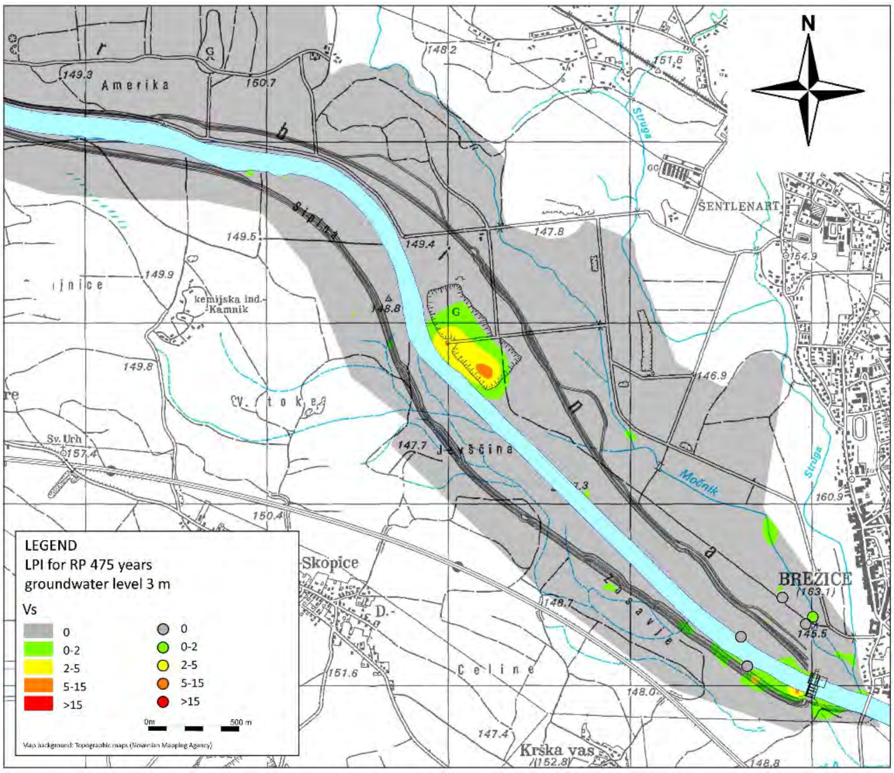

Figure 4-64: Liquefaction potential index - RP = 475 years, z_w = 3 m, v_s from SDMT.

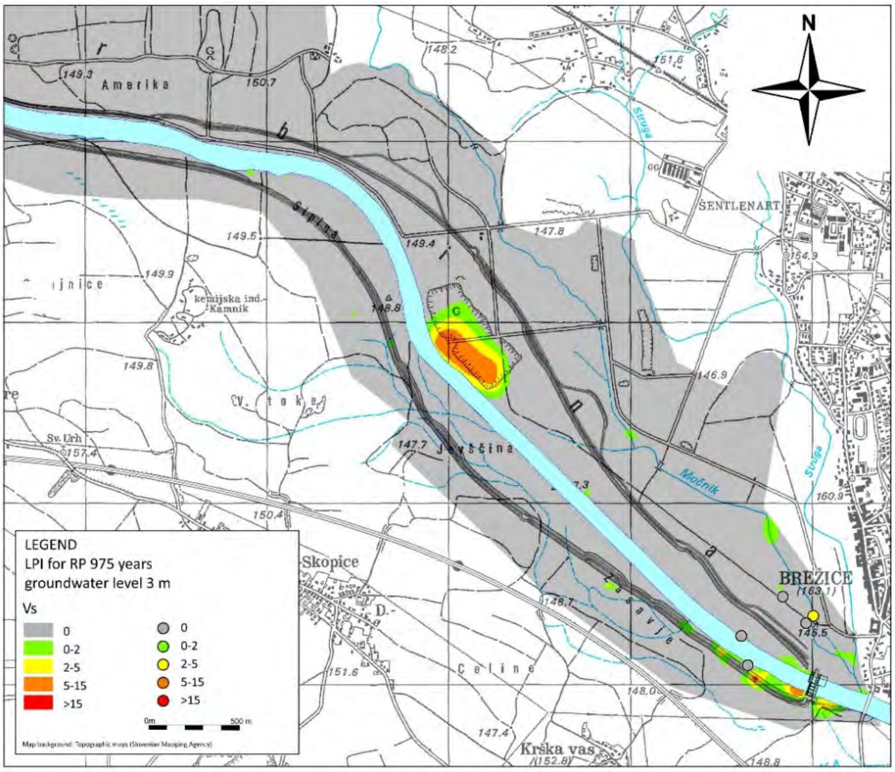

Figure 4-65: Liquefaction potential index - RP = 975 years, z_w = 3 m, v_s from SDMT.

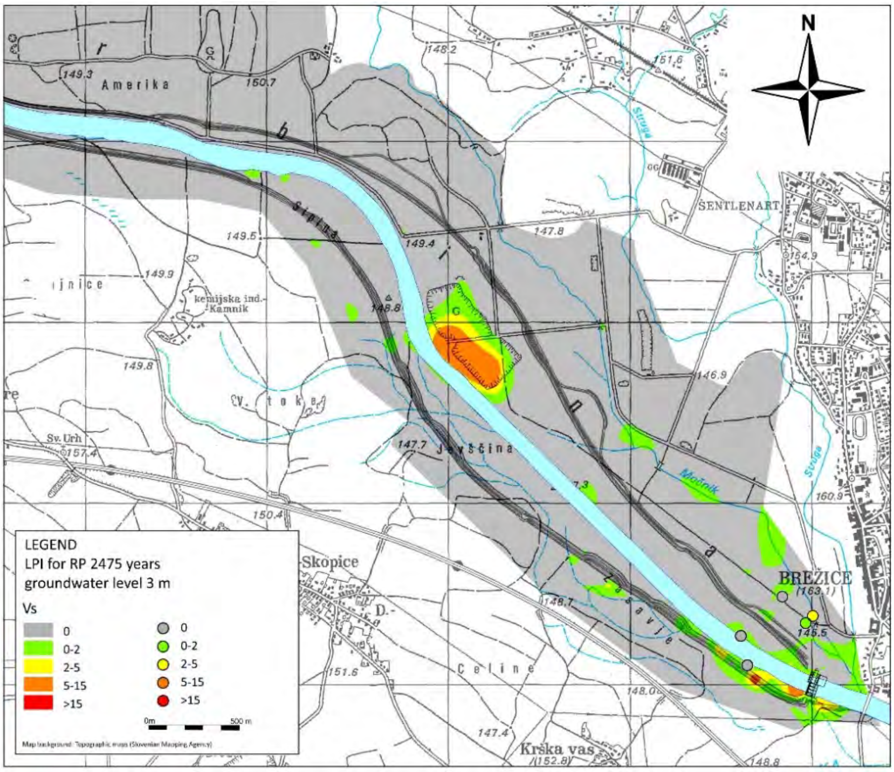

Figure 4-66: Liquefaction potential index - RP = 2475 years, z_w = 3 m, v_s from SDMT.

4.7.4 Discussion

The above results show that the silty sand layer that is present immediately under the surface of the study area is highly susceptible to liquefaction provided that it is fully saturated. The groundwater level during the earthquake event is therefore the decisive factor for the occurrence of liquefaction.

The expected earthquake excitation with return period of 475 years which has 10% probability of occurrence in 50 years is enough to cause liquefaction of saturated silty sand layer within study area.

Three different quantities obtained by CPT and SDMT in situ tests ($Q_{tn,cs}$, K_D, v_s) gave somewhat different LPI values for same seismic action and groundwater level. The highest LPI values were obtained from CPT results and the lowest with DMT (K_D) results. Due to relatively small number of available tests, any further conclusion would be inappropriate.

4.8 Conclusion

The study area upstream of newly constructed Hydro Power Plant Brežice proved to be interesting from liquefaction risk point of view. The area is highly susceptible to liquefaction, expected seismicity in the area is high, yet the occurrence of liquefaction has never been documented in this region. The main reason is the predominantly shallow depth of loose silty sand layer with depth of groundwater table that on the majority of the area lies below the silty sand. In this way the critical layer stayed most of the time unsaturated above the groundwater table.

High susceptibility for liquefaction of the Quaternary soil deposits of river Sava was proven during 1880 Zagreb earthquake (M=6.3) and the Kupa Valley earthquake (Veinović et al., 2007, Herak and Herak, 2010) when manifestation of liquefaction was observed in the vicinity of Zagreb some 20 km downstream, E-SE from Brežice.

The geological, geotechnical and geophysical models for the study area are based on high number of investigation points and geophysical profiles and can be considered reliable in this respect. On the other side, the number of in-situ tests that would enable more reliable quantification of liquefaction risk over the study area was low and their distribution not satisfactory. The reason was the intensive construction site during the in-situ investigations for Liquefact project.

The expected seismic action in the area is high with PGA on soil type A 0.32 g, 0.43 g and 0.63 g for return periods 475, 975 and 2475 years, respectively. The analyses have shown that the expected seismic action with return period of 475 years is strong enough to cause liquefaction of the submerged volume of silty sand layer.

No manifestation of liquefaction in the past is the consequence of relatively deep groundwater table. In the future, the water level is expected to rise due to newly built HPP Brežice. The final water level will depend on the successful implementation of watertight barriers along the dykes. All structures of the HPP Brežice are safe against liquefaction since the silty sand layer was removed and replaced by compacted gravel. It is important that any new construction on this territory follows the same simple and effective ground improvement method.

4.9 References

- Akkar S, Sandikkaya MA, Şenyurt M, Azari Sisi A, Ay BO, Traversa P, et al (2014) Reference database for seismic ground-motion in Europe (RESORCE). Bull Earthquake Engineering 12:311–39.
- ARSO (2001) Design peak ground acceleration in rock or firm soil with return period of 475 years. Ministry of the Environment and Spatial Planning, Slovenian Environment Agency, Geophysical Survey of Slovenia. http://www.arso.gov.si/potresi/potresna%20nevarnost/projektni_pospesek_tal.jpg (accessed 11/1/2017).
- Boulanger RW, Idriss IM (2014) CPT and SPT based liquefaction triggering procedures. Center for Geotechnical Modeling, Department of Civil & Environmental Engineering, University of California, Davis. Report No. UCD/CGM-14/01.
- Chiou BSJ, Darragh RB, Gregor NJ, Silva WJ (2008) NGA project strong-motion database. Earthquake Spectra 24:23–44.
- Dolšek M, Pulko B, Kosič M, Isaković T, Logar J, Fajfar P (2018). Neodvisno ekspertno mnenje o PGD za odlagališče NSRAO (2.faza). Ljubljana: University of Ljubljana, Faculty of Civil and Geodetic Engineering.

- EFEHR (2017) Seismic Map Viewer – interactive application. European Facility for Earthquake Hazard and Risk. http://www.efehr.org:8080/jetspeed/portal/HazardMaps.psml (accessed 11/1/2017).
- EFEHR (2017b) Hazard Curve Viewer – interactive application. European Facility for Earthquake Hazard and Risk. Available from: http://www.efehr.org:8080/jetspeed/portal/HazardCurves2.psml (accessed 11/1/2017).
- Fajfar P et al (2004), Revised PSHA for NPP Krško site, PSR-NEK-2.7.2, Revision 2, University of Ljubljana, Department of Civil Engineering, Institute of Structural and Earthquake Engineering, with subcontractors, Ljubljana 2004.
- Hashash YMA, Musgrove MI, Harmon JA, Okan I, Groholski DR, Phillips CA and Park D (2017) DEEPSOIL 7.0, User Manual.
- Herak D, Herak M (2010) The Kupa Valley (Croatia) Earthquake of 8 October 1909—100 Years Later. Seismol. Res. Lett. 81, 30. doi:10.1785/gssrl.81.1.30.
- Ishihara K, Troncoso J, Kawase Y and Takahashi Y (1980) Cyclic strength characteristics of tailings materials. Soils and Foundations, 20(4): 127-142.
- Lai et al. (2017). “Report on ground characterization of the four areas selected as testing sites by using novel technique and advances methodologies to perform in situ and laboratory tests”, LIQUEFACT Deliverable D2.1, Horizon 2020 EU funding for Research & Innovation Project ID: 700748 (www.liquefact.eu).
- Lapajne J, Šket Motnikar B, Zupančič P (2001) Probabilistic seismic hazard mapping in Slovenia. Twelfth World Conference on Earthquake Engineering, Auckland, New Zeland; Paper No. 0188.
- Lapajne J, Šket Motnikar B, Zupančič P (2003) Probabilistic seismic hazard assessment methodology for distributed seismicity. Bulletin of the Seismological Society of America 93, 6: 2502–2515.
- MATLAB R2017b, The MathWorks, Inc., Natick, Massachusetts, United States.
- Petkovšek A (2010) Geotehnična študija ravnanja z lokalnimi peski v temeljnih tleh in ocena njihove uporabnosti za vgradnjo v energetske nasipe. UL FGG Chair of Soil Mechanics with Laboratory, Ljubljana, E-02-10.
- Petkovšek A, Smolar J, Maček M (2016) Mechanically treated soils - test method validity and reliability: invited lecture. In: Jirasko D (ed.). Ground improvement, 44th Conference with international participation foundation engineering Brno, 14.-15.11. 2016. Brno: Foundation Engineering, 2016, pp. 5-29.
- Robertson P K, Wride C E (1998) Evaluating cyclic liquefaction potential using the cone penetration test. Canadian Geotechnical Journal. 35: 442-459.
- Robertson P K (2009) Interpretation of cone penetration tests – A unified approach. Canadian Geotechnical Journal. 46, 11: 1337-1355.
- Robertson P K (2012) Interpretation of in-situ tests – some insights. Mitchell Lecture – ISC`4 Brazil, 2012. 22 pp.
- Robertson PK, Cabal KL (2014) Guide to Cone Penetration Testing for Geotechnical Engineering. 6th ed. Signal Hill, California: Gregg Drilling & Testing, Inc.
- Seed HB & Idriss IM (1982) Ground Motions and Soil Liquefaction During Earthquakes. Berkeley, Earthquake Engineering Research Center.

- SHARE. European project EU-FP7 "Seismic Hazard Harmonization in Europe – SHARE", 2009-2013. Web page:
- Smolar J, Maček M, Petkovšek A (2012) Raziskave občutljivosti peskov na Krškem polju na likvifakcijo = Investigation of liquefaction potential of sands from Krško polje. V: PETKOVŠEK, Ana (ur.), KLOPČIČ, Jure (ur.). Razprave. Ljubljana: Slovensko geotehniško društvo.
- Smolar J, Maček M, Petkovšek A (2018) Potencial likvifakcije peskov na Krško-Brežiškem polju = Liquefaction potential of sands at Krško-Brežiško field. V: NOVAK, Matevž (ur.), RMAN, Nina (ur.). Zbornik povzetkov = Book of abstracts, 5. slovenski geološki kongres, Velenje, 3.-5. 10. 2018. Ljubljana: Geološki zavod Slovenije.
- Smolar J, Maček M, Petkovšek A (2019) Liquefaction potential of sands at the Krško-Brežice field, Slovenia. Geologia Croatica : a journal of the Institute of Geology Zagreb and Croatian Geological Society, ISSN 1330-030X, vol. 72, no. 2, str. 129-135, doi: 10.4154/gc.2019.12.
- Veinović Ž, Domitrović D, Lovrić T (2007) POJAVA LIKVEFAKCIJE NA PODRUČJU ZAGREBA U PROŠLOSTI I PROCJENA MOGUĆNOSTI PONOVNE POJAVE TIJEKOM JAČEG POTRESA. Rud.-Geol.-Naft. Zb. 19: 111–120.
- Vukadin V (2013) The improvement of the loosely deposited sands and silts with the Rapid Impact Compaction technique on Brežice testing sites. Eng. Geol. 160: 69–80. doi: 10.1016/j.enggeo.2013.03.025.
- Vukadin V (2014) Geološko geomehanski elaborat za HE Brežice. No. ic:397/14. Ljubljana, IRGO Consulting.
- Živčić M, Šket Motnikar B, Gosar A (2015), Izdelava projektne in druge dokumentacije za odlagališče NSRAO Vrbina v občini Krško. Izvedba seizmološke analize lokacije (seizmološki del) za objekt odlagališče NSRAO Vrbina – Revizija 1. Ministrstvo za okolje in prostor, Agencija za okolje, Urad za seizmologijo in geologijo.

This project has received funding from the European Union's Horizon 2020 research and innovation programme under grant agreement No. 700748

5. MICROZONATION OF THE TURKISH AREA IN THE MARMARA REGION

In this deliverable, entitled D2.7, "*Methodology for assessment of earthquake-induced risk of soil liquefaction at the four European testing sites (microzonation)",* microzonation studies that were carried out for Canakkale site (in Marmara Region) by Istanbul University-Cerrahpasa are presented. This report also summarizes the main findings from Deliverable 2.1, in which ground characterization was presented since this information is the main input in microzonation studies.

The location of the Canakkale city and the boundaries of the Canakkale city test site are shown in Figure 5-1. This site was selected on the basis of the following criteria: availability of geological and geotechnical data, presence of liquefiable soil deposits, representativeness of different geological settings and density of population in selected areas. Canakkale test site is in a high earthquake risk area and has historical importance due to the presence of Troia, Gallipoli, Assos, etc. in the region. High peak ground accelerations due to a probable earthquake are expected in the region coupled with suitable soil conditions for liquefaction occurrence. The structures in the test site are generally 4-6 storey reinforced concrete buildings with generally no basements or some with one basement. In the recent years, some high rise buildings, especially hotels and trade centers are being constructed in the area. In this context, the area is populated and the risk for liquefaction has to be defined.

Figure 5-1 Location of Canakkale City in Marmara Region and the boundaries of the test site

5.1 Definition of geological model

The first step in the microzonation studies began with understanding the geological and geomorphological setting of the test site and creating a geological model. This required the following steps;

1. Data collection and organization;
2. Data analysis;
3. Construction of Reference Geological Model;

4. Assessment of reliability of the model.

Site geomorphology was assessed through existing geomorphological maps, digital terrain models and detailed topographic maps. An important source for information was Canakkale Municipality Report (2013) prepared by Buyuksarac et al. (2013). The data in this report was analysed and was found to be reliable. A Geographical Information System (GIS) framework was then developed and used throughout the project.

The 3D engineering geological subsoil model created within the context of the project is given in Figure A-5-17. The 3D model revealed that Gazhanedere formation (Tmg), Alcitepe formation (Tmal), Alluvium (Qal) and Artificial fills (Qd) are encountered in the area. The Gazhanedere Formation, as designated by Saltik (1974) at Murefte city, is widely distributed on the Gelibolu Peninsula, the northern part of the Gulf of Saros and the Strait of Çanakkale (Dardanelles). In the study area, the formation consists of coarse clastics of meandering-river origin containing some coal seams and lacustrine clay deposits. The Alcitepe formation (described by Onem, 1974), represents shallow marine and lacustrine depositional environments (Yaltirak et al., 1998 and references therein). On the Gelibolu Peninsula, the Alçitepe formation is made up by sandy limestone, oolitic limestone, sandstone and Mactra-bearing limestone intercalations. The dispersion as well as formation of these alluvium were realized under the influence of Saricay stream. Saricay stream primarily accumulated in lowlands having plain nature by carrying the sediments from high levels throughout its previous stream bed as well as its recent bed. There is an artificial fill area (Qd) with approximately 25 m band width throughout the coast line which is formed under control by Canakkale Municipality. General topography of the field area has low slope angles ranging from 0-10%. The model shows that the test site includes liquefaction prone areas due to river meander points, estuarine deposits, alluvial ridges and reclamation fills. Geological map of the test site and the liquefiable areas are presented in Figure 5-2. The details are given in Istanbul University Report in Deliverable 2.1 (2017).

This project has received funding from the European Union's Horizon 2020 research and innovation programme under grant agreement No. 700748

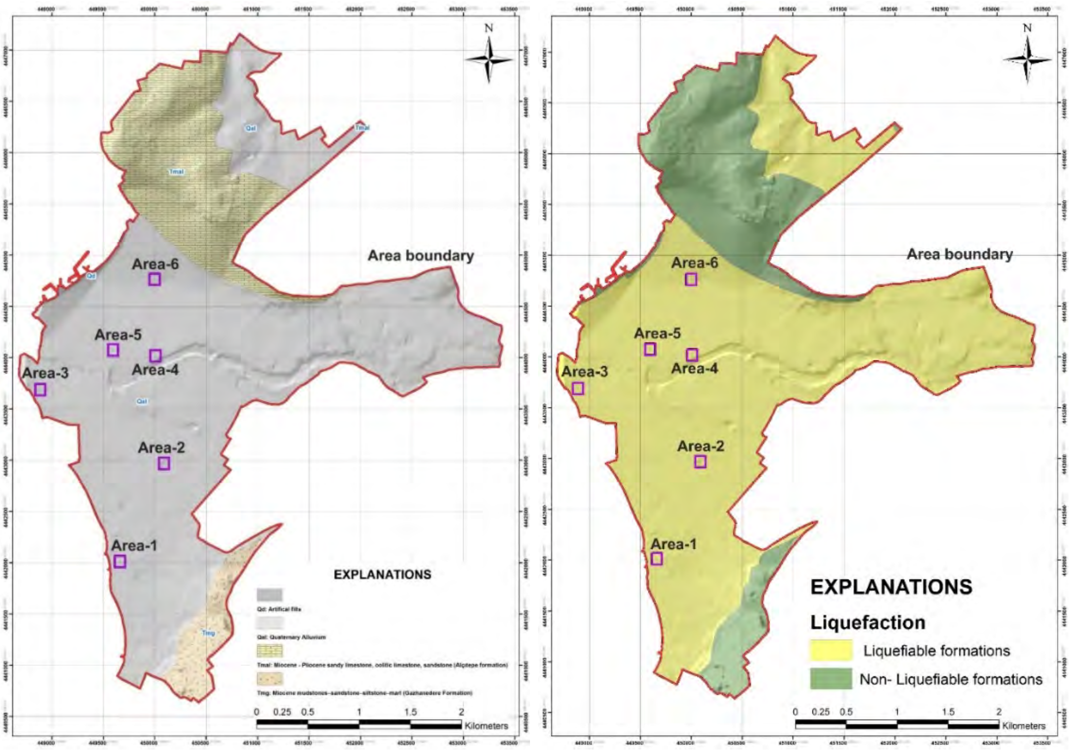

Figure 5-2 Geological map of the study area and liquefiable areas in the test site

The depth of groundwater is a very important parameter in liquefaction analyses. In this study, the depth to ground water table was acquired through existing ground water database for historical depths to ground water table and measurements performed during drilling of boring logs, water wells and in situ testing. Canakkale Plain is the largest in terms of area covered and feeding basin in the northern part of the Biga Peninsula, between the plains of the Dardanelles and the plains. Canakkale city's central residential area is established on this plain and it is poured into the sea through the residential area of Saricay which provides natural drainage of the plains. According to field observations made in the rainy and dry periods of 2003 and 2004 in the ground and surface waters of the Canakkale Plain, it was determined that the depth of the groundwater (after the heavy rainfall periods) increased significantly in the course of Saricay, the only stream in the same period. The depth of groundwater is 1 m in the western part of the plain and 12 m in the eastern part of the plain (Canakkale Municipality Report, 2013, Buyuksarac et al., 2013, Istanbul University Report in Deliverable 2.1., 2017).

5.2 Definition of geotechnical model

The geotechnical model was prepared based on the existing data and the complimentary investigation carried out within the context of this study. The details are given in Istanbul University Report in Deliverable 2.1. (2017). In order to obtain the previous information available for Canakkale city center, data from the governmental offices and private companies were gathered. As a result of this investigation, the data came from two main sources. The main data came from a detailed site investigation carried out for Canakkale

Municipality, which will be cited as Canakkale Municipality Report (2013) hereafter. This report was written by Buyuksarac et al. (2013), based on the soil investigation tests made by Canakkale Municipality. The second source of data was from a soil investigation report which was carried out by a private company, Geosan (2008). The locations of the boreholes from which the geotechnical model was presented are presented in Figure 5-3. The geotechnical model shows that;

- There are six different soil types in the test site. These are Artificial fills/top soil, Clean sands (SP, SW) (Holocene, Alluvium), Plastic Silts and Clays (ML, MH, CL, CH) (Holocene, Alluvium), Silty sands and sands (SW-SP-SC-SM) (Holocene, Alluvium), Clay, claystones and limestone (Miocene-Pliocene, Alcitepe Formation) and Claystone, sandstone (Miocene, Gazhanedere Formation).
- The first 15 meters of the subsoil consisted of mainly clean sands, sands and silty sands, with intrusions of plastic silts and clays. In the northern parts, Alcitepe Formation (Miocene-Pliocene aged) consisting of claystone and sandstone was encountered. Spots of "top soil" were encountered at several locations.
- At -20 m, plastic silts and clays were encountered at significant portion of the test site, while sands and silty sands and clean sands were still prevalent.
- At -25 m, the northern part was all Miocene-Pliocene claystone and limestones, while the southern parts consisted of mainly sands and silty sands, plastic silts and clays.
- At all depths, at the very southern part, Miocene sandstone was encountered.
- From a liquefaction susceptibility view, "Number 1, artificial fills, top soils", "Number 2, clean sands" and "Number 4, sands and silty sands" should be investigated further. "Number 3, Plastic Silts and Clays" are less susceptible to liquefaction and "Number 5, Miocene-Pliocene claystone and limestones" and "Number 6, Miocene sandstone" are not liquefiable units.
- Based on the soil lithology, it can be concluded that a large portion of the area consists of liquefiable soils to a considerable depth, as deep as 20 or 25 m. Ground water levels are very high in the test site, varying from being at the surface to about -4 m in a large portion of the area.

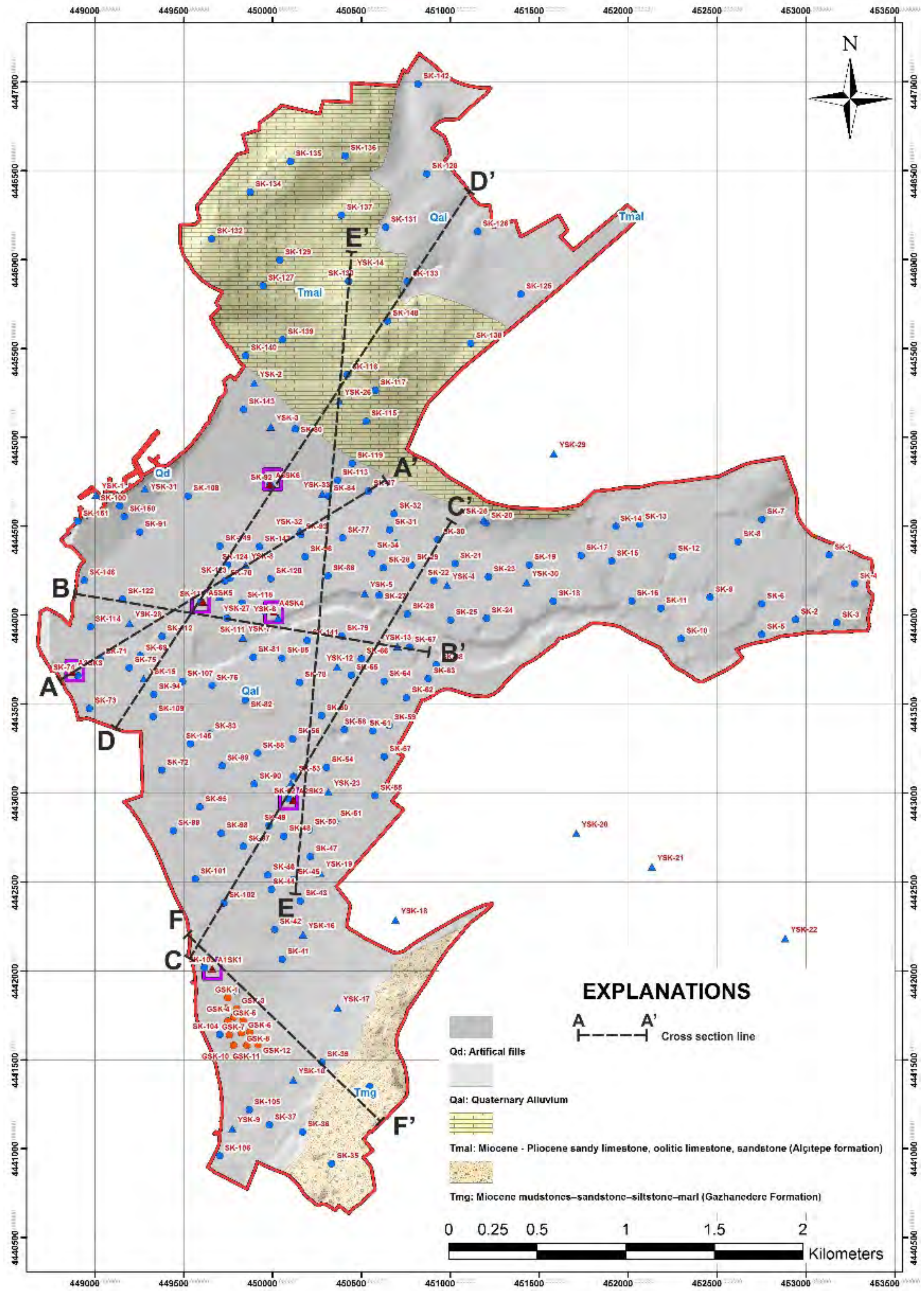

Figure 5-3 Locations of the field tests and geological map of the field area with the geological cross-section lines

After the data from the pre-existing soil investigation studies were evaluated, complementary tests were carried out in six selected areas. In these areas, additional boreholes were opened and SPT tests with energy measurements were performed. Additional CPT (CPTU and SCPT) and Marchetti Dilatometer (DMT) tests were carried out. In addition to seismic refraction, MASW and micro tremor measurements that had been carried out in pre-existing studies, downhole seismic, PS-logging, seismic refraction, 2D-ReMi, MASW, micro tremor (H/V Nakamura method), 2D resistivity and resonance acoustic profiling (RAP) were performed. Dynamic soil properties were investigated using resonant column and cyclic direct shear tests.

The complimentary testing survey revealed that shear wave velocities measured by different geophysical tests (PS-logging, downhole, MASW) were consistent with each other. Shear wave velocities calculated using SPT values were found to be generally consistent with the geophysical tests (PS-logging, downhole, MASW). Therefore based on the results of this study, the validity of Ohta and Goto (1978) equation for Quaternary Alluvial deposits was proven. This was valid for majority of the readings. The shear wave velocities measured in the six areas can be summarised as below;

- For all the areas, the shear wave velocities are low. In the first 10-15 meters, for all sections, the shear wave velocities are lower than 200 m/s. The distribution shear wave velocities in the first 30 m is given in Figure A-5-18.
- For gravel layers at about 20 m depth, there are increases in shear wave velocities, however in all cases, shear wave velocity values are lower than about 350 m/s.
- In terms of liquefaction consideration, all the sites are susceptible to liquefaction based on shear wave velocities.

The other main findings about the site were as follows;

- In the first 30 m, the corrected SPT values ($N_{1,60}$) are very low ranging from 2 and 27. The distribution of $N_{1,60}$ in the first 30 m is given in Shear wave velocities are between 130 m/s to 340 m/s.
- Soil types are sands, gravels, silts, silty sands, clays, silty clays, fills and sand-silt-clay mixtures.
- Fine contents values range from 2% to 54 % in average. Most of the time, low fine contents are dominating in the area.
- Soil classes can be listed as SP-SM, SP, SM, ML, SW, SW-SM, SC. It should be recalled that these soil classes are highly liquefiable.

An evaluation of all the tests were made and the characterization of the Canakkale test site was completed. Cross sections drawn in the test site are presented in Figs.

Another important information needed for the site for site response analyses is the depth of the bedrock level. A typical profile from the test site is given in Figure 5-4. The seismic bedrock is accepted to lie at a depth of 200 m based on the existing information (Istanbul University Report in Deliverable 2.1., 2017). Above it lie the Ground Type A and Type B, with varying thicknesess over the cross-sections. Depending on the location of the boreholes, the upper part of the soil strata consist of Ground Type C, D or E soil types.

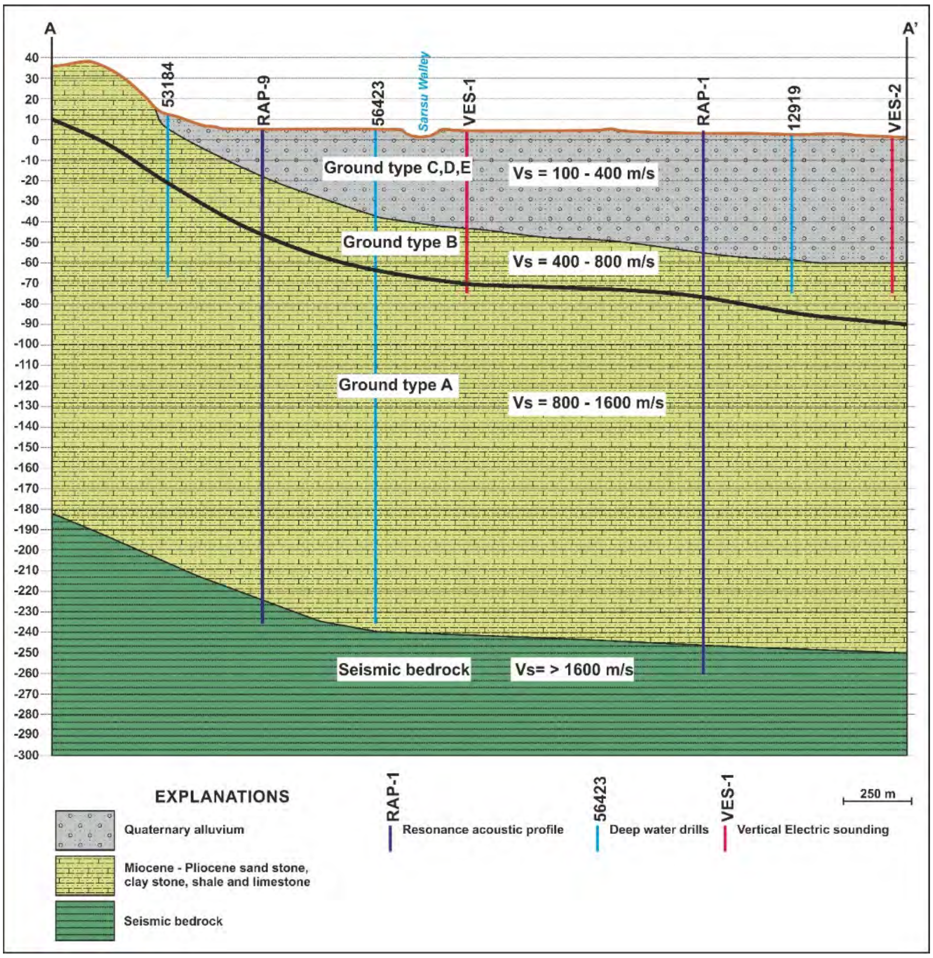

Figure 5-4 Soil profile in Canakkale test site and the bedrock level

5.3 Description of seismic input

Marmara Region is one of the most earthquake prone areas in Turkey. It is under the threat of North Anatolian Fault which is one of the most important and destructive earthquakes in the world. This fault intersects the northern part of Turkey approximately in E-W direction and it is a right lateral strike slip fault. Except for the one segment of the fault, the fault was broken in the 20th century. One of the sections which has not been broken yet in the Marmara Fault is approximately 160 km long and is located under the Marmara Sea. This fault is extremely important because of its proximity to Istanbul which has a 17 million of population. It is known that the energy accumulation on the Marmara Fault increased after the Izmit-Yalova earthquake in 1999 and there is a possibility that this fault will be broken in the coming decades. Many studies have been conducted to describe the tectonic structure of this important fault.

The historical earthquake records of the Marmara region follow a historical continuum and are almost complete (Ambraseys and Finkel, 1991; Ambraseys and Jackson, 2000 and Ambraseys, 2002). Estimated sources of important historical earthquakes that have affected the Marmara region based on macro seismic data are presented in Figure 5-5. Approximately 2000 years of earthquake history of the region shows that on average, every 50 years, earthquakes with intensities of (I_o = VII-VIII), and every 300 years, earthquakes with intensities of (I_o = VIII-IX) affect the region (Erdik et al., 2004). Data of the instrumental period in Turkey began with the establishment of the stations after the 1900 earthquake. The first half of the instrumental period in Turkey is between the years 1900-1970 where the seismic data was recorded with limited number of stations, whereas after the 1970 earthquake, due to the increased number of the stations, there was a quantitative and qualitative increase in the evaluations of the recorded earthquakes. It should be recalled that due to the limited number of stations between 1900-1970, number of earthquakes in the country may have been listed as lower than reality and this may cause misinterpretations.

Based on the present information, the seismicity of the region can be defined based on the following. Gazikoy, Etili, Biga, Sarıkoy and Yenice fault zones are known active members of NAFZ in Marmara region. The Saros–Gaziköy fault which is right lateral caused the 7.3 magnitude Murefte–Sarköy earthquake in 1912. The Can–Biga fault zone where a 6.4 magnitude earthquake occurred in 1935 is comprised of many northeast–southwest directional fault segments. The length observed on the surface of the Yenice–Gonen fault which caused the Ms = 7.2 magnitude earthquake in 1953, known as the Yenice–Gönen earthquake, is about 50 km (Herece 1990). The separation of the different faults which have generated large magnitudes in the Biga Peninsula allows us to divide this region into four sub-zones as was given in detail in Istanbul University Report in Deliverable 2.1., 2017, Akil and Bekler, 2013). Figure B-5-21 shows simplified seismotectonic features in Çanakkale and vicinity.

The long term seismicity of the Marmara Region is shown in Figure 5-5. Table 1-1 presents the significant earthquakes that have occurred in the region in the last century. The seismicity of the Marmara region is relatively high, as evidenced by both historical and contemporary period earthquakes. Fifteen destructive earthquakes occurred between 6.0 and 7.4 in the Marmara region between 1912 and 1999, Earthquakes with magnitudes higher than M = 6.0 after 12 November 1912.

This project has received funding from the European Union's Horizon 2020 research and innovation programme under grant agreement No. 700748

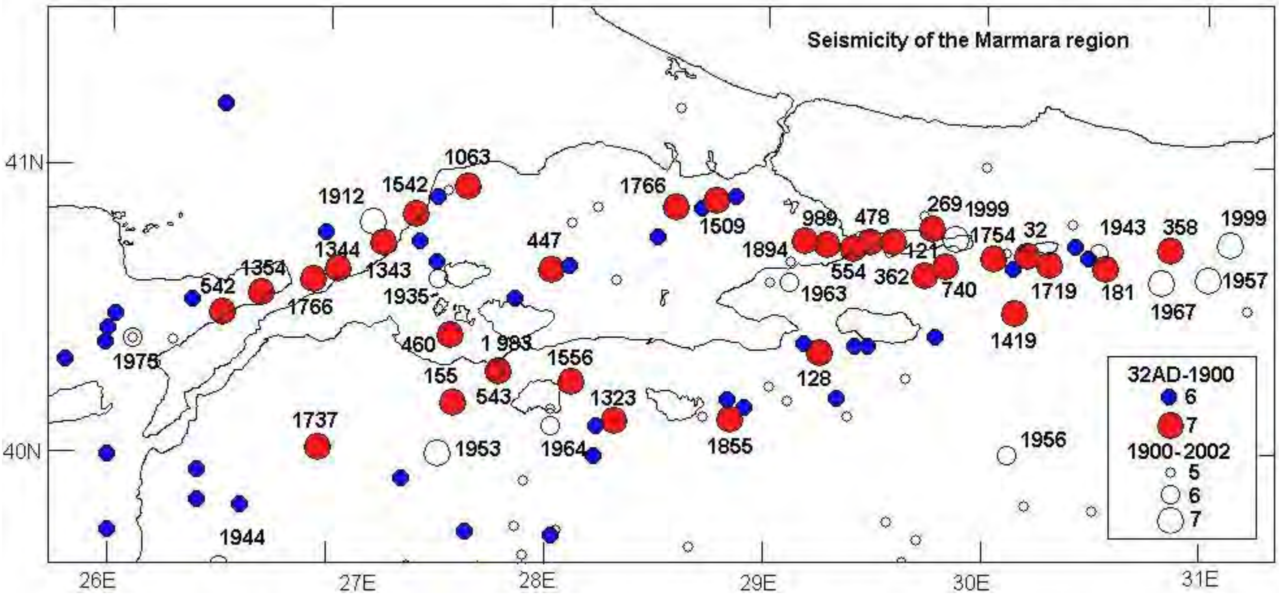

Figure 5-5 Long-term seismicity of the Marmara Region. (M.S. 32 .1983 from Ambraseys and Finkel, 1991) (Erdik et al., 2004)

Table 5-1 Significant earthquakes occurred in Marmara Region (M> 6.0) (KRDAE data)

No	Date	Latitute	Longitude	Magnitude	Location
1	09.08.1912	40.60	27.20	7.30	Şarköy-Mürefte
2	10.08.1912	40.60	27.10	6.30	Şarköy-Mürefte
3	02.05.1928	39.64	29.14	6.10	Bursa-Kütahya
4	04.01.1935	40.40	27.49	6.40	Marmara Island
5	04.01.1935	40.30	27.45	6.30	Marmara Island
6	15.11.1942	39.55	28.58	6.10	Balıkesir
7	20.06.1943	40.85	30.51	6.50	Sakarya
8	18.03.1953	39.99	27.36	7.20	Yenice-Gönen
9	20.02.1956	39.89	30.49	6.40	Bilecik-Eskişehir
10	26.05.1957	40.67	31.00	7.10	Abant
11	18.09.1963	40.77	29.12	6.30	Çınarcık
12	06.10.1964	40.30	28.23	7.00	Manyas
13	22.07.1967	40.67	30.69	7.20	Adapazarı-Mudurnu
14	17.08.1999	40.76	29.97	7.40	Gölcük
15	12.11.1999	40.74	31.21	7.20	Düzce

Erdik et al. (2004) presents the segmentation models developed according to OYO (2007) and these models are presented in Figure B-. It should be recalled that within the scope of this report, the segmentation model developed in SHARE project and EMCE project which is the sub-project of SHARE has been used.

5.3.1 Seismic Hazard and Non-Linear Site Response Analyses

After the seismicity of the region was determined, seismic hazard analyses and non-linear site response analyses were performed following different approaches. The aim was to determine the peak ground acceleration for microzonation studies. These approaches are presented in Figure 5-6 schematically and explained in detail below.

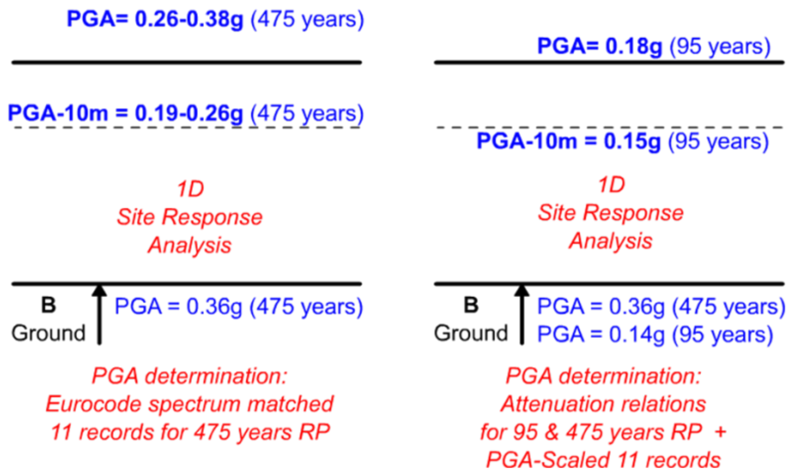

Figure 5-6 Calculated peak ground accelerations depending on two methods: (a) Eurocode; (b) Attenuation relations

Method 1: Full spectrum matched records were obtained at the bedrock level and this was followed by site response analyses.

- Full spectrum scaling (Seismo-Match) was carried out for selected 11 motions from PEER database to fit the Eurocode-8 type-1 spectrum for 475 years Return Period

Eurocode 8 states that the seismic action to be considered for design purposes should be taken on the estimation of the ground motion expected at each location in the future. Although peak ground acceleration is not a good descriptor of the severity of an earthquake and of its possible consequences on construction, for the sake of simplicity, EN1998-1 calculates the seismic hazard only by the value of the reference peak ground acceleration on ground type A (a_{gR}). As stated in the code, the seismic hazard is described by a zonation map defined by the National Authorities and the reference peak ground acceleration (a_{gR}) for each seismic zone, corresponds to the reference return period for the no collapse requirement; i.e.; for a return period of 475 years. This value is then corrected for the importance factor for the building. Eurocode 8 lists the building importance factors to range from 0.8 to 1.4. Accordingly, the design ground acceleration, a_g is calculated as below;

$$a_g = a_{gR} * \gamma_I$$

In this study, the design ground acceleration for a return period (RP) of 475 years was calculated as 0.36g, based on the a_{gR} value (from National Annex) of 0.3 and γ_I of 1.2. It should be recalled that this importance factor corresponds to buildings whose seismic resistance is of importance in view of the consequences associated with a collapse, e.g., schools, assembly holes, cultural institutions, etc.

The next step was to define the EC8 spectrum in SeismoMatch for soil type B level and 475 years return period. Eleven selected records given in Table 1-2 were then matched with the spectrum. The records were taken from PEER database. A schematic of this matching is presented in Figure 5-7 and Figure 5-8. The selected eleven records matched with the spectrum were also scaled for 0,36g, which was determined to be the design ground acceleration in the test site. These records were then accepted to be acting at the bedrock level.

Table 5-2 List of the selected eleven earthquakes

# of EQ	RSN	Event Name	Year	Magnitude	Fault Type	Rjb (km)	Rrup (km)	V_S (m/s)	PGA (g)	Target PGA	Scaling Factor
E01	280	Trinidad	1980	7.20	**SS**	76.06	76.26	311.75	0.150	0.360	2.400
E02	957	Northridge	1994	6.69	**RF**	15.87	16.88	581.93	0.352	0.360	1.023
E03	755	Loma Prieta	1989	6.93	**RF**	19.97	20.34	561.43	0.461	0.360	0.781
E04	3759	Landers	1992	7.28	**SS**	27.05	27.05	425.02	0.198	0.360	1.818
E05	1102	Kobe	1995	6.9	**SS**	49.91	49.91	609.00	0.110	0.360	3.273
E06	501	Hollister	1961	5.45	**SS**	11.15	12.32	608.67	0.192	0.360	1.875
E07	1618	Duzce	1999	7.14	**SS**	8.03	8.03	638.39	0.160	0.360	2.250
E08	125	Fruli	1976	6.50	**RF**	14.97	15.82	505.23	0.341	0.360	1.056
E09	2709	Chi-Chi	1999	6.20	**SS**	25.01	25.06	573.04	0.134	0.360	2.687
E10	6928	Darfield	2010	7.00	**SS**	25.21	25.67	649.17	0.240	0.360	1.500
E11	164	Imperial Val.	1979	6.53	**SS**	15.19	15.19	471.53	0.168	0.360	2.143

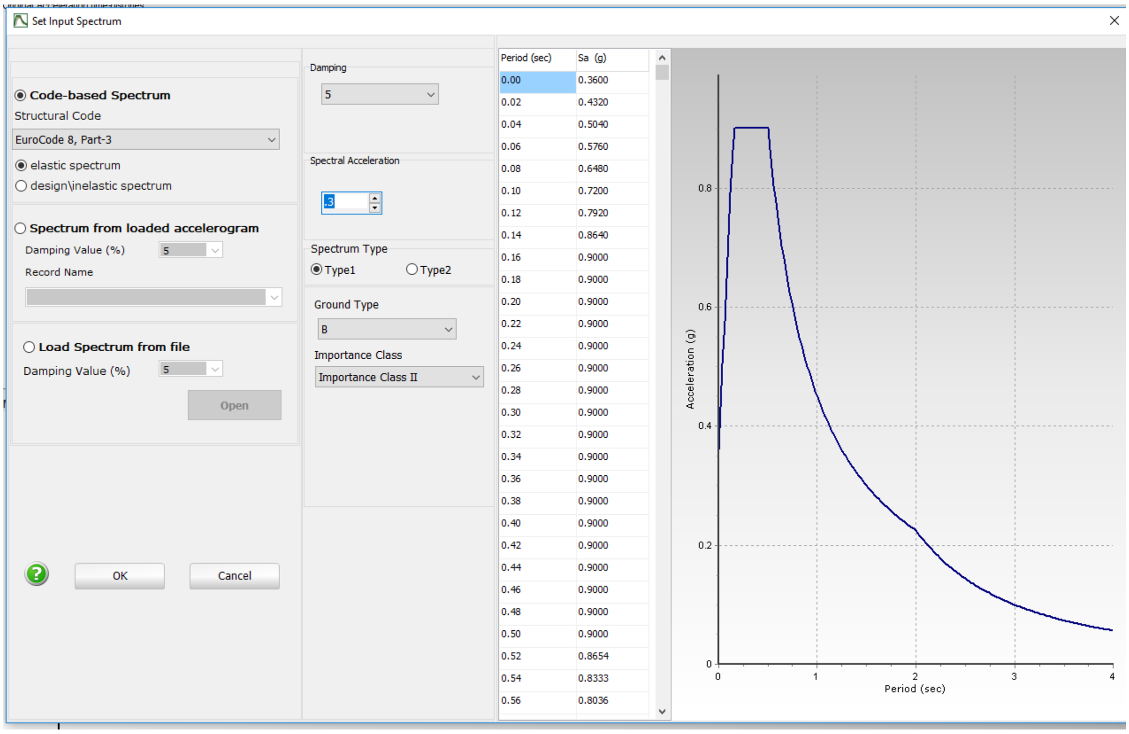

Figure 5-7 EC8 spectra matching in SeismoMatch

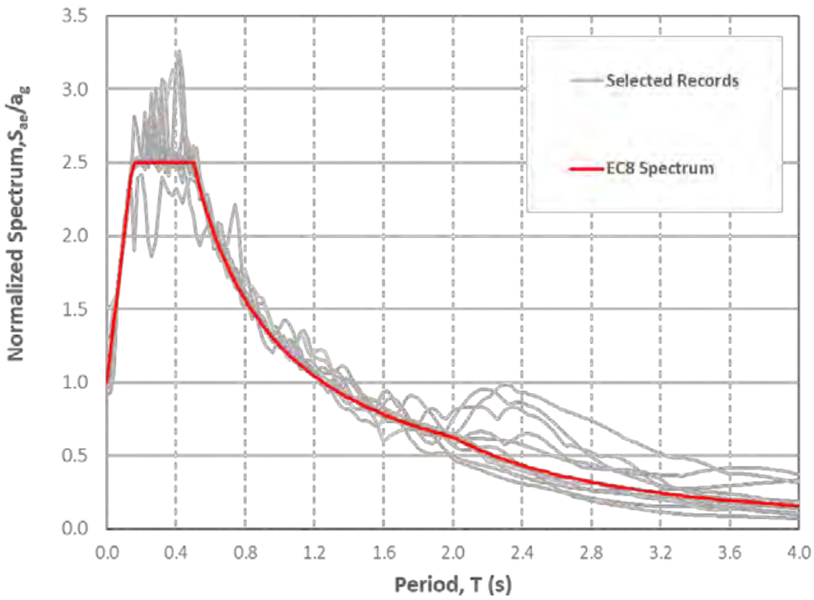

Figure 5-8 Matching of the selected records to EC8 spectra

- 1-D non-linear site response analyses were carried out via Plaxis (2019)

The final step was to carry out site response analyses. These analyses were performed using Plaxis 2D (2019) software. Definition of the geotechnical model for ground response analyses required knowledge of depth and geometry of the roof of geological or seismic bedrock; depth and geometry of piezometric surface, spatial distribution of geotechnical parameters for each lithological unit (e.g. thickness, soil unit weight, small-strain shear modulus and damping ratio, shear modulus and damping ratio reduction curves, grain size distribution, plasticity properties, etc.). All this information was obtained from the previous and the complimentary soil investigations in the test site. A typical soil profile is given in Figure 5-9. HS or HSsmall soil model was used. There was no need to define the lateral or bottom boundary conditions.

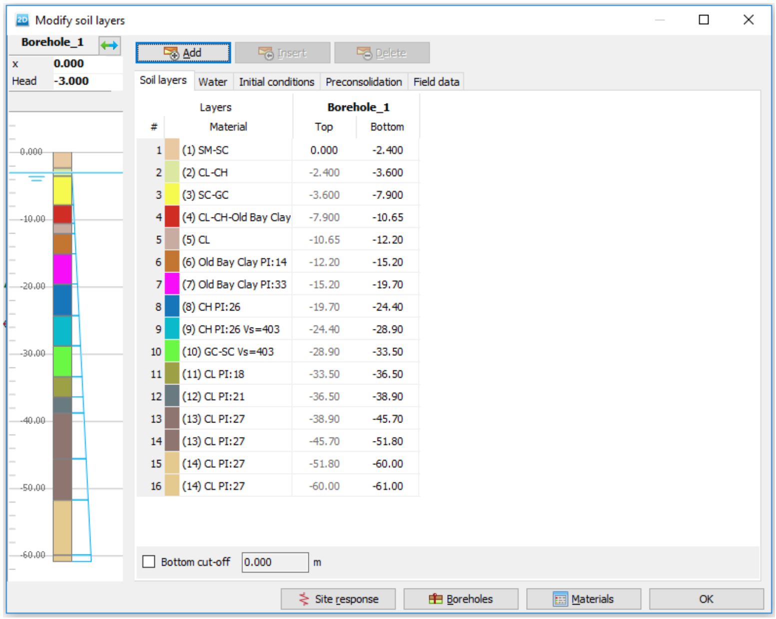

Figure 5-9 A typical soil profile used for ground response analyses

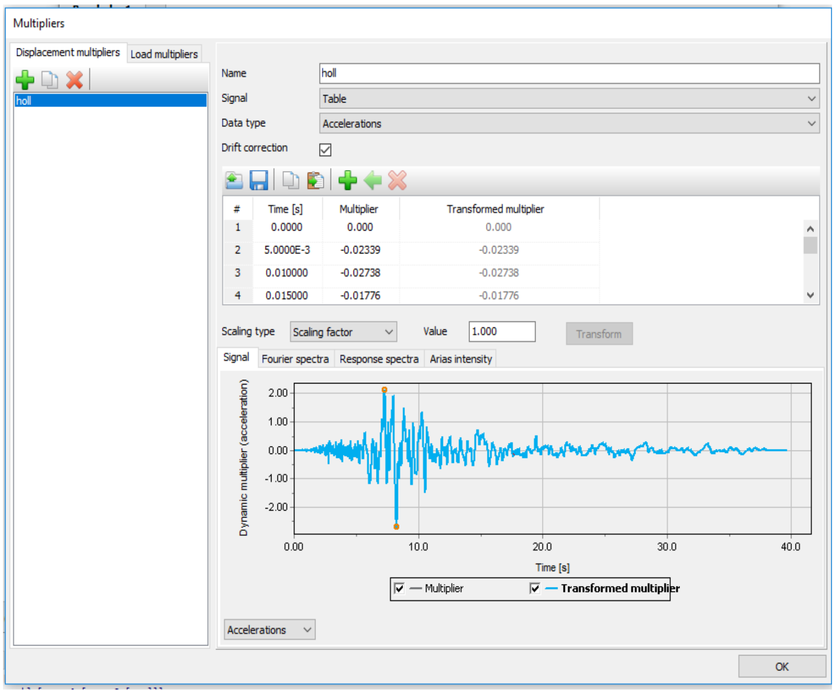

Figure 5-10 Screenshots from PLAXIS 2D (2019)

This project has received funding from the European Union's Horizon 2020 research and innovation programme under grant agreement No. 700748

For the site response analyses, soil profiles in Canakkale city center were used. A screenshot from the Plaxis2D (2019) analyses is shown in Figure 5-10. These ground response analyses were carried out with the recordings which were matched with the spectra and scaled for the peak ground acceleration. Peak ground acceleration (PGA) values at the surface, at 10 m depth and at the surface were determined for each borehole. The values at the surface were used in microzonation studies, however the values at 10 m depth were determined for possible use in further analyses.

The PGA values determined for each borehole were then put in SURFACE software as inputs and an interpolation was performed using the Kriging method. This made it possible to obtain the surface distribution of PGA values in the test site. The results show that PGA values at the surface range between 0.26g to 0.38g for 475 return period. At 10 m depth the values ranged between 0.19g to 0.26g.

Method 2: Attenuation relations were used together with PGD scaled records at the bedrock level. Site response analyses were then performed.

In this methodology, attenuation relations were taken from the probabilistic seismic hazard analyses that were carried out with R-Crisis v2015 and SHARE. The relationships that allow the modelling of the attenuation were selected from the database within the R-Crisis software. It was also possible to create hybrid models by determining the percentages of the selected attenuation relationships. The analyses were carried out for a return period of 475 years.

The parameters of linear and spatial sources that were used in R-CRISIS were taken from SHARE and EMME project. The satellite faults defined by the SHARE project is given in Figure B-5-23. Satellite image of background and spatial seismic resources defined by the SHARE project are given in Figure B-5-24 and Figure B-5-25.

Generation Next Generation Attenuation Relationships (NGA) were used as ground motion estimation models. Stafford et al. (2008) demonstrated the applicability of NGA models to the Euro-Mediterranean Region. Many ground motion prediction models were developed for Turkey in NGA project to be applied to different geographic regions. In this context, the relationships given by Akkar et al. (2014) and Abrahamson et al. (NGA-2, 2014) were selected as the attenuation relationships to be used in the study. The applied procedure was as follows; a circular area with a 100 km of diameter was defined. Linear and area sources in this circular area were defined both geometrically and seismically in R-crisis v2015 software. Linear seismic sources (Figure B-5-26), and spatial seismic sources (Figure B-5-27) are shown in the relevant figures. Acceleration, velocity and spectral acceleration values obtained from each source were calculated using the 50% of linear and background seismic sources and 50 % of the spatial seismic sources.

As attenuation models, Akkar et al. (2014) and Abrahamson et al. (NGA-2, 2014) models were selected, because these models are based dominantly on the Turkey and Middle East seismic region. A hybrid model was used as given below. It should be recalled that the selection of these coefficients were verified by the PGA value measured in Adapazari SKR-5401 station in 17 August 1999 earthquake.

This project has received funding from the European Union's Horizon 2020 research and innovation programme under grant agreement No. 700748

$$Hybrid\ Model = 0.7\ x\ Akkar\ et\ al.(2014) + 0.3\ x\ Abrahamson\ et\ al.(NGA-2, 2014)$$

This hybrid model was assigned to all the seismic sources in the software. In order to calculate the PGA of interested regions or sites, the results calculated from source and line sources analyses were averaged. Some equations used to convert information of source seismicity in the R-Crisis Software are given below;

$$\lambda(M) = \lambda_{min} * \frac{e^{-\beta * M} - e^{-\beta * M_{min}}}{e^{-\beta * M_{min}} - e^{-\beta * M_{max}}}$$

where,

$\lambda(M)$: Annual frequenc of exeedance of magnitude M

M : Magnitude

M_{min} : Minimum magnitude for which the catalog is considered

M_{max} : Maximum magnitude is considered for source

λ_{min} : Annual frequency of exceedance of the minimum magnitude,

$$\lambda_{min} = e^{\alpha - \beta * M_{min}}$$

In this equation, a and b are the parameters of Guterberg-Richter Model and $\alpha = 2.303\ x\ a; \beta = 2.303\ x\ b$

The ground motion estimation models used in the determination of earthquake hazard, the ground motion parameters (peak ground acceleration-PGA and spectral acceleration-SA) are calculated based on the location (magnitude and fault model), the fault distance and the soil profiles and hence site response. The fault sources are taken from SHARE and EMME projects. It should be noted that, catalog of fault sources uses Magnet Completeness (Mc), a and b values, as well as various statistical parameters. The "b" value used in the seismic hazard analysis is defined as the value of the linear regression slope and "a" value is the intercept of the "y" axis. Mc is defined as the smallest value in which the distribution remains linear.

After the application of this procedure to the region, PGA distribution at the bedrock level in the Canakkale city center was determined. The relevant figures are given in Figure B-5-28 and Figure B-5-29. PGA scaling was carried out for the selected motions from PEER database (given in Table 1-2). After this scaling, 1-D site response analysis was carried out via Plaxis.

The microzonation maps for PGA obtained with both methods are given in Figure 5-11. The results show that PGA values at the surface range between 0.26g to 0.38g for 475 return period. For the 95 years return period, the PGA values at the surface range between 0.13g to 0.18g.

This project has received funding from the European Union's Horizon 2020 research and innovation programme under grant agreement No. 700748

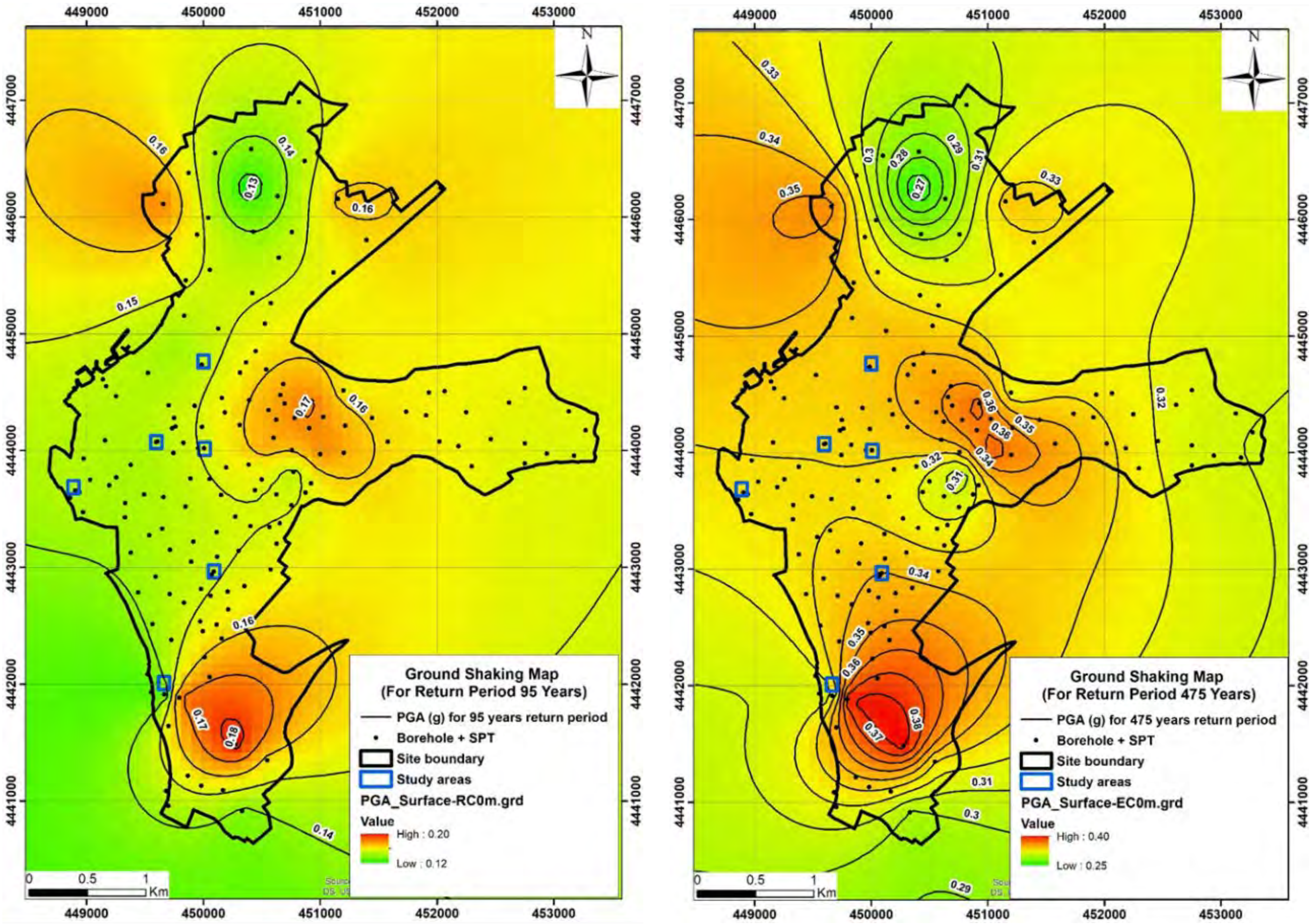

Figure 5-11 The distribution of PGA in the test site for 95 years and 475 years return periods

5.4 Microzonation for Liquefaction Risk

The microzonation for liquefaction risk was carried out for the test site taking into account the geotechnical data and the seismicity of the area. Geotechnical data was achieved through SPT testing. SPT is the most frequently used field test in Turkey and in this context, previous studies that had been carried out in Canakkale city center consisted of field investigation where SPT was the main field test. In selected six areas, CPT tests were carried out within the context of the complimentary testing, however these are limited in number. Therefore microzonation for liquefaction was based on SPT based approaches. The steps that were followed are given below;

- Definition of the soil profile
- Assignment of the soil properties based on SPT testing and laboratory tests

- Determination of safety factors for liquefaction for each soil layer in the profile
- Calculation of LPI and LSN values both from the ground surface and from the foundation base

An important step for SPT based liquefaction analyses is calculation of safety factors through depth in each soil profile. An EXCEL sheet was prepared in order to calculate the factor of safety values for liquefaction through the soil profile. This is called LiquIST, "liquefaction analyses programme developed by Istanbul University-Cerrahpasa." Figure 5-12 shows the screenshot of the LiquIST. The sheet is capable of automatically perform liquefaction analysis based on CSR and CRR. The calculation steps for CSR and CRR are given in detail in Appendix A. It should be recalled that the liquefaction factor of safety values were calculated for the free-field conditions.

After factor of safety values were calculated, microzonation for liquefaction was performed using liquefaction damage assessment indicators. The vulnerability indices chosen were Liquefaction Potential Index (LPI) and Liquefaction Severity Number (LSN). These two vulnerabilities were calculated both from the ground surface and from the foundation level. All the vulnerabilities were calculated both from the ground surface and from the foundation base.

Liquefaction Potential Index (LPI) was developed by Iwasaki et al. (1978) and is used to determine the vulnerability to liquefaction effects. LPI evaluates the liquefaction potential of the soil using the factor of safety, the thickness of the layer and the depth of the relevant layer. Liquefaction Potential Index is estimated as;

$$LPI = \int F_1 W(z) dz$$

where $F_1=1-FS$ for $FS \leq 1.0$, $F_1=0$ for $FS>1.0$ and $W(z)=10-0.5z$. The calculations are carried out for the top 20 m as it is accepted that liquefaction effect on the building is negligible at depths greater than 20 m. Liquefaction potential categories related to LPI are given in Table 1-3.

Table 5-3 Liquefaction Potential Index (LPI) – Iwasaki et al (1982) & Sonmez (2003)

LPI	Expected Damage Level
0	No liquefaction
0 - 2	Low
2 - 5	Moderate
5 - 15	High
≥ 15	Very high

Liquefaction Severity Index (LSN), is another parameter which defines the liquefaction related vulnerability of structures. It was developed by Tonkin and Taylor Ltd. (2013) based on the liquefaction damage observations resulting from 2010 and 2011 New Zealand earthquakes. This value depends on the volumetric densification values and the depth weighted factor. The volumetric strains are calculated for layers with FS less than 2.0 and these values are then used to calculate the LSN values as given below.

$$LSN = 1000 \int \frac{\varepsilon_v}{z} dz$$

In this equation, ε_v is the volumetric densification or strain for 1D post-liquefaction reconsolidation and is calculated using Zhang et al. (2002) or Idriss and Boulanger (2008). z is the depth to the layer of interest in meters below the ground surface. With 1/z depth weighing factor, the effect of the depth is much more influenced compared to LPI. The liquefaction potential categories based on LSN are given in Table 1-4.

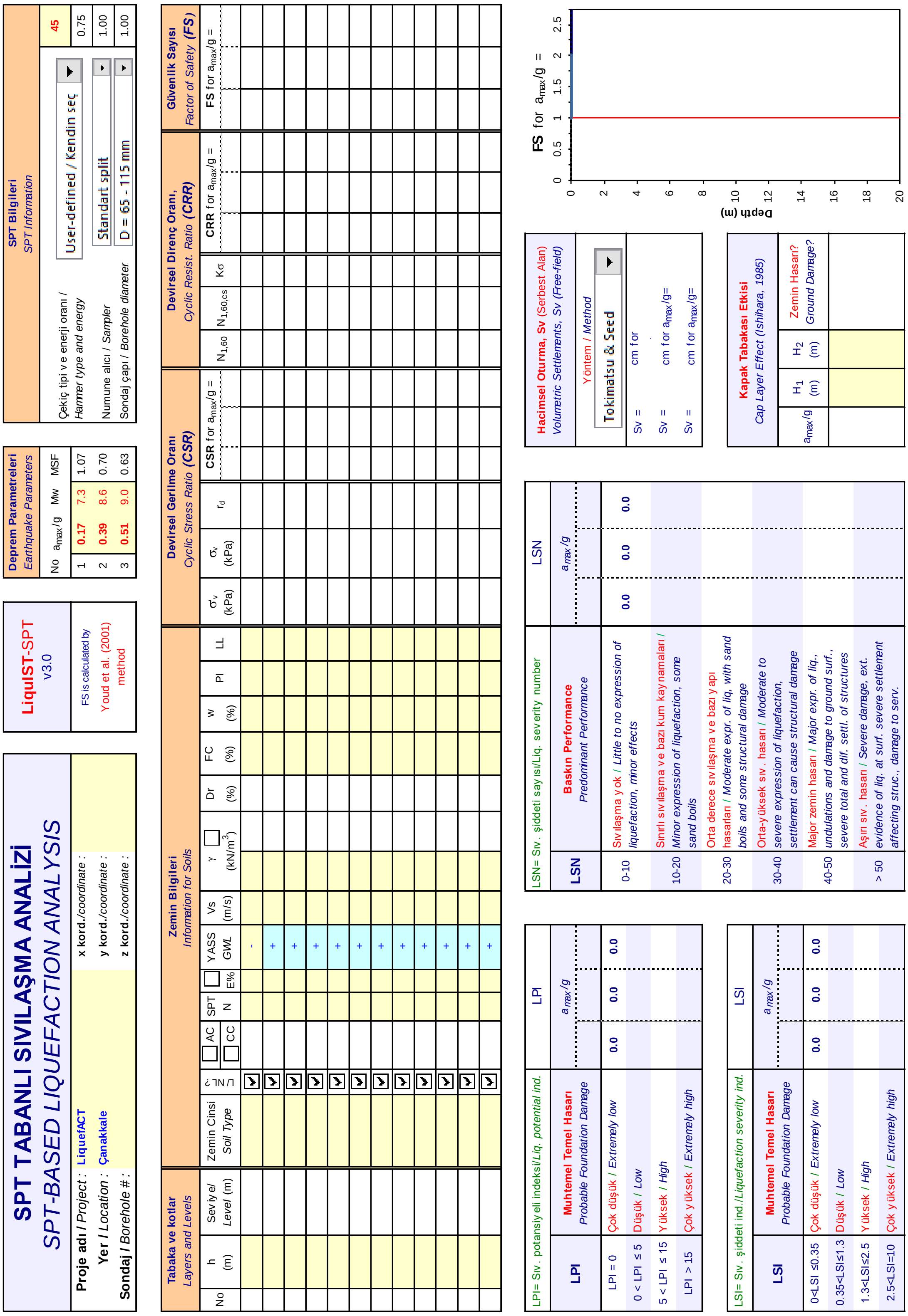

Figure 5-12 A screenshot from the EXCEL sheet, LIQUEIST

Table 5-4 Liquefaction Severity Number (LSN) by Tonkin and Taylor Ltd. (2013)

LSN	Expected Damage Level
< 10	None to Little
10 - 20	Minor
20 - 30	Moderate to Severe
30 - 40	Severe
40 - 50	Major
>50	Extensive

In this study, these two indicators; Liquefaction Potential Index and Liquefaction Severity Index; were applied in their original form and also from a modified point of view taking into account the soil system response. Cubrinovski et al. (2018) recommended "soil system response" to evaluate the liquefaction-induced damage. In this concept following main consideration was that liquefaction occurs in the first ten meters. The liquefaction is dominated by the critical layers (L_{crit}) and in this context, the shallowest critical layer is of outmost importance. In this approach critical layer is defined as the layer which is most likely to trigger and manifest liquefaction at the ground surface of a given site. The critical layer and the layers of low liquefaction resistance that are vertically continuous form the critical zone. The critical layer is characterized by $q_{c1ncs}<85$. The liquefiable layers between the critical layers and even the thin layers which are not liquefiable may contribute to the liquefaction. However, interbedded deposits of liquefiable and non-liquefiable soils were accepted to result in vertical discontinuity in soils that did not liquefy. The first 2.5 m layer from the ground surface which does not liquefy is called the crust layer and the presence of a crust layer prevents liquefaction. The soils above the groundwater table can liquefy due to seepage induced liquefaction. When liquefaction occurs in the critical zone, due to vertical communication of excess pore water pressures, the soil above the water table at shallow depths liquefies due to an upward flow from the critical zone.

Oztoprak et al. (2019) evaluated the soil system response and applied the liquefaction damage assessment tools to Adapazari cases in Kocaeli 1999 Earthquake. Their results showed that system response approach developed by Cubrinovski et al. (2018) could be applied with great success to Adapazari silty soils. Some modifications made by Oztoprak et al. (2019) are summarized as follows and it was shown that these modifications captured the real liquefaction damage in Adapazari with a more precision, therefore it was decided that they should also be applied to Canakkale case. This can also allow a comparison with the traditional methods. It should be recalled that the modified approaches were developed by Istanbul University-Cerrahpasa team within the context of the Liquefact project. The vulnerability indices carried out in this study both in their original form and in modified form are given in Table 1-5.

- A modification was made to the soil behavior index by Oztoprak et al. (2019), in order to include the soils with soil behavior index greater than 2.6 as being liquefiable depending on the Plasticity Index value. In this context, soils with soil behavior index greater than 2.6 and lower than 2.8 were accepted to liquefy in case their Plasticity Index (PI) values were less than 15. The PI criteria was based partially on the literature on the subject. Chinese criteria (Wang, 1979) classifies the soils with PI <12 and w_c/LL>0.85 (where w_c is natural water content) as liquefiable soils. Sancio et al. (2003) classifies the soils with PI <12 and

w_c/LL>0.85 as liquefiable soils. Sancio et al. (2003) determined that soils with PI>20 did not generate significant cyclic strains after a large number of cycles at low confining stresses representing the mean effective stress for soils under the corner of the mat foundation of typical 4 to 5 storey structures in Canakkale. In this context, PI of 15 was accepted to be a reasonable boundary. In the liquefaction analyses, the criteria for liquefaction of no liquefaction was based on this boundary. If the soil satisfied the liquefaction criteria, then the factor of safety was calculated, otherwise, it was accepted to not to liquefy.

- Cubrinovski et al. (2018) also warned that Seepage Induced Liquefaction (SIL) may occur in a soil layer above groundwater level, therefore in this study, seepage induced liquefaction was considered as one of the factors within the damage assessment indicators. In this context, the last group of analyses for Canakkale case were based on some modifications for I_c value boundary and seepage induced liquefaction concept recommended by Cubrinovski et al. (2018).
- The traditional approaches are LPI-1 and LSN-1. LPI-2 and LSN-2 were applied for the first 10 meters. The modified approaches are LPI-3, LPI-4, LSN-3 and LSN-4. As summarized in Table 1-5, LPI-3 and LSN-3 values consider an upper boundary of 2.8 for I_c values coupled with a Plasticity Index of 15%. This meant that the boundary for liquefiable soils was elevated in order to include silty soils with low plasticity indices. These indicators considered the top ten meters.
- For LPI-4 and LSN-4 values, seepage induced liquefaction was accepted to occur in soil layers above the ground water table. However, seepage induced liquefaction was accepted to occur in a soil layer only in cases where it satisfied the following criteria; the soil behavior type index (I_c) causing liquefaction is less than 2.8 coupled with a Plasticity Index of 15 and normalized clean sand equivalent cone tip resistance value is less than 85. The depth of the SIL was accepted to less than 1.5 m. It is clear that the depth of the GWL (with respect to the layer bottom) should affect this seepage induced liquefaction mechanism.
- It should be recalled that all the indicators were performed from the "ground surface"case and from "the foundation base" case.

The studied indicators are presented in Table 1-5. The criteria for the critical depth, for the I_c, PI and LL and for the Seepage Induced Liquefaction consideration are presented in the table. It should be recalled that LPI-1 and LSN-1 are the classical approaches and are calculated for the first 20 m.

Figure 5-13 shows the schematic for the application of the methodologies to Canakkale case. GS represents the ground surface and FB represents the foundation base. SIL is the Seepage Induced Layer, which is above the groundwater level, but in case some conditions are provided, it is accepted to liquefy.

Table 5-5 Criteria for liquefaction analyses for different LPI and LSN approaches

Criteria		**LPI-1 & LSN-1 (original form)**	**LPI-2 & LSN-2**	**LPI-3 & LSN-3 (for modified Ic and PI values)**	**LPI-4 & LSN-4 (modified Ic and PI values and seepage induced liquefaction)**
Criteria-1	Considered Depth	20 meters	10 meters	10 meters	10 meters
Criteria-2	Ic PI LL	<2.6 <12 <37	<2.6 <12 <37	<2.8 <15 <37	<2.8 <15 <37

Criteria-3	SIL $q_{c1,Ncs}$ thickness (m)	No - -	No - -	No - -	Yes <85 <1.5

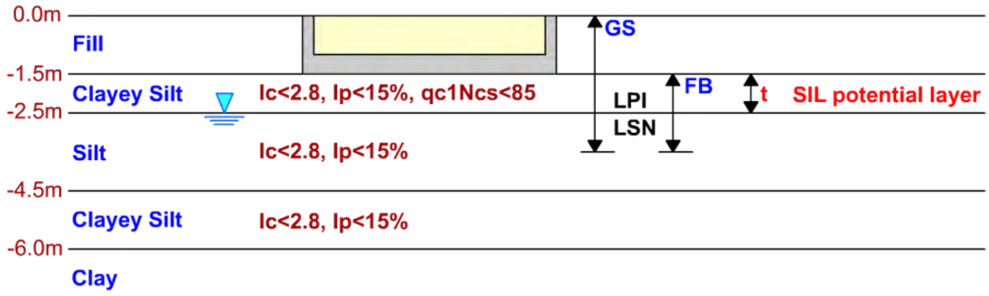

Figure 5-13 A schematic for the application of the methodologies to Canakkale case

Using LIQUIST and the criteria given in Table 1-5, liquefaction analyses were carried out for different return periods. The liquefaction assessment indicators were then calculated for each scenario and were mapped in GIS platform. Microzonation was then carried out and are presented below. The GIS platform used in this study is ArcInfo.

The microzonation for LSN-1 and LSN-2 for 475 years return periods are given in Figure 5-14. The results are presented for the "ground surface" (GS) case and "Foundation base" (FB) cases. The maps differ for LSN-1 and LSN-2 cases. Based on both indices, the maps showed that liquefaction is a very high risk in Canakkale test site, however depending on whether the calculations are carried out from the ground surface or from the foundation base affected the LSN values considerably. For the foundation base case, nearly all of the city center seems to be suffering from severe liquefaction damage, while for classical approaches which are carried out from the ground surface, the results are less severe. This is a novel contribution to the literature for liquefaction analyses. It shows that neglecting the depth of the foundation level may result in underestimation of liquefaction damage.

The microzonation maps for LPI-1 and LPI-2 are given in Figure 5-15. The calculations were carried out for 475 years return period. For LPI values, the maps did not differ for GS and FB cases. This shows that LPI values are not as sensitive to the depth of the foundation as much as the LSN values. The values differed slightly for LPI-1 and LPI-2, however the difference was not great. This may show that the first 10 meters governed the liquefaction damage in Canakkale city center.

The analyses were also carried out for a return period of 95 years. The results are given in the Appendix C in Figure C1 and C2 respectively for LSN and LPI values respectively. For LSN-1 and LSN-2 values, 95 years return period resulted in lower liquefaction damage in the area as expected. The analyses from the foundation base (FB) revealed higher liquefaction damage. Microzonation maps for LPI, revealed lower liquefaction damage compared to LSN, because the areas with the higher risk level contributed to a less area. This shows that liquefaction microzonation maps should be preapred using different liquefaction vulnerablility indices and an evaluation and comparison of the methods should be carried out.

5.4.1 Comparison of the microzonation maps with Tunusluoglu and Karaca (2018)

Based on the extensive study carried out by Buruksarac et al. (2013), a microzonation study was carried out by Tunusluoglu and Karaca (2018). Their maps for PGA=0.14g and for PGA= 0.32g are presented in Figure 5-16. The maps were drawn for LPI values. Their maps are similar to the findings in this study that were obtained with LPI microzonation. However the studies carried out in this project showed that LPI is not the only vulnerability index and other approaches should also be studied.

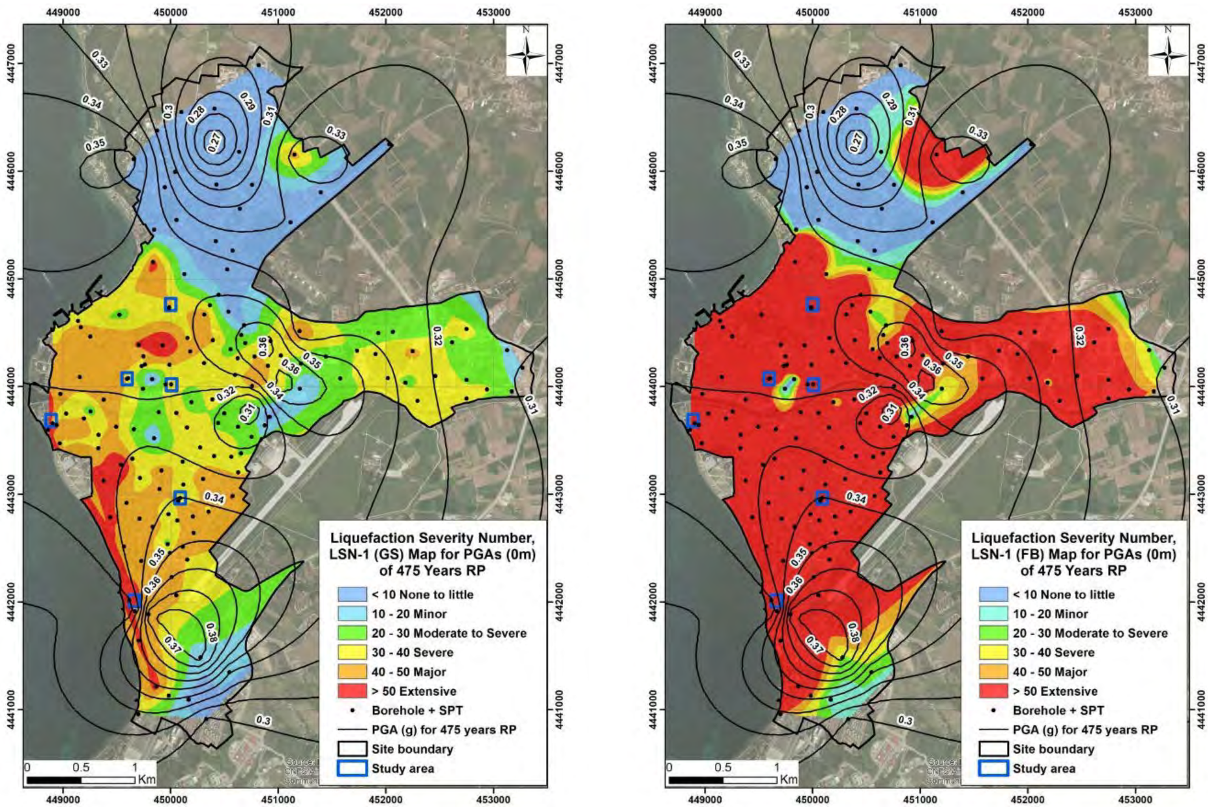

(a) LSN-1, GS, 475 years

(b) LSN-1, FB, 475 years

This project has received funding from the European Union's Horizon 2020 research and innovation programme under grant agreement No. 700748

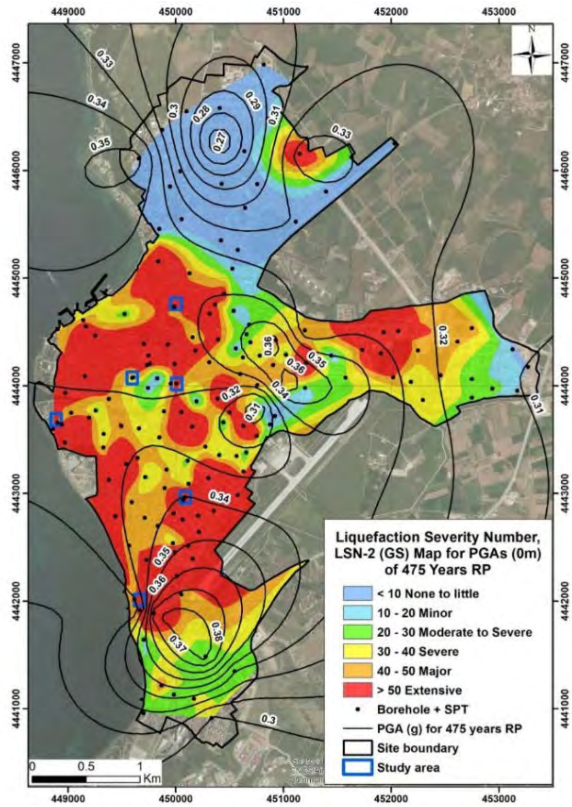

(c) LSN-2, GS, 475 years

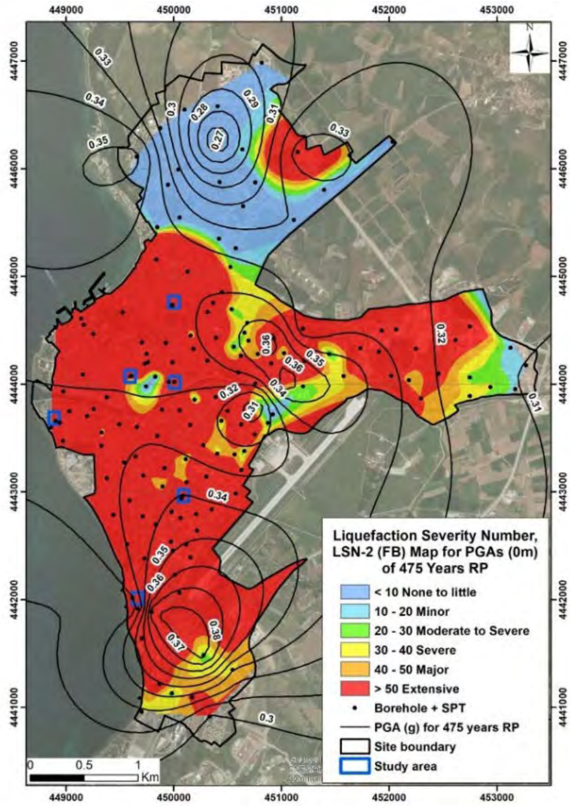

(d) LSN-2, FB, 475 years

Figure 5-14 Microzonation maps for LSN-1 and LSN-2 for 475 years return period

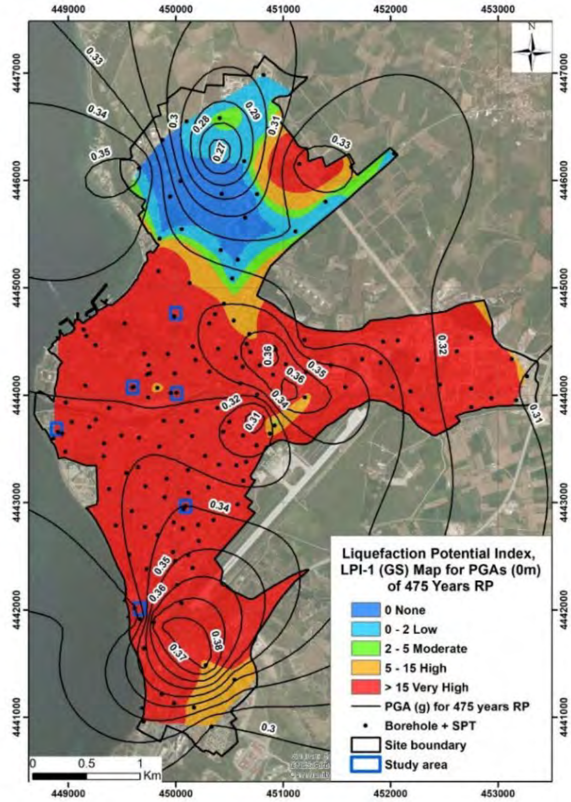

(a) LPI-1, GS, 475 years

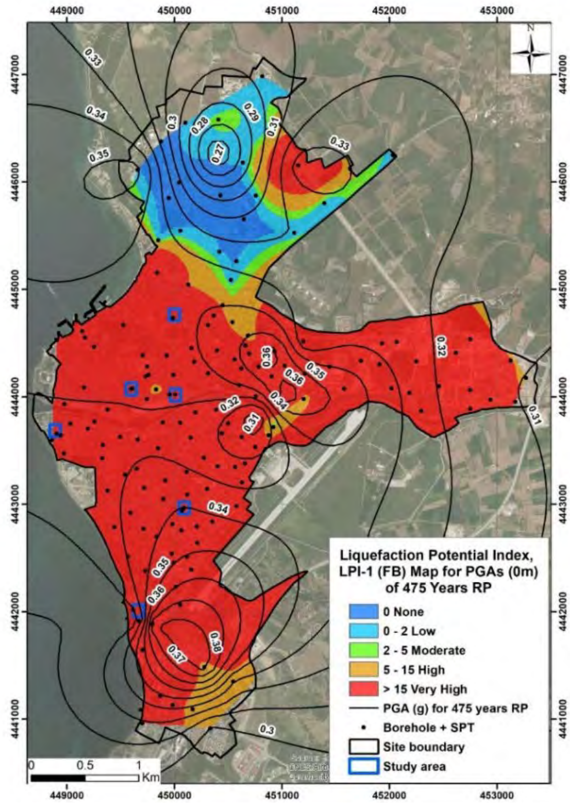

(a) LPI-1, FB, 475 years

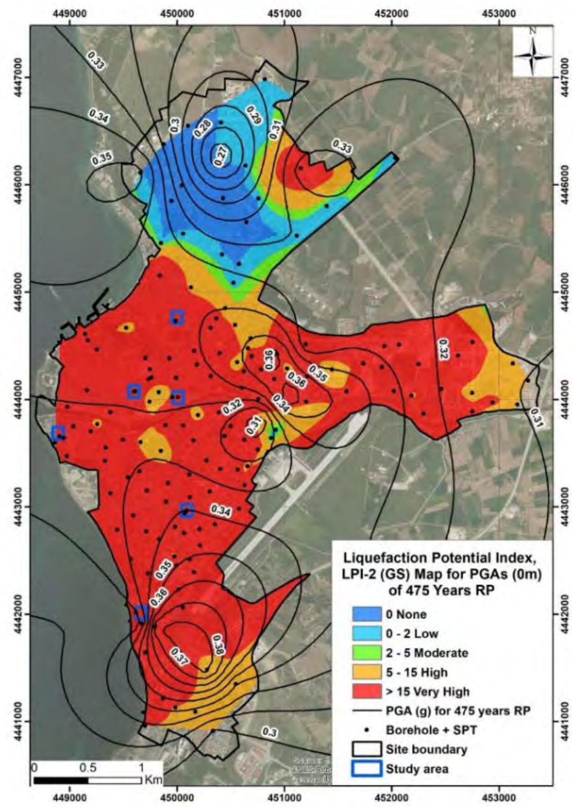

(a) LPI-2, GS, 475 years

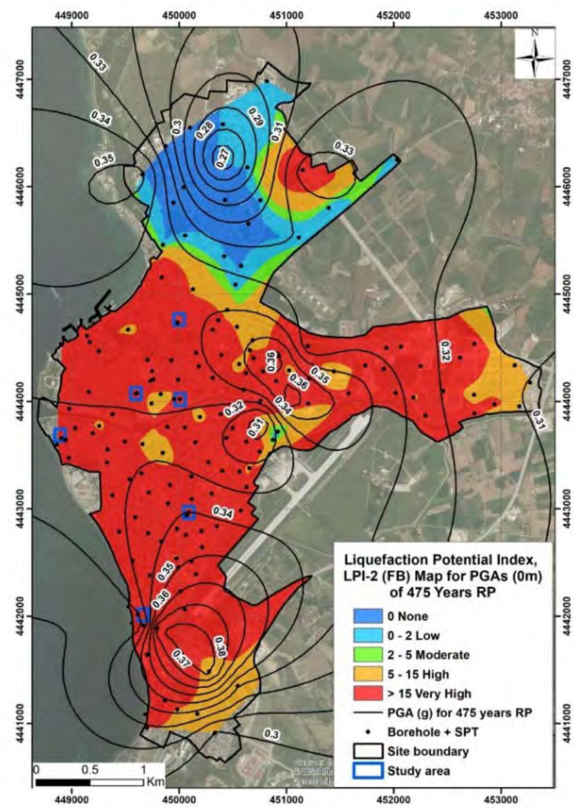

(a) LPI-2, FB, 475 years

Figure 5-15 Microzonation maps for LPI-1 and LPI-2 for 475 years return period

This project has received funding from the European Union's Horizon 2020 research and innovation programme under grant agreement No. 700748

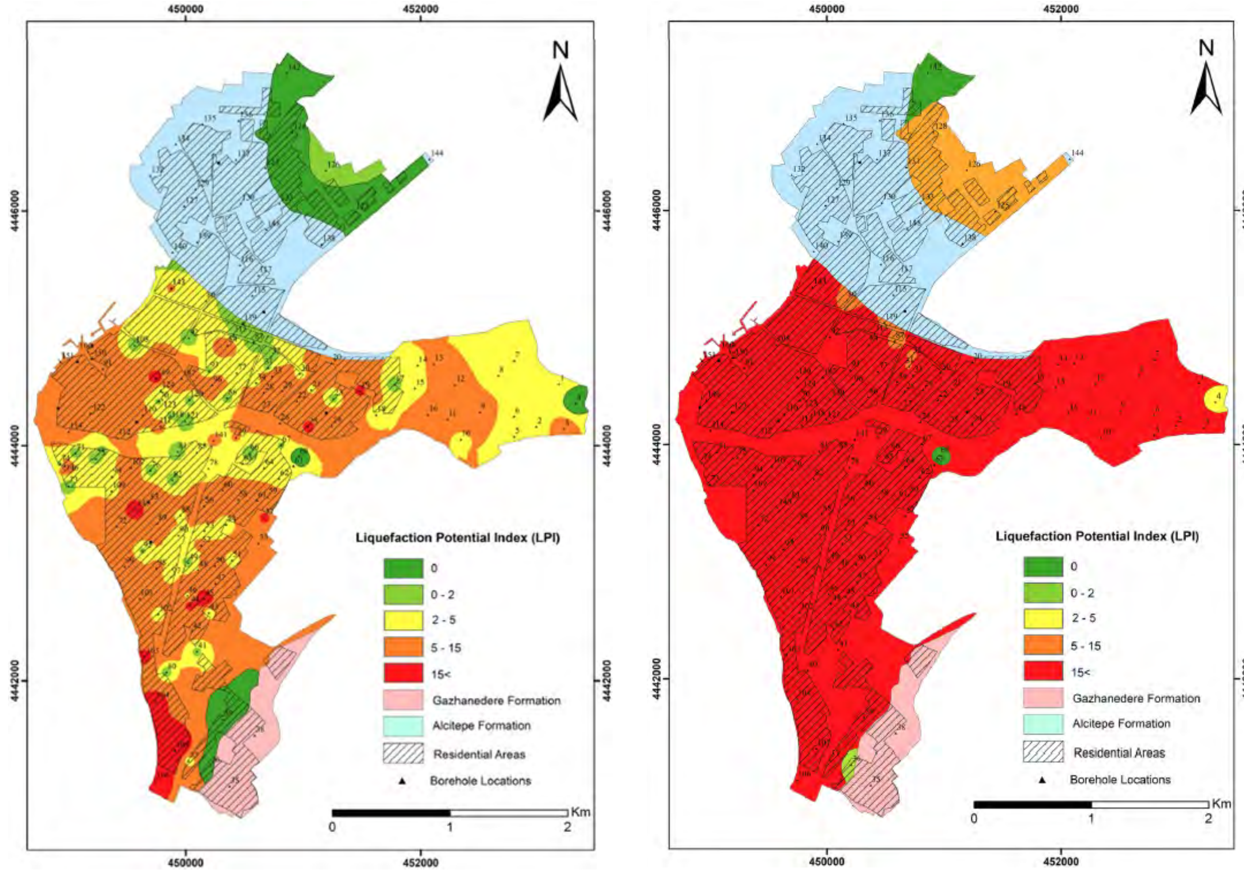

(a) PGA map for 95 years (a) PGA map for 475 years

Figure 5-16 PGA maps for 95 years (PGA=0.14g) and for 475 years (PGA=0.32g)

5.5 Conclusions

In this deliverable, entitled D2.7, "Methodology for assessment of earthquake-induced risk of soil liquefaction at the four European testing sites (microzonation)", microzonation studies that were carried out for Canakkale site (in Marmara Region) by Istanbul University-Cerrahpasa are presented.

The first stage in micronation studies was to characterize the Canakkale city center from a liquefaction point of view. In this context, existing data in the test site was compiled and an extensive complimentary study was performed in six selected areas. This data was used to create a reliable geological and geotechnical model.

The next step was to perform seismic hazard analyses. Seismic hazard analyses were carried out for the area using different methodologies, which were based on the most recent approaches. This brought novel contributions to the study. The aim was to obtain peak ground investigations at the bedrock level and then carry these peak ground accelerations to the ground surface. PGA values at the bedrock level were obtained by different approaches for different return periods. These values were then carried to the surface using Plaxis (2019) by site response analyses. This required a rigorous definition of the subsoil.

Microzonation for liquefaction was then performed using liquefaction damage assessment indicators. The vulnerability indices chosen were Liquefaction Potential Index (LPI) and Liquefaction Severity Number (LSN). These two vulnerabilities were calculated both from the ground surface and from the foundation level. This included definition of the soil profile, assignment of the soil properties based on SPT testing and laboratory tests, determination of safety factors for liquefaction for each soil layer in the profile and calculation of LPI and LSN values. Safety factors for liquefaction through depth in each soil profile was calculated by LIQUIST, which was created in EXCEL specially for this project. The two indicators; Liquefaction Potential Index and Liquefaction were applied in their original form and also from a modified point of view taking into account the soil system response. In this context, the soil system response recommended by Cubrinovski et al. (2018) to evaluate the liquefaction-induced damage was also taken into account. Seepeage induced liquefaction and modified soil behaviour indices were considered to see their effect on liquefaction hazard. The analyses were carried for the first 10 m for 20 m. Different maps for microzonation for prepared and evaluated. The maps are presented for different return periods and different vulnerability indices. The results showed that Canakkale city site carries a high risk of liquefaction.

5.6 References

- Abrahamson, N.A., Silva, W.J. and Kamai, R. (2014): "Summary of the ASK14 Ground Motion Relation for Active Crustal Regions", Earthquake Spectra, 30, 1025-1055
- Akil, B. and Bekler, T. (2013): "Analysis of Earthquake Hazard and Perceptibility Study in Çanakkale, NW Turkey, Nat Hazards", DOI:10.1007/s11069-013-0659-1
- Akkar, S., Sandikkaya, M.A. and Bommer, J.J. (2014): "Empirical ground-motion models for point- and extended-source crustal earthquake scenarios in Europe and the Middle East", Bulletin of Earthquake Engineering, 12, 359-387
- Ambraseys, N.N. and Finkel, C. (1991): "Long-term seismicity of Istanbul and of the Marmara Sea region". Terra Nova, 3, 527-539
- Ambraseys N.N. and Jackson, J.A. (2000): "Seismicity of the Sea of Marmara (Turkey) since 1500". Geophys J Int, 141(3):F1–F6.
- Ambraseys, N.N. (2002): "The seismic activity of the Marmara Sea region over the last 2000 years". Bulletin of the Seismological Society of America, 92-1, 1-18
- Buyuksarac, A., Tunusluoglu, M.C., Bekler, T, Yalciner, C.C., Karaca, O., Ekinci, Y., Demirci, A., Dinc, O. S. (2013): "Geological and geotechnical investigation project of Canakkale", Canakkale Municipality Report.
- Canakkale Municipality Report (2013), "Geological and geotechnical investigation project of Canakkale", (prepared for Buyuksarac et al (2013) for the municipality.)
- Code, Turkish Earthquake (2007): Specification for buildings to be built in seismic zones. Ministry of Public Works and Settlement, Government of Republic of Turkey (2007).
- Cubrinovski, M., Rhodes, A., Ntritsos, N., & Ballegooy, S. V. (2018): "System response of liquefiable deposits". Soil Dynamics and Earthquake Engineering, Pressed online. May 2018, https://doi.org/10.1016/j.soildyn.2018.05.013

- Erdik, M., Demircioglu, M., Sesetyan, K., Durukal, E. and Siyahi, B. (2004): "Earthquake Hazard in Marmara Region, Turkey", 13th World Conference on Earthquake Engineering, Vancouver, Canada
- Eurocode-8 (2004): "Eurocode-8: Design of structures for earthquake resistance", British Standard, BS EN 1998-1:2004
- Geosan (2008): Forum Canakkale geotechnical investigation report, Istanbul.
- Herece, E. (1990): "The fault trace of the 1953 Yenice-Gonen earthquake and the westernmost known extension of the NAF system in the Biga peninsula". Min Res Expl Bull Turkey, 111, 31-42.
- Idriss, I. M., & Boulanger, R. W. (2008): "Soil Liquefaction during Earthquakes". Oakland: Earthquake Engineering Research Institute; 2nd edition.
- Istanbul University Report in Deliverable 2.1 (2017): "Istanbul University-Cerrahpasa University Report in Deliverable 2.1", Liquefact Project H2020
- Iwasaki, T., Tatsuoka, F., Tokida, K., & Yasuda, S. (1978): "A practical method for assessing soil liquefaction potential based on case studies at various sites in Japan". Proc., 2nd Int. Conf. on Microzonation, pp. 885-896, San Francisco.
- Iwasaki, T., Arakawa, T., & Tokida , K. (1982): "Simplified procedures for assessing soil liquefaction during earthquakes". Proceedings of the Conference on Soil Dynamics and Earthquake Engineering, pp. 925-939, Southampton.
- Ohta, Y, and Goto, N. (1978): "Empirical shear wave velocity equations in terms of characteristic soil indexes", Earthq.Eng. Struct. Dyn., 6:167–187.
- Onem, Y. (1974): "Gelibolu Yarımadası ve Çanakkale dolaylarının jeolojisi". TPAO Rap, 877, 30.
- Oztoprak, S., Oser, C., Sargin, S., Bozbey, I., Aysal, N., Ozcep, F., Kelesoglu, M.K and Almasraf, M. (2019): "Evaluation of system response and liquefaction damage assessment tools applied to Adapazari cases in Kocaeli 1999 Earthquake". VII International Conference on Earthquake Geotechnical Engineering, Rome, Italy, 705-716
- Saltik, O. (1974): "Şarköy Mürefte sahaları jeolojisi ve petrol olanakları", TPAO report, 879
- Sancio, R. B., Bray, J. D., Riemer, M. F., & Durgunoglu, T. (2003): "An assessment of the liquefaction susceptibility of Adapazari Silt". Proc. of the7th Pacific Conference on Earthquake Engineering, pp. 172-179, Christchurch: New Zealand Society for Earthquake Engineering.
- Sonmez, H. (2003): "Modification of the liquefaction potential index and liquefaction susceptibility mapping for a liquefaction-prone area (Inegol, Turkey)". Environmental Geology, 44, 862-871.
- Stafford, P.J., Strasser, F.O. and Bommer, J.J. (2008): "An evaluation of the applicability of the NGA models to ground-motion prediction in the Euro-Mediterranean region", Bull Earthquake Eng., 6, 149-177, DOI 10.1007/s10518-007-9053-2
- Tonkin & Taylor Ltd. (2013): "Liquefaction Vulnerability Study. Canterbury: EARTHQUAKE COMMISSION". doi:https://www.eqc.govt.nz/sites/public_files/documents/liquefaction-vulnerability-study-final.pdf
- Tunusluoglu, M.C. and Karaca, O. (2018): "Liquefaction severity mapping based on SPT data: a case study in Canakkale city (NW Turkey)". Environmental Earth Sciences, 77;422
- Wang, W. (1979): "Some findings in soil liquefaction". Beijing: Water conservancy and hydroelectric power scientific research Institute.

- Yaltırak, C., Alpar, B. and Yüce, H. (1998): "Tectonic elements controlling the evolution of the Gulf of Saros (northeastern Aegean Sea, Turkey)".Tectonophysics, 300(1), 227-248.
- Zhang, G., Robertson, P. K., & Brachman, R. W. (2002): "Estimating liquefaction induced ground settlements from CPT for level ground". Canadian Geotechnical Journal, 39(5), 1168-1180. doi:10.1139/T02-047

This project has received funding from the European Union's Horizon 2020 research and innovation programme under grant agreement No. 700748

APPENDICES

APPENDIX 5A. Geological and Geotechnical Characterization

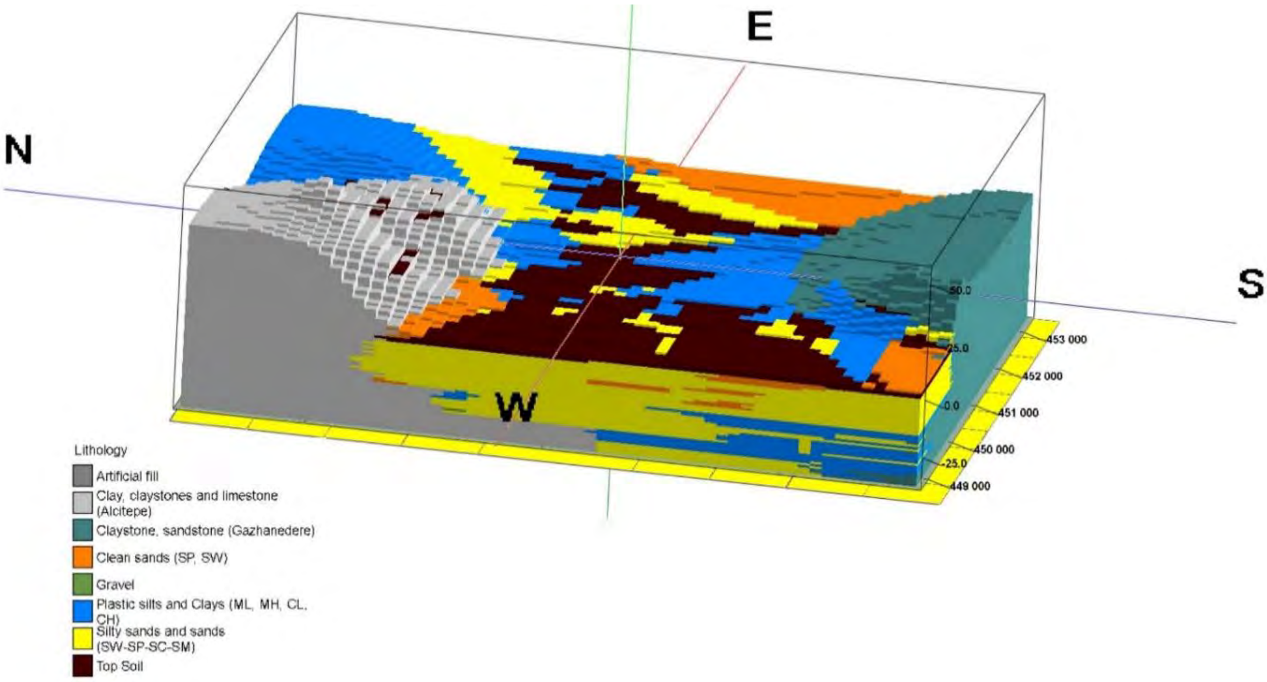

Figure A-5-17 3D engineering geological subsoil model-1

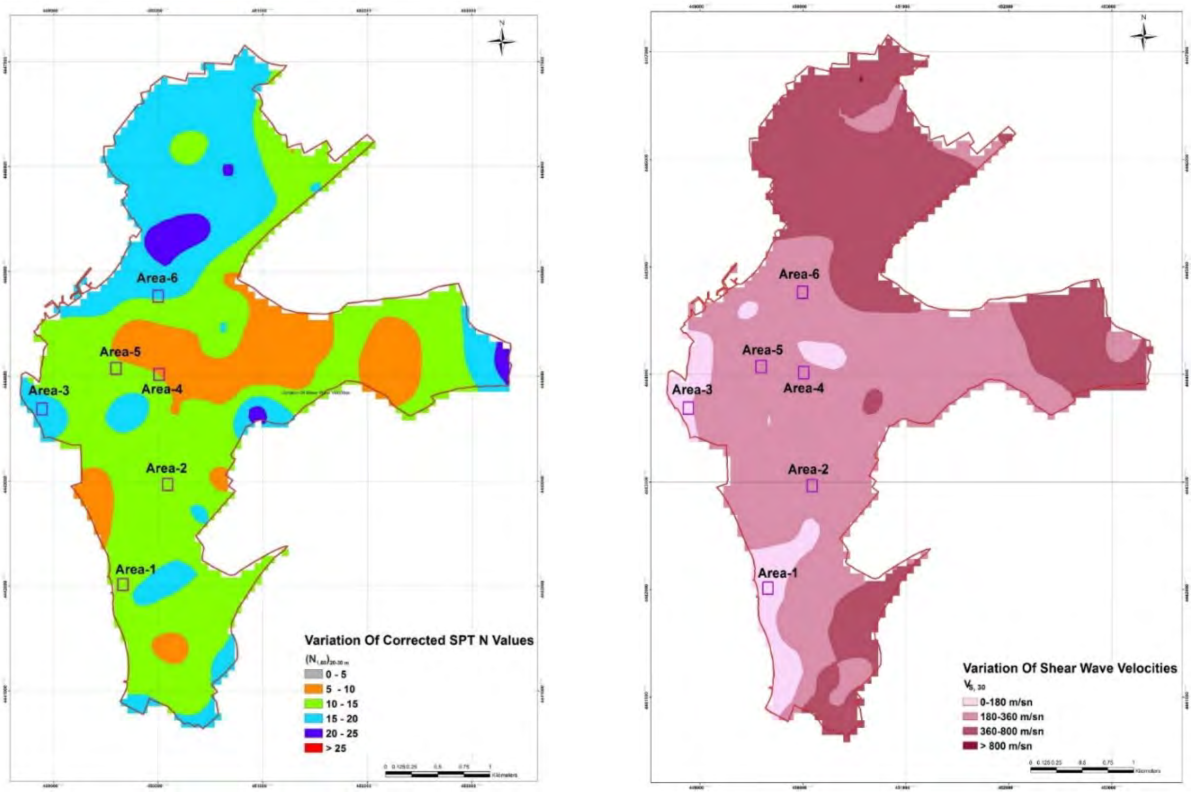

Figure A-5-18 Average N1,60 and shear wave velocity distribution in the top 30 m

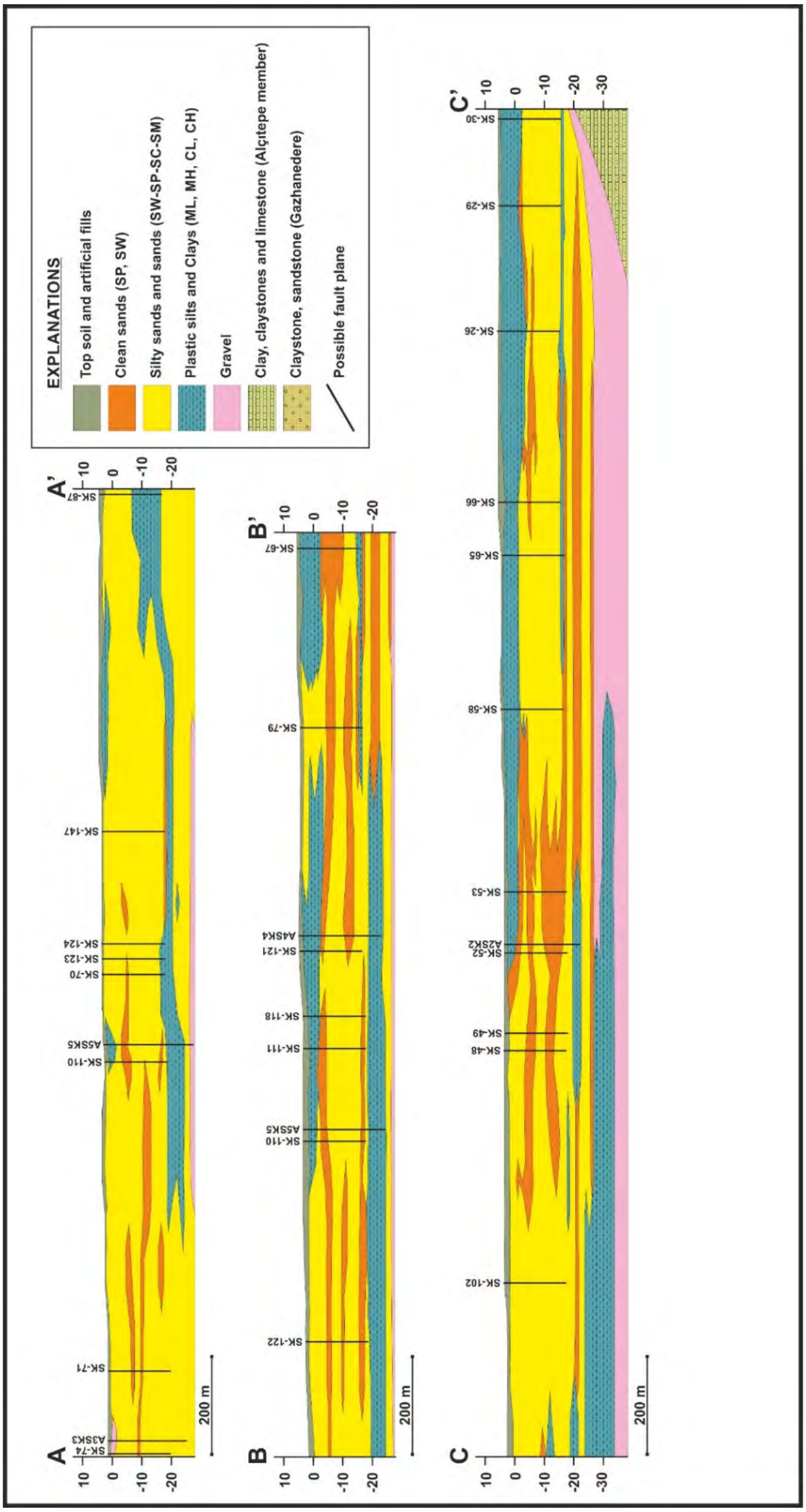

Figure A-5-19 Geolithologic cross-sections from Canakkale test region

This project has received funding from the European Union's Horizon 2020 research and innovation programme under grant agreement No. 700748

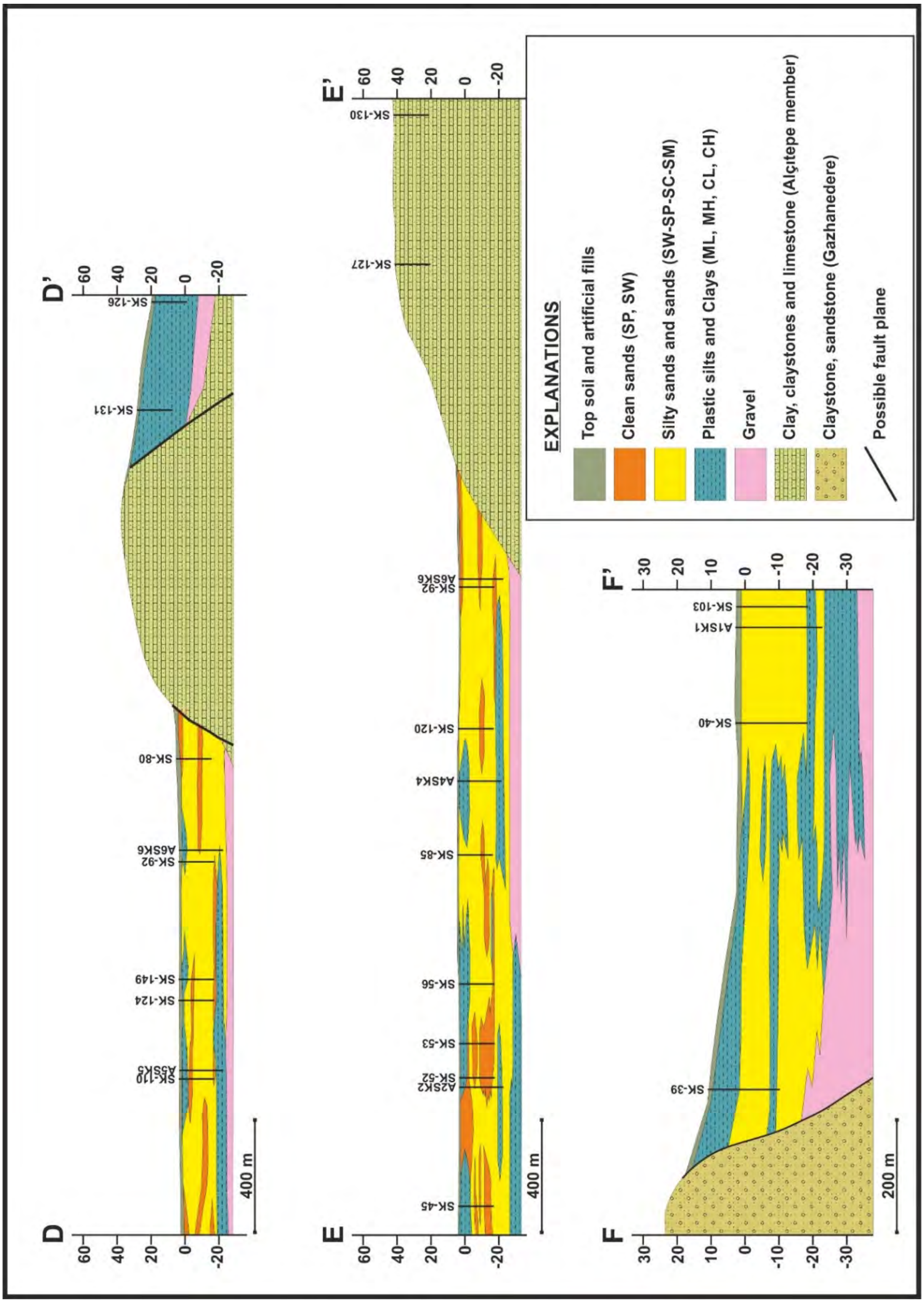

Figure A-5-20 Geolithologic cross-sections from Canakkale test region (continued)

This project has received funding from the European Union's Horizon 2020 research and innovation programme under grant agreement No. 700748

APPENDIX 5B. Seismicity and R-Crisis

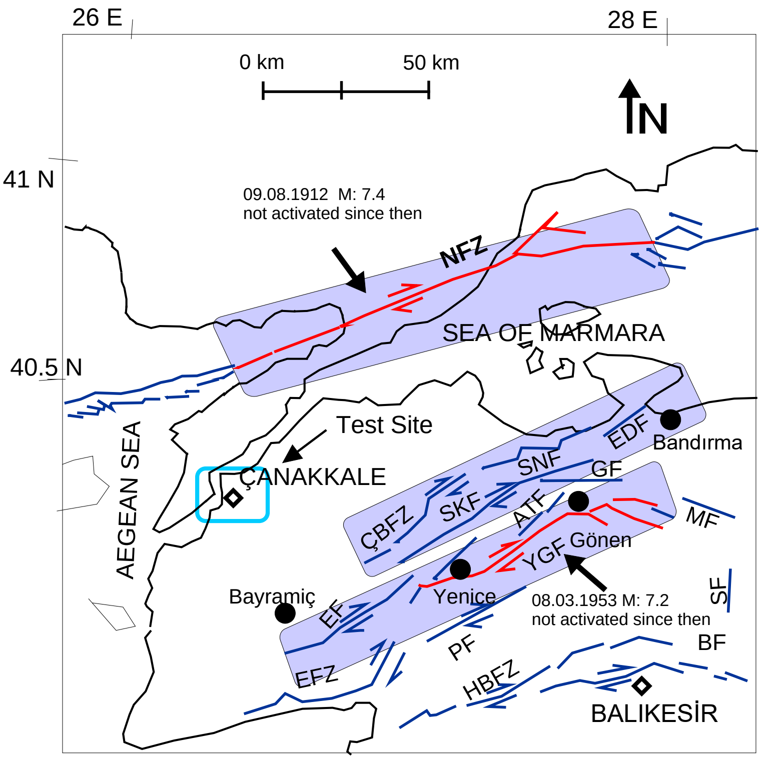

Figure B-5-21 Local seismic sub-zones in the study region (modified by Emre et al, 2013)

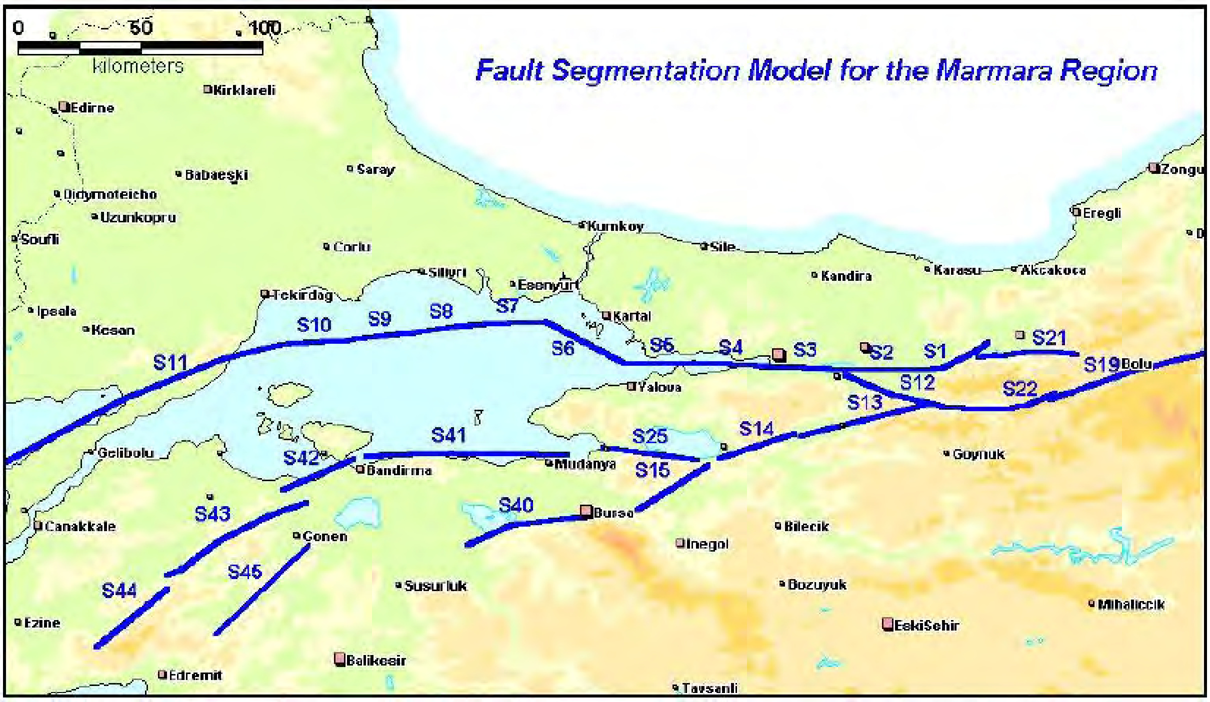

Figure B-5-22 The segmentation model developed by Erdik et al. (2004)

Figure B-5-23 The satellite faults defined by the SHARE project

This project has received funding from the European Union's Horizon 2020 research and innovation programme under grant agreement No. 700748

Figure B-5-24 Satellite image of background seismic sources defined by SHARE project

Figure B-5-25 Satellite image of the spatial seismic resources defined by the SHARE project

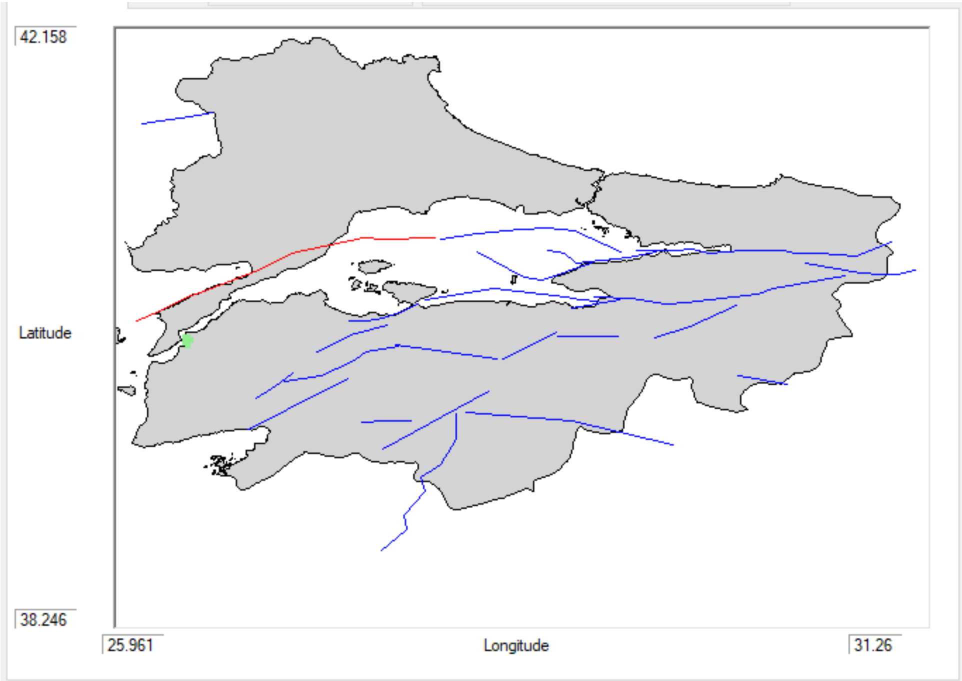

Figure B-5-26 Linear sources in R-Crisis

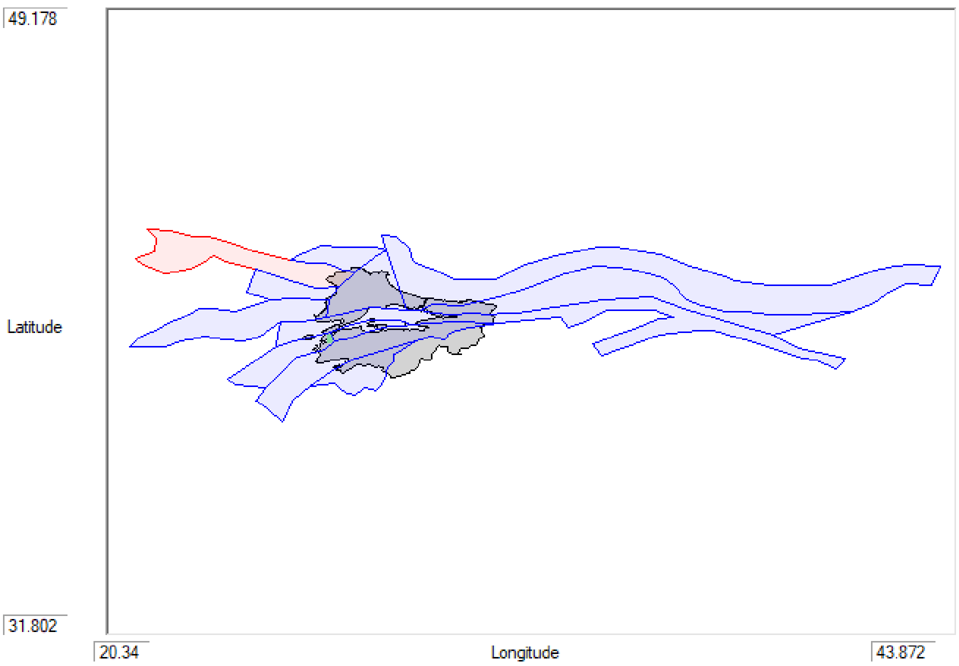

Figure B-5-27 Spatial sources in R-Crisis

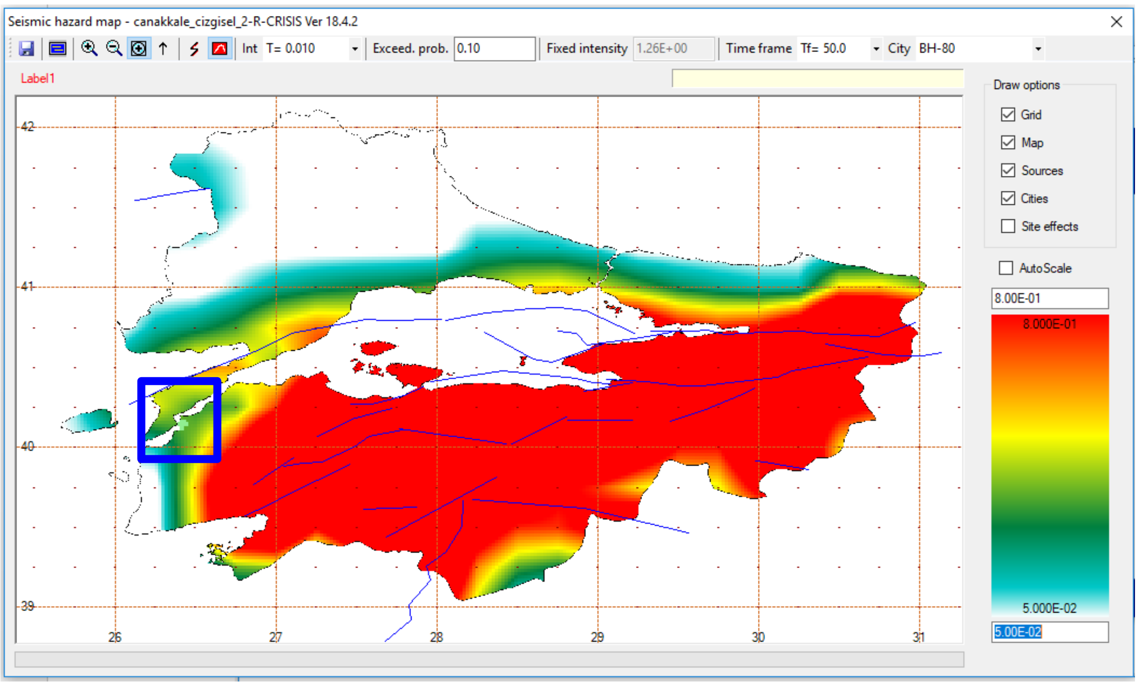

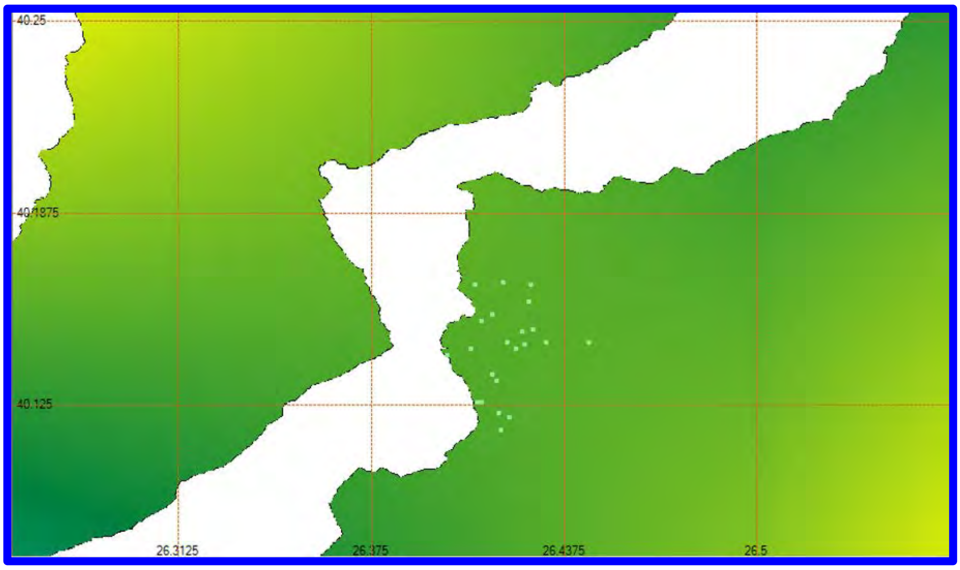

Figure B-5-28 PGA distribution at the bedrock level in Çanakkale city center using linear sources

This project has received funding from the European Union's Horizon 2020 research and innovation programme under grant agreement No. 700748

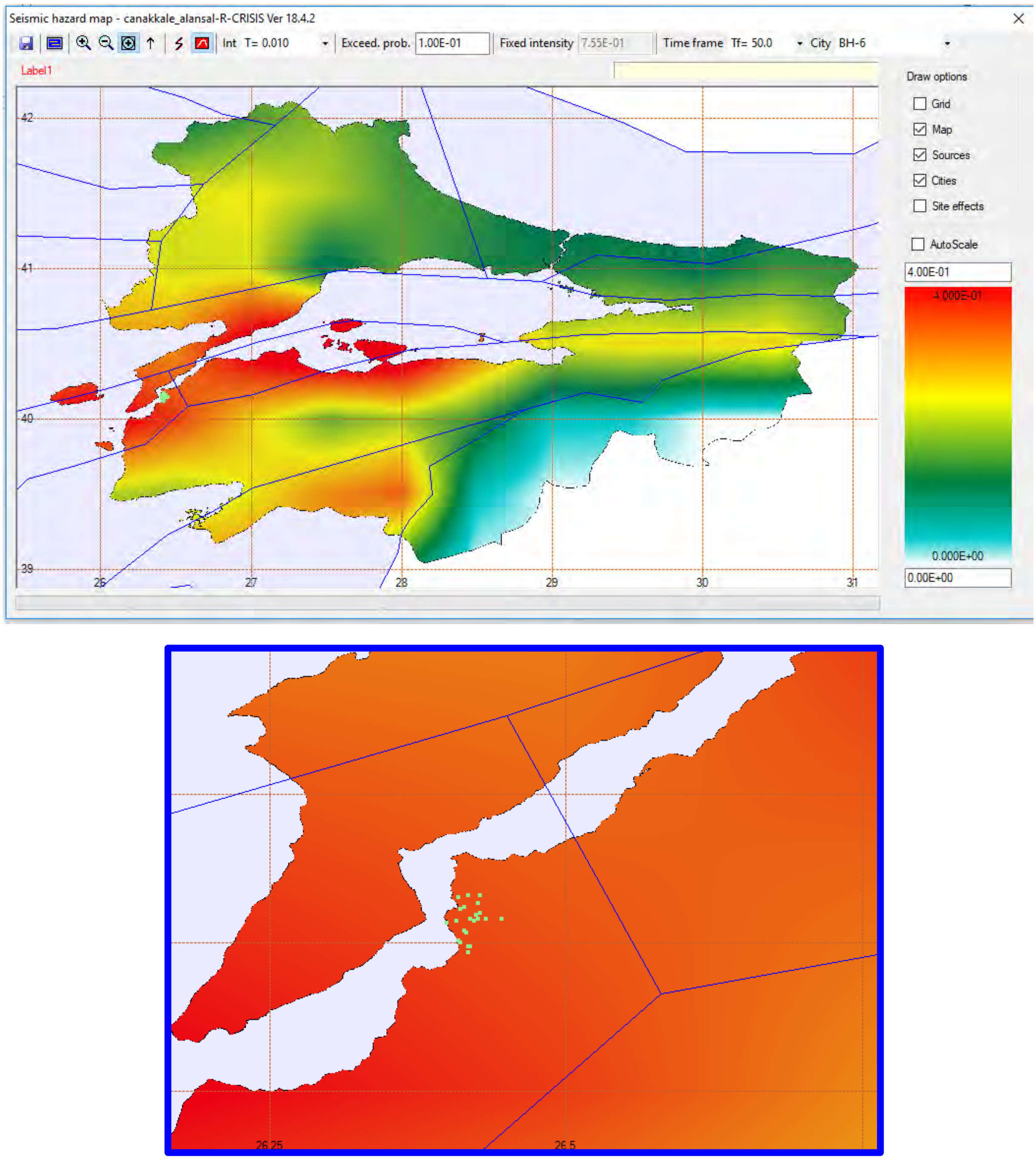

Figure B-5-29 PGA distribution at the bedrock level in Çanakkale city center using spatial sources

This project has received funding from the European Union's Horizon 2020 research and innovation programme under grant agreement No. 700748

APPENDIX 5C. Liquefaction Analyses

In this study, CRR was calculated as follows. Based on the empirical relationship between $(N_1)_{60}$ and the cyclic resistance ratio CRR can be estimated using the curves given by Seed et al. (1985) and by Seed et al. (2001). Figure 1.26 represents the relationship between the calculated CRR and the $(N_1)_{60}$ (corrected for an overburden pressure of about 100kPa and 60% of energy ratio with earthquake magnitude of 7.5.) The figure shows the strong dependency CRR values on the fines content. Depending on fine percent, (less than 5%, 15%, and 35%), CRR takes different values for any $(N_1)_{60}$ value. The following equations were used in the EXCEL sheet in order to calculate all the terms automatically.

$$FS_L = \frac{CRR}{CSR}$$

$$CRR = CRR_{M=7.5} \cdot MSF \cdot K_\sigma$$

$$CRR_{M=7.5} = \frac{1}{34-(N_1)_{60cs}} + \frac{(N_1)_{60cs}}{135} + \frac{50}{\left[10 \cdot (N_1)_{60cs} + 45\right]^2} - \frac{1}{200}$$

$$(N_1)_{60cs} = \alpha + \beta \cdot (N_1)_{60}$$

$$\alpha \begin{cases} = 0.0 & (FC \leq 5\%) \\ = \exp\left[1.76 - \left(\frac{190}{FC^2}\right)\right] & (5\% < FC < 35\%) \\ = 5.0 & (FC \geq 35\%) \end{cases}$$

$$\beta \begin{cases} = 1.0 & (FC \leq 5\%) \\ = 0.99 + \frac{FC^{1.5}}{1000} & (5\% < FC < 35\%) \\ = 1.2 & (FC \geq 35\%) \end{cases}$$

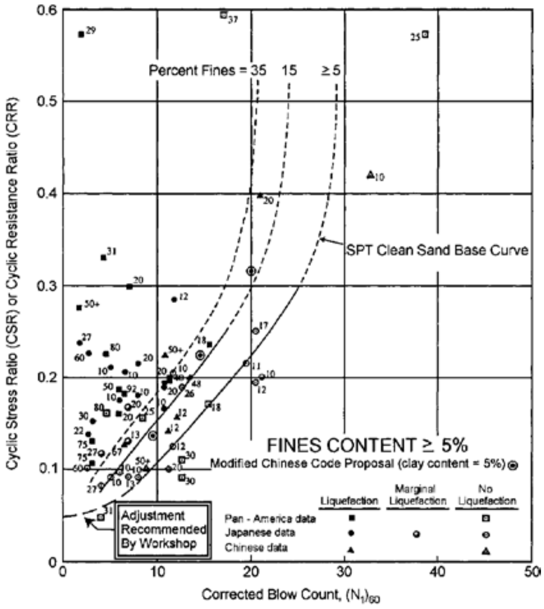

Figure C-5-30 Recommended curves for estimating CRR from (N1)60 (Youd et al., 2001).

$$MSF = \frac{10^{2.24}}{M_w^{2.56}}$$ $M_w < 7.5$

$$MSF = 1$$ $M_w = 7.5$

$$MSF = \left(\frac{M_w}{7.5}\right)^{-2.56}$$ $M_w > 7.5$

$$K_\sigma = \left(\frac{\sigma'_{vo}}{P_a}\right)^{f-1}$$

f = 0.8 $D_r \leq$ %40

f = 0.7 %40 < D_r < %60

f = 0.6 $D_r \geq$ %60

The Cyclic Stress Ratio (CSR) is calculated as below;

$$CSR = 0.65 \cdot \left(\frac{\sigma_v}{\sigma'_v}\right) \cdot \left(\frac{a_{max}}{g}\right) \cdot (r_d)$$

$r_d = 1 - 0{,}00765 \cdot z$ $z \leq 9{,}15$ m (2.11)

$r_d = 1{,}174 - 0{,}0267 \cdot z$ $9{,}15 < z \leq 23$ m (2.12)

6. CONCLUDING REMARKS

This Deliverable illustrates the efforts carried on and the results obtained within Task 2.6 of the Work Package 2 (WP2) of LIQUEFACT project to set-up a methodology for localized assessment of liquefaction potential (*microzonation*).

Four areas were investigated, located in Marmara region (Turkey), Ljubljana area (Slovenia), Lisbon area (Portugal) and Emilia region (Italy). The four testing sites were selected on the basis of the following criteria: availability of geological and geotechnical data, presence of liquefiable soil deposits, documented cases of liquefaction manifestations occurred in past earthquakes, representativeness of different geological setting, density of population in selected areas.

The roles of the partners involved in this activity is as follows:

- UNIPV-Eucentre has responsibility over the Emilia area;
- UPORTO has responsibility over the Lisbon area;
- ULJ has responsibility over the Ljubljana area;
- Istan-Uni has responsibility over the Marmara area.